



Det här verket är upphovrättskyddat enligt *Lagen (1960:729) om upphovsrätt till litterära och konstnärliga verk*. Det har digitaliserats med stöd av Kap. 1, 16 § första stycket p 1, för forskningsändamål, och får inte spridas vidare till allmänheten utan upphovsrättsinnehavarens medgivande.

Alla tryckta texter är OCR-tolkade till maskinläsbar text. Det betyder att du kan söka och kopiera texten från dokumentet. Vissa äldre dokument med dåligt tryck kan vara svåra att OCR-tolka korrekt vilket medför att den OCR-tolkade texten kan innehålla fel och därför bör man visuellt jämföra med verkets bilder för att avgöra vad som är riktigt.

This work is protected by Swedish Copyright Law (*Lagen (1960:729) om upphovsrätt till litterära och konstnärliga verk*). It has been digitized with support of Kap. 1, 16 § första stycket p 1, for scientific purpose, and may no be disseminated to the public without consent of the copyright holder.

All printed texts have been OCR-processed and converted to machine readable text. This means that you can search and copy text from the document. Some early printed books are hard to OCR-process correctly and the text may contain errors, so one should always visually compare it with the images to determine what is correct.



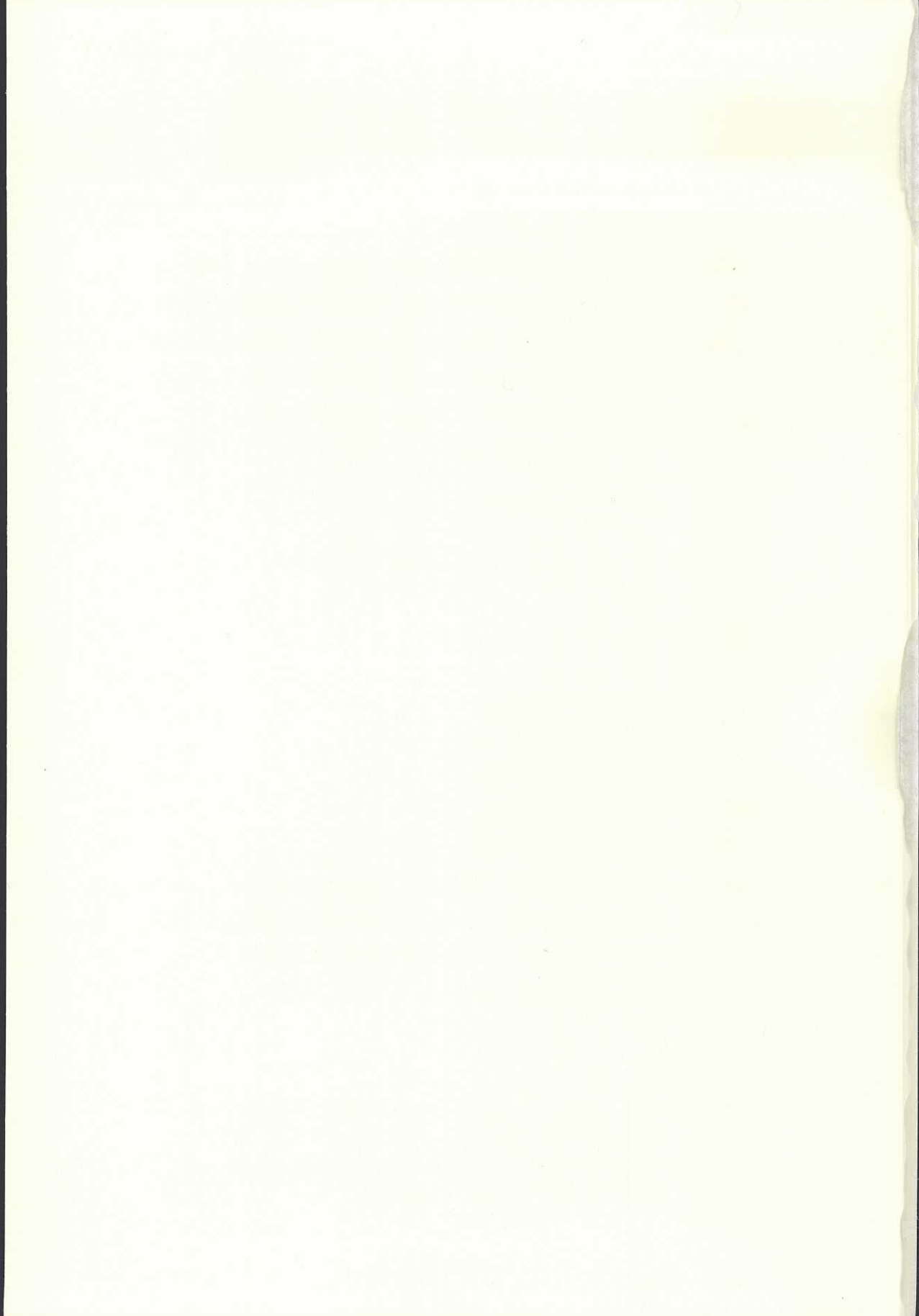


Complete One-Loop QED Calculations for Few-Electron Ions

–Applications to Electron-Electron
Interaction, the Zeeman Effect
and Hyperfine Structure

Per Sunnergren

Department of Experimental Physics
Göteborg University
Chalmers University of Technology
Göteborg 1998





Complete One-Loop QED Calculations for Few-Electron Ions

–Applications to Electron-Electron
Interaction, the Zeeman Effect
and Hyperfine Structure

Per Sunnergren

Akademisk avhandling, som för avläggande av filosofie doktorsexamen i Fysik
vid Göteborgs universitet, försvaras vid en offentlig disputation fredagen
den 16 oktober 1998 kl 10.15, sal KD, Kemigården 4,
Chalmers tekniska högskola, Göteborg.

Avhandlingen försvaras på engelska.

Fakultetsopponent: Professor Vladimir M. Shabaev
St. Petersburg, Ryssland.

Examinator: Professor Eleanor Campbell

Avdelningen för experimentell fysik
Göteborgs universitet
Chalmers tekniska högskola
Göteborg 1998

Abstract

In recent years a considerable improvement has been gained in precision measurements on heavy highly-charged ions. This has stimulated theory to perform accurate calculations for such systems, in the hope to uncover new effects or to verify the validity of existing theories in extreme situations. Specifically, the ground-state hyperfine splitting of hydrogenlike bismuth and the two-electron contribution to the ground-state energy of heliumlike systems have both been measured with high precision. These accurate measurements, together with a bound electron g -factor experiment in progress, motivate a detailed theoretical study of the one-loop QED corrections to these effects.

In this thesis we present the first complete calculation of these one-loop QED corrections. In particular, a rigorous scheme for evaluating the QED effects is developed by combining numerical methods and analytical renormalization techniques. The treatment is complete in the sense that all parts of the one-loop self-energy and vacuum polarization effects are taken into account. An important property of our approach is that the Coulomb interaction between the nucleus and the electrons is taken into account to all orders. This is in contrast to the traditional technique for performing bound-state QED calculations, in which the nuclear field is treated as a perturbation.

We present numerical results for the experiments mentioned and a comparison between theory and experiment is made for heavy highly-charged ions. These systems are extremely relativistic and they provide excellent test cases for bound-state QED in strong nuclear fields. The nuclear field felt by the electrons in such ions is so strong that an expansion in the nuclear potential is not meaningful. Here it is of crucial importance, in order to obtain a reliable theoretical prediction, to treat the bound-state QED effects to all orders in the nuclear interaction.¹

¹**Keywords:** bound-state QED, screened Lamb shift, hyperfine interaction, Zeeman effect, vacuum polarization, self-energy, heliumlike ions, hydrogenlike ions, highly-charged ions

Complete One-Loop QED Calculations for Few-Electron Ions

–Applications to Electron-Electron
Interaction, the Zeeman Effect
and Hyperfine Structure

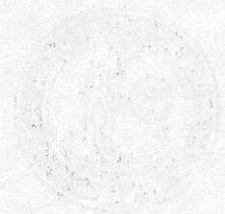
Per Sunnergren



Doctoral thesis for the degree of Doctor of Philosophy

Department of Experimental Physics
Göteborg 1998

Faint, illegible text, possibly bleed-through from the reverse side of the page.



ISBN 91-628-3192-5
Vasastadens Bokbinderi
Göteborg 1998

Abstract

In recent years a considerable improvement has been gained in precision measurements on heavy highly-charged ions. This has stimulated theory to perform accurate calculations for such systems, in the hope to uncover new effects or to verify the validity of existing theories in extreme situations. Specifically, the ground-state hyperfine splitting of hydrogenlike bismuth and the two-electron contribution to the ground-state energy of heliumlike systems have both been measured with high precision. These accurate measurements, together with a bound electron g -factor experiment in progress, motivate a detailed theoretical study of the one-loop QED corrections to these effects.

In this thesis we present the first complete calculation of these one-loop QED corrections. In particular, a rigorous scheme for evaluating the QED effects is developed by combining numerical methods and analytical renormalization techniques. The treatment is complete in the sense that all parts of the one-loop self-energy and vacuum polarization effects are taken into account. An important property of our approach is that the Coulomb interaction between the nucleus and the electrons is taken into account to all orders. This is in contrast to the traditional technique for performing bound-state QED calculations, in which the nuclear field is treated as a perturbation.

We present numerical results for the experiments mentioned and a comparison between theory and experiment is made for heavy highly-charged ions. These systems are extremely relativistic and they provide excellent test cases for bound-state QED in strong nuclear fields. The nuclear field felt by the electrons in such ions is so strong that an expansion in the nuclear potential is not meaningful. Here it is of crucial importance, in order to obtain a reliable theoretical prediction, to treat the bound-state QED effects to all orders in the nuclear interaction.¹

¹**Keywords:** bound-state QED, screened Lamb shift, hyperfine interaction, Zeeman effect, vacuum polarization, self-energy, heliumlike ions, hydrogenlike ions, highly-charged ions

Till Gisela,
Josefin och Pontus

"A poet once said, "The whole universe is in a glass of wine." We will probably never know in what sense he meant that, for poets do not write to be understood. But it is true that if we look at a glass of wine closely enough we see the entire universe. There are the things of physics: the twisting liquid which evaporates depending on the wind and weather, the reflections in the glass, and our imagination adds the atoms. The glass is a distillation of the earth's rocks, and in its composition we see the secrets of the universe's age, and the evolution of stars. What strange array of chemicals are in the wine? How did they come to be? There are the ferments, the enzymes, the substrates, and the products. There in wine is found the great generalization: all life is fermentation. Nobody can discover the chemistry of wine without discovering, as did Louis Pasteur, the cause of much disease. How vivid is the claret, pressing its existence into the consciousness that watches it! If our small minds, for some convenience, divide this glass of wine, this universe, into parts — physics, biology, geology, astronomy, psychology, and so on — remember that nature does not know it! So let us put it all back together, not forgetting ultimately what it is for. Let it give us one more final pleasure: drink it and forget it all!"

R. P. Feynman

Contents

List of Publications	3
1 Introduction	5
1.1 Thesis overview	6
2 First-Order Interactions	9
2.1 Interelectron interaction	9
2.1.1 One-photon exchange in momentum space	13
2.2 External potential interaction	16
2.2.1 Magnetic field interaction	17
2.2.2 Hyperfine interaction	17
3 Electron Self-Energy Corrections	19
3.1 First-order self-energy	19
3.2 Self-energy corrections in external potentials	23
3.2.1 Wavefunction correction	27
3.2.2 Vertex and binding-energy corrections	30
4 Vacuum Polarization Corrections	43
4.1 First-order vacuum polarization	43
4.2 Vacuum polarization corrections in external potentials	47
4.2.1 Wavefunction correction	47
4.2.2 Potential correction	48
4.2.3 Vacuum polarization correction to the nuclear magnetic moment	52
5 Numerical Procedure	55
5.1 Numerical solution of the Dirac equation	55
5.1.1 Symmetrical spectrum method	56
5.2 Wavefunctions	57
5.2.1 The reference wavefunction	57
5.2.2 The perturbed wavefunction	58
5.3 Numerical implementation of the self-energy	61
5.3.1 Many-potential terms	61
5.3.2 Zero- and one-potential terms	64
5.4 Numerical implementation of the vacuum polarization	71
6 Numerical Results and Discussion	73
6.1 Two-electron Lamb shift	73
6.2 Bound electron g factor	81
6.3 Hyperfine structure	85

7	Conclusions and Outlook	91
	Acknowledgements	93
	APPENDICES	95
A	Basic Theory of Bound State QED	97
A.1	Units and notations	97
A.2	The non-interacting electron field	99
A.3	The electromagnetic field	101
A.4	The interacting fields	105
A.4.1	Wick's theorem	107
A.5	Rules for Feynman diagrams	108
B	Interaction Potentials in Momentum Space	111
B.1	The electron potential	112
B.1.1	Coulomb potential	112
B.1.2	Breit potential	113
B.2	External magnetic potential	114
B.3	Hyperfine potential	115
C	Mass and Charge Renormalization	117
C.1	Photon self interaction	118
C.2	Electron self-energy	120
C.3	Vertex correction	121
D	Dimensional Regularization	123
D.1	Free electron self-energy operator	124
D.2	Free electron vertex operator	125
E	Derivation of the Binding-Energy Correction	129
F	Free Electron Solutions	133
F.1	Plane waves	133
F.2	Spherical waves	134
	BIBLIOGRAPHY	137

This thesis is based on the following publications

- I. "Radiative corrections to the hyperfine-structure splitting of hydrogenlike systems"
Per Sunnergren, Hans Persson, Sten Salomonson, Stefan M. Schneider, Ingvar Lindgren and Gerhard Soff.
Physical Review A, **58**, 1055, 1998.
- II. "Radiative corrections to the electron g-factor in H-like ions"
Hans Persson, Sten Salomonson, Per Sunnergren and Ingvar Lindgren.
Physical Review A, **56**, R4299, 1997.
- III. "Two-electron Lamb-shift calculations on heliumlike ions"
Hans Persson, Sten Salomonson, Per Sunnergren and Ingvar Lindgren.
Physical Review Letters, **76**, 204, 1996.
- IV. "Accurate vacuum-polarization calculations"
Hans Persson, Ingvar Lindgren, Sten Salomonson and Per Sunnergren.
Physical Review A, **48**, 2772, 1993.
- V. "Regularization corrections to the partial-wave renormalization procedure"
Hans Persson, Sten Salomonson and Per Sunnergren.
In proceedings of *Modern trends in atomic physics*,
Advances in Quantum Chemistry, **30**, 379, 1998.

Scientific publications not included in the thesis

- "Analysis of the electron self-energy for tightly bound electrons"
Ingvar Lindgren, Hans Persson, Sten Salomonson and Per Sunnergren.
Physical Review A, **58**, 1001, 1998.
- "A theoretical survey of QED tests in highly charged ions"
Hans Persson, Sten Salomonson, Per Sunnergren, Ingvar Lindgren and Martin G.H. Gustavsson.
In proceedings of the 2nd *Euroconference on atomic physics with stored highly charged ions*,
Hyperfine Interactions, **108**, 3, 1997.
- "QED effects in few-electron high- Z systems"
Ingvar Lindgren, Hans Persson, Sten Salomonson and Per Sunnergren.
In proceedings of the 15th *International conference on atomic physics*,
ICAP,
Atomic Physics, **15**, 271, 1997.
- "QED calculations on two- and three-electron ions"
Ingvar Lindgren, Hans Persson, Sten Salomonson and Per Sunnergren.
Physica Scripta, Nobel Symposium, **59**, 179, 1995.

- "Few-body problems in atomic physics"
Ingvar Lindgren, Hans Persson, Sten Salomonson and Per Sunnergren.
In proceedings of the XVth *European conference on few-body problems in physics*,
Few-Body Systems, 8, 60, 1995.

1 Introduction

The theory of quantum electrodynamics (QED) was formulated in the late 1920's as the result of the efforts to combine special relativity and quantum mechanics. The effect of relativity was found to be not merely quantitative — completely new phenomena arose, e.g., particle states with negative energy, spontaneous creation and annihilation of virtual particle-antiparticle pairs etc. It was soon recognized, however, that calculating QED effects in higher-order, which should yield small corrections, resulted in infinite answers. There was obviously some fundamental problem with the early formulation of QED. Several attempts were made to overcome this difficulty but the divergency problem remained unsolved for two decades.

During the 1930's and 40's experimental studies of the $2s_{1/2}$ and $2p_{1/2}$ states in atomic hydrogen suggested that these energy levels were not degenerate, which was in contrast to the Dirac theory. The technical development during the second world war made it possible to perform accurate spectroscopic studies, and in 1947 Lamb and Retherford measured the hydrogen shift to be ≈ 1000 MHz [1]. It was believed that this shift (the Lamb shift) could be of quantum electrodynamic origin but the contribution from vacuum polarization, which was the only higher-order QED effect one could evaluate, was too small (-27 MHz) to explain the observed splitting. The electron self-energy, on the other hand, gave infinite results and had therefore been neglected earlier. By adopting Kramers' idea of mass renormalization Bethe managed, however, to compute a finite contribution of 1040 MHz from the self-energy effect [2]. (The actual calculation was performed at a train ride after the Shelter Island conference in 1947, where mass renormalization and the Lamb shift were among the topics.) In the same year Schwinger [3] gave further an explanation of the anomalous magnetic moment of the electron, observed experimentally by Kusch and Foley [4], by using a quantum electrodynamic treatment. These successes brought QED back to the center of interest and led to the development of modern QED. The concept of renormalization was given a solid theoretical ground and it was shown that QED is renormalizable in all orders of perturbation theory [5-7].

QED has proven to be an extremely successful theory and the agreement between its predictions and experiment can only be described as stunning. The most spectacular example is the investigation of the anomalous magnetic moment of free electrons, which gives the remarkable agreement at the level of one part in 10^{11} . The theoretical calculation involves, in addition to the part evaluated by Schwinger in 1947, the computation of 970 different contributions!

Since QED describes the fundamental interaction of electrically charged particles, it can be viewed as the underlying theory of all everyday physics (excluding gravitational effects). It is, however, not necessary (or technically possible) to employ the pure theory for explaining most physical situations. The use of suitable approximations is usually sufficient, even in the majority of atomic

physics problems. Nevertheless, for certain systems and processes it is of crucial importance to use the full QED theory in order to obtain a satisfactory understanding of the physics involved.

In studying light elements, for which the nuclear electromagnetic field is relatively small, it is appropriate to start from free-electron QED and to consider the interaction with the nucleus as a perturbation. This treatment leads to an expansion in the characteristic coupling constant ($Z\alpha$) of the electron-nucleus interaction, where Z is the nuclear charge number and α is the fine structure constant $\alpha \approx 1/137$. With this approach it is possible to consider QED effects to relatively high-order, but the method is naturally restricted to low- Z systems where $(Z\alpha)$ is small. For high- Z systems the nuclear potential felt by the electrons is simply too strong for an expansion in the nuclear interaction to be meaningful. Here it is necessary to include the nuclear potential from the very beginning and to construct nonperturbative electron propagators. The lack of a simple analytical form for such propagators is one major complication of bound-state QED (QED in atoms) in comparison with free-electron QED. During the last decade several numerical techniques, mainly basis-set approaches, have been developed and employed in the calculations of bound-state QED effects in highly-charged ions.

Due to the recent progress in experimental technology, it is today possible to accurately study quite extreme ions like hydrogenlike uranium. Such heavy highly-charged ions are extremely relativistic and this enhances the relative importance of the QED effects. The principal aim for investigating this kind of systems is to test the validity of bound-state QED in strong nuclear fields. These developments have stimulated theoretical efforts to perform accurate calculations of bound-state QED effects — to which this work aims to contribute.

1.1 Thesis overview

A rather detailed presentation of the basic theory of bound-state QED is given in Appendix A, based on standard textbooks such as Sakurai [8], Mandl and Shaw [9], Jauch and Rohrlich [10] and Greiner [11]. The quantized electron and photon fields are introduced and their interaction in terms of the perturbative S-matrix expansion is discussed. The rules for bound-state Feynman diagrams, which pictures the interaction processes, is also stated at the end of the appendix. Units and notation conventions used in this thesis are further introduced (we will employ natural units in which $\hbar = c = \epsilon_0 = \mu_0 = 1$).

Chapter 2 introduces the lowest-order processes (referred to as the first-order interactions) which contributes to the physical effects studied in the thesis. These are: (1) the electron-electron interaction in ground-state two-electron systems, (2) the energy level splitting of ground-state one-electron ions due to the interaction with an external static homogeneous magnetic field (Zeeman effect) and (3) the corresponding splitting due to the interaction of the electron with the nuclear magnetic moment (hyperfine structure). The expressions for the first-order interactions are derived within the framework of bound-state QED and a discussion of the different potentials is given. In order to treat

these three different interactions on an equal footing, we will formulate also the inter-electron interaction as a one-electron problem, treating the potential from the other electron as an external potential.

The main subject of this thesis is the calculation of the one-loop radiative corrections to the first-order interactions. The theoretical formalism for these QED corrections is developed in Chapters 3 and 4 for the self-energy and the vacuum polarization parts, respectively. The presentation is rather detailed since we want to put emphasis on how the calculations are performed in practice. The radiative QED effects contain divergent pieces which are removed by means of mass and charge renormalization. A discussion about the basic ideas behind renormalization is given in Appendix C. Performing the renormalization in the actual calculations requires the use of a regularization procedure. We have adopted the concept of dimensional regularization and this technique is presented in Appendix D.

In Chapter 5 we discuss the numerical implementation of our calculation scheme. Besides a detailed presentation concerning the evaluation of the QED effects, we shortly describe the discretization technique which is central in the sense of providing us with a complete set of numerical solutions to the Dirac equation, used to represent the electron propagator.

Selected results for the three different projects covered in this work are presented and discussed in Chapter 6. The ambition is to complement the results given in the articles appended to the thesis. For the sake of completeness some results are, however, just re-quoted from the published papers. Comparisons with other calculations and with experimental results can also be found there.

Finally, in Chapter 7 we summarize the thesis and discuss some future goals and developments.

2 First-Order Interactions

In this thesis we will consider the contribution to the ground-state energy of two-electron systems due to the inter-electronic interaction (electron correlation). We will further study the energy level splitting in one-electron ions due to the interaction with an external homogeneous magnetic field (Zeeman effect) and with the nuclear magnetic potential (hyperfine structure). The lowest-order contributions to these effects are the one-photon exchange (Fig. 2.1 (a)) for the two-electron case, and the one-potential interaction (Fig. 2.1 (b)) for the one-electron system. These processes will be referred to as first-order interactions. The main concern of the thesis is the calculation of one-loop radiative corrections (which in the thesis also will be called *one-photon* radiative corrections) to these first-order interactions. The formal theory for the QED corrections is identical for the three different interaction types. By formulating the inter-electron interaction as a one-electron problem, considering the potential from the other electron as an external potential, we can treat the radiative corrections for all different interactions in a unified manner. In this chapter we will start with discussing the first-order interactions and the potentials in coordinate as well as in momentum space. The Fourier transformations to momentum space are treated in Appendix B. For later convenience we will further consider the first-order inter-electronic interaction in momentum space in some detail.

2.1 Interelectron interaction

For two-electron systems the lowest-order (one-photon) processes stem from the $\hat{S}_\gamma^{(2)}$ matrix elements. Using the formalism developed in Appendix A we have

$$\hat{S}_\gamma^{(2)} = \frac{(ie)^2}{2!} \int d^4x_1 \int d^4x_2 T \left\{ [\hat{\Psi}^\dagger \gamma^0 \hat{A} \hat{\Psi}]_{x_1} [\hat{\Psi}^\dagger \gamma^0 \hat{A} \hat{\Psi}]_{x_2} \right\} e^{-\gamma|t_1|} e^{-\gamma|t_2|}. \quad (2.1)$$

Rewriting the time-ordering by using Wick's theorem we find the following three contributions

$$\hat{S}_\gamma^{(2,1)} = -\frac{e^2}{2} \int d^4x_1 \int d^4x_2 N \left\{ (\hat{\Psi}^\dagger \alpha^\mu \hat{A}_\mu \hat{\Psi})_1 (\hat{\Psi}^\dagger \alpha^\nu \hat{A}_\nu \hat{\Psi})_2 \right\} e^{-\gamma|t_1|} e^{-\gamma|t_2|} \quad (2.2)$$

and

$$\hat{S}_\gamma^{(2,2)} = -\frac{e^2}{2} \int d^4x_1 \int d^4x_2 N \left\{ (\hat{\Psi}^\dagger \alpha^\mu \hat{A}_\mu \hat{\Psi})_1 (\hat{\Psi}^\dagger \alpha^\nu \hat{A}_\nu \hat{\Psi})_2 \right\} e^{-\gamma|t_1|} e^{-\gamma|t_2|} \quad (2.3)$$

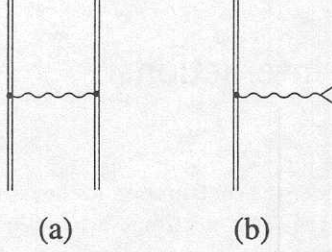


Figure 2.1: The Feynman diagrams for the first-order interactions, the one-photon exchange (a) for two-electron systems, and the one-potential interaction (b) for one-electron systems. The double lines represent electrons propagating in the nuclear electric field, and the wavy line indicates a photon interaction. The triangle represents the interaction with the external potential.

and

$$\hat{S}_\gamma^{(2,3)} = -\frac{e^2}{2} \int d^4x_1 \int d^4x_2 N \left\{ (\hat{\Psi}^\dagger \alpha^\mu \hat{A}_\mu \hat{\Psi})_1 (\hat{\Psi}^\dagger \hat{\Psi} \alpha^\nu \hat{A}_\nu)_2 \right\} e^{-\gamma|t_1|} e^{-\gamma|t_2|}. \quad (2.4)$$

The first of those expressions corresponds to the one-photon exchange (Fig. 2.1 (a)) and the second and third are the first-order electron self-energy (Fig. 2.2 (a)) and the first-order vacuum polarization (Fig. 2.2 (b)), respectively. The latter are radiative corrections, not to the one-photon exchange but rather to the energy eigenvalue of the Dirac equation. Note that these first-order radiative corrections do not contribute when considering the inter-electronic part of the two-electron ground-state energy. If one is interested to determine the total (true) ground state energy, they will of course contribute. This is also true for all higher-order radiative corrections which do not include any inter-electronic interaction.

Focus now on the energy contribution to the ground-state energy from the one-photon exchange between two electrons

$$\Delta E^1 = \lim_{\gamma \rightarrow 0} i\gamma \langle \Phi_{c,d}^0 | \hat{S}_\gamma^{(2,1)} | \Phi_{a,b}^0 \rangle, \quad (2.5)$$

where $\hat{S}_\gamma^{(2,1)}$ is given by Eq. (2.2). Identifying the contraction in that expression as the photon propagator yields

$$\begin{aligned} \hat{S}_\gamma^{(2,1)} &= -\frac{ie^2}{2} \int d^4x_1 \int d^4x_2 e^{-\gamma|t_1|} e^{-\gamma|t_2|} \\ &\times N \left\{ \hat{\Psi}^\dagger(x_1) \alpha^\mu \hat{\Psi}(x_1) D_{\mu\nu}^F(x_1 - x_2) \hat{\Psi}^\dagger(x_2) \alpha^\nu \hat{\Psi}(x_2) \right\}. \end{aligned} \quad (2.6)$$

The uncontracted field operators will, when calculating the matrix element $\langle \Phi_{c,d}^0 | \hat{S}_\gamma^{(2,1)} | \Phi_{a,b}^0 \rangle$, produce the atomic wave functions

$$\begin{aligned} \langle \Phi_{c,d}^0 | N \left\{ \hat{\Psi}^\dagger(x_1) \hat{\Psi}(x_1) \hat{\Psi}^\dagger(x_2) \hat{\Psi}(x_2) \right\} | \Phi_{a,b}^0 \rangle &\rightarrow \Phi_c^\dagger(\mathbf{x}_1) e^{iE_c t_1} \Phi_a(\mathbf{x}_1) e^{-iE_a t_1} \\ &\times \Phi_d^\dagger(\mathbf{x}_2) e^{iE_d t_2} \Phi_b(\mathbf{x}_2) e^{-iE_b t_2}. \end{aligned} \quad (2.7)$$

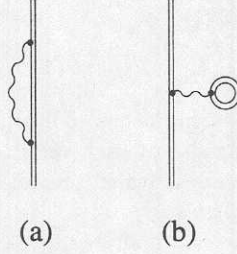


Figure 2.2: *First-order radiative corrections, the self-energy (a) and the vacuum polarization (b).*

Since the photon propagator has the time dependence $e^{-iz(t_1-t_2)}$, where z is the energy parameter of the propagator, we obtain the time-integrations

$$\begin{aligned} & \int_{-\infty}^{\infty} dt_1 \int_{-\infty}^{\infty} dt_2 e^{-\gamma|t_1|} e^{-\gamma|t_2|} e^{-it_1(E_a-E_c+z)} e^{-it_2(E_b-E_d-z)} \\ &= (2\pi)^2 \Delta_\gamma(E_a - E_c + z) \Delta_\gamma(E_b - E_d - z). \end{aligned} \quad (2.8)$$

Here we have introduced the Δ_γ -function, which is defined by

$$\Delta_\gamma(x) = \int_{-\infty}^{\infty} \frac{dt}{2\pi} e^{-ixt} e^{-\gamma|t|} = \frac{1}{\pi} \frac{\gamma}{x^2 + \gamma^2} \quad (2.9)$$

and has the following properties

$$\begin{aligned} \lim_{\gamma \rightarrow 0} \Delta_\gamma(x) &= \delta(x), \\ \lim_{\gamma \rightarrow 0} \pi\gamma \Delta_\gamma(x) &= \delta_{x,0}, \\ \lim_{\gamma \rightarrow 0} \Delta_\gamma(x-b)f(x) &= \lim_{\gamma \rightarrow 0} \Delta_\gamma(x-b)f(b), \\ \int_{-\infty}^{\infty} dx \Delta_{n\gamma}(x-a) \Delta_{m\gamma}(x-b) &= \Delta_{(n+m)\gamma}(a-b), \end{aligned} \quad (2.10)$$

where n and m are integers.

The expression for the matrix element takes now the form

$$\begin{aligned} \langle \Phi_{c,d}^0 | \hat{S}_\gamma^{(2,1)} | \Phi_{a,b}^0 \rangle &= -i\pi e^2 \int d^3\mathbf{x}_1 \int d^3\mathbf{x}_2 \int dz D_{\mu\nu}^F(\mathbf{x}_1 - \mathbf{x}_2, z) \\ &\quad \times \Delta_\gamma(E_a - E_c + z) \Delta_\gamma(E_b - E_d - z) \\ &\quad \times \Phi_c^\dagger(\mathbf{x}_1) \alpha^\mu \Phi_a(\mathbf{x}_1) \Phi_d^\dagger(\mathbf{x}_2) \alpha^\nu \Phi_b(\mathbf{x}_2). \end{aligned} \quad (2.11)$$

By using Eqs. (2.10) we can perform the z -integration

$$\begin{aligned} & \int_{-\infty}^{\infty} dz D_{\mu\nu}^F(\mathbf{x}_1 - \mathbf{x}_2, z) \Delta_\gamma(E_a - E_c + z) \Delta_\gamma(E_b - E_d - z) \\ &= D_{\mu\nu}^F(\mathbf{x}_1 - \mathbf{x}_2, E_c - E_a) \Delta_{2\gamma}(E_c + E_d - E_a - E_b), \end{aligned} \quad (2.12)$$

and taking the limit $\gamma \rightarrow 0$ yields

$$\lim_{\gamma \rightarrow 0} \pi 2\gamma \Delta_{2\gamma}(E_c + E_d - E_a - E_b) = \delta(E_c + E_d, E_a + E_b) . \quad (2.13)$$

The time-integrations leads thus, in the $\gamma \rightarrow 0$ limit, to energy conservation, not only for the entire diagram but also at each vertex. This is a general property of bound state QED for free atoms which prevails also in the presence of an time-independent external potential.

Summing everything up, we can finally write the energy contribution due to the one-photon exchange as

$$\begin{aligned} \Delta E^1 &= e^2 \delta(E_c + E_d, E_a + E_b) \int d^3 \mathbf{x}_1 \int d^3 \mathbf{x}_2 D_{\mu\nu}^F(\mathbf{x}_1 - \mathbf{x}_2, E_c - E_a) \\ &\quad \times \Phi_c^\dagger(\mathbf{x}_1) \alpha^\mu \Phi_a(\mathbf{x}_1) \Phi_d^\dagger(\mathbf{x}_2) \alpha^\nu \Phi_b(\mathbf{x}_2) . \end{aligned} \quad (2.14)$$

This is a general expression for the states a, b, c, d and the total one-photon process consists of the direct ($|c\rangle = |a\rangle$, $|d\rangle = |b\rangle$) and the exchange ($|c\rangle = |b\rangle$, $|d\rangle = |a\rangle$) parts

$$\begin{aligned} \Delta E_{ab}^1(\text{dir.} - \text{exc.}) &= e^2 \int d^3 \mathbf{x}_1 \int d^3 \mathbf{x}_2 D_{\mu\nu}^F(\mathbf{x}_1 - \mathbf{x}_2, 0) \\ &\quad \times \Phi_a^\dagger(\mathbf{x}_1) \alpha^\mu \Phi_a(\mathbf{x}_1) \Phi_b^\dagger(\mathbf{x}_2) \alpha^\nu \Phi_b(\mathbf{x}_2) \\ &\quad - e^2 \int d^3 \mathbf{x}_1 \int d^3 \mathbf{x}_2 D_{\mu\nu}^F(\mathbf{x}_1 - \mathbf{x}_2, E_b - E_a) \\ &\quad \times \Phi_b^\dagger(\mathbf{x}_1) \alpha^\mu \Phi_a(\mathbf{x}_1) \Phi_a^\dagger(\mathbf{x}_2) \alpha^\nu \Phi_b(\mathbf{x}_2) . \end{aligned} \quad (2.15)$$

For the $1s^2$ ground state the two electrons have the same energy and differ only in their spin states $m = \pm 1/2$. The two different processes can thus be included in the angular part of a given contribution. To be able to treat the inter-electronic interaction in the same manner as the g factor and the hyperfine structure later on, we formulate it in terms of the electron potential

$$A_\mu^{db}(\mathbf{x}_1) = -e \int d^3 \mathbf{x}_2 D_{\mu\nu}^F(\mathbf{x}_1 - \mathbf{x}_2, 0) \Phi_d^\dagger(\mathbf{x}_2) \alpha^\nu \Phi_b(\mathbf{x}_2) , \quad (2.16)$$

such that the first-order energy can be written as

$$\Delta E^1 = -e \int d^3 \mathbf{x}_1 \Phi_c^\dagger(\mathbf{x}_1) \alpha^\mu A_\mu^{db}(\mathbf{x}_1) \Phi_a(\mathbf{x}_1) . \quad (2.17)$$

The potential consists of a scalar part ($\alpha^0 = 1$) and a vector part ($\boldsymbol{\alpha}$). These will in the thesis be referred to as the Coulomb and Breit potentials, respectively. Their expressions in momentum space are derived in Appendix B and read

$$A_0^{db}(\mathbf{p} - \mathbf{p}') = \frac{-e}{(2\pi)^3} \sum_{k=0}^{\infty} (2k+1) V_k(p, p') \mathbf{C}^k(\hat{p}) \cdot \mathbf{C}^k(\hat{p}') , \quad (2.18)$$

for the Coulomb part, and

$$\begin{aligned} \mathbf{A}^{db}(\mathbf{p} - \mathbf{p}') &= \frac{-3e}{(2\pi)^3} \sum_{k=0}^{\infty} (2k+1) h_k(p, p') \mathbf{C}^k(\hat{p}) \cdot \mathbf{C}^k(\hat{p}') [p \mathbf{C}^1(\hat{p}) - p' \mathbf{C}^1(\hat{p}')] \\ &\quad \times \int d\Omega [\chi_\kappa^{m_a \dagger}(\hat{r}) \boldsymbol{\sigma} \mathbf{C}^1(\hat{r}) \chi_{-\kappa}^{m_b}(\hat{r}) - \chi_{-\kappa}^{m_a \dagger}(\hat{r}) \boldsymbol{\sigma} \mathbf{C}^1(\hat{r}) \chi_\kappa^{m_b}(\hat{r})] , \end{aligned} \quad (2.19)$$

for the Breit potential.

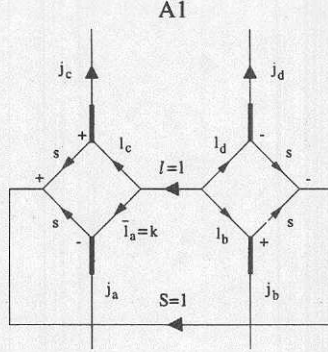


Figure 2.3: Angular momentum graph corresponding to the first term of $\Delta E_{\text{breit}}^1$ in Eq. (2.26) ($k = 1$). l is the tensor rank of the interaction in orbital space and S the tensor rank in spin space.

2.1.1 One-photon exchange in momentum space

Coulomb interaction

The first-order energy due to scalar photon exchange is in momentum space expressed as

$$\Delta E_{\text{cou}}^1 = -e \int d^3\mathbf{p} \int d^3\mathbf{p}' \Phi_c^\dagger(\mathbf{p}) A_0^{db}(\mathbf{p} - \mathbf{p}') \Phi_a(\mathbf{p}'), \quad (2.20)$$

with the potential A_0^{db} given in Eq. (2.18). The momentum space wavefunction is given by

$$\Phi(\mathbf{p}) = \frac{1}{(2\pi)^{3/2}} \int d^3\mathbf{r} e^{-i\mathbf{p}\cdot\mathbf{r}} \Phi(\mathbf{r}) = \begin{pmatrix} P(p) \chi_\kappa^m(\hat{p}) \\ Q(p) \chi_{-\kappa}^m(\hat{p}) \end{pmatrix}, \quad (2.21)$$

with the radial components

$$\begin{aligned} P(p) &= \sqrt{\frac{2}{\pi}} (-i)^l \int dr r^2 j_l(pr) f(r) \\ Q(p) &= \sqrt{\frac{2}{\pi}} (-i)^{\bar{l}-1} \int dr r^2 j_{\bar{l}}(pr) g(r), \end{aligned} \quad (2.22)$$

where $f(r)$ and $g(r)$ are the radial wavefunctions of the large and small components with orbital angular momenta l and \bar{l} , respectively. Inserting these expressions into Eq. (2.20) gives

$$\begin{aligned} \Delta E_{\text{cou}}^1 &= \frac{e^2}{(2\pi)^3} \sum_{k=0}^{\infty} (2k+1) \int d^3\mathbf{p} \int d^3\mathbf{p}' V_k(p, p') \\ &\times \left\{ P(p) P(p') \chi_\kappa^{m_c \dagger}(\hat{p}) \chi_\kappa^{m_a}(\hat{p}') C^k(\hat{p}) \cdot C^k(\hat{p}') \right. \\ &\quad \left. + Q(p) Q(p') \chi_{-\kappa}^{m_c \dagger}(\hat{p}) \chi_{-\kappa}^{m_a}(\hat{p}') C^k(\hat{p}) \cdot C^k(\hat{p}') \right\}. \end{aligned} \quad (2.23)$$

A2

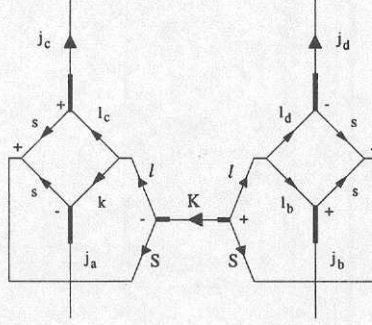


Figure 2.4: Angular momentum graph A1 with l and S coupled to K (summation over K).

The angular integrations leads to orthonormality conditions which yields $k = 0$ for the first term and $k = 1$ for the second and we obtain

$$\Delta E_{\text{cou}}^1 = \frac{2\alpha}{\pi} \int dp p^2 \int dp' p'^2 [P(p)P(p')V_0(p, p') + Q(p)Q(p')V_1(p, p')] . \quad (2.24)$$

Breit interaction

The energy contribution due to the vector photon exchange is given by

$$\Delta E_{\text{breit}}^1 = e \int d^3\mathbf{p} \int d^3\mathbf{p}' \Phi_c^\dagger(\mathbf{p}) \boldsymbol{\alpha} \cdot \mathbf{A}^{db}(\mathbf{p} - \mathbf{p}') \Phi_a(\mathbf{p}') , \quad (2.25)$$

where \mathbf{A}^{db} is given by Eq. (2.19). Inserting this expression together with the momentum space wavefunctions yields

$$\begin{aligned} \Delta E_{\text{breit}}^1 &= \frac{-3e^2}{(2\pi)^3} \sum_{k=0}^{\infty} (2k+1) \int d\Omega \left[\chi_{\kappa}^{m_d\dagger}(\hat{r}) \boldsymbol{\sigma} \mathbf{C}^1(\hat{r}) \chi_{-\kappa}^{m_b}(\hat{r}) - \chi_{-\kappa}^{m_d\dagger}(\hat{r}) \boldsymbol{\sigma} \mathbf{C}^1(\hat{r}) \chi_{\kappa}^{m_b}(\hat{r}) \right] \\ &\times \int d^3\mathbf{p} \int d^3\mathbf{p}' h_k(p, p') \\ &\times \left\{ P(p)pQ(p') \chi_{\kappa}^{m_c\dagger}(\hat{p}) \boldsymbol{\sigma} \chi_{-\kappa}^{m_a}(\hat{p}') \mathbf{C}^1(\hat{p}) \mathbf{C}^k(\hat{p}) \cdot \mathbf{C}^k(\hat{p}') \right. \\ &\quad - P(p)p'Q(p') \chi_{\kappa}^{m_c\dagger}(\hat{p}) \boldsymbol{\sigma} \chi_{-\kappa}^{m_a}(\hat{p}') \mathbf{C}^1(\hat{p}') \mathbf{C}^k(\hat{p}) \cdot \mathbf{C}^k(\hat{p}') \\ &\quad + Q(p)pP(p') \chi_{-\kappa}^{m_c\dagger}(\hat{p}) \boldsymbol{\sigma} \chi_{\kappa}^{m_a}(\hat{p}') \mathbf{C}^1(\hat{p}) \mathbf{C}^k(\hat{p}) \cdot \mathbf{C}^k(\hat{p}') \\ &\quad \left. - Q(p)p'P(p') \chi_{-\kappa}^{m_c\dagger}(\hat{p}) \boldsymbol{\sigma} \chi_{\kappa}^{m_a}(\hat{p}') \mathbf{C}^1(\hat{p}') \mathbf{C}^k(\hat{p}) \cdot \mathbf{C}^k(\hat{p}') \right\} . \quad (2.26) \end{aligned}$$

Each of the four terms in the curly bracket contains an orthonormality integral for the spherical harmonics, e.g., the \hat{p}' -integral in the first term. This leads to contributions with $k = 1, 0, 0, 1$ for the four different terms. Focus now on the first of these terms which has the angular part

$$\frac{4\pi}{2k+1} \langle l_c \parallel \mathbf{C}^1 \parallel k \rangle \cdot \langle l_d \parallel \mathbf{C}^1 \parallel l_b \rangle \langle \frac{1}{2} \parallel \boldsymbol{\sigma} \parallel \frac{1}{2} \rangle^2 \times A1 , \quad (2.27)$$

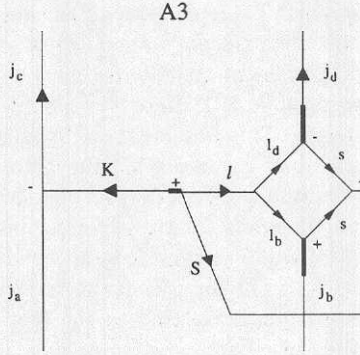


Figure 2.5: Angular momentum graph A2 after reducing the left-hand side.

where A1 is the angular momentum graph shown in Fig. 2.3. Note that l_d, l_b in this expression contributes as \bar{l}_d, l_b or l_d, \bar{l}_b . We can obtain the angular parts for the remaining three terms by replacing, $l_c \rightarrow k$ and $k \rightarrow \bar{l}_a$ for term two, $l_c \rightarrow \bar{l}_c$ for the third term and finally $l_c \rightarrow k$ and $k \rightarrow l_a$ for the last term. Apart from a sign change between the first two and the last two terms, all these cases give exactly the same result for the angular integration, and the final expression for the vector photon exchange can be written as

$$\Delta E_{\text{breit}}^1 = \frac{8\alpha}{\pi} \int dp p^2 \int dp' p'^2 \{ P(p)Q(p') [p' h_0(p, p') - p h_1(p, p')] + Q(p)P(p') [p h_0(p, p') - p' h_1(p, p')] \} . \quad (2.28)$$

Since $h_i(p, p')$ is symmetric with respect to p and p' , the two terms in the curly bracket gives the same contribution. We keep all terms here in order to see more clearly the correspondence with the terms in the free-electron vertex correction, which is considered in Chapter 3.

To see the relation with the g -factor and the hyperfine interactions (which also are vector type), we first rewrite diagram A1 by coupling l and S to K with a summation over K , as is shown in diagram A2 in Fig. 2.4. Diagram A2 can further be reduced to diagram A3 in Fig. 2.5 times a $9-j$ symbol, and we can write

$$A1 = \sum_K A2 ,$$

$$A2 = [(2j_c + 1)(2j_a + 1)(2K + 1)]^{1/2} \left\{ \begin{matrix} l_c & k & l \\ \frac{1}{2} & \frac{1}{2} & S \\ j_c & j_a & K \end{matrix} \right\} \times A3 . \quad (2.29)$$

A similar reduction can of course also be made on the right-hand side of the diagram, but we keep this form since the right-hand side will have different structure depending on the interaction considered. For the hyperfine interaction

the right-hand side of diagram A3 is replaced with the nuclear spin part and for the g -factor case we will have the external magnetic field at the right. Since only the nuclear magnetic dipole moment contributes for $j = 1/2$ states, it follows that both these interactions have $K = 1$. Here it is possible with $K = 0$ and $K = 1$, but only $K = 1$ contributes. This implies that the angular structure for the three different vector interactions is very similar, the factor relating diagrams A2 and A3 (Eq. (2.29)) is for example identical. The angular diagrams for higher-order effects can be treated generally for the different interactions, just having an outgoing $K = 1$ line. This will for example be utilized when considering the free-electron vertex correction. The angular factor associated with the vertex correction to the Breit interaction is related to the first-order angular factor, and this relation holds then also for the g -factor and hyperfine interactions. More generally, we can work out the angular parts for the QED corrections considering the Breit interaction. These angular parts can then be used also for the other vector interactions, simply by scaling with the corresponding angular factor for their first-order interaction.

2.2 External potential interaction

For one-electron ions in an external potential the lowest-order (one-potential) process comes from the $\hat{S}_\gamma^{(1)}$ matrix element

$$\hat{S}_\gamma^{(1)} = ie \int d^4x \hat{\Psi}^\dagger(x) \gamma^0 \mathcal{A}^{\text{ext}}(x) \hat{\Psi}(x) e^{-\gamma|t|}, \quad (2.30)$$

which corresponds to the Feynman diagram in Fig. 2.1 (b). This is the first-order process which contributes to the splitting caused by the external potential. First-order radiative corrections (Fig. 2.2 (a) and (b)), and all higher-order radiative corrections that do not mix with the external potential, will only contribute to the absolute values of the energy levels and not to the splittings.

The first-order energy contribution is given by

$$\begin{aligned} \Delta E^1 &= \lim_{\gamma \rightarrow 0} \frac{i\gamma}{2} \langle \Phi_b^0 | \hat{S}_\gamma^{(1)} | \Phi_a^0 \rangle \\ &= \lim_{\gamma \rightarrow 0} \frac{-e\gamma}{2} \int d^4x \Phi_b^\dagger(\mathbf{x}) \alpha^\mu A_\mu^{\text{ext}}(x) \Phi_a(\mathbf{x}) e^{-it(E_a - E_b)} e^{-\gamma|t|} \end{aligned} \quad (2.31)$$

and assuming the potential to be time-independent, $A_\mu^{\text{ext}} = A_\mu^{\text{ext}}(\mathbf{x})$, yields the time-integration

$$\int_{-\infty}^{\infty} dt e^{-\gamma|t|} e^{-it(E_a - E_b)} = 2\pi \Delta_\gamma(E_a - E_b). \quad (2.32)$$

Taking the limit, $\gamma \rightarrow 0$, leads to energy conservation

$$\lim_{\gamma \rightarrow 0} \pi \gamma \Delta_\gamma(E_a - E_b) = \delta(E_a, E_b), \quad (2.33)$$

as a consequence of the time-independence of the external potential. The first-order energy can now be written as

$$\Delta E^1 = -e \delta(E_a, E_b) \int d^3\mathbf{x} \Phi_b^\dagger(\mathbf{x}) \alpha^\mu A_\mu^{\text{ext}}(\mathbf{x}) \Phi_a(\mathbf{x}). \quad (2.34)$$

We will now discuss the two different external potentials which are treated in this work and we start with the case of a static homogeneous magnetic field.

2.2.1 Magnetic field interaction

For the Zeeman effect calculation we have the vector potential

$$\mathbf{A}^{\text{mag}}(\mathbf{r}) = -\frac{1}{2}\mathbf{r} \times \mathbf{B}, \quad (2.35)$$

where \mathbf{B} is the external homogeneous magnetic field. This potential transforms into the gradient of a delta function

$$\mathbf{r} \rightarrow -i\nabla_{\mathbf{q}}\delta^3(\mathbf{q}), \quad (2.36)$$

when going over to momentum space. We choose to represent this highly singular function by introducing a Gaussian cut-off function in coordinate space

$$\mathbf{r} \rightarrow \lim_{\rho \rightarrow 0} \mathbf{r} e^{-\left(\frac{\rho\mathbf{r}}{2}\right)^2}, \quad (2.37)$$

which yields the momentum transform

$$\mathbf{A}^{\text{mag}}(\mathbf{q}) = \frac{i}{\pi^{3/2}\rho^5} e^{-(q/\rho)^2} \mathbf{q} \times \mathbf{B}, \quad (2.38)$$

as is shown in Appendix B. Eventually, the limit $\rho \rightarrow 0$ should be taken, but in practice it is enough to have a small finite value of ρ so that the introduced inhomogeneity in the magnetic field is negligible over the extension of the ion.

2.2.2 Hyperfine interaction

In the magnetic point-dipole approximation, the nuclear vector potential is given by

$$\mathbf{A}^{\text{hfs}}(\mathbf{r}) = \frac{1}{4\pi} \frac{\boldsymbol{\mu} \times \mathbf{r}}{r^3} = \frac{g_I \mu_N}{4\pi} \frac{\mathbf{I} \times \mathbf{r}}{r^3}, \quad (2.39)$$

where $\boldsymbol{\mu}$ is the nuclear magnetic moment, g_I is the nuclear g factor, μ_N denotes the nuclear magneton and \mathbf{I} is the nuclear spin operator. The transformation to momentum space yields the expression

$$\mathbf{A}^{\text{hfs}}(\mathbf{q}) = \frac{-i}{(2\pi)^3} \frac{\boldsymbol{\mu} \times \mathbf{q}}{q^2}. \quad (2.40)$$

In this thesis we want further to study how the radiative corrections are affected by using an extended nuclear magnetization. To achieve this in a straightforward manner we have adopted a model for the magnetic moment distribution suggested by Finkbeiner *et al.* [12]. In this model a spherically symmetric distribution is assumed for the nuclear magnetic moment $\mathbf{M}(R) = \boldsymbol{\mu} w(R)$. The density function is given by $w(R) = k_n R^n$ for the interior of the nucleus and $w(R) = 0$ for the outside of the nucleus, n is the model parameter and k_n normalizes the distribution to the experimental magnetic moment. The hyperfine potential is then modified to read

$$\mathbf{A}^{\text{hfs},n}(\mathbf{r}) = \frac{1}{4\pi} \frac{\boldsymbol{\mu} \times \mathbf{r}}{r^3} V_n(r), \quad (2.41)$$

where

$$\begin{aligned} V_n(r) &= \left(\frac{r}{R_0}\right)^{n+3}, \quad r \leq R_0 \\ V_n(r) &= 1, \quad r > R_0 \end{aligned} \quad (2.42)$$

and where R_0 is the nuclear radius. With this parameterization we can consider different magnetic moment distributions, ranging from a homogeneous distribution ($n = 0$) up to the shell model ($n = \infty$) where the magnetic moment is located at the nuclear surface. The corresponding expression in momentum space can be evaluated as the sum

$$A^{\text{hfs},n}(\mathbf{q}) = \frac{-i}{(2\pi)^3} \frac{\boldsymbol{\mu} \times \mathbf{q}}{q} \left\{ \frac{1}{q} + \int_0^{R_0} dr j_1(qr) [V_n(r) - 1] \right\}, \quad (2.43)$$

such that the last term gives directly the extended magnetization correction (the Bohr-Weisskopf effect).

For the bismuth hyperfine calculation we have further employed the dynamical proton model (DPM) of Labzowsky *et al.* [13]. In this model the valence proton of the bismuth nucleus is treated as a Dirac particle bound in the Woods-Saxon potential of the lead core. The first-order hyperfine splitting is then given as a vector-photon exchange between the electron and the proton and the potential is given by

$$A_i^{\text{hfs,dpm}}(\mathbf{r}) = e \int d^3\mathbf{R} D_{i\nu}^F(\mathbf{r} - \mathbf{R}, 0) \Psi_N^\dagger(\mathbf{R}) \alpha^\nu \Psi_N(\mathbf{R}), \quad (2.44)$$

where Ψ_N is the proton wavefunction. The Fourier transform of this potential is very similar to the Breit potential for the inter-electronic case and is given in Eq. (B.35) of Appendix B.

3 Electron Self-Energy Corrections

In the previous chapter we considered the lowest-order processes which contribute to the physical effects studied in this thesis. We will now go on and study the one-photon radiative corrections to these first-order interactions. In this chapter the self-energy corrections are discussed and the vacuum polarization effects will be considered in Chapter 4. Taking these effects into account we expect corrections of the order α to the lowest-order result. However, when calculating radiative effects (not only one-photon) we encounter divergent integrals. This problem, which plagued the early development of QED, is resolved by renormalizing the mass and charge of the electron. A discussion of the basic principles of renormalization can be found in Appendix C, from which we will take some results when necessary. The renormalization technique enables us to extract the well-defined finite parts which yield detectable radiative corrections. To accomplish the renormalization explicitly, the divergent expressions have to be regularized such that the divergent and finite parts can be separated. We will here utilize the concept of dimensional regularization and the regularized expressions for the free-electron self-energy and vertex operators are derived in Appendix D.

The electron self-energy is the dominating QED correction, and also the most difficult to calculate. There is no unique scheme for evaluating the self-energy effects, and several procedures have been developed and employed using various kinds of divisions and regularizations during history [14–36]. Our calculation scheme is based on a generalization of the work of Snyderman [36], and a rigorous treatment of the self-energy corrections in external potentials is accomplished.

It is advantageous to start with a discussion of the Coulomb self-energy, i.e., in the presence of the nuclear Coulomb potential only — which we will also refer to as the first-order self-energy. Useful results are derived and our general approach for isolating the divergent parts and dividing up the calculation is introduced.

3.1 First-order self-energy

The renormalized first-order bound-state self-energy is shown in Fig. 3.1. From the Feynman diagram for the electron self-energy loop the *mass counterterm* δm is subtracted. The divergences inherent in the bound electron self-energy can be isolated by expanding in the background binding potential V . This is pictured in Fig. 3.2, where the self-energy is decomposed into a zero-potential term (zp), a one-potential term (op) and finally a many-potential term (mp). The first two terms in the expansion are divergent while the many-potential term is finite. This decomposition enables us to use the results for the free electron self-energy and vertex operators, derived in Appendices C and D.

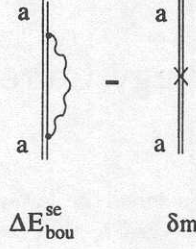


Figure 3.1: *The first-order bound-state self-energy.*

The energy contribution from the bound first-order self-energy is given by

$$\begin{aligned} \Delta E_{\text{ren}}^{\text{se}} &= \Delta E_{\text{bou}}^{\text{se}} - \langle a | \gamma^0 \delta m | a \rangle \\ &= \int d^3 \mathbf{x} \int d^3 \mathbf{y} \Phi_a^\dagger(\mathbf{x}) \Sigma^{\text{bou}}(\mathbf{x}, \mathbf{y}, E_a) \Phi_a(\mathbf{y}) - \delta m \int d^3 \mathbf{x} \Phi_a^\dagger(\mathbf{x}) \gamma^0 \Phi_a(\mathbf{x}), \end{aligned} \quad (3.1)$$

where we have defined the bound self-energy operator, Σ^{bou} , by

$$\Sigma^{\text{bou}}(\mathbf{x}, \mathbf{y}, E_a) = 4\pi i \alpha \int_{-\infty}^{\infty} \frac{dz}{2\pi} \alpha^\mu D_{\mu\nu}^F(\mathbf{x} - \mathbf{y}, z) S_F^{\text{bou}}(\mathbf{x}, \mathbf{y}, E_a - z) \alpha^\nu. \quad (3.2)$$

The bound electron propagator can be written as

$$\begin{aligned} S_F^{\text{bou}}(\mathbf{x}, \mathbf{y}, z) &= \sum_u \frac{\Phi_u(\mathbf{x}) \Phi_u^\dagger(\mathbf{y})}{z - E_u(1 - i\eta)} = \langle \mathbf{x} | \frac{1}{z - \hat{h}_{\text{bou}}(1 - i\eta)} | \mathbf{y} \rangle \\ &= \langle \mathbf{x} | \frac{1}{z - (\hat{h}_{\text{free}} + V)(1 - i\eta)} | \mathbf{y} \rangle, \end{aligned} \quad (3.3)$$

where \hat{h}_{bou} (\hat{h}_{free}) denotes the bound (free) Dirac Hamiltonian operator. Proceeding by using the identity

$$\begin{aligned} \frac{1}{z - \hat{h}_{\text{bou}}(1 - i\eta)} &= \frac{1}{z - \hat{h}_{\text{free}}(1 - i\eta)} + \frac{1}{z - \hat{h}_{\text{free}}(1 - i\eta)} V \frac{1}{z - \hat{h}_{\text{free}}(1 - i\eta)} \\ &+ \frac{1}{z - \hat{h}_{\text{free}}(1 - i\eta)} V \frac{1}{z - \hat{h}_{\text{bou}}(1 - i\eta)} V \frac{1}{z - \hat{h}_{\text{free}}(1 - i\eta)}, \end{aligned} \quad (3.4)$$

we obtain the following expansion of the electron propagator

$$\begin{aligned} S_F^{\text{bou}}(\mathbf{x}, \mathbf{y}, z) &= S_F^{\text{free}}(\mathbf{x}, \mathbf{y}, z) + \int d^3 \mathbf{x}_1 S_F^{\text{free}}(\mathbf{x}, \mathbf{x}_1, z) V(\mathbf{x}_1) S_F^{\text{free}}(\mathbf{x}_1, \mathbf{y}, z) \\ &+ \int d^3 \mathbf{x}_1 d^3 \mathbf{x}_2 S_F^{\text{free}}(\mathbf{x}, \mathbf{x}_1, z) V(\mathbf{x}_1) S_F^{\text{bou}}(\mathbf{x}_1, \mathbf{x}_2, z) V(\mathbf{x}_2) S_F^{\text{free}}(\mathbf{x}_2, \mathbf{y}, z). \end{aligned} \quad (3.5)$$

These three terms corresponds to, when inserted in the expression for Σ^{bou} , the zero-, one- and many-potential terms in Fig. 3.2. Consequently, we can write the energy contribution as

$$\Delta E_{\text{ren}}^{\text{se}} = \Delta E_{\text{zp}}^{\text{se}} + \Delta E_{\text{op}}^{\text{se}} + \Delta E_{\text{mp}}^{\text{se}} - \langle a | \gamma^0 \delta m | a \rangle. \quad (3.6)$$

$$\Delta E_{\text{bou}}^{\text{se}} - \delta m = \Delta E_{\text{zp}}^{\text{se}} = F1 + Q + \delta m + \Delta E_{\text{op}}^{\text{se}} = F2 - Q + \Delta E_{\text{mp}}^{\text{se}} - \delta m$$

Figure 3.2: The renormalized bound-state self-energy $\Delta E_{\text{ren}}^{\text{se}}$ decomposed into a zero-potential term $\Delta E_{\text{zp}}^{\text{se}}$, a one-potential term $\Delta E_{\text{op}}^{\text{se}}$ and a many-potential term $\Delta E_{\text{mp}}^{\text{se}}$. $F1$ and $F2$ are the finite parts of the zero- and one-potential terms, δm is the mass counterterm and Q the charge divergence. The single lines indicate the free-electron propagator.

The zero-potential term is just the expectation value of the free-electron self-energy operator

$$\Delta E_{\text{zp}}^{\text{se}} = \langle a | \gamma^0 \Sigma^{\text{free}} | a \rangle, \quad (3.7)$$

for which the mass divergent piece cancels against the mass counterterm. The γ^0 matrix appears here since we base our definition of the electron propagator on Ψ^\dagger rather than $\bar{\Psi} = \Psi^\dagger \gamma^0$, which is the standard definition (see Appendix A).

The one-potential term is obtained from the second term of Eq. (3.5), and corresponds to the matrix element of the free-electron vertex operator

$$\Delta E_{\text{op}}^{\text{se}} = -\langle a | \gamma^0 \Lambda_\mu^{\text{free}} e A^\mu | a \rangle, \quad (3.8)$$

with $V = -e \alpha_\mu A^\mu$. By using the last term of Eq. (3.5) we can similarly obtain the finite many-potential part.

To exploit the renormalization structure we transform the divergent parts to momentum space and by using the expansions (see Appendix C)

$$\Sigma^{\text{free}}(p) = \delta m + (\not{p} - m)(Z_2 - 1) + \Sigma^{\text{ren}}(p) \quad (3.9)$$

and

$$\Lambda_\mu^{\text{free}}(p, p') = \gamma_\mu(1 - Z_2) + \Lambda_\mu^{\text{ren}}(p, p'), \quad (3.10)$$

we can write

$$\begin{aligned} & \Delta E_{\text{zp}}^{\text{se}} + \Delta E_{\text{op}}^{\text{se}} - \langle a | \gamma^0 \delta m | a \rangle = \\ & = \int d^3 \mathbf{p} \Phi_a^\dagger(\mathbf{p}) \gamma^0 [\delta m + (\not{p} - m)(Z_2 - 1) + \Sigma^{\text{ren}}(p)] \Phi_a(\mathbf{p}) \\ & \quad - e \int d^3 \mathbf{p} \int d^3 \mathbf{p}' \Phi_a^\dagger(\mathbf{p}) \gamma^0 [\gamma_\mu(1 - Z_2) + \Lambda_\mu^{\text{ren}}(p, p')] A^\mu(\mathbf{p}, \mathbf{p}') \Phi_a(\mathbf{p}') \\ & \quad - \int d^3 \mathbf{p} \Phi_a^\dagger(\mathbf{p}) \gamma^0 \delta m \Phi_a(\mathbf{p}). \end{aligned} \quad (3.11)$$

Here we can see the explicit cancellation of δm between the zero-potential part and the mass counterterm. If we further use the Fourier transformed Dirac equation

$$(\not{p} - m)\Phi_a(\mathbf{p}) = -e \int d^3\mathbf{p}' \gamma_\mu A^\mu(\mathbf{p}, \mathbf{p}')\Phi_a(\mathbf{p}'), \quad (3.12)$$

on the term involving Z_2 in the zero-potential part, it follows that the charge divergent terms cancel (see Appendix C).

The energy shift due to the renormalized bound state self-energy is thus given by

$$\begin{aligned} \Delta E_{\text{ren}}^{\text{se}} &= \Delta E_{\text{mp}}^{\text{se}} + \int d^3\mathbf{p} \Phi_a^\dagger(\mathbf{p}) \gamma^0 \Sigma^{\text{ren}}(p) \Phi_a(\mathbf{p}) \\ &\quad - e \int d^3\mathbf{p} \int d^3\mathbf{p}' \Phi_a^\dagger(\mathbf{p}) \gamma^0 \Lambda_\mu^{\text{ren}}(p, p') A^\mu(\mathbf{p}, \mathbf{p}') \Phi_a(\mathbf{p}'). \end{aligned} \quad (3.13)$$

The ultraviolet finite parts of the zero- and one-potential terms, $\Sigma^{\text{ren}}(p)$ and $\Lambda_\mu^{\text{ren}}(p, p')$, can be shown to be separately infrared divergent (see next section), but in the sum the divergences cancel. This is for the Feynman gauge used here, but in the Fried-Yennie gauge all terms are infrared finite [36]. The contribution from the finite many-potential part $\Delta E_{\text{mp}}^{\text{se}}$ can be calculated directly from the expression obtained by the expansion Eq. (3.5) [35, 36]. Another possibility is to employ the subtraction scheme (see Fig. 3.2)

$$\Delta E_{\text{mp}}^{\text{se}} = \Delta E_{\text{bou}}^{\text{se}} - \Delta E_{\text{zp}}^{\text{se}} - \Delta E_{\text{op}}^{\text{se}}, \quad (3.14)$$

i.e., the unrenormalized zero- and one-potential terms are subtracted from the unrenormalized bound main term. Since each term is divergent in the integral over photon momentum, the subtraction is performed before the integration. We will adopt this latter procedure in the following.

Equation (3.13) expresses the self-energy in terms of matrix elements of renormalized operators. The remaining problem is now to find explicit forms of these operators, a subject which we will consider in the next section (and in Appendix D). Another approach is to evaluate $\Delta E_{\text{ren}}^{\text{se}}$ directly as the difference between the unrenormalized bound term and the mass counterterm, as it is expressed in Eq. (3.1). This procedure can be described as renormalizing the energy expression, in contrast to renormalizing the operators within that expression. Since both terms in Eq. (3.1) are divergent some regularization scheme has to be applied before the difference is taken. In the *partial-wave renormalization* (PWR) method, which was developed by Lindgren, Persson and Salomonson [33, 34] and by Quiney and Grant [37], the regularization is accomplished by expanding the photon propagator in spherical waves. The originally divergent integral over photon momentum is thereby convergent for each partial wave, and the divergence is moved to the sum over partial waves. By taking the difference between the bound term and the mass term for each partial wave, the resulting partial wave sum is convergent. PWR is discussed thoroughly in Ref. [38] and we will not go into details here. This method works well for the first-order self-energy but in the presence of an external field one

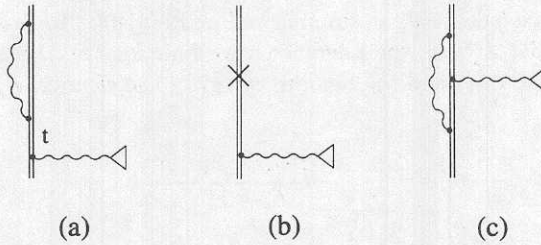


Figure 3.3: *The one-photon self-energy corrections. (a) the external line self-energy correction, (b) the corresponding mass counterterm, and (c) the vertex correction.*

has to correct for the non-covariance of PWR. Such an analysis shows that the regularization correction terms cancel in a Coulomb field but gives finite corrections in a magnetic field, see Paper V.

3.2 Self-energy corrections in external potentials

We are now ready to deal with the self-energy corrections to the interaction with an external potential. In doing so we can make extensive use of the methods and results derived in the preceding section. The Feynman diagrams for the one-photon self-energy corrections are shown in Fig. 3.3. These contain various kinds of singularities and divergences, and we will start the discussion with a brief overview of how these difficulties are treated.

The first diagram (a), obtained by inserting a self-energy loop on the outgoing electron line, contains both a reducible as well as an irreducible part. The reducible term originates from the intermediate states $|t\rangle$, which are degenerate with the reference state $|a\rangle$. The singularity associated with the degeneracy is cancelled by subtracting away the corresponding counterparts, as prescribed by Sucher's formula Eq. (A.60). There is also a remainder which is called, for reasons that will be made clear below, the *binding-energy correction* (be). This correction is both infrared and ultraviolet divergent but the divergences cancel between this diagram and the *vertex correction* (ve), diagram (c). Finally, we have the irreducible part of diagram (a) which is called the *wavefunction correction* (wf). This part is mass divergent and we thus have to subtract the corresponding mass counterterm, diagram (b). Note that the binding-energy correction needs no mass renormalization, since it contains only a charge divergent piece.

The expressions for the one-photon self-energy corrections can be derived in a formal way, using the S-matrix formalism discussed in Appendix A. Such a derivation of the binding-energy correction is presented in Appendix E. A somewhat different approach based on the two-time Green function method is presented in Ref. [39].

An alternative way of deriving the corrections in the presence of an external potential, which gives expressions identical to those derived from Sucher's formula Eq. (A.60), is to perturb the first-order Coulomb self-energy Eq. (3.1)

with the external potential, as summarized in Ref. [40]. To first-order in the external potential $A_\mu^{\text{ext}}(\mathbf{r})$, the reference wave function $|a\rangle$, the propagator for the bound electron S_F , and the binding energy of the electron E_a are modified as follows

$$\begin{aligned} |a\rangle &\rightarrow |a\rangle - \sum_{E_t \neq E_a} \frac{|t\rangle \langle t| e\alpha^\mu A_\mu^{\text{ext}}(\mathbf{r}) |a\rangle}{E_a - E_t} + \dots \\ &= |a\rangle + |\delta a\rangle + \dots, \end{aligned} \quad (3.15)$$

$$\begin{aligned} S_F(\mathbf{x}_2, \mathbf{x}_1, z) &\rightarrow S_F(\mathbf{x}_2, \mathbf{x}_1, z) \\ &\quad - \int d^3\mathbf{x}_3 S_F(\mathbf{x}_2, \mathbf{x}_3, z) e\alpha^\mu A_\mu^{\text{ext}}(\mathbf{x}_3) S_F(\mathbf{x}_3, \mathbf{x}_1, z) + \dots, \end{aligned} \quad (3.16)$$

$$\begin{aligned} E_a &\rightarrow E_a - \langle a| e\alpha^\mu A_\mu^{\text{ext}}(\mathbf{r}) |a\rangle + \dots \\ &= E_a + \Delta E_a^1 + \dots. \end{aligned} \quad (3.17)$$

The wavefunction modification term, originating from the replacement given in Eq. (3.15), takes the form

$$\begin{aligned} \Delta E_{\text{se}}^{\text{wf}} &= - \sum_{E_t \neq E_a} \frac{\langle a| (\Sigma^{\text{bou}} - \delta m) |t\rangle \langle t| e\alpha^\mu A_\mu^{\text{ext}} |a\rangle}{E_a - E_t} \\ &= \langle a| (\Sigma^{\text{bou}} - \delta m) |\delta a\rangle, \end{aligned} \quad (3.18)$$

where $|\delta a\rangle$ is the external field perturbed wavefunction.

The modification of the propagator in Eq. (3.16), leads to the vertex correction

$$\Delta E_{\text{se}}^{\text{vc}} = -\langle a| e\Lambda_{\text{bou}}^\mu A_\mu^{\text{ext}} |a\rangle, \quad (3.19)$$

where Λ_{bou}^μ is the bound vertex function. For the binding-energy term, replace ment Eq. (3.17), the formula reads as follows

$$\begin{aligned} \Delta E_{\text{se}}^{\text{be}} &= -\langle a| e\alpha^\mu A_\mu^{\text{ext}} |a\rangle \times \langle a| \left[\frac{\partial}{\partial E} \Sigma^{\text{bou}}(E) \right]_{E=E_a} |a\rangle \\ &= \Delta E_a^1 \times \langle a| \left[\frac{\partial}{\partial E} \Sigma^{\text{bou}}(E) \right]_{E=E_a} |a\rangle, \end{aligned} \quad (3.20)$$

where ΔE_a^1 is the first-order energy in the external potential. Note that the mass counterterm is absent since it does not depend on E_a .

To handle the divergences present in these three terms, we expand the bound self-energy and vertex operators in the nuclear Coulomb potential. The mass- and charge-divergences will then be isolated in the lowest-order terms and can be cancelled analytically between different diagrams. This procedure is done working in momentum space and using dimensional regularization for the divergent integrals. The finite higher-order terms are then calculated in coordinate-space

by taking the difference between the full unrenormalized expression and the divergent parts in the expansion, similarly as for the first-order self-energy (Eq. (3.14)).

We start here with considering the free-electron self-energy and vertex operators using dimensional regularization. These expressions will be used later when discussing the calculation of the three different contributions. Note that in the expressions for $\Sigma(p)$ and $\Lambda_\mu(p, p')$, the notations p (k) denotes the four-momentum, whereas it indicates the absolute values $p = |\mathbf{p}|$ ($k = |\mathbf{k}|$) elsewhere in this work.

From Appendix D we have the mass renormalized self-energy operator in dimensional regularization

$$\begin{aligned}\Sigma_{\text{ren}}^{\text{mass}}(p) &= \Sigma(p) - \delta m \\ &= -\frac{\alpha}{4\pi} \left\{ (\not{p} - m) \left[\Delta + 2 + \frac{\rho}{1-\rho} \left(1 + \frac{2-\rho}{1-\rho} \ln \rho \right) \right] \right. \\ &\quad \left. + \frac{m\rho}{1-\rho} \left(1 - \frac{2-3\rho}{1-\rho} \ln \rho \right) \right\} .\end{aligned}\quad (3.21)$$

Here $\Delta = 2/\epsilon - \gamma_E + \ln 4\pi$ is the ultraviolet part of the charge renormalization constant after dimensional regularization, ϵ is the dimensional regularization parameter and γ_E is Euler's constant. We have further introduced the dimensionless variable

$$\rho = \frac{m^2 - E^2 + \mathbf{p}^2}{m^2} = -\frac{(\not{p} - m)(\not{p} + m)}{m^2}, \quad (3.22)$$

which is positive definite for a bound electron. Equation (3.21) is mass renormalized but still contains the charge divergence. The charge renormalization constant can be extracted from (Eq. (C.18))

$$Z_2 - 1 = \left. \frac{\partial \Sigma(p)}{\partial \not{p}} \right|_{\not{p}=m}, \quad (3.23)$$

which yields

$$Z_2 - 1 = -\frac{\alpha}{4\pi} [\Delta + 4 + 4 \ln \rho] \Big|_{\rho \rightarrow 0}. \quad (3.24)$$

The logarithmic term represents the infrared divergence of the charge renormalization constant. Thus, even though the expression for $\Sigma_{\text{ren}}^{\text{mass}}(p)$ is infrared finite, extracting the full charge renormalization constant will introduce infrared divergences. The same is also true for the vertex operator and it is therefore sufficient to cancel the ultraviolet divergency Δ , which vanishes due to Ward's identity, between these two operators to obtain finite expressions.

Taking into account the energy dependence of ρ , the derivative of the free self-energy operator with respect to the energy is given by

$$\begin{aligned} \frac{\partial \Sigma(p)}{\partial E} = & -\frac{\alpha}{4\pi} \left\{ \gamma_0 \left[\Delta + 2 + \frac{\rho}{1-\rho} \left(1 + \frac{2-\rho}{1-\rho} \ln \rho \right) \right] \right. \\ & + \frac{\not{p}}{m^2} \left[-\frac{2E}{(1-\rho)^2} \left(3 - \rho + \frac{2}{1-\rho} \ln \rho \right) \right] \\ & \left. + \frac{8E}{m(1-\rho)} \left[1 + \frac{1}{1-\rho} \ln \rho \right] \right\}. \end{aligned} \quad (3.25)$$

Note that there are misprints in the corresponding expression in Ref. [36] (Eq. (5.43) in that paper). The expression (3.25) is free from the mass divergence, since δm is a constant which vanishes in the differentiation. This operator is needed for the computation of the free-electron part of the binding-energy correction.

Finally, from Appendix D we get the free electron vertex operator

$$\begin{aligned} \Lambda_\mu(p, p') = & \frac{\alpha}{4\pi} \left\{ \gamma_\mu \left[4C_{24} - 2 + 2m^2 C_0 - 4p \cdot p' (C_0 + C_{11} + C_{12} + C_{23}) \right. \right. \\ & \left. \left. - 2p^2 (C_{11} + C_{21}) - 2p'^2 (C_{12} + C_{22}) \right] \right. \\ & + \not{p} p_\mu [4(C_{11} + C_{21})] \\ & + \not{p}' p'_\mu [4(C_0 + C_{11} + C_{12} + C_{23})] \\ & + \not{p}' p'_\mu [4(C_0 + C_{11} + C_{12} + C_{23})] \\ & + \not{p}' p'_\mu [4(C_{12} + C_{22})] \\ & - \not{p} \gamma_\mu \not{p}' [2(C_0 + C_{11} + C_{12})] \\ & - p_\mu [4m(C_0 + 2C_{11})] \\ & \left. \left. - p'_\mu [4m(C_0 + 2C_{12})] \right\}, \end{aligned} \quad (3.26)$$

where the coefficient functions C_{ij} are functions of p , p' and are given by Feynman parameter integrals. Here, the ultraviolet divergency Δ is contained in C_{24} , which is the only divergent coefficient function. For later convenience we also write down the explicit form of the zeroth component of the vertex function

$$\begin{aligned} \Lambda_0(p, p') = & \frac{\alpha}{4\pi} \left\{ \gamma_0 \left[4C_{24} - 2 + 2m^2 C_0 - 4p \cdot p' (C_0 + C_{11} + C_{12} + C_{23}) \right. \right. \\ & \left. \left. - 2p^2 (C_{11} + C_{21}) - 2p'^2 (C_{12} + C_{22}) \right] \right. \\ & + \not{p} E [4(C_0 + 2C_{11} + C_{12} + C_{21} + C_{23})] \\ & + \not{p}' E [4(C_0 + C_{11} + 2C_{12} + C_{22} + C_{23})] \\ & - \not{p} \gamma_0 \not{p}' [2(C_0 + C_{11} + C_{12})] \\ & \left. \left. - 8mE [C_0 + C_{11} + C_{12}] \right\}, \end{aligned} \quad (3.27)$$

where we have used $p_0 = p'_0 = E$, which is valid for all potentials considered in this work.

As previously mentioned it is appropriate to organize the different terms into two different sub-groups: (1) wavefunction correction and (2) vertex plus binding-energy corrections, depending on the structure of the divergences in the diagrams.

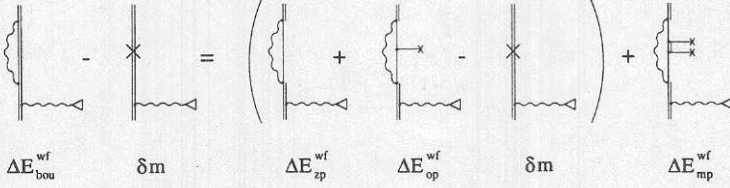


Figure 3.4: *Feynman graphs representing the wavefunction correction. In order to isolate divergences, the internal self-energy electron propagator is expanded in the nuclear Coulomb potential which is denoted by a horizontal line with a cross. The divergent zero-potential, one-potential and the mass-counter term are grouped together. The remaining many-potential term is finite.*

3.2.1 Wavefunction correction

The structure of divergences in the wavefunction correction is the same as for the first-order self-energy. We can therefore isolate and subtract the divergences by means of a potential expansion (Eq. (3.4)) of the self-energy operator into a free self-energy operator (zp), a one-potential term (op) and a finite many-potential part (mp), see Fig. 3.4. The many-potential part is treated in coordinate space while the zero- and one-potential terms are calculated in momentum space. The wavefunction correction is thus separated as follows

$$\begin{aligned} \Delta E_{se}^{wf} &= \langle a | (\Sigma^{\text{bou}} - \delta m) | \delta a \rangle \\ &= \langle a | \gamma^0 \Sigma_{\text{ren}}^{\text{mass}}(p) | \delta a \rangle + \langle a | \gamma^0 \Lambda_0(p, p') V_{\text{nuc}}(\mathbf{p}, \mathbf{p}') | \delta a \rangle + \Delta E_{\text{mp}}^{wf}, \end{aligned} \quad (3.28)$$

where $V_{\text{nuc}}(\mathbf{p}, \mathbf{p}')$ is the nuclear Coulomb potential, $\Sigma_{\text{ren}}^{\text{mass}}(p)$ is given by Eq. (3.21) and $\Lambda_0(p, p')$ is the zeroth component of the vertex function Eq. (3.27). We will in the following consider the ket-state as the perturbed wavefunction, but there is of course also a symmetrical diagram where instead the bra-state is perturbed by the external potential. For the electron-electron interaction we must further consider the self-energy loop inserted on both electrons.

The ultraviolet divergence Δ cancels between the zero- and one-potential terms in the same way as for the first-order self-energy. In the following discussion it is therefore implicitly assumed that the terms proportional to Δ is omitted.

Zero-potential term

To discuss the calculation of the zero-potential part we first separate the tensor structure by writing $\Sigma_{\text{ren}}^{\text{mass}}(p) = a(\rho) + \not{p} b(\rho)$, which yields

$$\begin{aligned} \Delta E_{\text{zp}}^{wf} &= \langle a | \gamma^0 \Sigma_{\text{ren}}^{\text{mass}}(p) | \delta a \rangle \\ &= \int d^3 \mathbf{p} \Phi_a^\dagger(\mathbf{p}) \gamma^0 [a(\rho) + \not{p} b(\rho)] \Phi_{\delta a}(\mathbf{p}), \end{aligned} \quad (3.29)$$

where

$$\begin{aligned} a(\rho) &= \frac{\alpha}{4\pi} 2m \left[1 + 2 \frac{\rho}{1-\rho} \ln \rho \right], \\ b(\rho) &= -\frac{\alpha}{4\pi} \left[2 + \frac{\rho}{1-\rho} \left(1 + \frac{2-\rho}{1-\rho} \ln \rho \right) \right]. \end{aligned} \quad (3.30)$$

For the a -part, which is diagonal, the angular integrations can be done straightforwardly giving

$$A(p) = \int d\Omega \Phi_a^\dagger(\mathbf{p}) \gamma^0 \Phi_{\delta a}(\mathbf{p}) = P_a(p) P_{\delta a}(p) - Q_a(p) Q_{\delta a}(p). \quad (3.31)$$

For the b -term we use the explicit form

$$\not{p} = \begin{pmatrix} E & -\boldsymbol{\sigma} \cdot \mathbf{p} \\ \boldsymbol{\sigma} \cdot \mathbf{p} & -E \end{pmatrix}, \quad (3.32)$$

together with the identity $\boldsymbol{\sigma} \cdot \mathbf{p} \chi_\kappa^m(\hat{p}) = -p \chi_{-\kappa}^m(\hat{p})$, to obtain

$$\begin{aligned} B(p) &= \int d\Omega \Phi_a^\dagger(\mathbf{p}) \gamma^0 \not{p} \Phi_{\delta a}(\mathbf{p}) \\ &= E_a [P_a(p) P_{\delta a}(p) + Q_a(p) Q_{\delta a}(p)] \\ &\quad + p [P_a(p) Q_{\delta a}(p) + P_{\delta a}(p) Q_a(p)]. \end{aligned} \quad (3.33)$$

We are finally left with the radial integral

$$\Delta E_{zp}^{\text{wf}} = \int dp p^2 [A(p)a(\rho) + B(p)b(\rho)]. \quad (3.34)$$

One-potential term

The one-potential part is given by

$$\begin{aligned} \Delta E_{\text{op}}^{\text{wf}} &= \langle a | \gamma^0 \Lambda_0(p, p') V_{\text{nuc}}(\mathbf{p}, \mathbf{p}') | \delta a \rangle \\ &= \int d^3\mathbf{p} d^3\mathbf{p}' \Phi_a^\dagger(\mathbf{p}) \gamma^0 [\gamma_0 f_1(p, p', \cos \vartheta) + \not{p} f_2(p, p', \cos \vartheta) \\ &\quad + \not{p}' f_3(p, p', \cos \vartheta) + \not{p} \gamma_0 \not{p}' f_4(p, p', \cos \vartheta) \\ &\quad + f_5(p, p', \cos \vartheta)] V_{\text{nuc}}(\mathbf{p}, \mathbf{p}') \Phi_{\delta a}(\mathbf{p}'), \end{aligned} \quad (3.35)$$

where ϑ is the angle between \mathbf{p} and \mathbf{p}' , and where the f_i -functions are abbreviations for the coefficient functions in Eq. (3.27). The angular dependence of the wavefunctions can be reduced to a dependence on the intermediate angle by utilizing the identity

$$\frac{1}{2j+1} \sum_{m=-j}^j \chi_\kappa^{m\dagger}(\hat{p}) \chi_\kappa^m(\hat{p}') = \frac{1}{4\pi} P_{|\kappa+1/2|-1/2}(\cos \vartheta), \quad (3.36)$$

where $P_{|\kappa+1/2|-1/2}(\cos \vartheta)$ is a Legendre polynomial. Performing the matrix multiplication and using this identity we obtain for the 1s-state

$$\begin{aligned}
4\pi\Phi_a^\dagger(\mathbf{p})\gamma^0\Lambda_0(p,p')\Phi_{\delta a}(\mathbf{p}') &= f_1 [PP' + QQ' \cos \vartheta] \\
&+ f_2 [EPP' + pQP' + (pPQ' + EQQ') \cos \vartheta] \\
&+ f_3 [EPP' + p'PQ' + (p'QP' + EQQ') \cos \vartheta] \\
&+ f_4 [E^2PP' + pEQP' + p'EPQ' + pp'QQ' + \\
&\quad (pp'PP' + pEPQ' + p'EQP' + E^2QQ') \cos \vartheta] \\
&+ f_5 [PP' - QQ' \cos \vartheta] ,
\end{aligned} \tag{3.37}$$

where $P = P_a(p)$ and $P' = P_{\delta a}(p')$ and similarly for Q . The expression for the one-potential part is thus reduced to a three-dimensional integral over p , p' and $\cos \vartheta$.

Many-potential term

The many-potential part is convergent and is calculated from the expression

$$\Delta E_{\text{mp}}^{\text{wf}} = \Delta E_{\text{bou}}^{\text{wf}} - \Delta E_{\text{zp}}^{\text{wf}} - \Delta E_{\text{op}}^{\text{wf}} , \tag{3.38}$$

where all terms at the right are unrenormalized. Starting from Eqs. (3.1) and (3.2) we can write for the bound main term

$$\begin{aligned}
\Delta E_{\text{bou}}^{\text{wf}} &= \langle a | \Sigma^{\text{bou}} | \delta a \rangle \\
&= 4\pi i \alpha \int d^3 \mathbf{x}_1 \int d^3 \mathbf{x}_2 \int_{-\infty}^{\infty} \frac{dz}{2\pi} \\
&\quad \times \Phi_a^\dagger(\mathbf{x}_1) \alpha^\mu D_{\mu\nu}^F(\mathbf{x}_1 - \mathbf{x}_2, z) S_F(\mathbf{x}_1, \mathbf{x}_2, E_a - z) \alpha^\nu \Phi_{\delta a}(\mathbf{x}_2) \\
&= -4\pi i \alpha \int d^3 \mathbf{x}_1 \int d^3 \mathbf{x}_2 \int \frac{d^3 \mathbf{k}}{(2\pi)^3} \int_{-\infty}^{\infty} \frac{dz}{2\pi} \\
&\quad \times \sum_n \frac{\Phi_a^\dagger(\mathbf{x}_1) \alpha^\mu e^{i\mathbf{k}\cdot\mathbf{x}_1} \Phi_n(\mathbf{x}_1) \Phi_n^\dagger(\mathbf{x}_2) e^{-i\mathbf{k}\cdot\mathbf{x}_2} \alpha_\mu \Phi_{\delta a}(\mathbf{x}_2)}{[z^2 - \mathbf{k}^2 + i\delta][E_a - z - E_n(1 - i\eta)]} .
\end{aligned} \tag{3.39}$$

The z -integration gives

$$\int_{-\infty}^{\infty} \frac{dz}{2\pi} \frac{1}{[z^2 - \mathbf{k}^2 + i\delta][E_a - z - E_n(1 - i\eta)]} = -\frac{i}{2k[E_a - E_n - \text{sign}(E_n)k]} , \tag{3.40}$$

which leads to

$$\begin{aligned}
\Delta E_{\text{bou}}^{\text{wf}} &= -2\pi\alpha \int d^3 \mathbf{x}_1 \int d^3 \mathbf{x}_2 \int \frac{d^3 \mathbf{k}}{(2\pi)^3} \frac{1}{k} \\
&\quad \times \sum_n \frac{\Phi_a^\dagger(\mathbf{x}_1) \alpha^\mu e^{i\mathbf{k}\cdot\mathbf{x}_1} \Phi_n(\mathbf{x}_1) \Phi_n^\dagger(\mathbf{x}_2) e^{-i\mathbf{k}\cdot\mathbf{x}_2} \alpha_\mu \Phi_{\delta a}(\mathbf{x}_2)}{E_a - E_n - \text{sign}(E_n)k} \\
&= -2\pi\alpha \int \frac{d^3 \mathbf{k}}{(2\pi)^3} \frac{1}{k} \sum_n \frac{\langle a | \alpha^\mu e^{i\mathbf{k}\cdot\mathbf{x}_1} | n \rangle \langle n | e^{-i\mathbf{k}\cdot\mathbf{x}_2} \alpha_\mu | \delta a \rangle}{E_a - E_n - \text{sign}(E_n)k} .
\end{aligned} \tag{3.41}$$

Furthermore, by performing the angular part of the \mathbf{k} -integration and using the spherical wave expansion

$$\frac{\sin(k|\mathbf{x}_1 - \mathbf{x}_2|)}{k|\mathbf{x}_1 - \mathbf{x}_2|} = \sum_{l=0}^{\infty} (2l+1) \mathbf{C}^l(1) \cdot \mathbf{C}^l(2) j_l(kr_1) j_l(kr_2), \quad (3.42)$$

we obtain

$$\begin{aligned} \Delta E_{\text{bou}}^{\text{wf}} &= -\frac{\alpha}{\pi} \sum_{l=0}^{\infty} (2l+1) \int k dk \\ &\times \sum_n \frac{\langle a | \alpha^\mu j_l(kr_1) \mathbf{C}^l(1) | n \rangle \langle n | j_l(kr_2) \mathbf{C}^l(2) \alpha_\mu | \delta a \rangle}{E_a - E_n - \text{sign}(E_n) k}. \end{aligned} \quad (3.43)$$

The zero-potential term is given by the same expression but with free intermediate states. The one-potential part is the matrix element of the free vertex operator, and its coordinate space expression will be derived in the following section. Putting all this together we finally obtain for the many-potential term

$$\begin{aligned} \Delta E_{\text{mp}}^{\text{wf}} &= -\frac{\alpha}{\pi} \sum_{l=0}^{\infty} (2l+1) \int k dk \\ &\times \left\{ \sum_n \frac{\langle a | \alpha^\mu j_l(kr_1) \mathbf{C}^l | n \rangle \langle n | j_l(kr_2) \mathbf{C}^l \alpha_\mu | \delta a \rangle}{E_a - E_n - \text{sign}(E_n) k} \right. \\ &\quad - \sum_q \frac{\langle a | \alpha^\mu j_l(kr_1) \mathbf{C}^l | q \rangle \langle q | j_l(kr_2) \mathbf{C}^l \alpha_\mu | \delta a \rangle}{E_a - E_q - \text{sign}(E_q) k} \\ &\quad \left. - \sum_{p,q} \frac{\langle a | \alpha^\mu j_l(kr_1) \mathbf{C}^l | p \rangle \langle p | V_{\text{nuc}} | q \rangle \langle q | j_l(kr_2) \mathbf{C}^l \alpha_\mu | \delta a \rangle}{[E_a - E_p - \text{sign}(E_p) k][E_a - E_q - \text{sign}(E_q) k]} \times F \right\}, \end{aligned} \quad (3.44)$$

where $|n\rangle$ denotes bound and $|p\rangle, |q\rangle$ free electron states and where the function F is given by

$$F = 1 + [\text{sign}(E_p) - \text{sign}(E_q)] \frac{k}{E_p - E_q}. \quad (3.45)$$

3.2.2 Vertex and binding-energy corrections

The vertex and the binding-energy terms, which are shown in Fig. 3.5, are both infrared divergent and ultraviolet charge divergent, but the divergences cancel between the two terms. To formulate an unambiguous regularization, we expand the intermediate bound electron propagators into free electron propagators interacting zero, one or several times with the nuclear potential. The divergent zero-potential terms are grouped together and by the use of dimensional regularization the ultraviolet divergences can be identified and cancelled. The finite remainder is thereafter evaluated in momentum space. After separating out and cancelling the infrared divergences, the one-potential and many-potential terms (higher-order terms (h.o.)) are finite and are calculated in coordinate space. Our standard approach for evaluating the higher-order terms is to subtract the zero-potential terms from the bound terms (see Fig. 3.5):

$$\Delta E_{\text{h.o.}}^{\text{ve+be}} = (\Delta E_{\text{sc}}^{\text{ve}} - \Delta E_{\text{zp}}^{\text{ve}}) + (\Delta E_{\text{sc}}^{\text{be}} - \Delta E_{\text{zp}}^{\text{be}}), \quad (3.46)$$

$$\Delta E^1 \times \frac{d}{dE} \left[\text{Self-energy diagram} \right] + \left[\text{Vertex diagram} \right] = \left(\Delta E^1 \times \frac{d}{dE} \left[\text{Self-energy diagram} \right] + \left[\text{Vertex diagram} \right] \right) + \Delta E_{\text{h.o.}}^{\text{ve+be}}$$

$\Delta E_{\text{se}}^{\text{be}}$ $\Delta E_{\text{se}}^{\text{ve}}$ $\Delta E_{\text{zp}}^{\text{be}}$ $\Delta E_{\text{zp}}^{\text{ve}}$

Figure 3.5: Feynman graphs representing the binding energy and vertex correction. In this part the divergences occur only in the zero-potential terms, which are grouped together. ΔE^1 denotes the first-order energy in the external field.

which works well for medium and high Z calculations. Going down in Z it is, however, hard to obtain this part with high accuracy, as it turns out that the one-potential terms (implicitly present in Eq. (3.46)) has a very slow partial wave convergence. This was particularly pronounced for the g -factor calculation where we handled this problem by subtracting away also the one-potential terms from the bound main terms. The one-potential terms of course have to re-added, calculated in some different way which can take care of the slow partial wave convergence. This separate calculation was performed in a semi-analytical fashion, which is very stable and therefore can be extended up to very high partial waves (well beyond $l = 100$). This procedure led to a substantial improvement of the numerical accuracy in the computation of the higher-order terms.

The calculation of the vertex and binding-energy corrections are thus arranged as follows

$$\begin{aligned} \Delta E_{\text{se}}^{\text{ve+be}} &= \Delta E_{\text{zp}}^{\text{ve}} + \Delta E_{\text{zp}}^{\text{be}} + \Delta E_{\text{h.o.}}^{\text{ve+be}} \\ &= -\langle a | \gamma^0 e \Lambda_{\text{free}}^\mu(p, p') A_\mu^{\text{ext}}(\mathbf{p}, \mathbf{p}') | a \rangle + \Delta E_a^1 \times \langle a | \gamma^0 \frac{\partial}{\partial E} \Sigma^{\text{free}}(p) | a \rangle \\ &\quad + \Delta E_{\text{h.o.}}^{\text{ve+be}}, \end{aligned} \quad (3.47)$$

where $\Lambda_{\text{free}}^\mu(p, p')$ and $\frac{\partial}{\partial E} \Sigma^{\text{free}}(p)$ are given by Eqs. (3.26) and (3.25), respectively.

Zero-potential terms

We consider first the cancellation of the ultraviolet charge divergent parts between the zero-potential terms. Using the formal expansions Eqs. (3.9) and (3.10) we obtain

$$\begin{aligned} \Delta E_{\text{zp}}^{\text{be}} &= \Delta E_a^1 \times \langle a | \gamma^0 \frac{\partial}{\partial E} [\delta m + (\not{p} - m)(Z_2 - 1) + \Sigma^{\text{ren}}(p)] | a \rangle \\ &= \Delta E_a^1 \times \langle a | \gamma^0 \left[\gamma^0 (Z_2 - 1) + \frac{\partial}{\partial E} \Sigma^{\text{ren}}(p) \right] | a \rangle \\ &= \Delta E_a^1 \times (Z_2 - 1) + \Delta E_a^1 \times \langle a | \gamma^0 \frac{\partial}{\partial E} \Sigma^{\text{ren}}(p) | a \rangle, \end{aligned} \quad (3.48)$$

and

$$\begin{aligned}
\Delta E_{zp}^{ve} &= -\langle a|\gamma^0 e[\gamma^\mu(1-Z_2) + \Lambda_{\text{ren}}^\mu(p, p')] A_\mu^{\text{ext}}(\mathbf{p}, \mathbf{p}')|a\rangle \\
&= -\langle a|e\alpha^\mu A_\mu^{\text{ext}}(\mathbf{p}, \mathbf{p}')(1-Z_2)|a\rangle - \langle a|\gamma^0 e\Lambda_{\text{ren}}^\mu(p, p')A_\mu^{\text{ext}}(\mathbf{p}, \mathbf{p}')|a\rangle \\
&= \Delta E_a^1 \times (1-Z_2) - \langle a|\gamma^0 e\Lambda_{\text{ren}}^\mu(p, p')A_\mu^{\text{ext}}(\mathbf{p}, \mathbf{p}')|a\rangle, \tag{3.49}
\end{aligned}$$

from which we can see the cancellation of the charge divergence. From the expressions in dimensional regularization Eqs. (3.26) and (3.25), and using $C_{24} = \Delta/4 + \dots$ (see Appendix D), we see that the ultraviolet divergence Δ cancels in this way. Since the remaining terms are finite we just remove, in the calculations, the terms proportional to Δ in the zero-potential terms. Any constant added to Δ in the vertex and binding-energy corrections will cancel in the same way as Δ — only the total self-energy correction has a physical meaning. In order to allow for a detailed comparison between our results and those of Refs. [41, 42], we have added a constant term = 2, in the numerical implementation of the expressions Eqs. (3.25) and (3.26).

The momentum space expression for the zero-potential binding-energy correction is given by

$$\Delta E_{zp}^{\text{bs}} = \Delta E_a^1 \times \int d^3\mathbf{p} \Phi_a^\dagger(\mathbf{p})\gamma^0 \left[\frac{\partial}{\partial E} \Sigma^{\text{free}}(\mathbf{p}, E) \right]_{E=E_a} \Phi_a(\mathbf{p}). \tag{3.50}$$

The integral structure is similar to the zero-potential wavefunction part and the calculation follows the same scheme. By explicit differentiation we separate the tensor structure as

$$\frac{\partial \Sigma^{\text{free}}}{\partial E} = \frac{\partial a(\rho)}{\partial E} + \not{p} \frac{\partial b(\rho)}{\partial E} + \gamma^0 b(\rho), \tag{3.51}$$

with $a(\rho)$ and $b(\rho)$ given by Eq. (3.30). The angular integrations then yields the expression

$$\Delta E_{zp}^{\text{bs}} = \Delta E_a^1 \times \int dp p^2 \left[\tilde{A}(p) \frac{\partial a(\rho)}{\partial E} + \tilde{B}(p) \frac{\partial b(\rho)}{\partial E} + \tilde{C}(p) b(\rho) \right]_{E=E_a}, \tag{3.52}$$

where we have defined

$$\begin{aligned}
\tilde{A}(p) &= P_a^2(p) - Q_a^2(p), \\
\tilde{B}(p) &= E_a [P_a^2(p) + Q_a^2(p)] + 2p P_a(p) Q_a(p), \\
\tilde{C}(p) &= P_a^2(p) + Q_a^2(p), \tag{3.53}
\end{aligned}$$

and where

$$\begin{aligned}
\frac{\partial a(\rho)}{\partial E} &= -\frac{\alpha}{4\pi} \frac{8E}{m(1-\rho)} \left[1 + \frac{\rho}{1-\rho} \ln \rho \right], \\
\frac{\partial b(\rho)}{\partial E} &= \frac{\alpha}{4\pi} \frac{2E}{m^2(1-\rho)^2} \left[3 - \rho + \frac{2}{1-\rho} \ln \rho \right]. \tag{3.54}
\end{aligned}$$

We now turn to the zero-potential part of the vertex correction which is given by

$$\Delta E_{zp}^{ve} = - \int d^3\mathbf{p} \int d^3\mathbf{p}' \Phi_a^\dagger(\mathbf{p}) \gamma^0 \Lambda_{free}^\mu(p, p') e A_\mu^{\text{ext}}(\mathbf{p}, \mathbf{p}') \Phi_a(\mathbf{p}') . \quad (3.55)$$

The case of a scalar external potential is equivalent to the one-potential wavefunction part with $V_{\text{nuc}} \rightarrow -eA_0^{\text{ext}}$ and $\Phi_{\delta a} \rightarrow \Phi_a$ in Eq. (3.35). We will thus focus here on the vector part of Eq. (3.55), which is given by the following integral

$$\begin{aligned} \Delta E_{zp}^{ve} &= \frac{\alpha}{4\pi} \int d^3\mathbf{p} \int d^3\mathbf{p}' \Phi_a^\dagger(\mathbf{p}) \gamma^0 \\ &\quad \times [\gamma f_1(p, p', \cos \vartheta) + \not{\mathbf{p}} f_2(p, p', \cos \vartheta) + \not{\mathbf{p}}' f_3(p, p', \cos \vartheta) \\ &\quad + \not{\mathbf{p}}' \mathbf{p} f_4(p, p', \cos \vartheta) + \not{\mathbf{p}}' \mathbf{p}' f_5(p, p', \cos \vartheta) + \not{\mathbf{p}} \gamma \not{\mathbf{p}}' f_6(p, p', \cos \vartheta) \\ &\quad + \mathbf{p} f_7(p, p', \cos \vartheta) + \mathbf{p}' f_8(p, p', \cos \vartheta)] \cdot e A^{\text{ext}}(\mathbf{p} - \mathbf{p}') \Phi_a(\mathbf{p}') , \end{aligned} \quad (3.56)$$

where the f_i -functions are abbreviations for the coefficient functions of the vector part of Eq. (3.26). Due to the vector structure of this expression, we can not reduce the angular part to some simple dependence on the intermediate angle as was done for the zeroth component of the vertex function. By defining, for the different interaction types, the functions

$$\begin{aligned} V_i^{\text{breit}}(p, p', \cos \vartheta) &= \frac{f_i(p, p', \cos \vartheta)}{|\mathbf{p} - \mathbf{p}'|^3} \int dr r^2 j_1(|\mathbf{p} - \mathbf{p}'|r) f(r) g(r) , \\ V_i^{\text{hfs}}(p, p', \cos \vartheta) &= f_i(p, p', \cos \vartheta) \frac{1}{|\mathbf{p} - \mathbf{p}'|^2} , \\ V_i^{\text{mag}}(p, p', \cos \vartheta) &= f_i(p, p', \cos \vartheta) e^{-(|\mathbf{p} - \mathbf{p}'|/\rho)^2} , \end{aligned} \quad (3.57)$$

and expanding those according to Eq. (B.14), the angular dependencies can be separated. The angular integrations can thereby be performed analytically by using angular diagram techniques [43] as will be demonstrated below. The final expression then contains the expansion integral Eq. (B.15) and the radial integrals over p and p' , which are performed numerically.

Let us start with considering the structure of the different terms in the vertex operator. The first term of Eq. (3.56), proportional to $\gamma^0 \gamma = \alpha$, has exactly the form of the first-order interaction and its contribution is given by (cf. Eqs. (2.25), (2.28) and Eq. (18) in Paper I)

$$\begin{aligned} \Delta E_{zp,1}^{ve} &= C^{\text{int}} \frac{\alpha}{4\pi} \int dp p^2 \int dp' p'^2 \left\{ P(p) Q(p') [p' V_{1,0}^{\text{int}}(p, p') - p V_{1,1}^{\text{int}}(p, p')] \right. \\ &\quad \left. + Q(p) P(p') [p V_{1,0}^{\text{int}}(p, p') - p' V_{1,1}^{\text{int}}(p, p')] \right\} , \end{aligned} \quad (3.58)$$

where C^{int} is the overall constant in the first-order expression ($= 8\alpha/\pi$ for the Breit interaction). Performing the matrix multiplications for the remaining terms gives the following result

$$\begin{aligned} \Phi_c^\dagger(\mathbf{p}) \gamma^0 \not{\mathbf{p}} \Phi_a(\mathbf{p}') &= \mathbf{p} \left\{ E \left[P(p) P(p') \chi_\kappa^{m_c \dagger}(\hat{p}) \chi_\kappa^{m_a}(\hat{p}') + Q(p) Q(p') \chi_{-\kappa}^{m_c \dagger}(\hat{p}) \chi_{-\kappa}^{m_a}(\hat{p}') \right] \right. \\ &\quad \left. + p \left[P(p) Q(p') \chi_{-\kappa}^{m_c \dagger}(\hat{p}) \chi_{-\kappa}^{m_a}(\hat{p}') + Q(p) P(p') \chi_{\kappa}^{m_c \dagger}(\hat{p}) \chi_{\kappa}^{m_a}(\hat{p}') \right] \right\} , \end{aligned} \quad (3.59)$$

$$\begin{aligned} \Phi_c^\dagger(\mathbf{p})\gamma^0\not{\mathbf{p}}\mathbf{p}'\Phi_a(\mathbf{p}') &= \mathbf{p}' \left\{ E \left[P(p)P(p')\chi_\kappa^{m_c\dagger}(\hat{p})\chi_\kappa^{m_a}(\hat{p}') + Q(p)Q(p')\chi_{-\kappa}^{m_c\dagger}(\hat{p})\chi_{-\kappa}^{m_a}(\hat{p}') \right] \right. \\ &\quad \left. + p \left[P(p)Q(p')\chi_{-\kappa}^{m_c\dagger}(\hat{p})\chi_{-\kappa}^{m_a}(\hat{p}') + Q(p)P(p')\chi_\kappa^{m_c\dagger}(\hat{p})\chi_\kappa^{m_a}(\hat{p}') \right] \right\}, \end{aligned} \quad (3.60)$$

$$\begin{aligned} \Phi_c^\dagger(\mathbf{p})\gamma^0\not{\mathbf{p}}\mathbf{p}\Phi_a(\mathbf{p}') &= \mathbf{p} \left\{ E \left[P(p)P(p')\chi_\kappa^{m_c\dagger}(\hat{p})\chi_\kappa^{m_a}(\hat{p}') + Q(p)Q(p')\chi_{-\kappa}^{m_c\dagger}(\hat{p})\chi_{-\kappa}^{m_a}(\hat{p}') \right] \right. \\ &\quad \left. + p' \left[P(p)Q(p')\chi_\kappa^{m_c\dagger}(\hat{p})\chi_\kappa^{m_a}(\hat{p}') + Q(p)P(p')\chi_{-\kappa}^{m_c\dagger}(\hat{p})\chi_{-\kappa}^{m_a}(\hat{p}') \right] \right\}, \end{aligned} \quad (3.61)$$

$$\begin{aligned} \Phi_c^\dagger(\mathbf{p})\gamma^0\not{\mathbf{p}}'\mathbf{p}'\Phi_a(\mathbf{p}') &= \mathbf{p}' \left\{ E \left[P(p)P(p')\chi_\kappa^{m_c\dagger}(\hat{p})\chi_\kappa^{m_a}(\hat{p}') + Q(p)Q(p')\chi_{-\kappa}^{m_c\dagger}(\hat{p})\chi_{-\kappa}^{m_a}(\hat{p}') \right] \right. \\ &\quad \left. + p' \left[P(p)Q(p')\chi_\kappa^{m_c\dagger}(\hat{p})\chi_\kappa^{m_a}(\hat{p}') + Q(p)P(p')\chi_{-\kappa}^{m_c\dagger}(\hat{p})\chi_{-\kappa}^{m_a}(\hat{p}') \right] \right\}, \end{aligned} \quad (3.62)$$

$$\begin{aligned} \Phi_c^\dagger(\mathbf{p})\gamma^0\not{\mathbf{p}}\not{\mathbf{p}}'\mathbf{p}'\Phi_a(\mathbf{p}') &= \\ &- E^2 \left[P(p)Q(p')\chi_\kappa^{m_c\dagger}(\hat{p})\boldsymbol{\sigma}\chi_{-\kappa}^{m_a}(\hat{p}') + Q(p)P(p')\chi_{-\kappa}^{m_c\dagger}(\hat{p})\boldsymbol{\sigma}\chi_\kappa^{m_a}(\hat{p}') \right] \\ &- p'E \left[P(p)P(p')\chi_\kappa^{m_c\dagger}(\hat{p})\boldsymbol{\sigma}\chi_{-\kappa}^{m_a}(\hat{p}') + Q(p)Q(p')\chi_{-\kappa}^{m_c\dagger}(\hat{p})\boldsymbol{\sigma}\chi_\kappa^{m_a}(\hat{p}') \right] \\ &- pE \left[P(p)P(p')\chi_{-\kappa}^{m_c\dagger}(\hat{p})\boldsymbol{\sigma}\chi_\kappa^{m_a}(\hat{p}') + Q(p)Q(p')\chi_\kappa^{m_c\dagger}(\hat{p})\boldsymbol{\sigma}\chi_{-\kappa}^{m_a}(\hat{p}') \right] \\ &- pp' \left[P(p)Q(p')\chi_{-\kappa}^{m_c\dagger}(\hat{p})\boldsymbol{\sigma}\chi_\kappa^{m_a}(\hat{p}') + Q(p)P(p')\chi_\kappa^{m_c\dagger}(\hat{p})\boldsymbol{\sigma}\chi_{-\kappa}^{m_a}(\hat{p}') \right], \end{aligned} \quad (3.63)$$

$$\Phi_c^\dagger(\mathbf{p})\gamma^0\mathbf{p}\Phi_a(\mathbf{p}') = \mathbf{p} \left[P(p)P(p')\chi_\kappa^{m_c\dagger}(\hat{p})\chi_\kappa^{m_a}(\hat{p}') - Q(p)Q(p')\chi_{-\kappa}^{m_c\dagger}(\hat{p})\chi_{-\kappa}^{m_a}(\hat{p}') \right], \quad (3.64)$$

$$\Phi_c^\dagger(\mathbf{p})\gamma^0\mathbf{p}'\Phi_a(\mathbf{p}') = \mathbf{p}' \left[P(p)P(p')\chi_\kappa^{m_c\dagger}(\hat{p})\chi_\kappa^{m_a}(\hat{p}') - Q(p)Q(p')\chi_{-\kappa}^{m_c\dagger}(\hat{p})\chi_{-\kappa}^{m_a}(\hat{p}') \right]. \quad (3.65)$$

In deriving these expressions we have used the relations

$$\gamma^0\not{\mathbf{p}} = \begin{pmatrix} E & -\boldsymbol{\sigma} \cdot \mathbf{p} \\ -\boldsymbol{\sigma} \cdot \mathbf{p} & E \end{pmatrix}, \quad (3.66)$$

and

$$\begin{aligned} \boldsymbol{\sigma} \cdot \mathbf{p} \chi_{\pm\kappa}^m(\hat{p}) &= -p \chi_{\mp\kappa}^m(\hat{p}) \\ \chi_{\pm\kappa}^{m\dagger}(\hat{p}) \boldsymbol{\sigma} \cdot \mathbf{p} &= -p \chi_{\mp\kappa}^{m\dagger}(\hat{p}), \end{aligned} \quad (3.67)$$

and similarly for $p^{\mu'} = (E, \mathbf{p}')$. We will here concentrate on the evaluation of the angular parts for the electron-electron Breit interaction. This do not, however, imply any loss of generality since we reduce (evaluate) only the part of the angular diagram which is associated with the vertex operator. As discussed

VA1

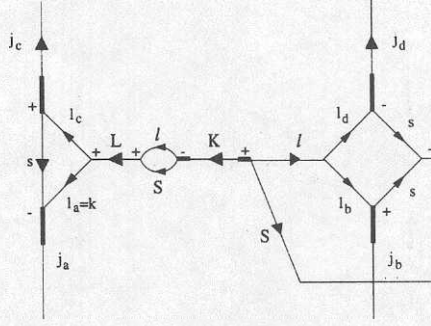


Figure 3.6: Angular momentum graph corresponding to the $\mathbf{p} \mathbf{C}^1(\hat{p})$ part of the second term of the vertex operator.

in Chapter 2 the results obtained are valid for all $K = 1$ vector interactions, in particular for the g factor and the hyperfine structure calculations.

Focus now on the contribution from the second term in the vertex operator $\gamma^0 \not{p}$, Eq. (3.59). Inserting the Breit potential Eq. (2.19), we obtain

$$\begin{aligned} \Delta E_{zp,2}^{ve} &= \frac{-3\alpha e^2}{4\pi(2\pi)^3} \sum_{k=0}^{\infty} (2k+1) \\ &\times \int d\Omega \left[\chi_{\kappa}^{m_a \dagger}(\hat{r}) \boldsymbol{\sigma} \mathbf{C}^1(\hat{r}) \chi_{-\kappa}^{m_b}(\hat{r}) - \chi_{-\kappa}^{m_a \dagger}(\hat{r}) \boldsymbol{\sigma} \mathbf{C}^1(\hat{r}) \chi_{\kappa}^{m_b}(\hat{r}) \right] \\ &\times \int d^3\mathbf{p} \int d^3\mathbf{p}' V_{2,k}(p, p') \mathbf{C}^k(\hat{p}) \cdot \mathbf{C}^k(\hat{p}') \left[p \mathbf{p} \mathbf{C}^1(\hat{p}) - p' \mathbf{p}' \mathbf{C}^1(\hat{p}') \right] \\ &\times \left\{ E \left[P(p) P(p') \chi_{\kappa}^{m_c \dagger}(\hat{p}) \chi_{\kappa}^{m_a}(\hat{p}') + Q(p) Q(p') \chi_{-\kappa}^{m_c \dagger}(\hat{p}) \chi_{-\kappa}^{m_a}(\hat{p}') \right] \right. \\ &\quad \left. + p \left[P(p) Q(p') \chi_{-\kappa}^{m_c \dagger}(\hat{p}) \chi_{-\kappa}^{m_a}(\hat{p}') + Q(p) P(p') \chi_{\kappa}^{m_c \dagger}(\hat{p}) \chi_{\kappa}^{m_a}(\hat{p}') \right] \right\}. \end{aligned} \quad (3.68)$$

By decomposing the \mathbf{p} -vector as

$$\mathbf{p} = p \sum_{t=-1}^1 (-1)^t C_t^1(\hat{p}) \hat{e}_{-t}^{[1]}, \quad (3.69)$$

and using the expansion

$$C_{m_1}^1(\hat{p}) C_{m_2}^1(\hat{p}) = \sum_{LM} a_{LM} C_M^L(\hat{p}), \quad L = 0, 2, \quad M = m_1 + m_2, \quad (3.70)$$

we obtain the angular diagram VA1 (Fig. 3.6) for the $\mathbf{p} \mathbf{C}^1(\hat{p})$ -term and diagram VA2 (Fig. 3.7) for the $\mathbf{p} \mathbf{C}^1(\hat{p}')$ -term. From diagram VA1 it follows that $L = K$ for nonvanishing contributions. Since $K = 1$ and L only can take the values $L = 0, 2$, it follows that this term does not contribute.

The VA2 diagram can be transformed to the first-order angular diagram A3 in Fig. 2.5 by removing the triangles, which yields the relation

$$\text{VA2} = (-1)^{l_c} [(2j_c + 1)(2j_a + 1)(2K + 1)]^{1/2} \left\{ \begin{matrix} l_a & K & l_c \\ S & k & l \end{matrix} \right\} \left\{ \begin{matrix} j_a & K & j_c \\ l_c & \frac{1}{2} & l_a \end{matrix} \right\} \times \text{A3}. \quad (3.71)$$

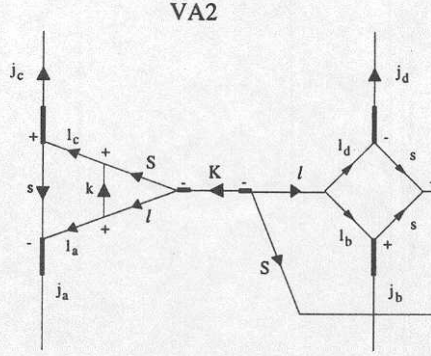


Figure 3.7: Angular momentum graph corresponding to the $\mathbf{p} \mathbf{C}^1(\hat{p}')$ part of the second term of the vertex operator.

It follows further from triangular conditions that only the \bar{l}_c, \bar{l}_a parts contribute. The expansion parameter k can thus take the values $k = 0, 2$ and the total angular factor is given by

$$\begin{aligned} & \frac{4\pi}{3} [(2j_c + 1)(2j_a + 1)(2K + 1)]^{1/2} \langle \frac{1}{2} \parallel \sigma \parallel \frac{1}{2} \rangle \langle l_d \parallel \mathbf{C}^1 \parallel l_b \rangle \\ & \times \langle \bar{l}_c \parallel \mathbf{C}^k \parallel S \rangle \langle l \parallel \mathbf{C}^k \parallel \bar{l}_a \rangle \left\{ \begin{matrix} \bar{l}_a & K & \bar{l}_c \\ S & k & l \end{matrix} \right\} \left\{ \begin{matrix} j_a & K & j_c \\ \bar{l}_c & \frac{1}{2} & \bar{l}_a \end{matrix} \right\} \times A3. \end{aligned} \quad (3.72)$$

Comparing this factor with the angular part of the first-order interaction Eqs. (2.27) and (2.29), it can be seen that the latter is a factor of 3 (-3) times larger than for the vertex $k = 2$ ($k = 0$) part. The contribution from the $\gamma^0 \not{p} \mathbf{p}$ -term can thus after angular integrations be written as

$$\begin{aligned} \Delta E_{zp,2}^{ve} &= \frac{2\alpha^2}{\pi^2} \frac{1}{3} \int dp p^2 \int dp' p'^2 pp' [V_{2,2}(p, p') - V_{2,0}(p, p')] \\ & \times [EQ(p)Q(p') + pP(p)Q(p')] . \end{aligned} \quad (3.73)$$

Consider now the remaining terms of the vertex operator listed in Eqs. (3.60)–(3.65). By comparing Eqs. (3.59) and (3.60) it is straightforward to see that the contribution from the $\gamma^0 \not{p} \mathbf{p}'$ -term is similar to the contribution for the $\gamma^0 \not{p} \mathbf{p}$ -term

$$\begin{aligned} \Delta E_{zp,3}^{ve} &= \frac{2\alpha^2}{\pi^2} \frac{1}{3} \int dp p^2 \int dp' p'^2 pp' [V_{3,2}(p, p') - V_{3,0}(p, p')] \\ & \times [EQ(p)Q(p') + pP(p)Q(p')] . \end{aligned} \quad (3.74)$$

Here it is the $\mathbf{p}' \mathbf{C}^1(\hat{p})$ part which contributes while the contribution in Eq. (3.73) comes from the $\mathbf{p} \mathbf{C}^1(\hat{p}')$ part. The momentum vector and the \mathbf{C}^1 -tensor thus have to depend on different coordinates to obtain non-vanishing contributions. For equal coordinates it is not possible to form the required rank one tensor ($K = 1$).

Also the $\gamma^0 \not{p}' \mathbf{p}$ and the $\gamma^0 \not{p}' \mathbf{p}'$ -terms (Eqs. (3.61) and (3.62)) leads to the same angular diagrams and their contributions are given by

$$\Delta E_{zp,4}^{ve} = \frac{2\alpha^2}{\pi^2} \frac{1}{3} \int dp p^2 \int dp' p'^2 pp' [V_{4,2}(p, p') - V_{4,0}(p, p')] \times [EQ(p)Q(p') + p'P(p')Q(p)] , \quad (3.75)$$

and

$$\Delta E_{zp,5}^{ve} = \frac{2\alpha^2}{\pi^2} \frac{1}{3} \int dp p^2 \int dp' p'^2 pp' [V_{5,2}(p, p') - V_{5,0}(p, p')] \times [EQ(p)Q(p') + p'P(p')Q(p)] . \quad (3.76)$$

The $\gamma^0 \not{p} \gamma \not{p}'$ -term (Eq. (3.63)) has the same angular structure as the first-order interaction and differs only in the radial parts

$$\Delta E_{zp,6}^{ve} = -\frac{2\alpha^2}{\pi^2} \int dp p^2 \int dp' p'^2 \{ [p'V_{6,0}(p, p') - pV_{6,1}(p, p')] \times [p'E P(p)P(p') + p E Q(p)Q(p') + pp'P(p')Q(p) + E^2 P(p)Q(p')] + [p V_{6,0}(p, p') - p'V_{6,1}(p, p')] \times [p'E Q(p)Q(p') + p E P(p)P(p') + pp'P(p)Q(p') + E^2 P(p')Q(p)] \} . \quad (3.77)$$

The two last terms of the vertex operator, $\gamma^0 \mathbf{p}$ and $\gamma^0 \mathbf{p}'$, has the same form as the parts proportional to E in Eqs. (3.59) and (3.60), and their contributions are given by

$$\Delta E_{zp,7}^{ve} = -\frac{2\alpha^2}{\pi^2} \frac{1}{3} \int dp p^2 \int dp' p'^2 pp' [V_{7,2}(p, p') - V_{7,0}(p, p')] Q(p)Q(p') , \quad (3.78)$$

and

$$\Delta E_{zp,8}^{ve} = -\frac{2\alpha^2}{\pi^2} \frac{1}{3} \int dp p^2 \int dp' p'^2 pp' [V_{8,2}(p, p') - V_{8,0}(p, p')] Q(p)Q(p') . \quad (3.79)$$

The contributions in Eqs. (3.73)–(3.79) are derived for the Breit part of the electron-electron interaction. They are, however, valid for all $K = 1$ vector interactions considered in this thesis. Just replace the overall factor from the first-order interaction and re-define the V_i -functions for the relevant interaction type.

Higher-order terms

The remaining contributions beyond the zero-potential part of the vertex and binding-energy corrections are convergent and can be obtained from the subtraction

$$\Delta E_{h.o.}^{ve+be} = \left(\Delta E_{se}^{ve} - \Delta E_{zp}^{ve} \right) + \left(\Delta E_{se}^{be} - \Delta E_{zp}^{be} \right) , \quad (3.80)$$

or in the alternative approach

$$\begin{aligned} \Delta E_{\text{h.o.}}^{\text{ve+be}} &= \left(\Delta E_{\text{se}}^{\text{ve}} - \Delta E_{\text{zp}}^{\text{ve}} - \Delta E_{\text{op}}^{\text{ve}} \right) + \left(\Delta E_{\text{se}}^{\text{be}} - \Delta E_{\text{zp}}^{\text{be}} - \Delta E_{\text{op}}^{\text{be}} \right) \\ &\quad + \Delta E_{\text{op}}^{\text{ve}} + \Delta E_{\text{op}}^{\text{be}} . \end{aligned} \quad (3.81)$$

This latter scheme has so far only been implemented for the g -factor calculation, and the discussion of the one-potential terms in that expression is given at the end of this section.

For the bound vertex diagram we have from Feynman rules

$$\begin{aligned} \Delta E_{\text{se}}^{\text{ve}} &= -4\pi i \alpha \int d^3 \mathbf{x}_1 \int d^3 \mathbf{x}_2 \int d^3 \mathbf{x}_3 \int_{-\infty}^{\infty} \frac{dz}{2\pi} \Phi_b^\dagger(\mathbf{x}_1) \alpha^\mu D_{\mu\nu}^F(\mathbf{x}_1 - \mathbf{x}_2, z) \\ &\quad \times S_F(\mathbf{x}_1, \mathbf{x}_3, E_a - z) \alpha^\sigma e A_\sigma^{\text{ext}}(\mathbf{x}_3) S_F(\mathbf{x}_3, \mathbf{x}_2, E_a - z) \alpha^\nu \Phi_a(\mathbf{x}_2) \\ &= 4\pi i \alpha \int \frac{d^3 \mathbf{k}}{(2\pi)^3} \int_{-\infty}^{\infty} \frac{dz}{2\pi} \\ &\quad \times \sum_{m,n} \frac{\langle a | \alpha_\mu e^{i\mathbf{k}\cdot\mathbf{x}_1} | m \rangle \langle m | \alpha^\sigma e A_\sigma^{\text{ext}}(\mathbf{x}_3) | n \rangle \langle n | e^{-i\mathbf{k}\cdot\mathbf{x}_2} \alpha^\nu | a \rangle}{[z^2 - \mathbf{k}^2 + i\delta][E_a - z - E_m(1 - i\eta)][E_a - z - E_n(1 - i\eta)]} . \end{aligned} \quad (3.82)$$

The z -integration yields

$$\begin{aligned} &\int_{-\infty}^{\infty} \frac{dz}{2\pi} \frac{1}{[E_a - z - E_m(1 - i\eta)][E_a - z - E_n(1 - i\eta)](z^2 - \mathbf{k}^2 + i\delta)} \\ &= -\frac{i}{2k} \frac{1}{[E_a - E_m - \text{sign}(E_m)k][E_a - E_n - \text{sign}(E_n)k]} \times F , \end{aligned} \quad (3.83)$$

where

$$F = 1 + [\text{sign}(E_n) - \text{sign}(E_m)] \frac{k}{E_n - E_m} . \quad (3.84)$$

Performing the angular part of the \mathbf{k} -integration and using the spherical wave expansion Eq. (3.42), we finally obtain

$$\begin{aligned} \Delta E_{\text{se}}^{\text{ve}} &= \frac{\alpha}{\pi} \sum_{l=0}^{\infty} (2l+1) \int k dk \\ &\quad \times \sum_{m,n} \frac{\langle a | \alpha_\mu j_l(kr_1) \mathbf{C}^l | m \rangle \langle m | e \alpha^\sigma A_\sigma^{\text{ext}}(\mathbf{x}_3) | n \rangle \langle n | j_l(kr_2) \mathbf{C}^l \alpha^\nu | a \rangle}{[E_a - E_m - \text{sign}(E_m)k][E_a - E_n - \text{sign}(E_n)k]} \times F . \end{aligned} \quad (3.85)$$

From Appendix E we obtain similarly for the bound binding-energy correction

$$\begin{aligned} \Delta E_{\text{se}}^{\text{be}} &= \Delta E_a^1 \times \langle a | \left[\frac{\partial}{\partial E} \Sigma^{\text{bou}}(E) \right]_{E=E_a} | a \rangle \\ &= \Delta E_a^1 \times \frac{\alpha}{\pi} \sum_{l=0}^{\infty} (2l+1) \int k dk \sum_m \frac{\langle a | \alpha_\mu j_l(kr_1) \mathbf{C}^l | m \rangle \langle m | j_l(kr_2) \mathbf{C}^l \alpha^\nu | a \rangle}{[E_a - E_m - \text{sign}(E_m)k]^2} . \end{aligned} \quad (3.86)$$

The bound terms given by Eqs. (3.85) and (3.86) contains an infrared divergence in the k -integration when $l = 0$ and the intermediate states are degenerate with the reference state. This situation occurs for scalar self-energy interaction ($\mu = 0$), and we can write for the divergent vertex part

$$\begin{aligned}\Delta E_{se}^{ve,div} &= \frac{\alpha}{\pi} \int \frac{dk}{k} \langle a|j_0(kr_1)|a\rangle \langle a|e\alpha^\sigma A_\sigma^{\text{ext}}(\mathbf{x}_3)|a\rangle \langle a|j_0(kr_2)|a\rangle \\ &= -\Delta E_a^1 \times \frac{\alpha}{\pi} \int \frac{dk}{k} \langle a|j_0(kr_1)|a\rangle \langle a|j_0(kr_2)|a\rangle ,\end{aligned}\quad (3.87)$$

where we have used $\Delta E_a^1 = -\langle a|e\alpha^\sigma A_\sigma^{\text{ext}}(\mathbf{x}_3)|a\rangle$. The divergent part of the binding-energy correction is similarly

$$\Delta E_{se}^{be,div} = \Delta E_a^1 \times \frac{\alpha}{\pi} \int \frac{dk}{k} \langle a|j_0(kr_1)|a\rangle \langle a|j_0(kr_2)|a\rangle ,\quad (3.88)$$

from which we see that the infrared divergent parts cancel between the vertex and binding-energy corrections. The cancellation holds for each k and we can thus exclude the relevant terms of the l and m, n summations in the numerical calculation.

The contribution from higher-order vertex and binding-energy terms is thus given by

$$\begin{aligned}\Delta E_{h.o.}^{ve} &= \frac{\alpha}{\pi} \sum_{l=0}^{\infty} (2l+1) \int k dk \\ &\times \left\{ \sum_{m,n} \frac{\langle a|\alpha_\mu j_l(kr_1)C^l|m\rangle \langle m|e\alpha^\sigma A_\sigma^{\text{ext}}(\mathbf{x}_3)|n\rangle \langle n|j_l(kr_2)C^l\alpha^\mu|a\rangle}{[E_a - E_m - \text{sign}(E_m)k][E_a - E_n - \text{sign}(E_n)k]} \times F \right. \\ &\quad \left. - \sum_{p,q} \frac{\langle a|\alpha_\mu j_l(kr_1)C^l|p\rangle \langle p|e\alpha^\sigma A_\sigma^{\text{ext}}(\mathbf{x}_3)|q\rangle \langle q|j_l(kr_2)C^l\alpha^\mu|a\rangle}{[E_a - E_p - \text{sign}(E_p)k][E_a - E_q - \text{sign}(E_q)k]} \times F \right\} ,\end{aligned}\quad (3.89)$$

and

$$\begin{aligned}\Delta E_{h.o.}^{be} &= \Delta E_a^1 \times \frac{\alpha}{\pi} \sum_{l=0}^{\infty} (2l+1) \int k dk \\ &\times \left\{ \sum_m \frac{\langle a|\alpha_\mu j_l(kr_1)C^l|m\rangle \langle m|j_l(kr_2)C^l\alpha^\mu|a\rangle}{[E_a - E_m - \text{sign}(E_m)k]^2} \right. \\ &\quad \left. - \sum_p \frac{\langle a|\alpha_\mu j_l(kr_1)C^l|p\rangle \langle p|j_l(kr_2)C^l\alpha^\mu|a\rangle}{[E_a - E_p - \text{sign}(E_p)k]^2} \right\} ,\end{aligned}\quad (3.90)$$

where $|m\rangle, |n\rangle$ denotes bound electron states and $|p\rangle, |q\rangle$ free electron states.

One-potential terms

As previously mentioned we can improve the accuracy of the higher-order terms by taking the one-potential terms, shown in Fig. 3.8, into account explicitly using the calculation scheme of Eq. (3.81). The re-added one-potential terms are calculated separately in a semi-analytical way, with the radial integrals evaluated analytically.

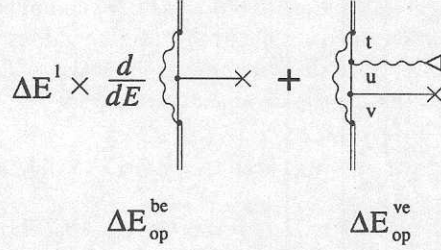


Figure 3.8: Feynman diagrams for the one-potential terms of the binding energy and the vertex correction. The triangle represents the interaction with the external potential and the line with the cross represents the nuclear Coulomb potential.

The expression for the one-potential vertex correction is given by

$$\begin{aligned} \Delta E_{\text{op}}^{\text{ve}} &= \frac{2\alpha}{\pi} \sum_{l=0}^{\infty} (2l+1) \int_0^{\infty} dk k^2 \\ &\quad \times \sum_{t,u,v} G(t,u,v) \langle a | \alpha^{\mu} j_l(kr) \mathbf{C}^l | t \rangle \langle t | e \alpha^{\sigma} A_{\sigma}^{\text{ext}} | u \rangle \langle u | V_{\text{nuc}} | v \rangle \langle v | \alpha_{\mu} j_l(kr') \mathbf{C}^l | a \rangle, \end{aligned} \quad (3.91)$$

where t, u, v labels free electron states. There are eight different combinations with respect to the sign of intermediate energies which is described by the function $G(t, u, v)$

$$\begin{aligned} G(+, +, +) &= \frac{1}{2k[E_a - E_t - k][E_a - E_u - k][E_a - E_v - k]}, \\ G(-, -, -) &= \frac{1}{2k[E_a - E_t + k][E_a - E_u + k][E_a - E_v + k]}, \\ G(+, +, -) &= \frac{1}{2k[E_a - E_t - k][E_a - E_u - k][E_a - E_v + k]} \\ &\quad + \frac{1}{[E_u - E_v][E_a - E_t - k][E_a - E_u - k][E_a - E_v + k]} \\ &\quad - \frac{1}{[E_u - E_v][E_t - E_v][E_a - E_t - k][E_a - E_v + k]}, \\ G(-, -, +) &= \frac{1}{2k[E_a - E_t + k][E_a - E_u + k][E_a - E_v - k]} \\ &\quad + \frac{1}{[E_v - E_u][E_a - E_t + k][E_a - E_u + k][E_a - E_v - k]} \\ &\quad + \frac{1}{[E_v - E_u][E_v - E_t][E_a - E_t + k][E_a - E_v - k]}. \end{aligned} \quad (3.92)$$

The remaining four cases are obtained by interchanging $t \leftrightarrow v$ and $u \leftrightarrow v$ in the last two formulas.

The one-potential binding-energy term can be obtained by differentiating Eq. (3.85) (replacing $e\alpha^\sigma A_\sigma^{\text{ext}} \rightarrow -V_{\text{nuc}}$)

$$\begin{aligned} \Delta E_{\text{op}}^{\text{be}} &= \Delta E_a^1 \times 2 \frac{\alpha}{\pi} \sum_{l=0}^{\infty} (2l+1) \int k dk \\ &\times \sum_{t,u} \frac{\langle a | \alpha_\mu j_l(kr_1) \mathbf{C}^l | t \rangle \langle t | V_{\text{nuc}} | u \rangle \langle u | j_l(kr_2) \mathbf{C}^l \alpha^\mu | a \rangle}{[E_a - E_t - \text{sign}(E_t)k][E_a - E_u - \text{sign}(E_u)k]^2} \times F, \end{aligned} \quad (3.93)$$

where $|t\rangle, |u\rangle$ are free electron states. The factor of two is due to the symmetry of the diagram. From the beginning there is also a term where the first factor in the denominator is squared, but these two terms give the same contribution. Using the scheme of Eq. (3.81) the fully numerical part is now given by Eqs. (3.89) and (3.90) where also the expressions of Eqs. (3.91) and (3.93) are subtracted.

In the semi-analytical treatment of the one-potential terms, we make use of the analytical solutions of the free Dirac equation given in Appendix F. The summations over the free intermediate states goes then over to integrations and we can write

$$\begin{aligned} \Delta E_{\text{op}}^{\text{ve}} &= \frac{2\alpha}{\pi} \sum_{l=0}^{\infty} (2l+1) \sum_{r,s,s'} \int_0^\infty dk k^2 \int d^3\mathbf{t} \int d^3\mathbf{u} \int d^3\mathbf{v} G(t, u, v) \\ &\times \langle a | \alpha_\mu j_l(kr) \mathbf{C}^l | t, r \rangle \langle t, r | e\alpha^\sigma A_\sigma^{\text{ext}} | u, s \rangle \langle u, s | V_{\text{nuc}} | v, s' \rangle \langle v, s' | j_l(kr') \mathbf{C}^l \alpha^\mu | a \rangle, \end{aligned} \quad (3.94)$$

and

$$\begin{aligned} \Delta E_{\text{op}}^{\text{be}} &= \Delta E_a^1 \times 2 \frac{\alpha}{\pi} \sum_{l=0}^{\infty} (2l+1) \sum_{r,s} \int k dk \int d^3\mathbf{t} \int d^3\mathbf{u} \\ &\times \frac{\langle a | \alpha_\mu j_l(kr_1) \mathbf{C}^l | t, r \rangle \langle t, r | V_{\text{nuc}} | u, s \rangle \langle u, s | j_l(kr_2) \mathbf{C}^l \alpha^\mu | a \rangle}{[E_a - E_t - \text{sign}(E_t)k][E_a - E_u - \text{sign}(E_u)k]^2} \times F, \end{aligned} \quad (3.95)$$

where the ket $|t, r\rangle$ describes the free-electron state with momentum \mathbf{t} and spinor component r . The radial matrix elements can here be evaluated analytically as is discussed further in Chapter 5.

4 Vacuum Polarization Corrections

A virtual electron-positron pair created in the vicinity of a nucleus will be polarized by the nuclear Coulomb field. The effective result can be described as a re-distribution of the nuclear charge, which in turn implies corrections to the atomic energy levels. This effect is called the vacuum polarization (VP). In analogy to the induced charge distribution in the electrical field of the nucleus, the nuclear magnetic field induces vacuum currents. These currents can be associated with an induced magnetic moment. In contrast to the electrical case which results in a zero net charge, the induced magnetic moment is non-zero.

The vacuum polarization consists of two parts: the Uehling (Ue) part and the Wichmann-Kroll (WK) part. The Uehling term is the finite remainder after performing charge renormalization (see Appendix C) and it was derived already in 1935 by Uehling [44] — despite that there was no clear formulation of renormalization at that time. The Uehling part originates from the first non-zero term in the $(Z\alpha)$ -expansion of the polarization loop and the finite Wichmann-Kroll part represents the remaining higher-order terms.

We start this chapter by reviewing the calculation of the first-order vacuum polarization, following the work in Paper IV. Since the VP corrections in an external potential is rather similar we can benefit greatly from the first-order discussion. In Section 4.2.3 we will further consider the vacuum polarization correction to the measured nuclear magnetic moment.

4.1 First-order vacuum polarization

As for the electron self-energy we can isolate the divergent part of the vacuum polarization by expanding in the binding potential. Using the propagator expansion Eq. (3.5), the vacuum polarization diagram is decomposed into a zero-potential term (zp), a divergent one-potential term (op) and finally a finite many-potential term (mp), see Fig. 4.1. The first term, ΔE_{zp}^{vp} , vanish due to Furry's theorem, which states that the contributions of diagrams which contain a free electron loop with an odd number of vertices vanish. The one-potential term, ΔE_{op}^{vp} , contains a charge divergence (Q) which can be absorbed in the charge renormalization, see Appendix C. The finite remainder is known as the Uehling term ΔE_{ue}^{vp} . The many-potential term, ΔE_{mp}^{vp} , contains in addition to the finite Wichmann-Kroll part ΔE_{wk}^{vp} , also a spurious gauge-dependent piece, S_2 , that has to be removed.

The energy shift due to vacuum polarization can be expressed in terms of a vacuum-polarization potential U_{bou}^{vp} , by writing

$$\Delta E_{bou}^{vp} = \int d^3\mathbf{x}_1 \Phi_a^\dagger(\mathbf{x}_1) U_{bou}^{vp}(\mathbf{x}_1) \Phi_a(\mathbf{x}_1), \quad (4.1)$$

$$\Delta E_{\text{bou}}^{\text{vp}} = \Delta E_{\text{zp}}^{\text{vp}} = 0 + \Delta E_{\text{op}}^{\text{vp}} = Q + \Delta E_{\text{ue}}^{\text{vp}} + \Delta E_{\text{mp}}^{\text{vp}} = S2 + \Delta E_{\text{wk}}^{\text{vp}}$$

Figure 4.1: The first-order vacuum polarization $\Delta E_{\text{bou}}^{\text{vp}}$ decomposed into the zero-potential term $\Delta E_{\text{zp}}^{\text{vp}} = 0$, the one-potential term $\Delta E_{\text{op}}^{\text{vp}} = Q + \Delta E_{\text{ue}}^{\text{vp}}$ and the many-potential term $\Delta E_{\text{mp}}^{\text{vp}} = S2 + \Delta E_{\text{wk}}^{\text{vp}}$. $\Delta E_{\text{ue}}^{\text{vp}}$ and $\Delta E_{\text{wk}}^{\text{vp}}$ are the finite Uehling and Wichmann-Kroll parts, Q is the charge divergence and $S2$ the spurious part of the many-potential term.

where

$$U_{\text{bou}}^{\text{vp}}(\mathbf{x}_1) = -4\pi i \alpha \int d^3 \mathbf{x}_2 \int_{-\infty}^{\infty} \frac{dz}{2\pi} \alpha^\nu D_{\nu\mu}^F(\mathbf{x}_2 - \mathbf{x}_1, 0) \text{Tr}[\alpha^\mu S_F^{\text{bou}}(\mathbf{x}_2, \mathbf{x}_2, z)]. \quad (4.2)$$

Inserting the expansion of the electron propagator in the nuclear field Eq. (3.5), we obtain for the one-potential term

$$U_{\text{op}}^{\text{vp}}(\mathbf{x}_1) = -4\pi i \alpha \int d^3 \mathbf{x}_2 \int d^3 \mathbf{x}_3 \int_{-\infty}^{\infty} \frac{dz}{2\pi} \times \alpha^\nu D_{\nu\mu}^F(\mathbf{x}_2 - \mathbf{x}_1, 0) \text{Tr}[\alpha^\mu S_F^{\text{free}}(\mathbf{x}_2, \mathbf{x}_3, z) V_{\text{nuc}}(\mathbf{x}_3) S_F^{\text{free}}(\mathbf{x}_3, \mathbf{x}_2, z)]. \quad (4.3)$$

Transforming this to momentum space yields

$$U_{\text{op}}^{\text{vp}}(\mathbf{q}) = -4\pi \alpha \frac{V_{\text{nuc}}(\mathbf{q})}{\mathbf{q}^2} \alpha_\nu \Pi^{\nu 0, (1)}(q), \quad (4.4)$$

where $q = (0, \mathbf{q})$ and $\Pi^{\nu 0, (1)}(q)$ is the first-order unrenormalized polarization tensor Eq. (C.2). Performing the charge renormalization (see Appendix C) we can extract the renormalized Uehling potential

$$U_{\text{ue}}^{\text{vp}}(\mathbf{q}) = -4\pi \alpha V_{\text{nuc}}(\mathbf{q}) \Pi^{\text{ren}}(\mathbf{q}^2), \quad (4.5)$$

where $\Pi^{\text{ren}}(\mathbf{q}^2)$ is given by Eq. (C.12). Going back to coordinate space we obtain the well known expression

$$U_{\text{ue}}^{\text{vp}}(\mathbf{x}_1) = 2\pi \alpha \int \frac{d^3 \mathbf{x}_3}{(2\pi)^3} \frac{\rho_{\text{nuc}}(\mathbf{x}_3)}{|\mathbf{x}_1 - \mathbf{x}_3|} \int_1^\infty dt \sqrt{t^2 - 1} \left(\frac{2}{3t^2} + \frac{1}{3t^4} \right) e^{-2mt|\mathbf{x}_1 - \mathbf{x}_3|}, \quad (4.6)$$

where ρ_{nuc} is the nuclear charge density.

To obtain the finite Wichmann-Kroll contribution we adopt the subtraction scheme suggested by Soff and Mohr [45]:

$$\Delta E_{\mathbf{w}\mathbf{k}}^{\text{vp}} = \Delta E_{\text{bou}}^{\text{vp}} - \Delta E_{\text{op}}^{\text{vp}} - S2. \quad (4.7)$$

By making the spherical-wave decomposition

$$\Delta E_{\mathbf{w}\mathbf{k}}^{\text{vp}} = \sum_{|\kappa|=1}^{\infty} \left(\Delta E_{\text{bou}}^{\text{vp},|\kappa|} - \Delta E_{\text{op}}^{\text{vp},|\kappa|} - S2^{|\kappa|} \right), \quad (4.8)$$

we can handle the spurious term $S2$ in the following way. If the summation over the angular momentum number $|\kappa|$ is restricted to a finite number of terms $|\kappa| = 1, 2, \dots, |\kappa_{\text{max}}|$, then the explicit contribution from the $S2^{|\kappa|}$ term can be shown to vanish [45–47]. The $S2$ -term can thus be omitted and the subtraction scheme can be simplified to read

$$\Delta E_{\mathbf{w}\mathbf{k}}^{\text{vp}} = \lim_{|\kappa_{\text{max}}| \rightarrow \infty} \sum_{|\kappa|=1}^{|\kappa_{\text{max}}|} \left(\Delta E_{\text{bou}}^{\text{vp},|\kappa|} - \Delta E_{\text{op}}^{\text{vp},|\kappa|} \right). \quad (4.9)$$

Note that this subtraction involves the unrenormalized bound and one-potential terms, which is analogous with the calculation of the electron self-energy many-potential terms.

We now go on to find the explicit partial-wave expressions for the bound and one-potential terms. The bound term is from Eq. (4.2) given by

$$U_{\text{bou}}^{\text{vp}}(\mathbf{x}_1) = -4\pi i \alpha \int d^3 \mathbf{x}_2 \int \frac{d^3 \mathbf{k}}{(2\pi)^3} \frac{e^{i\mathbf{k} \cdot (\mathbf{x}_2 - \mathbf{x}_1)}}{k^2} \int_{-\infty}^{\infty} \frac{dz}{2\pi} \alpha_{\mu} \sum_t \frac{\text{Tr}[\alpha^{\mu} \Phi_t(\mathbf{x}_2) \Phi_t^{\dagger}(\mathbf{x}_2)]}{z - E_t(1 - i\eta)}. \quad (4.10)$$

By performing the trace, integrating over the angular part of \mathbf{k} and using the partial-wave expansion Eq. (3.42) we obtain

$$U_{\text{bou}}^{\text{vp}}(\mathbf{x}_1) = -\frac{2i\alpha}{\pi} \sum_{l=0}^{\infty} (2l+1) \int_0^{\infty} dk \int_{-\infty}^{\infty} \frac{dz}{2\pi} \\ \times j_l(kr_1) C^l(1) \alpha_{\mu} \sum_t \frac{\langle t | j_l(kr_2) C^l(2) \alpha^{\mu} | t \rangle}{z - E_t(1 - i\eta)}. \quad (4.11)$$

Since we sum over all orientations m of j_{κ} for a specific κ in the $t = (n, \kappa, m)$ summation, one can show that l and μ have to be zero for nonvanishing contributions. Performing the z -integration, which picks up half pole contributions, integrating over angular coordinates and summing over m , we finally obtain

$$U_{\text{bou}}^{\text{vp}}(r_1) = -\frac{\alpha}{\pi} \int_0^{\infty} dk j_0(kr_1) \sum_{n,\kappa} (2j_{\kappa} + 1) \text{sign}(E_{n,\kappa}) \langle n, \kappa | j_0(kr_2) | n, \kappa \rangle. \quad (4.12)$$

This expression is divergent since it contains the unrenormalized electric charge. However, if we replace the bound intermediate states with free electron states we obtain the zero-potential term which, according to Furry's theorem, is exactly

zero. This comes out since there is an exact cancellation between the positive and negative energy states for the free electron spectra with a given $|\kappa|$ value. To be specific, in the case when $|\kappa| = 1$ the cancellation takes place between the positive (negative) spectra of the $s_{1/2}$ angular symmetry and the negative (positive) spectra of the $p_{1/2}$ angular symmetry. This cancellation is discussed in detail in Chapter 5. For bound spectra the cancellation is not exact giving rise to the divergent expression for $U_{\text{bou}}^{\text{vp}}$.

Starting from Eq. (4.3) we obtain for the one-potential term

$$U_{\text{op}}^{\text{vp}}(\mathbf{x}_1) = -\frac{2i\alpha}{\pi} \sum_{l=0}^{\infty} (2l+1) \int_0^{\infty} dk \int_{-\infty}^{\infty} \frac{dz}{2\pi} \\ \times j_l(kr_1) \mathbf{C}^l(1) \alpha_{\mu} \sum_{r,s} \frac{\langle r | j_l(kr_2) \mathbf{C}^l(2) \alpha^{\mu} | s \rangle \langle s | V_{\text{nuc}}(\mathbf{x}_3) | r \rangle}{[z - E_r(1 - i\eta)][z - E_s(1 - i\eta)]}, \quad (4.13)$$

where r, s denotes free electron states. This expression for the one-potential term corresponds to Eq. (4.11) for the bound term. As for that expression only $l = \mu = 0$ gives a non-zero contribution. If r, s are both positive (negative) states, we can close the z -integration in the upper (lower) plane and get zero contribution. Only the situation with one positive and one negative state, i.e., a virtual electron-positron pair, thus contributes in the r, s summation. Performing the angular integrations and the z -integration then gives

$$U_{\text{op}}^{\text{vp}}(r_1) = -\frac{4\alpha}{\pi} \int_0^{\infty} dk j_0(kr_1) \sum_{\kappa} (2j_{\kappa} + 1) \\ \times \sum_p^+ \sum_{p'}^- \frac{\langle p, \kappa | j_0(kr_2) | p', \kappa \rangle \langle p', \kappa | V_{\text{nuc}}(r_3) | p, \kappa \rangle}{E_{p,\kappa} - E_{p',\kappa}}, \quad (4.14)$$

where we have also summed over the m quantum numbers and used that $r = (p, \kappa, m)$ and $s = (p', \kappa, m)$ must have the same κ and m . An extra factor of two occurs since we have restricted r to be a positive energy state.

Equations (4.12) and (4.14) represents the partial-wave decompositions of the bound and one-potential terms, and we can thus express the Wichmann-Kroll potential as

$$U_{\text{wk}}^{\text{vp}}(r_1) = -\frac{\alpha}{\pi} \sum_{|\kappa|=1}^{|\kappa_{\text{max}}|} (2j_{\kappa} + 1) \int_0^{\infty} dk j_0(kr_1) \\ \times \left[\sum_n \text{sign}(E_{n,\kappa}) \langle n, \kappa | j_0(kr_2) | n, \kappa \rangle \right. \\ \left. - 4 \sum_p^+ \sum_{p'}^- \frac{\langle p, \kappa | j_0(kr_2) | p', \kappa \rangle \langle p', \kappa | V_{\text{nuc}}(r_3) | p, \kappa \rangle}{E_{p,\kappa} - E_{p',\kappa}} \right]. \quad (4.15)$$

To summarize, the renormalized first-order vacuum polarization can be expressed in terms of an energy independent potential

$$U_{\text{ren}}^{\text{vp}}(\mathbf{x}) = U_{\text{ue}}^{\text{vp}}(\mathbf{x}) + U_{\text{wk}}^{\text{vp}}(\mathbf{x}), \quad (4.16)$$

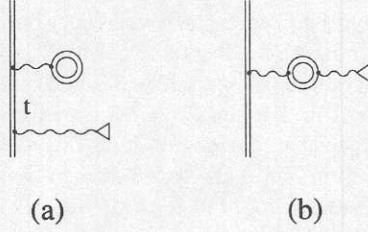


Figure 4.2: *The one-loop vacuum polarization corrections. Diagram (a) is the external line correction and (b) the potential correction.*

where $U_{\text{uc}}^{\text{vp}}$ and $U_{\text{wk}}^{\text{vp}}$ are given by Eqs. (4.6) and (4.15), respectively. The corresponding energy shift is given by

$$\Delta E_{\text{ren}}^{\text{vp}} = \langle a | U_{\text{ren}}^{\text{vp}} | a \rangle. \quad (4.17)$$

Since the potential is energy independent we can actually include it when solving the Dirac equation, and thereby obtain the vacuum polarization effect to all orders.

4.2 Vacuum polarization corrections in external potentials

The one-photon vacuum polarization corrections to the interaction with an external potential are shown in Fig. 4.2. Diagram (a) results from inserting the vacuum polarization potential in the outgoing electron line. The irreducible part, with $E_t \neq E_a$, can be expressed in terms of a perturbed wavefunction $|\delta a\rangle$, similarly as for the self-energy case, and is accordingly referred to as the *vacuum polarization wavefunction correction* $\Delta E_{\text{vp}}^{\text{wf}}$. In contrast to the corresponding self-energy diagram, there is here no contribution from the reducible part of diagram (a). This can be seen explicitly by subtracting away the lower-order diagrams in Sucher's formula Eq. (A.60). Taking the view of perturbing the first-order vacuum polarization by the external potential, this result follows from the fact that the vacuum polarization potential does not depend on E_a , leading to a vanishing binding-energy correction.

The insertion of a polarization loop in the interaction line leads to diagram Fig. 4.2 (b), which is called the *potential correction*, $\Delta E_{\text{vp}}^{\text{pc}}$. This part corresponds to the propagator modification Eq. (3.16) of the first-order vacuum polarization.

The calculation of the vacuum polarization effects in an external potential is similar to the first-order vacuum polarization, and the results and methods of the previous section will be used frequently in the following.

4.2.1 Wavefunction correction

The contribution from the wavefunction correction is given by

$$\Delta E_{\text{vp}}^{\text{wf}} = \langle a | U_{\text{ren}}^{\text{vp}} | \delta a \rangle, \quad (4.18)$$

where $|\delta a\rangle$ is the external field perturbed wavefunction and where $U_{\text{ren}}^{\text{vp}}$ is the renormalized vacuum polarization potential Eq. (4.16). There is also a symmetrical diagram where instead the bra-state is perturbed by the external potential, giving the same contribution. For the two electron case also an extra factor of two must be included since the polarization loop can then be inserted on both electron lines. The wavefunction correction has exactly the same structure as the first-order vacuum polarization, but here the matrix element is taken with one perturbed wavefunction. We thus evaluate $U_{\text{ren}}^{\text{vp}}$ in the same way as for the first-order case, and obtain the (charge renormalized) Uehling part

$$\Delta E_{\text{vp}}^{\text{wf-ue}} = \langle a | U_{\text{ue}}^{\text{vp}} | \delta a \rangle, \quad (4.19)$$

and the Wichmann-Kroll part

$$\Delta E_{\text{vp}}^{\text{wf-wk}} = \langle a | U_{\text{wk}}^{\text{vp}} | \delta a \rangle. \quad (4.20)$$

The wavefunction contribution can also be computed to all orders in the vacuum polarization potential by including $U_{\text{ren}}^{\text{vp}}$ when solving the Dirac equation. If we denote the resulting wavefunctions by $|a^{\text{vp}}\rangle$, we obtain the correction as

$$\Delta E_{\text{vp},\infty}^{\text{wf}} = \langle a^{\text{vp}} | (-e) \alpha^\mu A_\mu^{\text{ext}} | a^{\text{vp}} \rangle - \langle a | (-e) \alpha^\mu A_\mu^{\text{ext}} | a \rangle. \quad (4.21)$$

4.2.2 Potential correction

Similarly as for the first-order vacuum polarization, we decompose the potential correction into a zero-potential term, a one-potential part and finally higher-order terms, see Fig. 4.3. Here it is the zero-potential term which is divergent and requires charge renormalization. The remaining part after renormalization is recognized as the Uehling contribution. The one-potential part vanishes due to Furry's theorem and the finite higher-order part, the Wichmann-Kroll term, can be obtained by a subtracting scheme analogously to the first-order case.

Uehling part

The Uehling part is conveniently treated in momentum space and its energy contribution is given by

$$\Delta E_{\text{vp}}^{\text{pc-ue}} = -e \int d^3 \mathbf{p} \int d^3 \mathbf{p}' \Phi_a^\dagger(\mathbf{p}) \alpha^\mu A_\mu^{\text{ext-ue}}(\mathbf{p} - \mathbf{p}') \Phi_a(\mathbf{p}'), \quad (4.22)$$

where

$$A_\mu^{\text{ext-ue}}(\mathbf{p} - \mathbf{p}') = -e^2 \Pi^{\text{ren}}(|\mathbf{p} - \mathbf{p}'|^2) A_\mu^{\text{ext}}(\mathbf{p} - \mathbf{p}'). \quad (4.23)$$

For the g -factor calculation it turns out that the Uehling contribution vanishes, which can be seen in the following way. The renormalized polarization tensor

$$e^2 \Pi^{\text{ren}}(\mathbf{q}^2) = -\frac{\alpha}{\pi} \int_1^\infty dt \sqrt{t^2 - 1} \left(\frac{2}{3t^2} + \frac{1}{3t^4} \right) \frac{\mathbf{q}^2}{\mathbf{q}^2 + 4m^2 t^2} \quad (4.24)$$

$$\Delta E_{\text{bou}}^{\text{pc}} = \Delta E_{\text{zp}}^{\text{pc}} = Q + \Delta E_{\text{vp}}^{\text{pc-ue}} + 2 \Delta E_{\text{op}}^{\text{pc}} = 0 + (\Delta E_{\text{h.o.}}^{\text{pc}} = S2 + \Delta E_{\text{vp}}^{\text{pc-wk}})$$

Figure 4.3: *The potential correction due to vacuum polarization, decomposed into a zero-potential term, a (vanishing) one-potential term and finally higher-order terms. $\Delta E_{\text{vp}}^{\text{pc-ue}}$ is the renormalized Uehling part, $\Delta E_{\text{vp}}^{\text{pc-wk}}$ the Wichmann-Kroll part, Q is the charge divergence and $S2$ the spurious term.*

can, for small momentum transfer $\mathbf{q} \approx 0$, be expanded as

$$e^2 \Pi^{\text{ren}}(\mathbf{q}^2) = -\frac{\alpha}{\pi} \left[\frac{1}{15} \left(\frac{\mathbf{q}^2}{m^2} \right) - \frac{1}{140} \left(\frac{\mathbf{q}^2}{m^2} \right)^2 + O(\mathbf{q}^6) \right]. \quad (4.25)$$

From Eq. (B.25) we have the magnetic vector potential

$$\mathbf{A}^{\text{mag}}(\mathbf{q}) = \frac{i}{2} \nabla_{\mathbf{q}} \delta^3(\mathbf{q}) \times \mathbf{B}, \quad (4.26)$$

which makes the Uehling contribution proportional to

$$\int d^3\mathbf{p} \int d^3\mathbf{p}' \Phi_a^\dagger(\mathbf{p}) \Pi^{\text{ren}}(|\mathbf{p} - \mathbf{p}'|^2) \boldsymbol{\alpha} \cdot [\nabla_{\mathbf{p}} \delta^3(\mathbf{p} - \mathbf{p}') \times \mathbf{B}] \Phi_a(\mathbf{p}'). \quad (4.27)$$

By partial integration it is seen that this expression vanishes since $\Pi^{\text{ren}} \approx \mathbf{q}^2$ as $\mathbf{q}^2 \rightarrow 0$.

Wichmann-Kroll part

To obtain the contribution from the Wichmann-Kroll term we employ the subtraction scheme

$$\Delta E_{\text{vp}}^{\text{pc-wk}} = \lim_{|\kappa_{\text{max}}| \rightarrow \infty} \sum_{|\kappa|=1}^{|\kappa_{\text{max}}|} (\Delta E_{\text{bou}}^{\text{pc},|\kappa|} - \Delta E_{\text{zp}}^{\text{pc},|\kappa|}), \quad (4.28)$$

where the spurious part $S2$ has been dropped due to the partial wave decomposition (see Ref. [47] for the vector part). The zero-potential term is given by the same expression as for the bound term with the bound intermediate states replaced with free electron states. The problem is thus reduced to finding a partial-wave decomposition of the bound term.

The potential correction diagram is very similar to the one-potential part of the first-order vacuum polarization, see Fig. 4.1. From the expression Eq. (4.3) we can thus easily obtain (replacing $V_{\text{nuc}} \rightarrow -e\alpha^\sigma A_\sigma^{\text{ext}}$ and $S_F^{\text{free}} \rightarrow S_F^{\text{bou}}$)

$$\Delta E_{\text{bou}}^{\text{pc}} = 4\pi i \alpha \int d^3\mathbf{x}_1 \int d^3\mathbf{x}_2 \int d^3\mathbf{x}_3 \int_{-\infty}^{\infty} \frac{dz}{2\pi} \Phi_a^\dagger(\mathbf{x}_1) \boldsymbol{\alpha}^\nu \Phi_a(\mathbf{x}_1)$$

$$\begin{aligned}
& \times D_{\nu\mu}^F(\mathbf{x}_2 - \mathbf{x}_1, 0) \text{Tr} \left[\alpha^\mu S_F^{\text{bou}}(\mathbf{x}_2, \mathbf{x}_3, z) e \alpha^\sigma A_\sigma^{\text{ext}}(\mathbf{x}_3) S_F^{\text{bou}}(\mathbf{x}_3, \mathbf{x}_2, z) \right] \\
= & 4\pi i \alpha \int d^3 \mathbf{x}_1 \int d^3 \mathbf{x}_2 \int d^3 \mathbf{x}_3 \int \frac{d^3 \mathbf{k}}{(2\pi)^3} \frac{e^{i\mathbf{k} \cdot (\mathbf{x}_2 - \mathbf{x}_1)}}{k^2} \int_{-\infty}^{\infty} \frac{dz}{2\pi} \Phi_a^\dagger(\mathbf{x}_1) \alpha_\mu \Phi_a(\mathbf{x}_1) \\
& \times \sum_{t,u} \frac{\text{Tr} \left[\alpha^\mu \Phi_u(\mathbf{x}_2) \Phi_u^\dagger(\mathbf{x}_3) e \alpha^\sigma A_\sigma^{\text{ext}}(\mathbf{x}_3) \Phi_t(\mathbf{x}_3) \Phi_t^\dagger(\mathbf{x}_2) \right]}{[z - E_t(1 - i\eta)][z - E_u(1 - i\eta)]}. \quad (4.29)
\end{aligned}$$

Performing the trace and the z -integration, which gives contributions only for positive-negative pairs, yields

$$\begin{aligned}
\Delta E_{\text{bou}}^{\text{pc}} &= 8\pi\alpha \int \frac{d^3 \mathbf{k}}{(2\pi)^3} \frac{1}{k^2} \langle a | \alpha_\mu e^{-i\mathbf{k} \cdot \mathbf{x}_1} | a \rangle \\
& \times \sum_t^+ \sum_u^- \frac{\langle t | e^{i\mathbf{k} \cdot \mathbf{x}_2} \alpha^\mu | u \rangle \langle u | e \alpha^\sigma A_\sigma^{\text{ext}}(\mathbf{x}_3) | t \rangle}{E_t - E_u}, \quad (4.30)
\end{aligned}$$

where a factor of two is due to restricting t to be a positive energy state. Proceeding with the angular part of the \mathbf{k} -integration and using the expansion Eq. (3.42), we obtain

$$\begin{aligned}
\Delta E_{\text{bou}}^{\text{pc}} &= \frac{4\alpha}{\pi} \sum_l (2l+1) \int dk \langle a | \alpha_\mu j_l(kr_1) C^l | a \rangle \\
& \times \sum_t^+ \sum_u^- \frac{\langle t | j_l(kr_2) C^l \alpha^\mu | u \rangle \langle u | e \alpha^\sigma A_\sigma^{\text{ext}}(\mathbf{x}_3) | t \rangle}{E_t - E_u}. \quad (4.31)
\end{aligned}$$

By identifying the electron potential (cf. Eq. (2.16))

$$eA_\mu^{\text{el}}(\mathbf{x}_2) = -\frac{2\alpha}{\pi} \sum_{l=0}^{\infty} (2l+1) C^l(\hat{r}_2) \int dk j_l(kr_2) \langle a | \alpha_\mu j_l(kr_1) C^l(\hat{r}_1) | a \rangle, \quad (4.32)$$

we can write down the compact form

$$\Delta E_{\text{bou}}^{\text{pc}} = -2 \sum_t^+ \sum_u^- \frac{\langle t | e \alpha^\mu A_\mu^{\text{el}}(\mathbf{x}_2) | u \rangle \langle u | e \alpha^\sigma A_\sigma^{\text{ext}}(\mathbf{x}_3) | t \rangle}{E_t - E_u}. \quad (4.33)$$

Considering a scalar external potential (e.g., the Coulomb potential in the two-electron case) this expression becomes very similar to the one-potential term of the first-order case (Eq. (4.14)), and we can write down the Wichmann-Kroll contribution

$$\begin{aligned}
\Delta E_{\text{vp-sca}}^{\text{pc-wk}} &= -2 \sum_{|\kappa|=1}^{|\kappa_{\text{max}}|} (2j_\kappa + 1) \\
& \times \left\{ \sum_n^+ \sum_{n'}^- \frac{\langle n, \kappa | e A_0^{\text{el}}(r_2) | n', \kappa \rangle \langle n', \kappa | e A_0^{\text{ext}}(r_3) | n, \kappa \rangle}{E_{n,\kappa} - E_{n',\kappa}} \right. \\
& \left. - \sum_p^+ \sum_{p'}^- \frac{\langle p, \kappa | e A_0^{\text{el}}(r_2) | p', \kappa \rangle \langle p', \kappa | e A_0^{\text{ext}}(r_3) | p, \kappa \rangle}{E_{p,\kappa} - E_{p',\kappa}} \right\}, \quad (4.34)
\end{aligned}$$

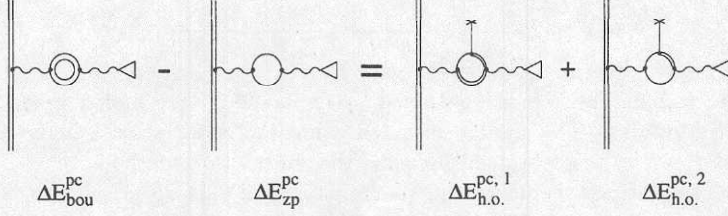


Figure 4.4: Rewriting the higher-order terms in terms of $\Delta E_{\text{bou}}^{\text{pc}}$ and $\Delta E_{\text{h.o.}}^{\text{pc},2}$.

where n, n' are bound and p, p' are free intermediate states. Here we have also used that the matrix indices μ, σ of Eq. (4.33) are connected such that $\mu = 0 \Leftrightarrow \sigma = 0$, i.e., only scalar-scalar or vector-vector interaction contributes.

For the vector case it is possible with non-diagonal terms, such that the two $|\kappa|$ -values can differ by one unit, and we obtain the Wichmann-Kroll contribution as

$$\begin{aligned}
 \Delta E_{\text{vp-vec}}^{\text{pc-wk}} &= -2 \sum_{|\kappa|=1}^{|\kappa_{\text{max}}|} \sum_{|\kappa'|=|\kappa|-1}^{|\kappa|+1} \\
 &\times \left\{ \sum_n^+ \sum_{n'}^- \frac{\langle n, \kappa, m | e\boldsymbol{\alpha} \cdot \mathbf{A}^{\text{el}}(\mathbf{x}_2) | n', \kappa', m' \rangle \langle n', \kappa', m' | e\boldsymbol{\alpha} \cdot \mathbf{A}^{\text{ext}}(\mathbf{x}_3) | n, \kappa, m \rangle}{E_{n, \kappa} - E_{n', \kappa'}} \right. \\
 &\left. - \sum_p^+ \sum_{p'}^- \frac{\langle p, \kappa, m | e\boldsymbol{\alpha} \cdot \mathbf{A}^{\text{el}}(\mathbf{x}_2) | p', \kappa', m' \rangle \langle p', \kappa', m' | e\boldsymbol{\alpha} \cdot \mathbf{A}^{\text{ext}}(\mathbf{x}_3) | p, \kappa, m \rangle}{E_{p, \kappa} - E_{p', \kappa'}} \right\} \quad (4.35)
 \end{aligned}$$

where the summation over m, m' is implicit.

The Wichmann-Kroll part can also be calculated in a more direct way by utilizing the identity pictured in Fig. 4.4. The contribution is then obtained by adding two finite parts instead of as the difference of two (separately divergent) terms. Assuming the partial-wave decomposition we can write

$$\begin{aligned}
 \Delta E_{\text{vp}}^{\text{pc-wk}} &= \Delta E_{\text{bou}}^{\text{pc}} - \Delta E_{\text{zp}}^{\text{pc}} \\
 &= \Delta E_{\text{h.o.}}^{\text{pc},1} + \Delta E_{\text{h.o.}}^{\text{pc},2} \\
 &= \sum_{s,p,u} \langle p | V_{\text{nuc}} | s \rangle \langle s | e\boldsymbol{\alpha}^\sigma A_\sigma^{\text{ext}} | u \rangle \langle u | e\boldsymbol{\alpha}^\mu A_\mu^{\text{el}} | p \rangle \times G(s, p, u) \\
 &\quad + \sum_{s,p,p'} \langle p | V_{\text{nuc}} | s \rangle \langle s | e\boldsymbol{\alpha}^\sigma A_\sigma^{\text{ext}} | p' \rangle \langle p' | e\boldsymbol{\alpha}^\mu A_\mu^{\text{el}} | p \rangle \times G(s, p, p'), \quad (4.36)
 \end{aligned}$$

where $|s\rangle, |u\rangle$ denote bound states and $|p\rangle, |p'\rangle$ free states. The function $G(\alpha, \beta, \gamma)$ describes the denominators for different signs on the intermediate states

$$\begin{aligned}
 G(+, +, +) &= 0, \\
 G(-, -, -) &= 0, \\
 G(+, +, -) &= \frac{1}{(E_\alpha - E_\gamma)(E_\beta - E_\gamma)},
 \end{aligned}$$

$$G(-, -, +) = -\frac{1}{(E_\gamma - E_\alpha)(E_\gamma - E_\beta)}. \quad (4.37)$$

The four remaining cases are obtained by replacing $\beta \leftrightarrow \gamma$ and $\alpha \leftrightarrow \gamma$ in the last two formulas. The results obtained using this calculation scheme agrees completely with those obtained by using the subtraction method.

The calculation scheme for the Wichmann-Kroll part discussed above gives generally unambiguous and finite results. Employing the nonrecoil point-dipole model for the hyperfine interaction yields, however, a divergent Wichmann-Kroll contribution. This is due to the singular $1/r^2$ dependence of the radial potential of that model. The origin of the divergence is the unphysical nature of the description of the nucleus. When considering an extended nuclear magnetization the divergence is absent and we can obtain finite results. The divergence occurs also when considering the Wichmann-Kroll correction to the measured nuclear magnetic moment, and we can cancel the divergence by combining the two effects, as will be discussed below.

4.2.3 Vacuum polarization correction to the nuclear magnetic moment

Similarly as for the electron g factor case, the Wichmann-Kroll effect gives a correction to the measured nuclear magnetic moment, see Fig. 4.5. This correction, as well as the WK potential correction to the hyperfine structure, diverges in the point-dipole hyperfine model. Cutting off the small distances leads to a logarithmic divergence in the cut-off radius. This logarithmic behavior is well known from calculations of the anomalous magnetic moment of the muon [48–50], and also from earlier treatments of the nuclear magnetic moment correction [51, 52].

In an external homogeneous magnetic field \mathbf{B} , described by the vector potential $\mathbf{A}^{\text{mag}} = -(\mathbf{r} \times \mathbf{B})/2$, the correction to the nuclear magnetic moment can be written as (assuming a $|\kappa|$ decomposition)

$$\Delta\mu_{\text{wk}} = -\frac{2\mu_{\text{bare}}}{g_I m_I \mu_N |\mathbf{B}|} \left\{ \sum_n^+ \sum_m^- \frac{\langle n | e\boldsymbol{\alpha} \cdot \mathbf{A}^{\text{mag}} | m \rangle \langle m | e\boldsymbol{\alpha} \cdot \mathbf{A}^{\text{hfs}} | n \rangle}{E_n - E_m} - \sum_p^+ \sum_q^- \frac{\langle p | e\boldsymbol{\alpha} \cdot \mathbf{A}^{\text{mag}} | q \rangle \langle q | e\boldsymbol{\alpha} \cdot \mathbf{A}^{\text{hfs}} | p \rangle}{E_p - E_q} \right\}, \quad (4.38)$$

where μ_{bare} is the bare magnetic moment, i.e., the unperturbed nuclear magnetic moment. This correction is included in the measured nuclear magnetic moment

$$\mu_{\text{exp}} = \mu_{\text{bare}} + \Delta\mu_{\text{wk}} = \mu_{\text{bare}}(1 + \epsilon), \quad (4.39)$$

and can not be separated out. In order to avoid double counting, the bare magnetic moment should be used when calculating the hyperfine structure. Specifically, one should correct for the shift in the magnetic moment when calculating the first-order hyperfine splitting

$$\Delta E_{\text{hfs}}^{1, \text{bare}} = \Delta E_{\text{hfs}}^{1, \text{exp}}(1 - \epsilon). \quad (4.40)$$

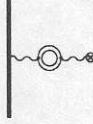


Figure 4.5: Feynman diagram representing the vacuum polarization correction to the nuclear magnetic moment. The filled line indicates the nuclear wavefunction and the crossed circle represents the interaction with the external homogeneous magnetic field.

This opens the possibility to “renormalize” the point-dipole divergency in the corrections Eqs. (4.35) and (4.40). We therefore employ the calculation scheme

$$\begin{aligned}
 \Delta E_{\text{vp}}^{\text{pc-wk-ren}} &= \Delta E_{\text{vp-hfs}}^{\text{pc-wk}} - \Delta E_{\text{hfs}}^{1,\text{exp}} \times \epsilon \\
 &= -2 \left\{ \sum_n^+ \sum_m^- \frac{\langle n | e\boldsymbol{\alpha} \cdot (\mathbf{A}^{\text{el}} - \beta \mathbf{A}^{\text{mag}}) | m \rangle \langle m | e\boldsymbol{\alpha} \cdot \mathbf{A}^{\text{hfs}} | n \rangle}{E_n - E_m} \right. \\
 &\quad \left. - \sum_p^+ \sum_q^- \frac{\langle p | e\boldsymbol{\alpha} \cdot (\mathbf{A}^{\text{el}} - \beta \mathbf{A}^{\text{mag}}) | q \rangle \langle q | e\boldsymbol{\alpha} \cdot \mathbf{A}^{\text{hfs}} | p \rangle}{E_p - E_q} \right\}, \tag{4.41}
 \end{aligned}$$

where $\beta = \Delta E_{\text{hfs}}^{1,\text{exp}} / (g_I m_I \mu_N |\mathbf{B}|)$. With this scheme the $1/r^2$ divergence is eliminated and we can obtain the combined effect of the Wichmann-Kroll correction to the hyperfine structure and to the nuclear magnetic moment.

It should be pointed out that we take the effect of the corrected magnetic moment into account only in the first-order hyperfine splitting, since it would lead to uncontrolled higher-order effects when applied to the QED corrections.

5 Numerical Procedure

5.1 Numerical solution of the Dirac equation

One major difficulty in bound-state QED is to construct accurate electron propagators and we shall in this section discuss how we achieve this. In the eigenfunction representation the propagator is given by

$$S_F(\mathbf{x}_2, \mathbf{x}_1, z) = \sum_s \frac{\Phi_s(\mathbf{x}_2)\Phi_s^\dagger(\mathbf{x}_1)}{z - E_s(1 - i\eta)} \quad (5.1)$$

where the sum is over the complete Dirac spectrum. The spectrum is obtained by using the method of discretization introduced by Salomonson and Öster [53], and we shall here briefly discuss the method and its properties.

The time-independent Dirac equation in the nuclear potential, $V(\mathbf{x}) = -e\phi_{\text{nuc}}(\mathbf{x})$, is given by

$$[\boldsymbol{\alpha} \cdot \mathbf{p} + \beta m + V(\mathbf{x})] \Phi_s(\mathbf{x}) = \begin{pmatrix} V(\mathbf{x}) + m & \boldsymbol{\sigma} \cdot \mathbf{p} \\ \boldsymbol{\sigma} \cdot \mathbf{p} & V(\mathbf{x}) - m \end{pmatrix} \Phi_s(\mathbf{x}) = E_s \Phi_s(\mathbf{x}).$$

For a spherically symmetric nuclear potential, $V = V(r)$, we can separate the Dirac spinor into an angular and a radial part as

$$\Phi_s(\mathbf{x}) = \begin{pmatrix} f_{n,\kappa}(r) \chi_\kappa^m(\hat{r}) \\ i g_{n,\kappa}(r) \chi_{-\kappa}^m(\hat{r}) \end{pmatrix} = \frac{1}{r} \begin{pmatrix} F_{n,\kappa}(r) \chi_\kappa^m(\hat{r}) \\ i G_{n,\kappa}(r) \chi_{-\kappa}^m(\hat{r}) \end{pmatrix}, \quad (5.2)$$

where $f_{n,\kappa}(r)$ and $g_{n,\kappa}(r)$ are the large and small radial components of the wave function, respectively, and $\chi_\kappa^m(\hat{r})$ is the ls -coupled spin-angular function. The Dirac equation then leads to the coupled radial equations

$$\begin{pmatrix} V(r) + m & -\frac{d}{dr} + \frac{\kappa}{r} \\ \frac{d}{dr} + \frac{\kappa}{r} & V(r) - m \end{pmatrix} \begin{pmatrix} F_{n,\kappa}(r) \\ G_{n,\kappa}(r) \end{pmatrix} = E_{n,\kappa} \begin{pmatrix} F_{n,\kappa}(r) \\ G_{n,\kappa}(r) \end{pmatrix} \quad (5.3)$$

which are solved by numerical discretization. The basic idea is to confine the atom in a large cavity and discretize the radial space into N grid points. In this way a corresponding $2N \times 2N$ symmetric matrix equation is obtained. The solution of this eigenvalue problem yields a complete set of $2N$ (N positive and N negative) orthogonal radial eigenvectors and corresponding real eigenvalues. The lowest lying positive energy states accurately reproduce the bound atomic states.

Using this approach it is easy to incorporate different models for the nuclear charge distribution and to vary the parameters of these models. We have in this work mainly used the point-, the uniform- and the Fermi-model in the

calculations but the discretization procedure sets no restriction on the choice of nuclear charge distribution. Setting $V = 0$ gives a complete set of numerical free electron states which are used to represent the free electron propagator. It is further straightforward to include additional model potentials in order to calculate higher-order effects.

Using different nuclear potentials will of course impose different boundary conditions at the inner limit of the box. Outside the box we use the constraint that the radial wave functions are forced to be zero. No observable discrepancy has been detected using this boundary condition. To get a good representation of the physical interactions near the nucleus the grid points are distributed exponentially. This implies that the high energy solutions are restricted to oscillate at the inner part of the box and they tend dramatically to zero at the outer part of the box. Empirically, this seems to cause no difficulties for bound state problems. The box size is chosen to be sufficiently large, not to affect the figures of interest. Usually it is sufficient to have a box size which covers the specific reference state.

To summarize, the method described seems to be a rigorous and practical way of constructing accurate electron propagators in an arbitrary potential.

5.1.1 Symmetrical spectrum method

When solving the discretized Dirac equation there might appear spurious states in the spectrum [53]. The spurious states are basically high-energy solutions which, due to the numerical problems of representing highly oscillating functions, appears in the low-energy part of the spectrum. This problem can be avoided by defining the large and small components of the wavefunction on alternating sites of the lattice. As a consequence we have to interpolate the wavefunctions whenever calculating matrix elements which connects the large and small components. The interpolation procedure will of course impair the numerical accuracy and this can lead to serious problems for contributions with slowly converging partial wave sums. By utilizing the inherent symmetries of the Dirac equation we can, however, avoid the interpolation.

From the Dirac equation Eq. (5.3) it follows that changing the sign of κ , E and $V(r)$ leads to the same equation if also F and G is interchanged. We can thus write down the relation

$$F_{\pm\kappa,\pm V}^{\pm E}(r) = G_{\mp\kappa,\mp V}^{\mp E}(r), \quad (5.4)$$

and this can be used to avoid interpolation. Consider for example the radial integral

$$\int dr h(r) [F_{n s_{1/2}}(r) G_{m p_{1/2}}(r) + G_{n s_{1/2}}(r) F_{m p_{1/2}}(r)], \quad (5.5)$$

where n , m are the principal quantum numbers and $h(r)$ is some potential. To evaluate this integral we now generate, with the discretization method, two separate $s_{1/2}$ spectra. One ordinary spectrum and one spectrum with reversed sign on the potential. For the latter we interchange the large and small components as well as the positive- and negative-energy solutions. This spectrum is now

used in Eq. (5.5) for the $p_{1/2}$ states and we can evaluate the integral without any interpolation, since the large (small) $p_{1/2}$ component is generated directly in the G (F) grid.

This procedure for generating radial wavefunctions has further important consequences for the calculation of vacuum polarization effects. Here it is essential to fulfill Furry's theorem, which states that the contribution of any closed free-electron loop with an odd number of vertices vanishes. Numerically this follows from a cancellation between positive and negative energy free-electron spectra for a given $|\kappa|$ value. To obtain the cancellation the numerical wavefunctions has to fulfill Eq. (5.4) exactly. In the method described above we make explicit use of Eq. (5.4) to obtain the wavefunctions and Furry's theorem is therefore automatically satisfied. This subject will be discussed in some more detail in Section 5.4.

5.2 Wavefunctions

We will in this section discuss the reference radial wavefunctions needed in the calculations. These are the wavefunctions in the matrix elements of the Self-energy and vacuum polarization operators, and the accuracy of their numerical representation is essential for the overall numerical uncertainty. Both coordinate and momentum space representation is needed.

5.2.1 The reference wavefunction

For a point nucleus the radial Dirac equation Eq. (5.3) can be solved analytically, and for the $1s$ -state we obtain the radial functions

$$\begin{aligned} f(r) &= \sqrt{\frac{1+\gamma}{2\Gamma(1+2\gamma)}} (2mZ\alpha)^{\gamma+\frac{1}{2}} r^{\gamma-1} e^{-mZ\alpha r} \\ g(r) &= \left(\frac{\gamma-1}{Z\alpha}\right) f(r), \end{aligned} \quad (5.6)$$

where $\gamma = \sqrt{1 - (Z\alpha)^2}$. When employing an extended nuclear model the radial equations have to be solved numerically and we do this by using the space-discretization method discussed in the previous section.

We need also the reference wavefunction in momentum space which is defined through

$$\Phi_a(\mathbf{p}) = \frac{1}{(2\pi)^{3/2}} \int d^3\mathbf{r} e^{-i\mathbf{p}\cdot\mathbf{r}} \Phi_a(\mathbf{r}) = \begin{pmatrix} P(p) \chi_{\kappa}^m(\hat{p}) \\ Q(p) \chi_{-\kappa}^m(\hat{p}) \end{pmatrix}, \quad (5.7)$$

with the radial components

$$\begin{aligned} P(p) &= \sqrt{\frac{2}{\pi}} (-i)^l \int dr r^2 j_l(pr) f(r) \\ Q(p) &= \sqrt{\frac{2}{\pi}} (-i)^{l-1} \int dr r^2 j_l(pr) g(r), \end{aligned} \quad (5.8)$$

where l and \bar{l} are the orbital angular momenta of the large and small components, respectively. Using a finite nuclear model these integrals has to be evaluated numerically and we do this by using Lagrange interpolation as discussed in Section 5.3.1. For the point nucleus we can obtain analytical forms for the momentum space wavefunctions as follows. The radial dependence of the wavefunctions in Eq. (5.6) and the explicit forms of $j_0(pr)$ and $j_1(pr)$ ($l = 0$ and $\bar{l} = 1$ for the 1s-state) implies that the Fourier integrals involve two types of integrals

$$\begin{aligned} \int_0^\infty dx x^a e^{-bx} \sin x &= \frac{\Gamma(a+1)}{(1+b^2)^{\frac{a}{2}+\frac{1}{2}}} \sin \left[(a+1) \arctan \left(\frac{1}{b} \right) \right], \\ \int_0^\infty dx x^a e^{-bx} \cos x &= \frac{\Gamma(a+1)}{(1+b^2)^{\frac{a}{2}+\frac{1}{2}}} \cos \left[(a+1) \arctan \left(\frac{1}{b} \right) \right]. \end{aligned} \quad (5.9)$$

Using these we obtain the following expressions for the radial wavefunctions in momentum space

$$\begin{aligned} P(p) &= \sqrt{\frac{1+\gamma}{\pi\Gamma(1+2\gamma)}} (2mZ\alpha)^{\gamma+\frac{1}{2}} \Gamma(\gamma+1) \\ &\quad \times \frac{p^{-\gamma-2}}{\left(1+\frac{m^2Z^2\alpha^2}{p^2}\right)^{\frac{\gamma}{2}+\frac{1}{2}}} \sin \left[(\gamma+1) \arctan \left(\frac{p}{mZ\alpha} \right) \right] \end{aligned} \quad (5.10)$$

and

$$\begin{aligned} Q(p) &= \left(\frac{\gamma-1}{Z\alpha} \right) \sqrt{\frac{1+\gamma}{\pi\Gamma(1+2\gamma)}} (2mZ\alpha)^{\gamma+\frac{1}{2}} \Gamma(\gamma) \\ &\quad \times \left\{ \frac{p^{-\gamma-2}}{\left(1+\frac{m^2Z^2\alpha^2}{p^2}\right)^{\frac{\gamma}{2}}} \sin \left[\gamma \arctan \left(\frac{p}{mZ\alpha} \right) \right] \right. \\ &\quad \left. - \frac{\gamma p^{-\gamma-2}}{\left(1+\frac{m^2Z^2\alpha^2}{p^2}\right)^{\frac{\gamma}{2}+\frac{1}{2}}} \cos \left[(\gamma+1) \arctan \left(\frac{p}{mZ\alpha} \right) \right] \right\}. \end{aligned} \quad (5.11)$$

5.2.2 The perturbed wavefunction

The reference wavefunction perturbed by an external potential is given by

$$|\delta a\rangle = - \sum_{t, E_t \neq E_a} \frac{|t\rangle \langle t | \alpha^\sigma e A_\sigma^{\text{ext}} | a \rangle}{E_a - E_t}, \quad (5.12)$$

where the summation is over the complete (non-degenerate) Dirac spectrum. This expression is, for extended nuclear models, evaluated by numerical integration of the external potential and explicit summation over the discretized Dirac spectrum. The momentum space wavefunction is further obtained by

numerical integration of Eqs. (5.8) using the Lagrange interpolation method (Section 5.3.1).

One of the largest uncertainties in our calculations stems from the zero- and one-potential wavefunction correction terms. These are (momentum space) matrix elements between the unperturbed and perturbed reference wavefunctions with the free-electron self-energy and vertex operators, see Section 3.2.1. Here it is desirable to improve the accuracy of the wavefunctions through a more analytical treatment. For the unperturbed wavefunction analytical forms can, for a point nucleus, be found as described above. Also for the perturbed wavefunction one can in the point nucleus case derive analytical expressions, and we will now describe a way to achieve this for the g factor and hyperfine interactions. A more general approach for this can be found in Refs. [54, 55].

The intermediate states $|t\rangle$ are eigenstates of the single-particle Hamiltonian $\hat{h}|t\rangle = E_t|t\rangle$, where \hat{h} is given in Eq. (5.3). We can thus write down the following equation for the perturbed wavefunction

$$\begin{aligned}
(E_a - \hat{h})|\delta a\rangle &= - \sum_{t, E_t \neq E_a} \frac{(E_a - \hat{h})|t\rangle\langle t|\alpha^\sigma e A_\sigma^{\text{ext}}|a\rangle}{E_a - E_t} \\
&= - \sum_{t, E_t \neq E_a} |t\rangle\langle t|\alpha^\sigma e A_\sigma^{\text{ext}}|a\rangle \\
&= - \sum_t |t\rangle\langle t|\alpha^\sigma e A_\sigma^{\text{ext}}|a\rangle + \sum_{t, E_t = E_a} |t\rangle\langle t|\alpha^\sigma e A_\sigma^{\text{ext}}|a\rangle \\
&= -\alpha^\sigma e A_\sigma^{\text{ext}}|a\rangle + \sum_{t, E_t = E_a} |t\rangle\langle t|\alpha^\sigma e A_\sigma^{\text{ext}}|a\rangle, \tag{5.13}
\end{aligned}$$

where we have completed the sum and used the completeness relation. For the corrections considered in this thesis $|\delta a\rangle$ has the same angular structure as $|a\rangle = |1s\rangle$. We therefore focus on the radial part of the equation and write

$$\begin{aligned}
(E_a - \hat{h}(r))|\delta a(r)\rangle &= -\alpha^\sigma e A_\sigma^{\text{ext}}(r)|a(r)\rangle + |a(r)\rangle\langle a(r)|\alpha^\sigma e A_\sigma^{\text{ext}}(r)|a(r)\rangle \\
&= -\alpha^\sigma e A_\sigma^{\text{ext}}(r)|a(r)\rangle - \Delta E_r^1|a(r)\rangle \\
&= [-\alpha^\sigma e A_\sigma^{\text{ext}}(r) - \Delta E_r^1]|a(r)\rangle, \tag{5.14}
\end{aligned}$$

where we have introduced $\Delta E_r^1 = -\langle a(r)|\alpha^\sigma e A_\sigma^{\text{ext}}(r)|a(r)\rangle$ for the radial part of the first-order energy in the external potential.

We will now briefly consider how to obtain the perturbed wavefunction in an external magnetic field. To simplify the notation we put the electron mass (m) equal to one in the following. The radial potential $A^{\text{mag}}(r) = r$ leads to

$$\Delta E_r^{1, \text{mag}} = 2 \int r^2 dr f_{1s}(r) r g_{1s}(r) = -\frac{2\gamma + 1}{2}, \tag{5.15}$$

and inserting this together with $E_{1s} = \gamma$ in Eq. (5.14) gives the differential equation

$$\begin{pmatrix} \gamma - 1 + \frac{Z\alpha}{r} & \frac{d}{dr} + \frac{1}{r} \\ -\frac{d}{dr} + \frac{1}{r} & \gamma + 1 + \frac{Z\alpha}{r} \end{pmatrix} \begin{pmatrix} F_{\delta 1s}(r) \\ G_{\delta 1s}(r) \end{pmatrix} = r \begin{pmatrix} G_{1s}(r) \\ F_{1s}(r) \end{pmatrix} + \frac{2\gamma + 1}{2} \begin{pmatrix} F_{1s}(r) \\ G_{1s}(r) \end{pmatrix} \tag{5.16}$$

By inserting the ansatz

$$\begin{aligned} F_{\delta 1s}(r) &= F_{1s}(r) \sum_n a_n r^n \\ G_{\delta 1s}(r) &= G_{1s}(r) \sum_n b_n r^n \end{aligned} \quad (5.17)$$

we obtain the coefficients

$$a_0 = b_0 = -\frac{2\gamma + 1}{2}, \quad (5.18)$$

and

$$\begin{aligned} a_1 &= \frac{2\gamma + 3}{2(\gamma + 1)} Z\alpha \\ b_1 &= \frac{2\gamma - 1}{2(\gamma - 1)} Z\alpha, \end{aligned} \quad (5.19)$$

and all other vanishes. The coefficients a_0, b_0 are found by orthogonalizing the solutions against the unperturbed wavefunctions. We can thus write the magnetic field perturbed wavefunction as

$$\begin{aligned} F_{\delta 1s}^{\text{mag}}(r) &= F_{1s}(r) \left[\frac{2\gamma + 3}{2(\gamma + 1)} Z\alpha r - \frac{2\gamma + 1}{2} \right] \\ G_{\delta 1s}^{\text{mag}}(r) &= G_{1s}(r) \left[\frac{2\gamma - 1}{2(\gamma - 1)} Z\alpha r - \frac{2\gamma + 1}{2} \right]. \end{aligned} \quad (5.20)$$

For the hyperfine interaction it is also necessary with a logarithmic term in the ansatz and this yields the functions

$$\begin{aligned} F_{\delta 1s}^{\text{hfs}}(r) &= F_{1s}(r) \frac{Z\alpha}{2\gamma - 1} \left[\frac{1}{Z\alpha r} + 2\gamma + 3 - \frac{3}{\gamma} + \frac{2}{\gamma} \Psi(2\gamma + 1) - 2Z\alpha r - \frac{2}{\gamma} \ln(2Z\alpha r) \right] \\ G_{\delta 1s}^{\text{hfs}}(r) &= G_{1s}(r) \frac{Z\alpha}{2\gamma - 1} \left[\frac{3}{Z\alpha r} + 2\gamma + 3 - \frac{1}{\gamma} + \frac{2}{\gamma} \Psi(2\gamma + 1) - 2Z\alpha r - \frac{2}{\gamma} \ln(2Z\alpha r) \right] \end{aligned} \quad (5.21)$$

where Ψ is the digamma function

$$\Psi(x) = \frac{d \ln \Gamma(x)}{dx} = \frac{\Gamma'(x)}{\Gamma(x)}. \quad (5.22)$$

Comparing Eqs. (5.20) and (5.21) we see that the perturbation of the magnetic field does not change the behavior at the boundary $r = 0$, whereas the hyperfine perturbation does. This fact leads to numerical difficulties when generating $|\delta a\rangle^{\text{hfs}}$ by explicit summation over the intermediates states t in Eq. (5.12). One then tries to represent the perturbed wavefunction by an expansion in $|ns\rangle$ states, which have a different functional form for small r .

The perturbed wavefunctions can be transformed to momentum space by using the formulas in Eq. (5.9). The only new thing is the logarithmic term in the hyperfine case, which leads to digamma functions.

5.3 Numerical implementation of the self-energy

The full expressions for the self-energy corrections contain divergent pieces which are identified by expanding the relevant electron propagators in the nuclear potential. The divergences will then be isolated in the lowest-order terms and can be cancelled analytically between different diagrams. This procedure is done working in momentum space and using dimensional regularization for the divergent integrals. The finite higher-order terms are then calculated in coordinate space by taking the difference between the full unrenormalized expression and the divergent parts in the expansion. We will here discuss in some detail how the numerical computations of the different parts are performed.

5.3.1 Many-potential terms

The many-potential terms of a given Feynman diagram are evaluated as the difference between the full expression and the lowest-order terms from the expansion of the electron propagator (zero- or zero- plus one-potential). All terms in the subtraction are computed simultaneously and in exactly the same way. The only difference is the potential used when generating the intermediate states (and energies) in the electron propagator. It is thus sufficient to discuss here the numerical implementation of the full expression for a particular contribution.

Focus now on the bound vertex correction, see Fig. 3.5

$$\begin{aligned} \Delta E_{se}^{ve} &= \frac{\alpha}{\pi} \sum_{l=0}^{\infty} (2l+1) \int k dk \\ &\times \sum_{u,t} \frac{\langle a | \alpha_{\mu} j_l(kr) C^l | u \rangle \langle u | e \alpha^{\nu} A_{\nu}^{ext} | t \rangle \langle t | j_l(kr') C^l \alpha^{\mu} | a \rangle}{[E_a - E_u - \text{sign}(E_u)k][E_a - E_t - \text{sign}(E_t)k]} \times F, \end{aligned} \quad (5.23)$$

where the function F is given by Eq. (3.84). The radial and the angular integrations are separated and the angular parts are treated analytically by using graphical angular momentum techniques [43, 56]. We will here focus on the radial part only.

For the case of a scalar external potential the intermediate states $|u\rangle$ and $|t\rangle$ in Eq. (5.23) must have the same angular symmetry. The vector potentials lead also to non-diagonal symmetries, such that the j -values for the intermediate states can differ by one unit. For these potentials we further have radial integrals between the large and small components of the wavefunctions. The accuracy of these non-diagonal terms is substantially increased by avoiding the grid interpolation through the use of the symmetrical spectrum method (Section 5.1.1).

The integration over k (photon momentum) is performed along the real axis and a general radial matrix element takes therefore the form

$$\langle a | j_l(kr) | u \rangle = \sum_i \int_{r_i}^{r_i+1} dr j_l(kr) [F_a(r)F_u(r) + G_a(r)G_u(r)] \quad (5.24)$$

where $|a\rangle$ and $|u\rangle$ are discrete numerical states and $j_l(kr)$ is a continuous spherical Bessel function. In calculating radiative effects we obtain important contri-

butions from a wide range of photon momenta. The Bessel functions oscillates strongly in the high momentum region and it is therefore not good enough to just sum up the discrete points in evaluating the integral. We therefore choose to interpolate the discrete numerical states to continuous space by using Lagrange polynomials in r . We can then, to a large extent, treat the Bessel functions analytically and the radial integrals can obtained with high accuracy. The numerical implementation of this procedure is performed as follows. The wavefunctions in square brackets in Eq. (5.24) are here denoted by $h(r)$ and we further introduce the notation (i) to refer to the specific interval $[r_i, r_{i+1}]$. The function $h(r)$ is now interpolated in this interval with the Lagrangian polynomial

$$h^{(i)}(r) = \sum_{j=i-2}^{i+3} h_j p_j^{(i)}(r), \quad (5.25)$$

where $h_j = h(r_j)$, and

$$p_j^{(i)}(r) = \sum_{m=0}^5 a_{j,m}^{(i)} r^m, \quad (5.26)$$

is a polynomial defined such that it takes the value 1 at the point j , and is zero in the remaining five gridpoints. The wavefunctions are thus interpolated by a fifth-order polynomial which depends on the values at two points before and after the interval (i) . A fifth-order polynomial is empirically found to be appropriate for this calculation. The integral over the interval (i) can now be written as

$$\int_{r_i}^{r_{i+1}} dr j_l(kr) h^{(i)}(r) = \sum_{j=i-2}^{i+3} h_j \sum_{m=0}^5 a_{j,m}^{(i)} \int_{r_i}^{r_{i+1}} dr j_l(kr) r^m. \quad (5.27)$$

From this expression it follows that the contribution to the total integral from the particular value h_n , is contained in the partial sum

$$\sum_{i=n-3}^{n+2} \int_{r_i}^{r_{i+1}} dr j_l(kr) h^{(i)}(r) = \sum_{i=n-3}^{n+2} \sum_{j=i-2}^{i+3} h_j \sum_{m=0}^5 a_{j,m}^{(i)} \int_{r_i}^{r_{i+1}} dr j_l(kr) r^m \quad (5.28)$$

and it is given by

$$h_n \sum_{s=n-3}^{n+2} \sum_{m=0}^5 a_{n,m}^{(s)} \int_{r_s}^{r_{s+1}} dr j_l(kr) r^m = h_n w_n \quad (5.29)$$

where w_n is the weight for h_n . The total integral is thus reduced to a sum over the discrete values of the wavefunctions times a weighting factor

$$\langle a | j_l(kr) | u \rangle = \sum_i w_i [F_a(r_i) F_u(r_i) + G_a(r_i) G_u(r_i)]. \quad (5.30)$$

The weights can be calculated once and for all in the chosen r - and k -grids for the relevant range of l -values. To achieve this we have to evaluate the integral

$$\int_{r_i}^{r_{i+1}} dr j_l(kr) r^m \quad (5.31)$$

for all combinations of m and l . We start with $m = l = 0$

$$\int_{kr_i}^{kr_{i+1}} dx j_0(x) = si(kr_{i+1}) - si(kr_i) \quad (5.32)$$

where $si(kr_i)$ is the sine integral which is evaluated numerically. This is the only integral which has to be calculated explicitly. The integrals with other combinations of m and l is obtained by using the following recursion relations

$$\begin{aligned} j_l(x) &= \left(\frac{l-1}{l}\right) j_{l-2}(x) - \left(\frac{2l-1}{l}\right) \frac{d}{dx} [j_{l-1}(x)] \\ x^{m+1} j_l(x) &= (l-m+1) x^m j_{l+1}(x) + \frac{d}{dx} [x^{m+1} j_{l+1}(x)] \\ j_l(x) &= \left(\frac{2l+3}{x}\right) j_{l+1}(x) - j_{l+2}(x). \end{aligned} \quad (5.33)$$

The next step is to perform the k -integration. Since this integration is performed along the real axis we have to perform principal-value integrals whenever a pole appears. Considering QED corrections to the atomic ground state, here $1s$ and $1s^2$, there are no poles, but for excited states both simple and double poles will appear. Special care must be taken when integrating over these poles in order to maintain the numerical accuracy. Consider now the case of a simple pole at $k = \omega$. The integral can then be written as

$$\int dk \frac{f(k)}{k - \omega} \quad (5.34)$$

where the numerator $f(k)$ is a discrete valued function in the chosen k -grid. In a similar manner as for the radial integrals, we use a Lagrange polynomial in $(k - k_i)$ to interpolate $f(k)$ to a continuous function. The integral above then reduces to a number of k -integrals which look like

$$\int_{k_i}^{k_{i+1}} dk \frac{(k - k_i)^m}{k - \omega}. \quad (5.35)$$

These integrals are easily evaluated analytically and the principal-value integrals are obtained with high accuracy. For the case of double poles we have instead the integral

$$\int dk \frac{f(k)}{(k - \omega)^2}. \quad (5.36)$$

By rewriting the numerator as $f(k) = f(\omega) + (f(k) - f(\omega))$, the double pole is isolated in the first term and the remainder is again of simple pole structure. The double pole can be integrated analytically and we obtain

$$\begin{aligned} \int_0^\infty dk \frac{f(k)}{(k - \omega)^2} &= \int_0^\mathcal{K} dk \frac{f(\omega)}{(k - \omega)^2} + \int_0^\mathcal{K} dk \frac{f(k) - f(\omega)}{(k - \omega)^2} + \int_\mathcal{K}^\infty dk \frac{f(k)}{(k - \omega)^2} \\ &= \frac{f(\omega)\mathcal{K}}{\omega(\omega - \mathcal{K})} + \int_0^\mathcal{K} dk \frac{f(k) - f(\omega)}{(k - \omega)^2} + \int_\mathcal{K}^\infty dk \frac{f(k)}{(k - \omega)^2}, \end{aligned} \quad (5.37)$$

where the integration limit \mathcal{K} is defined such that all possible poles lies in the interval $[0, \mathcal{K}]$. The second term is calculated using the scheme for simple poles outlined above and the last term, together with all other pole free k -integrations, is computed using Gauss-Legendre and Gauss-Laguerre quadrature.

The calculation procedure discussed above is now executed for different numbers of radial grid points N for each given partial wave (l -value). The values obtained are then grid extrapolated to $N = \infty$. We evaluate several partial waves, the maximum number of l depending on the convergence properties of the given contribution, and finally we extrapolate to $l = \infty$ to obtain the finite remainder. We typically use five grids in the range of 300 – 500 radial grid points and evaluate partial wave terms up to $l = 20$.

A main problem with the discussed numerical approach is to obtain high numerical accuracy for high-energy photons. The radial integral of a highly oscillating numerical state and a high frequency Bessel function, is causing a slow convergence in the number of radial grid points. A way to handle this problem is to subtract a counter term which has a similar high-energy dependence. By performing the integrations for the main term and the counter term in exactly the same way, a numerically stable difference can be obtained. In the case of the wavefunction correction the subtracted zero- and one-potential terms acts as natural counter terms (see Eq. (3.38)). For the vertex and binding energy corrections it is sufficient to subtract the zero-potential terms in order to obtain the finite many-potential term (Eq. (3.80)). Here it is, however, possible to improve the numerical accuracy by subtracting also the one-potential terms (Eq. (3.81)), which contain high-energy parts. The one-potential terms of course have to be re-added. This separate calculation of the one-potential terms can be performed semi-analytically, with the radial integrations evaluated analytically. This procedure has so far only been elaborated for the g -factor calculation and its numerical implementation will be discussed in the next section.

5.3.2 Zero- and one-potential terms

The zero- and one-potential terms are calculated in momentum space and involves the matrix elements of the renormalized free-electron vertex and self-energy operators (see Chapter 3). We start with the wavefunction and binding-energy corrections which can be treated generally, without reference to the specific type of external potential in which the corrections are evaluated.

Wavefunction Correction

The zero-potential part of the wavefunction correction (Fig. 3.4) is in momentum space given by

$$\Delta E_{zp}^{\text{wf}} = \int d^3\mathbf{p} \Phi_a^\dagger(\mathbf{p}) \gamma^0 \Sigma_{\text{ren}}^{\text{mass}}(p) \Phi_{\delta a}(\mathbf{p}), \quad (5.38)$$

where $\Phi_{\delta a}(\mathbf{p})$ is perturbed by some external potential. The angular integrations are performed analytically and we are left with the radial integral

$$\Delta E_{zp}^{\text{wf}} = \int dp p^2 [A(p)a(\rho) + B(p)b(\rho)], \quad (5.39)$$

where $a(\rho)$, $b(\rho)$ and $A(p)$, $B(p)$ are given by Eqs. (3.30), (3.31) and (3.33). The radial wavefunctions are transformed to momentum space by the methods described earlier and the final radial integral in Eq. (5.39) is performed using Gauss-Legendre quadrature.

The one-potential part is given by the integral

$$\Delta E_{\text{op}}^{\text{wf}} = \int d^3\mathbf{p} d^3\mathbf{p}' \Phi_a^\dagger(\mathbf{p}) \gamma_0 [\gamma_0 f_1(p, p', \cos \vartheta) + \not{p} f_2(p, p', \cos \vartheta) + \not{p}' f_3(p, p', \cos \vartheta) + \not{p} \gamma_0 \not{p}' f_4(p, p', \cos \vartheta) + f_5(p, p', \cos \vartheta)] V_{\text{nuc}}(\mathbf{q}) \Phi_{\delta a}(\mathbf{p}'), \quad (5.40)$$

where the f_i -functions are abbreviations for the coefficient functions of the vertex operator Λ_0 (Eq. (3.27)), and where $V_{\text{nuc}}(\mathbf{q})$ is the Fourier-transformed nuclear potential ($\mathbf{q} = \mathbf{p} - \mathbf{p}'$). The angular dependence of the wavefunctions can be reduced to a dependence on the intermediate angle and we can write

$$\Delta E_{\text{op}}^{\text{wf}} = 2\pi \int dp p^2 \int dp' p'^2 \int d\vartheta \sin \vartheta h(p, p', \cos \vartheta) V_{\text{nuc}}(\mathbf{q}) \quad (5.41)$$

where $h(p, p', \cos \vartheta)$ is given by Eq. (3.37). To obtain the nuclear potential in momentum space for arbitrary extended nuclear models we use the relation

$$(2\pi^2) V_{\text{nuc}}^{\text{ext}}(\mathbf{q}) = -\frac{Z\alpha}{q^2} + \int_0^{R_{\text{nuc}}} dr r^2 j_0(qr) \left[V_{\text{nuc}}^{\text{ext}}(r) - \left(-\frac{Z\alpha}{r} \right) \right], \quad (5.42)$$

which is valid since the extended and point nuclear potentials differ only inside the nuclear radius R_{nuc} (using that $1/r$ transforms into $1/q^2$). The one-potential part can now be rewritten in the following way

$$\Delta E_{\text{op}}^{\text{wf}} = \int_0^\infty dp \int_0^\infty dp' \int_{-1}^1 dz \frac{\tilde{h}(p, p', z)}{q^2} \quad (5.43)$$

where we have separated out the Coulomb singularity $1/q^2$, and changed variable $z = \cos \vartheta$. The integrable Coulomb singularity is handled by the variable transformations suggested by Blundell [27]. Changing the variables in Eq. (5.43) according to

$$\begin{aligned} v &= -\frac{1}{2pp'} \ln(q^2) = -\frac{1}{2pp'} \ln(p^2 + p'^2 - 2pp'z) \\ x &= p + p' \\ y &= p - p' \end{aligned} \quad (5.44)$$

and using the symmetry under $y \rightarrow -y$, the integral becomes

$$\int_0^\infty dx \int_0^x dy \int_{v_{\text{min}}}^{v_{\text{max}}} dv \tilde{h} \left(\frac{x+y}{2}, \frac{x-y}{2}, z(x, y, v) \right) \quad (5.45)$$

where

$$\begin{aligned} v_{\text{min}} &= -\frac{1}{pp'} \ln(x) \\ v_{\text{max}} &= -\frac{1}{pp'} \ln(y). \end{aligned} \quad (5.46)$$

We still have a singularity in the y -integration as $y \rightarrow 0$, which is removed with the substitution

$$s = y \ln \left(\frac{y}{x} \right) - y \quad (5.47)$$

for small y -values ($0 \leq y \leq x/10$). Since the coefficient functions (C_{ij}) of the vertex operator are defined through one-dimensional integrals (see Appendix D), the total expression for the one-potential part is a four-dimensional integral. All of these four integrals are computed using Gauss-Legendre quadrature.

Binding-energy correction

The momentum space expression for the zero-potential binding-energy correction, Fig. 3.5, is given by

$$\Delta E_{zp}^{be} = \Delta E_a^1 \times \int d^3 \mathbf{p} \Phi_a^\dagger(\mathbf{p}) \gamma^0 \left[\frac{\partial}{\partial E} \Sigma^{\text{free}}(\mathbf{p}, E) \right]_{E=E_a} \Phi_a(\mathbf{p}), \quad (5.48)$$

where ΔE_a^1 is the first-order energy in the given external potential. The evaluation of the binding-energy correction is very similar to the zero-potential wavefunction part and follow the same scheme. After angular integrations we have the radial integral

$$\Delta E_{zp}^{be} = \Delta E_a^1 \times \int dp p^2 \left[\tilde{A}(p) \frac{\partial a(\rho)}{\partial E} + \tilde{B}(p) \frac{\partial b(\rho)}{\partial E} + \tilde{C}(p) b(\rho) \right]_{E=E_a}, \quad (5.49)$$

where the functions in the square bracket are given by Eqs. (3.53) and (3.54). The radial p -integration is again computed with Gauss-Legendre quadrature.

Vertex correction

For the case of a scalar external potential, the zero-potential vertex correction is identical to the one-potential part of the wavefunction correction discussed above. Just replace the nuclear potential with the external potential and use unperturbed reference wavefunctions in those expressions.

Consider now the zero-potential part of the vertex correction for a external vector potential, see Section 3.2.2. All terms of the vertex correction (Eqs. (3.58) and (3.73)-(3.79)) are treated in the same manner and we will here focus on the first of those terms for a general ($K = 1$) vector interaction

$$\Delta E_{zp,1}^{ve} = 2C^{\text{int}} \frac{\alpha}{4\pi} \int dp p^2 \int dp' p'^2 P(p) Q(p') \left[p' V_{1,0}^{\text{int}}(p, p') - p V_{1,1}^{\text{int}}(p, p') \right], \quad (5.50)$$

where the extra factor of 2 comes from the two identical terms in the original expression Eq. (3.58). The expansion coefficients are given by (cf. Eq. (B.15))

$$V_{1,k}^{\text{int}}(p, p') = \frac{1}{2} \int_{-1}^1 dz V_1^{\text{int}}(p, p', z) P_k(z), \quad (5.51)$$

where we have for the different interaction types

$$\begin{aligned}
 V_1^{\text{breit}}(p, p', z) &= f_1(p, p', z) \frac{1}{|\mathbf{p} - \mathbf{p}'|^3} \int dr r^2 j_1(|\mathbf{p} - \mathbf{p}'|r) f(r) g(r) , \\
 V_1^{\text{hfs}}(p, p', z) &= f_1(p, p', z) \frac{1}{|\mathbf{p} - \mathbf{p}'|^2} , \\
 V_1^{\text{mag}}(p, p', z) &= f_1(p, p', z) e^{-(|\mathbf{p} - \mathbf{p}'|/\rho)^2} .
 \end{aligned} \tag{5.52}$$

Recall that the f_1 -function is a abbreviation for the coefficient functions of the vertex operator and that $z = \cos \vartheta$ where ϑ is the angle between \mathbf{p} and \mathbf{p}' .

All the interaction potentials peaks at $\mathbf{q} = \mathbf{p} - \mathbf{p}' = \mathbf{0}$, i.e. at $p = p'$ and $z = 1$, and the major part of the total contribution comes from this region of zero momentum transfer. All numerical grids are therefore adjusted in order to get a good representation in the vicinity of that region. The potential from the external magnetic field is the most singular and for this case it is particularly important to be careful around the point $\mathbf{q} = \mathbf{0}$. Consider for example the following cancellation problem. Using $P_0(z) = 1$ and $P_1(z) = z$ we write the contribution as

$$\begin{aligned}
 \Delta E_{zp,1}^{\text{ve}} &= C^{\text{int}} \frac{\alpha}{4\pi} \int d\mathbf{p} p^2 \int d\mathbf{p}' p'^2 \int_{-1}^1 dz P(p) Q(p') V_1^{\text{int}}(p, p', z) [p' - pz] \\
 &= C^{\text{int}} \frac{\alpha}{4\pi} \int d\mathbf{p} p^2 \int d\mathbf{p}' p'^2 \int_{-1}^1 dz P(p) Q(p') \\
 &\quad \times V_1^{\text{int}}(p, p', z) [(p' - p) + p(1 - z)] .
 \end{aligned} \tag{5.53}$$

In the interesting region we see that there is a numerical cancellation problem in the second term, due to the very narrow peak of $V_1^{\text{int}}(p, p', z)$ at $z = 1$. To avoid numerical loss of figures close to this point we change variable $s = 1 - z$ which leads to a direct integration of the important region ($s \approx 0$).

One-potential vertex and binding-energy terms

In this section we will discuss the implementation of the semi-analytical treatment of the one-potential vertex and binding-energy terms (see Fig. 3.8). The implementation of the binding-energy part is identical to that for the vertex part, and we will here focus on the latter. The one-potential parts has further the same angular structure as the corresponding bound terms and we will thus concentrate on the radial parts only. We therefore write down the simplified form

$$\begin{aligned}
 \Delta E_{\text{op}}^{\text{ve}} &\propto \sum_{l=0}^{\infty} (2l+1) \int_0^{\infty} dk k^2 \int d^3\mathbf{t} \int d^3\mathbf{u} \int d^3\mathbf{v} \int d^3\mathbf{p} \int d^3\mathbf{p}' G(t, u, v) \\
 &\quad \times \langle a|p\rangle \langle p|j_l(kr)|t\rangle \langle t|\alpha^\alpha A_\alpha^{\text{ext}}|u\rangle \langle u|V_{\text{nuc}}|v\rangle \langle v|j_l(kr')|p'\rangle \langle p'|a\rangle ,
 \end{aligned} \tag{5.54}$$

where we have expanded the bound reference states in terms of free states. We will divide the above expression into different parts and consider them separately.

The overlap $\langle a|p\rangle$, is a radial integral between a numerical discrete bound state and a continuous analytical spherical Bessel function (see Appendix F)

$$\begin{aligned} \langle a|p\rangle = & \int dr \left\{ F_a^{\text{num}}(r) \sqrt{\frac{E_p + m}{\pi E_p}} pr j_{l'}(pr) \right. \\ & \left. + G_a^{\text{num}}(r) \sqrt{\frac{E_p - m}{\pi E_p}} pr j_{l''}(pr) \right\}, \end{aligned} \quad (5.55)$$

where $E_p = \pm\sqrt{p^2 + m^2}$ is the energy of the free electron. For a point nucleus the integral can be done analytically and otherwise we use the Lagrange interpolation procedure discussed above. The overlap function is stored in a preassigned momentum grid and is later interpolated to any choice of momentum. The overlap function peaks at $p \approx Z$, where Z is the nuclear charge, which require a large number of points to represent the steep behavior. Apart from this peak it is well behaved and the asymptotic tail falls off roughly as the inverse cube of the momentum.

The next part is the ‘‘side’’ radial matrix element, which in the case of a $s_{1/2}$ -reference function is given by

$$\begin{aligned} \langle p|j_l(kr)|t\rangle = & \sqrt{\frac{E_p + m}{\pi E_p}} \sqrt{\frac{E_t + m}{\pi E_t}} pt \int dr r^2 j_0(pr) j_l(kr) j_l(tr) \\ & + \sqrt{\frac{E_p - m}{\pi E_p}} \sqrt{\frac{E_t - m}{\pi E_t}} pt \int dr r^2 j_1(pr) j_l(kr) j_{l\pm 1}(tr), \end{aligned} \quad (5.56)$$

where we have used that the sum of the three characteristic l -values of the Bessel functions must be an integer to give a non-vanishing contribution. To calculate the radial matrix element, we follow a scheme originally outlined by Quiney and Grant [32]. The basic skeleton we use is the integral taken from the table by Prudnikov *et al* [57]

$$\begin{aligned} \int_0^\infty dr r^{2-l'} j_{l'}(pr) j_l(kr) j_l(tr) = & \\ & \begin{cases} \frac{\pi}{4pkt} \left(\frac{kt}{p}\right)^{l'} \sin^{l'}(\theta_1) P_l^{-l'}(\cos\theta_1), & |p-t| \leq k \leq p+t \\ 0, & \text{otherwise} \end{cases} \end{aligned} \quad (5.57)$$

where $\cos(\theta_1) = \frac{k^2 + t^2 - p^2}{2kt}$ and where $P_l^m(x)$ are the associated Legendre functions of the first kind. It is also convenient to introduce the recursion relation

$$j_{l+1}(x) = \frac{(2l+1)}{x} j_l(x) - j_{l-1}(x). \quad (5.58)$$

When the reference state has the angular symmetry $j = 1/2$ ($s_{1/2}, p_{1/2}$) there will be two types of radial integrals to evaluate. This is also the true when we

evaluate the vector part α . The two types are

$$\begin{aligned} I_1(l, l) &= \frac{4kpt}{\pi} \int_0^\infty dr r^2 j_0(pr) j_l(kr) j_l(tr), \\ I_2(l, l \pm 1) &= \frac{4kpt}{\pi} \int_0^\infty dr r^2 j_1(pr) j_l(kr) j_{l \pm 1}(tr). \end{aligned} \quad (5.59)$$

To evaluate $I_1(l, l)$ we use Eq. (5.57) with $l' = 0$ which yields

$$I_1(l, l) = P_l^0(\cos\theta_1). \quad (5.60)$$

The Legendre functions are readily evaluated using the standard recursion relation

$$(l - m + 1)P_{l+1}^m(x) = (2l + 1)xP_l^m(x) - (l - m)P_{l-1}^m(x), \quad (5.61)$$

which is stable in the direction of increasing l , with the subsidiary condition $l + m \geq 0$. Furthermore, to evaluate $I_2(l, l \pm 1)$ we employ the recursion relation in Eq. (5.58) which yields

$$\begin{aligned} I_2(l, l + 1) &= \frac{4pkt(2l + 1)}{\pi t} \int dr r j_1(pr) j_l(kr) j_l(tr) - I_2(l, l - 1) \\ &= \frac{(2l + 1)k}{p} \sin(\theta_1) P_l^{-1}(\cos\theta_1) - I_2(l, l - 1) \end{aligned} \quad (5.62)$$

where Eq. (5.57) is used with $l' = 1$. In a similar way we obtain

$$I_2(l + 1, l) = \frac{(2l + 1)t}{p} \sin(\theta_1) P_l^{-1}(\cos\theta_1) - I_2(l - 1, l). \quad (5.63)$$

By combining both these recursion relations and using the starting value $I_2(0, 1) = P_1^0(\cos\theta_1)$ all needed integrals can be evaluated.

Consider now the matrix element of the nuclear potential for a point nucleus

$$\begin{aligned} \langle u | V_{\text{nuc}}(r) | v \rangle &= \sqrt{\frac{E_u + m}{\pi E_u}} \sqrt{\frac{E_v + m}{\pi E_v}} uv \int dr r^2 j_l(u r) \left(-\frac{Z\alpha}{r} \right) j_l(v r) \\ &\quad + \sqrt{\frac{E_u - m}{\pi E_u}} \sqrt{\frac{E_v - m}{\pi E_v}} uv \int dr r^2 j_l(u r) \left(-\frac{Z\alpha}{r} \right) j_l(v r). \end{aligned} \quad (5.64)$$

To evaluate this integral we use the general formula taken from [58]

$$\begin{aligned} \int_0^\infty dx J_\nu(px) J_\mu(p'x) x^{-\lambda} &= \frac{p^\nu}{2^\lambda p'^{\nu-\lambda+1}} \frac{\Gamma(\frac{\nu+\mu-\lambda+1}{2})}{\Gamma(\nu+1)\Gamma(\frac{\mu-\nu+\lambda+1}{2})} \\ &\quad \times F\left(\frac{\nu+\mu-\lambda+1}{2}, \frac{\nu-\mu-\lambda+1}{2}; \nu+1; \frac{p^2}{p'^2}\right), \end{aligned} \quad (5.65)$$

for $p' > p$, and

$$\int_0^\infty dx J_\nu(px) J_\mu(p'x) x^{-\lambda} = \frac{p^\mu}{2^\lambda p^{\mu-\lambda+1}} \frac{\Gamma(\frac{\nu+\mu-\lambda+1}{2})}{\Gamma(\mu+1)\Gamma(\frac{\nu-\mu+\lambda+1}{2})} \times F\left(\frac{\nu+\mu-\lambda+1}{2}, \frac{\mu-\nu-\lambda+1}{2}; \mu+1; \frac{p'^2}{p^2}\right), \quad (5.66)$$

for $p > p'$. Here $J_{n+1/2}(x) = \sqrt{\frac{2x}{\pi}} j_n(x)$ is a cylindrical Bessel function and $F(\alpha, \beta; \gamma; z)$ is the hypergeometric function

$$F(\alpha, \beta; \gamma; z) = \sum_{n=0}^{\infty} \frac{(\alpha+n-1)!(\beta+n-1)!(\gamma-1)!}{(\alpha-1)!(\beta-1)!(\gamma+n-1)!n!} z^n. \quad (5.67)$$

At $u = v$ we encounter the integrable Coulomb singularity and we handle this in the following way. Consider the part for the $G(+, +, +)$ case (refer to Chapter 3)

$$\begin{aligned} B_l(k, u) &= \int dv \int dp' \frac{\langle u | V_{\text{nuc}} | v \rangle \langle v | j_l(kr') | p' \rangle \langle p' | a \rangle}{[E_a - E_u - k][E_a - E_v - k]} \\ &= \int dv \langle u | V_{\text{nuc}} | v \rangle h_l(k, v, u), \end{aligned} \quad (5.68)$$

where we have defined

$$h_l(k, v, u) = \int dp' \frac{\langle v | j_l(kr') | p' \rangle \langle p' | a \rangle}{[E_a - E_u - k][E_a - E_v - k]}. \quad (5.69)$$

We now rewrite the v -integral as follows

$$\begin{aligned} B_l(k, u) &= \int dv \langle u | V_{\text{nuc}} | v \rangle [h_l(k, v, u) - h_l(k, u, u)] \\ &\quad + h_l(k, u, u) \int dv \langle u | V_{\text{nuc}} | v \rangle. \end{aligned} \quad (5.70)$$

The difference $h_l(k, v, u) - h_l(k, u, u)$ goes fast enough to zero in the limit $u \rightarrow v$ and the last term can be evaluated analytically.

The treatment of the matrix element of the external potential depends on the interaction type considered. In the hyperfine case we can use integrals similar to Eqs. (5.65) and (5.66) to evaluate the matrix element. In the g factor and two-electron case we instead transform the interaction potential into momentum space, in order to obtain integrals of the form

$$\begin{aligned} \langle t | \alpha^\alpha A_\alpha^{\text{ext}}(\mathbf{r}) | u \rangle &= \langle t | \int d^3 \mathbf{q} e^{i\mathbf{q}\cdot\mathbf{r}} \alpha^\alpha A_\alpha^{\text{ext}}(\mathbf{q}) | u \rangle \\ &\propto \int q^2 dq A^{\text{ext}}(q) \langle t | j_l(qr) | u \rangle. \end{aligned} \quad (5.71)$$

The radial integral has the structure of Eq. (5.57) and the q -integration is performed numerically.

The general calculation scheme is ordered in the following way. First the p and p' integrations are performed and then we define the parts (considering here the $G(+, +, +)$ combination)

$$\begin{aligned} A_l(k, u) &= \int dt \int dp \frac{\langle a|p\rangle \langle p|j_l(kr)|t\rangle \langle t|\alpha^\sigma A_\sigma^{\text{ext}}|u\rangle}{2k[E_a - E_t - k]}, \\ B_l(k, u) &= \int dv \int dp' \frac{\langle u|V_{\text{nuc}}|v\rangle \langle v|j_l(kr')|p'\rangle \langle p'|a\rangle}{[E_a - E_u - k][E_a - E_v - k]}. \end{aligned} \quad (5.72)$$

The total contribution is then given by

$$\Delta E_{\text{op}}^{\text{ve}} \propto \sum_{l=0}^{\infty} (2l+1) \int_0^\infty dk k^2 \int du A_l(k, u) B_l(k, u). \quad (5.73)$$

This separation is possible for most cases of denominators but not for all. In those cases where t and v have different signs there are denominators which couple these two outermost momenta, and the scheme above can not be used. However, in the g factor case we could still use the above separation by utilizing the fact that the matrix element in Eq. (5.71) contributes only in a small region around $t = u$.

5.4 Numerical implementation of the vacuum polarization

The numerical calculation of the Uehling parts is straightforward and we will here concentrate on the Wichmann-Kroll contributions. The calculation scheme is further identical for all Wichmann-Kroll corrections considered in this thesis. Focus now on the correction to the interaction line, see Fig. 4.3, which is given by the subtraction

$$\begin{aligned} \Delta E_{\text{vp}}^{\text{pc-wk}} &= \frac{4\alpha}{\pi} \sum_{l=0}^{\infty} (2l+1) \int dk \langle a|\alpha_\mu j_l(kr_1)\mathbf{C}^l|a\rangle \\ &\times \left\{ \sum_t^+ \sum_u^- \frac{\langle t|\alpha^\mu j_l(kr_2)\mathbf{C}^l|u\rangle \langle u|e\alpha^\sigma A_\sigma^{\text{ext}}(\mathbf{x}_3)|t\rangle}{E_t - E_u} \right. \\ &\quad \left. - \sum_p^+ \sum_q^- \frac{\langle p|\alpha^\mu j_l(kr_2)\mathbf{C}^l|q\rangle \langle q|e\alpha^\sigma A_\sigma^{\text{ext}}(\mathbf{x}_3)|p\rangle}{E_p - E_q} \right\}, \end{aligned} \quad (5.74)$$

where $|t\rangle$, $|u\rangle$ denotes bound intermediate states and $|p\rangle$, $|q\rangle$ the corresponding free states. The numerical evaluation of this expression is very similar to the computation of the self-energy many-potential terms. The angular part is calculated separately using angular diagram techniques. The radial integrations are performed exactly as in the self-energy case and the k -integration is done using Gauss-Legendre quadrature. Also in the direct calculation of the Wichmann-Kroll parts, without the subtraction scheme, the same numerical procedure is used.

There is one ambiguity which has to do with the numerical spectra we use. According to Furry's theorem any closed free-electron loop with an odd number

of vertices vanishes. Numerically this has to do with a cancellation between the positive and negative energy free electron spectra, due to the complete symmetry of those spectra, for a given $|\kappa|$ value. To be specific, consider the zero-potential term in the vacuum polarization potential

$$U_{\text{zp}}^{\text{vp}}(r) = -\frac{\alpha}{\pi} \int_0^\infty dk j_0(kr) \sum_{q,\kappa} (2j_\kappa + 1) \text{sgn}(E_{q,\kappa}) \langle q, \kappa | j_0(kr') | q, \kappa \rangle, \quad (5.75)$$

which is Eq. (4.12) with free intermediate electron states $|q, \kappa\rangle$. The radial integral will for $|\kappa| = 1$ contain the terms

$$\begin{aligned} & \sum_q \int dr' j_0(kr') \left\{ \left[F_{qs_{1/2}}^2(r') + G_{qs_{1/2}}^2(r') \right] + \left[F_{qp_{1/2}}^2(r') + G_{qp_{1/2}}^2(r') \right] \right. \\ & \quad \left. - \left[F_{-qs_{1/2}}^2(r') + G_{-qs_{1/2}}^2(r') \right] - \left[F_{-qp_{1/2}}^2(r') + G_{-qp_{1/2}}^2(r') \right] \right\}, \quad (5.76) \end{aligned}$$

where $-q$ denotes the principal quantum number in the negative energy continuum. Due to the relation Eq. (5.4) the first square bracket term will cancel against the last term and similarly the second square bracket term will cancel the third term. Such cancellations will occur for each $|\kappa|$ value and the zero-potential term will thus vanish completely.

In a similar manner there are numerical cancellations (but not exact) for the main term, with bound intermediate states, for a given $|\kappa|$ value. To correctly obtain these cancellations numerically, one has to be very careful with the boundary conditions of the radial grid, such that the wavefunctions exactly fulfill the symmetry relation Eq. (5.4). This was not achieved completely in Paper IV where this problem was handled by numerically subtracting the zero-potential term (Eq. (5.75)) from the main term. The zero-potential term should then be re-added calculated analytically, but this is just exactly zero. This procedure resulted in a stable and accurate evaluation of the Wichmann-Kroll contribution.

This subtraction procedure can be avoided by using the symmetrical spectrum method described in Section 5.1.1. Here we utilize the symmetry relation Eq. (5.4) explicitly to obtain the radial wavefunctions within a given $|\kappa|$ value. Furry's theorem is then fulfilled identically also numerically and we obtain the correct cancellations in the main term.

These two approaches gives, to the relevant accuracy, exactly the same numerical results. We have here discussed the procedures to correctly obtain the the Furry theorem cancellations for the vacuum polarization potential. The argumentation is valid also for the vacuum polarization correction on the interaction line, but here it is instead the terms with an odd number of nuclear Coulomb interactions which should vanish, see Fig. 4.3.

6 Numerical Results and Discussion

"It's more fun to compute"

Kraftwerk

We will in this chapter present our numerical results for the one-photon radiative corrections to the different effects studied in this thesis, i.e., the electron-electron interaction, the Zeeman effect and the hyperfine splitting. These different calculations will be discussed separately in sections 6.1, 6.2 and 6.3, respectively. The results presented here are meant to supplement the results given in the articles appended to this thesis. The hyperfine structure calculation is given in Paper I, the g factor investigation in Paper II and the study of the two-electron corrections is found in Paper III. The calculations cover the range of nuclear charges from $Z = 1$ up to hydrogenlike and heliumlike uranium, $Z = 92$. In the low- Z region we compare our numerical results with the known parts of $(Z\alpha)$ -expansions. We find excellent agreement between the two approaches. Experimental studies have been carried out on the two-electron contribution to the ground-state energy of some heliumlike ions [59] and more recently also on the hyperfine splitting in highly-charged hydrogenlike systems [60–63]. A Penning-trap experiment is further in progress in a Mainz-GSI collaboration to perform measurements on the bound-electron g -factor in H-like ions [64]. Numerical results for these experimentally interesting systems are presented and compared with the measurements. In addition to the comparison with the $(Z\alpha)$ -expansions and with experiment, we also list several results from theoretical calculations performed by other research groups. The agreement between the various theoretical results is generally very good, which suggests that we have today a good theoretical understanding of the evaluation of the one-photon radiative corrections.

6.1 Two-electron Lamb shift

In Paper III we presented the first complete calculation of the one-loop two-electron Lamb shift for some heavy heliumlike ions. Here we present more accurate results and we have further extended the calculations into the low- Z region, where a comparison with the $(Z\alpha)$ -expansion is meaningful. The results for the self-energy correction to the Breit interaction presented in Paper III are slightly wrong. This originates from the erroneous assumption that only the terms proportional to f_1 and f_6 in the zero-potential vertex part Eq. (3.56) were non-vanishing. The new results presented here for the Breit interaction replace those given in the article.

The two-electron contribution to the ground-state energy of heliumlike ions can be determined by comparing the ionization energy of heliumlike and hy-

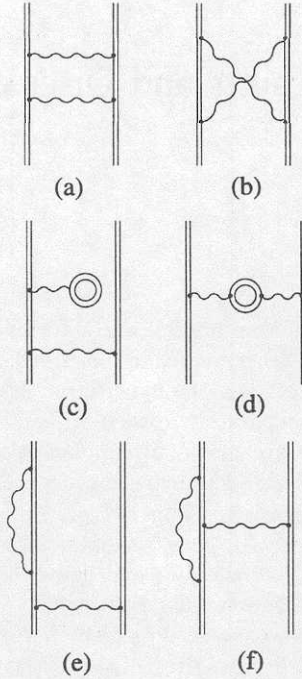


Figure 6.1: Feynman diagrams representing the two-photon contribution to the electron-electron interaction for heliumlike ions. The first row, the “ladder” (a) and the “crossed-photon” (b) diagrams, represent the non-radiative part and the remaining diagrams the two-electron Lamb shift.

drogenlike ions of the same elements [59]. In such an analysis the dominating one-body parts are completely eliminated. This implies for instance that the dependence on the nuclear structure is strongly suppressed, which motivates accurate calculations of the two-electron QED corrections. The two-electron Lamb shift can to a first approximation be regarded as a screening of the single-electron Lamb shift. This screening can be estimated by means of a modification of the potential in which the electron states are generated [27,28,65,66]. In this way, however, it is not possible to treat the exchange process and the effect due to transverse photons in an exact way. To reach high accuracy it is important to calculate the two-electron Lamb shift without any approximations as in our approach. In Fig. 6.1 all two-photon diagrams that contribute to the electron-electron interaction are displayed. The first two graphs (a) and (b), contain both ordinary relativistic many-body effects (RMBPT) as well as “non-radiative” QED effects, which were recently calculated by Lindgren *et al.* [56] and Blundell *et al.* [67]. The remaining diagrams (c)-(f), represents the two-electron Lamb shift. To complete the two-electron contribution to the ground-state energy, up to second order, the one-photon exchange Fig. 2.1 (a) must also be included.

QED corrections to the energy of heliumlike ions, correct to order α^3 , were

Table 6.1: The low Z Uehling vacuum polarization corrections given in terms of the function F . In the first row the constants from the $(Z\alpha)$ -expansion are given. The numbers in parenthesis indicating the power of ten.

Z	$E_{\text{cou}}^{\text{pc}}$	$E_{\text{br}}^{\text{pc}}$	$E_{\text{cou}}^{\text{wf}}$	$E_{\text{br}}^{\text{wf}}$	Sum
const.	0.0333333		0.356074		
1	0.0333349	3.5500(-6)	0.353032	2.7355(-5)	0.386371
2	0.0333402	1.4198(-5)	0.350228	1.0852(-4)	0.383582
3	0.0333487	3.1941(-5)	0.347627	2.4227(-4)	0.381008
4	0.0333606	5.6772(-5)	0.345211	4.2746(-4)	0.378628
5	0.0333760	8.8683(-5)	0.342965	6.6308(-4)	0.376430
6	0.0333948	1.2767(-4)	0.340879	9.4821(-4)	0.374401
7	0.0334170	1.7371(-4)	0.338943	1.2820(-3)	0.372534
8	0.0334427	2.2682(-4)	0.337151	1.6637(-3)	0.370820
9	0.0334719	2.8697(-4)	0.335495	2.0925(-3)	0.369254
10	0.0335046	3.5416(-4)	0.333970	2.5680(-3)	0.367829

derived already in the 1950s by Araki and Sucher [68]. Considering the two-photon two-electron contribution only the leading terms in the $(Z\alpha)$ -expansion are included in their expressions. They found the following expressions (in atomic units) for the vacuum polarization

$$\Delta E_{\text{vp}}^{\text{AS}} = \frac{4}{15}\alpha^3 \{ \langle \delta(\mathbf{r}_{12}) \rangle - [Z\langle \delta(\mathbf{r}_1) \rangle + Z\langle \delta(\mathbf{r}_2) \rangle] \}, \quad (6.1)$$

and for the self-energy

$$\Delta E_{\text{se}}^{\text{AS}} = \frac{2}{3}\alpha^3 \left\{ 2 \left[\frac{5}{6} - \ln 2\alpha^2 \right] [Z\langle \delta(\mathbf{r}_1) \rangle + Z\langle \delta(\mathbf{r}_2) \rangle - 2\langle \delta(\mathbf{r}_{12}) \rangle] - \langle \boldsymbol{\sigma}_1 \cdot \boldsymbol{\sigma}_2 \delta(\mathbf{r}_{12}) \rangle \right\} - \frac{2}{3\pi} M'', \quad (6.2)$$

where M'' is a part of the Bethe logarithm [56]. The expectation values are to be taken with fully correlated non-relativistic two-electron wavefunctions, i.e., exact solutions to the Schrödinger two-electron equation. They can be expressed in terms of a $1/Z$ expansion

$$\begin{aligned} \langle \delta(\mathbf{r}) \rangle &= \frac{Z^3}{\pi} \left[1 - \left(\frac{19}{16} - \frac{3}{4} \ln 2 \right) \left(\frac{1}{Z} \right) + 0.1781 \left(\frac{1}{Z} \right)^2 + \dots \right] \\ \langle \delta(\mathbf{r}_{12}) \rangle &= \frac{Z^3}{\pi} \left[\frac{1}{8} - 0.2418673 \left(\frac{1}{Z} \right) + 0.1810 \left(\frac{1}{Z} \right)^2 + \dots \right], \end{aligned} \quad (6.3)$$

where the power of $1/Z$ indicates the number of (instantaneous) Coulomb interactions. This leads to the following contributions, correct at the level $(Z\alpha)^3$,

$$\Delta E_{\text{vp}}^{\text{AS}}(Z\alpha) = \frac{(Z\alpha)^3}{\pi} \left[\frac{1}{30} + \left(\frac{19}{30} - \frac{2}{5} \ln 2 \right) \right], \quad (6.4)$$

and

$$\Delta E_{\text{se}}^{\text{AS}}(Z\alpha) = \frac{(Z\alpha)^3}{\pi} \left[\frac{1}{4} + 2.588819 + \left(\frac{7}{2} - 2 \ln 2 \right) \ln 2(Z\alpha)^2 \right], \quad (6.5)$$

Table 6.2: Two-electron vacuum-polarization contributions to the ground-state energy of some heliumlike ions (in eV).

Nuclear charge Z	VP wavefunction correction				VP potential correction				Total VP Effect
	Coulomb		Breit		Coulomb		Breit		
	Uehl	WK	Uehl	WK	Uehl	WK	Uehl	WK	
18	0.0064	-0.0000	0.0002	-0.0000	0.0007	-0.0000	0.0000	0.0000	0.0072
24	0.0151	-0.0001	0.0006	-0.0000	0.0016	-0.0000	0.0001	0.0000	0.0173
32	0.0361	-0.0003	0.0027	-0.0000	0.0039	-0.0000	0.0004	0.0000	0.0427
44	0.0987	-0.0016	0.0131	-0.0002	0.0106	-0.0001	0.0020	0.0001	0.1226
54	0.1964	-0.0044	0.0371	-0.0008	0.0208	-0.0004	0.0057	0.0003	0.2547
66	0.409	-0.012	0.106	-0.003	0.042	-0.002	0.016	0.001	0.557
74	0.647	-0.024	0.198	-0.007	0.064	-0.003	0.030	0.003	0.908
83	1.076	-0.046	0.379	-0.016	0.100	-0.007	0.056	0.008	1.549
92	1.792	-0.088	0.701	-0.034	0.155	-0.016	0.101	0.019	2.630

where we have also used that $\langle \sigma_1 \cdot \sigma_2 \rangle = -3$ for singlet states. The first term in the square bracket of the vacuum polarization part corresponds to the potential correction diagram Fig. 6.1 (d), and the second term to the wavefunction correction Fig. 6.1 (c). Note that the expression for the vacuum polarization, Eq. (6.4), only takes the Coulomb interaction into account and is further restricted to the Uehling approximation. For the self-energy part the first term (1/4) yields the Schwinger correction to the first-order Breit interaction and the remaining terms are associated with the Coulomb interaction. To compare our numerical results with the $(Z\alpha)$ -expansions it is convenient to introduce the function F defined by

$$\Delta E_{\text{QED}} = \frac{(Z\alpha)^3}{\pi} F. \quad (6.6)$$

In the low Z limit our numerically calculated F values should coincide with the expressions in square brackets of Eqs. (6.4) and (6.5). The deviation occurring for higher Z represents contributions from higher-order terms in $(Z\alpha)$.

In Table 6.1 we present the low Z Uehling vacuum polarization results in terms of the function F . In column two and three we have the potential correction (pc) parts and the wavefunction (wf) corrections are given in column four and five followed by the total sum in the last column. As can be inferred from the table the Coulomb parts approaches the results of Eq. (6.4) as $Z \rightarrow 0$. (1/30 for the potential correction and $19/30 - 2 \ln 2/5 = 0.356074\dots$ for the wf correction). We see also that the contributions from higher-order terms are quite small in this Z range.

The complete vacuum polarization results, in electron-volts (eV), are given in Table 6.2 for the high Z region. These values and all others for $Z \geq 18$ are obtained using a uniform nuclear charge distribution with the R_{rms} values as given in Table 6.5.

The self-energy corrections to the Breit interaction are displayed in Table 6.3 in terms of the F function. The total value is composed of various parts

Table 6.3: The Breit self-energy corrections given in terms of the function F . The constant (1/4) from the $(Z\alpha)$ -expansion is given in the first row.

Z	E_{se}^{wf}	E_{zp}^{be}	E_{zp}^{ve}	$E_{h.o.}^{ve+be}$	Total
const.					0.2500
1	-0.0007	3.8945	-3.3747	-0.2705	0.2486
2	-0.0022	3.2031	-2.6860	-0.2694	0.2456
3	-0.0042	2.8002	-2.2867	-0.2678	0.2414
4	-0.0067	2.5156	-2.0066	-0.2661	0.2362
5	-0.0096	2.2961	-1.7921	-0.2643	0.2302
6	-0.0128	2.1179	-1.6192	-0.2623	0.2236
7	-0.0163	1.9682	-1.4753	-0.2602	0.2164
8	-0.0200	1.8394	-1.3526	-0.2581	0.2087
9	-0.0239	1.7267	-1.2462	-0.2561	0.2005
10	-0.0280	1.6267	-1.1526	-0.2540	0.1920
18	-0.0655	1.0882	-0.6691	-0.2390	0.1146
24	-0.0971	0.8421	-0.4647	-0.2305	0.0498
32	-0.1420	0.6124	-0.2885	-0.2232	-0.0412
44	-0.2142	0.3819	-0.1320	-0.2200	-0.1843
54	-0.2797	0.2487	-0.0552	-0.2234	-0.3096
66	-0.3676	0.1303	0.0003	-0.2336	-0.4705
74	-0.4347	0.0682	0.0224	-0.2435	-0.5876
83	-0.5220	0.0096	0.0364	-0.2571	-0.7332
92	-0.6268	-0.0398	0.0404	-0.2729	-0.8991

as described in Chapter 3. Also here we find good agreement with the $(Z\alpha)$ -expansion result for low Z , but for high Z there is a substantial deviation (even wrong sign). The term $(Z\alpha)^3/(4\pi)$ in the $(Z\alpha)$ -expansion corresponds to the Schwinger correction to the first-order Breit interaction, as shown below. The first-order point nucleus Breit energy can be evaluated analytically and the result for the $1s^2$ configuration is given by

$$\begin{aligned}
 \Delta E_{\text{Breit}}^1 &= \frac{2}{3} \frac{Z^3 \alpha^2}{\gamma(2\gamma-1)} \left[2\gamma + 1 - \frac{6\gamma + 1}{2^{4\gamma}} \frac{\Gamma(4\gamma + 1)}{\Gamma^2(2\gamma + 1)} \right] \\
 &= \frac{Z^3 \alpha^2}{4} + \left(\frac{5}{2} - \frac{7}{2} \ln 2 \right) Z^5 \alpha^4 + \dots
 \end{aligned} \tag{6.7}$$

Denoting the leading term by $\Delta E_{\text{Breit}}^{1,\text{lead}} = Z^3 \alpha^2/4$, we can write

$$\Delta E_{\text{se,Breit}}^{\text{AS}}(Z\alpha) = 2\Delta E_{\text{Breit}}^{1,\text{lead}} \times \left(\frac{\alpha}{2\pi} \right), \tag{6.8}$$

where $\alpha/(2\pi)$ is just the Schwinger correction factor. The extra factor of 2 in front comes from the fact that both electrons are modified by the radiative corrections.

Table 6.4 shows the self-energy corrections to the Coulomb interaction in terms of the function F . As can be seen from the table this calculation suffers from strong numerical cancellations in the low Z range. Nevertheless, we obtain

Table 6.4: The self-energy corrections to the Coulomb interaction given in terms of the function F . In the last column the logarithmic term of the $(Z\alpha)$ -expansion is subtracted from the total value in column six. The constant in the first row in the “Total” column is the $Z = 1$ result from the $(Z\alpha)$ -expansion. The constant of the last column represents the limiting value as $Z \rightarrow 0$ for the values in this column.

Z	E_{se}^{wf}	E_{zp}^{be}	E_{zp}^{ve}	$E_{h.o.}^{ve+be}$	Total	Tot.-log.term
const.					-16.746	2.589
1	-12.92	182837.08	-179320.33	-3520.6	-16.8	2.5(2)
2	-11.09	37595.12	-36720.70	-877.37	-14.03	2.37(5)
3	-9.83	14607.27	-14221.57	-388.24	-12.38	2.31(3)
4	-8.890	7381.800	-7166.857	-217.282	-11.229	2.245
5	-8.170	4312.255	-4176.161	-138.273	-10.349	2.182
6	-7.593	2762.256	-2668.872	-95.437	-9.645	2.115
7	-7.109	1886.056	-1818.337	-69.670	-9.060	2.049
8	-6.704	1349.627	-1298.503	-52.988	-8.569	1.975
9	-6.355	1001.097	-961.301	-41.585	-8.144	1.902
10	-6.043	763.972	-732.241	-33.452	-7.764	1.837
18	-4.4476	157.8801	-149.4595	-9.7721	-5.7990	
24	-3.7672	68.7931	-64.6746	-5.2960	-4.9448	
32	-3.1701	28.1927	-26.3460	-2.8594	-4.1829	
44	-2.6268	9.3342	-8.7306	-1.4512	-3.4744	
54	-2.3586	4.0536	-3.8615	-0.9479	-3.1144	
66	-2.1781	1.4323	-1.4791	-0.6357	-2.8607	
74	-2.1260	0.5999	-0.7382	-0.5135	-2.7778	
83	-2.1287	0.0679	-0.2788	-0.4220	-2.7616	
92	-2.2014	-0.2312	-0.0373	-0.3626	-2.8326	

fair agreement with the $(Z\alpha)$ -expansion results; the latter gives $-16.746\dots$ for $Z = 1$ in comparison with our numerical value -16.8 with an error of two units in the last digit. To explore the results further we present in the last column the total values after subtracting the dominating logarithmic term of the $(Z\alpha)$ -expansion. The resulting values should then approach the constant 2.588819 as $Z \rightarrow 0$. We can see a clear tendency for that and the values of the last column also indicates the presence of a linear higher-order term. Our accuracy is, however, not high enough to perform a detailed fitting.

In Table 6.5 the self-energy and vacuum polarization corrections are added to obtain the two-electron Lamb shift. As a comparison we have collected results from Refs. [47] (VP) and [69] (SE) and displayed those in the last column. The agreement between the two results is almost perfect.

In order to investigate the influence of the nuclear structure on the results, the dominating first-order energy was calculated varying nuclear parameters and by using uniform as well as Fermi charge distribution models. The results of these considerations are presented in Table 6.6. The fourth column shows the result when using a Fermi nuclear charge distribution with R_{rms} given in column two and a (related to the skin thickness) given in column three, taken

Table 6.5: Two-electron vacuum-polarization and self-energy contributions to the ground-state energy of some heliumlike ions (in eV).

Nucleus $Z, (R_{\text{rms}})$	Vacuum polarization			Self-energy			Two-electron Lamb shift	Refs. [47, 69]
	Coul.	Breit	Total	Coul.	Breit	Total		
18 (3.423)	0.0070	0.0002	0.0072	-0.1138	0.0022	-0.1116	-0.1044	
24 (3.643)	0.0166	0.0007	0.0173	-0.2301	0.0023	-0.2278	-0.2104	
32 (4.07)	0.0397	0.0031	0.0427	-0.4613	-0.0045	-0.4659	-0.4232	-0.4232
44 (4.480)	0.1077	0.0150	0.1226	-0.9962	-0.0528	-1.0490	-0.9264	
54 (4.78)	0.212	0.042	0.255	-1.651	-0.164	-1.815	-1.560	-1.560
66 (5.21)	0.436	0.120	0.557	-2.768	-0.455	-3.224	-2.667	-2.666
74 (5.37)	0.684	0.224	0.908	-3.789	-0.801	-4.590	-3.682	-3.682
83 (5.519)	1.122	0.427	1.549	-5.315	-1.411	-6.726	-5.176	-5.176
92 (5.860)	1.844	0.786	2.630	-7.424	-2.357	-9.781	-7.151	-7.150

from [70]. In the fifth column the R_{rms} is the same as in the fourth column but the skin thickness is set to zero, i.e., a homogeneous nuclear charge distribution is used. In the last column we repeat the Fermi calculation using the same skin thickness, but now with a R_{rms} which is reduced with approximately one percent compared to the value in column two. The results of Table 6.6 show that the nuclear structure model affects the results very weakly. The dominating numerical uncertainty comes from the uncertainty in the nuclear radius R_{rms} .

In Table 6.7 we collect the various contributions to the two-electron part of the energy and compare with recent experimental results of Marrs *et al.* [59]. The all-order relativistic many-body result (RMBPT) is also calculated and the non-radiative QED contribution is taken from [56]. All RMBPT calculations are performed within the no-virtual-pair approximation (NVPA), neglecting the effects of negative-energy states, and without retardation. The “2nd order RMBPT” values refers to the ladder diagram Fig. 6.1 (a). Taking the difference between the full ladder diagram, including negative intermediate states and retardation, and the corresponding RMBPT value yields the QED part of the ladder diagram. The non-radiative QED effect is defined as the sum of that QED contribution together with the entire crossed photon diagram Fig. 6.1 (b). The “ ≥ 3 rd order RMBPT” values include only one Breit interaction together

Table 6.6: Comparison between different nuclear models used in calculating the first-order RMBPT (in eV).

Nuclear charge	R_{rms} fm	a fm	1st order Fermi	1st order Uniform	R_{rms} fm	1st order Fermi
32	4.07	0.59	567.609	567.609	4.02	567.610
54	4.78	0.60	1036.558	1036.558	4.73	1036.560
66	5.21	0.60	1347.450	1347.450	5.15	1347.458
74	5.37	0.54	1586.929	1586.927	5.31	1586.945
83	5.52	0.47	1897.565	1897.561	5.46	1897.602
92	5.86	0.61	2265.888	2265.872	5.80	2265.974

Table 6.7: Various components of the two-electron contribution to the ground-state energy of some heliumlike ions and a comparison with experiment (in eV). The errors assigned for the “1st order RMBPT” values are due to a variation of the nuclear R_{rms} value by one percent.

Nuclear charge	RMBPT			Non-rad. QED	Lamb shift	Total theory	Experiment Marris <i>et al.</i> [59]
	1st ord.	2nd ord.	≥ 3 rd ord.				
18	310.22	-4.58	0.02	0.00	-0.10	305.56	\pm
24	417.92	-4.81	0.02	0.01	-0.21	412.94	\pm
32	567.61	-5.22	0.02	0.03	-0.42	562.02	562.5 ± 1.6
44	810.56	-6.07	0.03	0.08	-0.93	803.66	\pm
54	1036.56	-7.04	0.03	0.16	-1.56	1028.15	1027.2 ± 3.5
66	1347.45(1)	-8.59	0.03	0.35	-2.67	1336.58	1341.6 ± 4.3
74	1586.93(2)	-9.91	0.04	0.53	-3.68	1573.90	1568 ± 15
83	1897.56(4)	-11.77	0.04	0.85	-5.18	1881.51	1876 ± 14
92	2265.87(10)	-14.16	0.05	1.28	-7.15	2245.90	\pm

with iterated Coulomb interactions. Thus, the total theoretical result is complete up to second order.

If we now consider the Breit values of Table 6.5 together with the non-radiative QED results in Table 6.7, we see that these contributions cancel each other to a large extent. This is particularly evident for uranium ($Z = 92$) and bismuth ($Z = 83$), where the resulting contribution of the three terms amounts only to one tenth of the SE part which enters the sum. Thus, for the high- Z region one can obtain quite good estimates of the final theoretical value, just by using ordinary RMBPT together with the Coulomb-screened Lamb shift.

In Table 6.8 we compare the results of several recent theoretical calculations of the two-electron energy contribution. The results of Refs. [71–73] include only approximate treatments of the two-electron Lamb shift as discussed in Paper III. The work of Yerokhin *et al.* [69] is analogous to ours and a comparison shows excellent agreement between the two calculations. (Their results for the radiative part are displayed in Table 6.5.) The agreement between the various theoretical results is generally quite good, which indicates that the earlier estimates of the Lamb-shift contributions have been quite accurate. Drake’s result [71] suffers, for heavy elements, from the inaccuracy of the $(Z\alpha)$ -expansion used for the QED and relativistic effects, which becomes particularly evident for

Table 6.8: Comparison between various theoretical calculations (in eV).

Z	Plante [72]	Indelicato [73]	Drake [71]	Yerokhin [69]	Present work
32	562.05	562.1	562.1	562.02	562.02
54	1028.4	1028.2	1028.8	1028.16	1028.15
66	1337.2	1336.5	1338.2	1336.58	1336.58
74	1574.8	1573.6	1576.6	1573.92	1573.90
83		1880.8	1886.3	1881.50	1881.51
92				2245.92	2245.90

the bismuth result. On the other hand, Drake uses correlated hydrogenic wave functions and thus includes also higher-order Coulomb correlation in the QED effects. The relative effect of correlation is largest for light elements, where the absolute effect is smaller. Therefore, the missing correlation effect in our QED values is estimated to be at most of the order of 0.1eV for all elements.

To summarize, the results presented in this section shows that our numerical calculations agrees well with the predictions of the leading terms of the $(Z\alpha)$ -expansion for low Z . We find further an excellent agreement for medium and high Z with the calculation of Yerokhin *et al.* [69]. For the comparison with experiment we have shown that the total two-electron energy contribution depends very weakly on the nuclear structure. We can conclude that the nuclear uncertainties do not affect the QED contribution at the present level of accuracy. The agreement between the experimental and theoretical results supports the accuracy of the experimental and the many-body results, but the experimental accuracy is not yet high enough to seriously test the QED part of the calculation. An improvement of the experimental accuracy by one order of magnitude would, however, provide a good experimental test of the two-electron Lamb shift.

6.2 Bound electron g factor

The calculations on the radiative corrections to the bound electron g factor was first presented in Paper II. Here we will summarize the results of that paper and some more detailed results for the self-energy corrections will be given.

An experiment that will provide a good testing ground for QED in strong fields is the measurement of the bound electron g factor for high- Z ions. In the first stage of the Mainz-GSI experiment [64] one plans to perform measurements on ions in the nuclear range $Z = 6 - 20$, and at a later stage on heavier elements up to uranium. The expected accuracy of the measurements is of the order of 10^{-7} and this stimulates efforts on the theoretical side to reach the same accuracy.

In the Dirac theory the g factor of a free electron is exactly $g = 2$. Due to self-interactions with the radiation field, the free electron possesses an anomalous magnetic moment g_e , first accounted for by Schwinger [3]. The investigations of g_e have reached very far, and give at present the outstanding agreement at the level of one part in 10^{11} between theory and experiment [74]. The corrections to the g factor of an atomic electron originate not only from the interactions with the radiation field, but also from the interaction with the nuclear field.

Table 6.9: The self-energy corrections to the electron g factor given in terms of the function $C^{(2)}(Z\alpha)$. For $Z \leq 18$ the point nucleus model is used and for higher Z a uniform charge distribution is employed (R_{rms} values are given in Table 6.10).

Z	$E_{\text{se}}^{\text{wf}}$	$E_{\text{zp}}^{\text{be}}$	$E_{\text{zp}}^{\text{ve}}$	$E_{\text{mp}}^{\text{ve+be}}$	$E_{\text{op}}^{\text{ve+be}}$	Total SE
1	0.00032916	7.78876809	-7.28920807	0.00000712	0.00010817	0.50000447
2	0.00112071	6.40541501	-5.90688089	0.00002811	0.00033520	0.50001815
3	0.00226516	5.59868638	-5.10159977	0.00006217	0.00062788	0.50004182
4	0.00370586	5.02855574	-4.53325307	0.00010823	0.00095974	0.50007650
5	0.0054045	4.5883788	-4.0951388	0.0001651	0.0013137	0.5001234
6	0.0073326	4.2306065	-3.7396648	0.0002314	0.0016778	0.5001835
7	0.0094678	3.9298448	-3.4414033	0.0003059	0.0020432	0.5002584
8	0.0117920	3.6709159	-3.1851489	0.0003871	0.0024032	0.5003492
9	0.0142903	3.4440153	-2.9610744	0.0004735	0.0027529	0.5004576
10	0.0169500	3.2424383	-2.7624556	0.0005635	0.0030884	0.5005846
11	0.0197602	3.0613947	-2.5844857	0.0006566	0.0034067	0.5007325
12	0.0227118	2.8973415	-2.4236073	0.0007504	0.0037056	0.5009020
13	0.025797	2.747584	-2.277113	0.000844	0.003983	0.501095
14	0.029008	2.610022	-2.142891	0.000936	0.004239	0.501313
15	0.032339	2.482990	-2.019267	0.001024	0.004471	0.501556
16	0.035784	2.365140	-1.904885	0.001109	0.004679	0.501829
17	0.039340	2.255372	-1.798633	0.001189	0.004864	0.502130
18	0.043000	2.152767	-1.699590	0.001261	0.005024	0.502463
24	0.066991	1.651651	-1.220441		0.006994 ^a	0.505194
32	0.10379	1.18261	-0.78117		0.00600 ^a	0.51123
44	0.16842	0.71369	-0.35549		0.00056 ^a	0.52719
54	0.23122	0.44799	-0.12319		-0.00702 ^a	0.54901
66	0.31917	0.22166	0.06709		-0.01849 ^a	0.58941
74	0.38727	0.11057	0.15684		-0.02672 ^a	0.62795
83	0.4756	0.0146	0.2315		-0.0355 ^a	0.6863
92	0.5800	-0.0559	0.2838		-0.0425 ^a	0.7655

^a These values are the sum of $E_{\text{mp}}^{\text{ve+be}}$ and $E_{\text{op}}^{\text{ve+be}}$ (see text).

Beyond the relativistic Breit correction [75], Grotch and Hegstrom [76–78] derived the leading bound radiative correction of order $\alpha(Z\alpha)^2$ and the leading recoil corrections of order $(Z\alpha)^2 m/M$, $\alpha(Z\alpha)^2 m/M$ and $(Z\alpha)^2 (m/M)^2$, where m/M is the electron-nucleus mass ratio. However, to obtain accurate theoretical results for heavy ions, one has to go beyond the $(Z\alpha)$ -expansion and include the nuclear interaction nonperturbatively.

The first-order contribution to the bound electron g factor can, in the point nucleus case, be evaluated analytically and this yields

$$g_j^{\text{Breit}} = \frac{2}{3} \left[1 + 2\sqrt{1 - (Z\alpha)^2} \right], \quad (6.9)$$

which was first derived by Breit in 1928 [75]. Taking radiative corrections into account it is convenient to expand the g factor into zero-, one-, etc. photon contributions. Specifically, for an electron bound to an infinitely heavy point

Table 6.10: The total ($g_j - 2$) correction (see text) is collected for some H-like ions. The free-electron QED value $2319.3043 \cdot 10^{-6}$ is also added. All values are given in terms of 10^{-6} .

Z	R_{rms} (fm)	QED- α/π	Nuc. Size	Recoil	$g_j^{\text{Breit}} - 2$	Total
1		0.021	0.0	0.029	-35.501	2283.853
2		0.084	0.0	0.029	-142.011	2177.406
3		0.194	0.0	0.037	-319.546	1999.988
4		0.354	0.0	0.051	-568.136	1751.573
5		0.569	0.0	0.066	-887.818	1432.121
6		0.844	0.0	0.087	-1278.646	1041.590
7	2.540(20)	1.18	0.0	0.10	-1740.68	579.91
8	2.737(8)	1.60	0.0	0.12	-2274.00	47.02
9	2.90(2)	2.08	0.0	0.12	-2878.68	-557.17
10	2.992(8)	2.65	0.0	0.14	-3554.83	-1232.72
11	2.94(6)	3.31	0.01	0.15	-4302.55	-1979.78
12	3.08(5)	4.06	0.01	0.17	-5121.97	-2798.42
13	3.035(2)	4.91	0.01	0.18	-6013.21	-3688.80
14	3.086(18)	5.86	0.02	0.20	-6976.43	-4651.04
15	3.191(5)	6.92	0.03	0.21	-8011.78	-5685.31
16	3.230(5)	8.10	0.04	0.23	-9119.42	-6791.75
17	3.388(17)	9.39	0.05	0.24	-10299.54	-7970.55
18	3.423(14)	10.82	0.07	0.23	-11552.34	-9221.91
24	3.643(3)	22.2	0.27	0.3	-20607.8	-18265.6
32	4.088(8)	46.4	1.24	0.4	-36862.5	-34495.1
44	4.480(22)	106.3	6.92(6)	0.6	-70598.8	-68165.8
54	4.782(2)	182.4	23.4(2)	0.6	-107885.4	-105359.5
66	5.211(26)	311.9	90.9(8)	0.8	-164830.3	-162107.5
74	5.374(22)	424.9	205.6(14)	0.9	-211116.8	-208166.2
83	5.519(4)	580.4	500.0(6)	1.0	-272389.2	-268988.6
92	5.860(2)	766.1	1274.1(6)	1.0	-345153.9	-340793.4

nucleus, the expansion is given by (the power of α/π indicates the number of virtual photons)

$$g_j = 2 \left\{ \frac{1}{3} \left[1 + 2\sqrt{1 - (Z\alpha)^2} \right] + \frac{\alpha}{\pi} \left[\frac{1}{2} + \frac{(Z\alpha)^2}{12} + \dots \right] + \left(\frac{\alpha}{\pi} \right)^2 \left[A^{(4)} + \dots \right] + \left(\frac{\alpha}{\pi} \right)^3 \left[A^{(6)} + \dots \right] + \dots \right\}, \quad (6.10)$$

where $A^{(4)} = -0.328478 \dots$ and $A^{(6)} = 1.18 \dots$ etc. are the known free-electron contributions [74]. Focus now on the one-photon contributions in Eq. (6.10) described by the function $C^{(2)}(Z\alpha) = 1/2 + (Z\alpha)^2/12 + \dots$ where the first term is the Schwinger correction and $(Z\alpha)^2/12$ is the Grotch term [77]. Both these are due to the self-energy corrections. For low Z , $1/2$ strongly dominates (for $Z = 1$ by five orders of magnitude). Thus, to achieve the QED corrections beyond the Schwinger term, one needs a very high numerical accuracy in the calculations

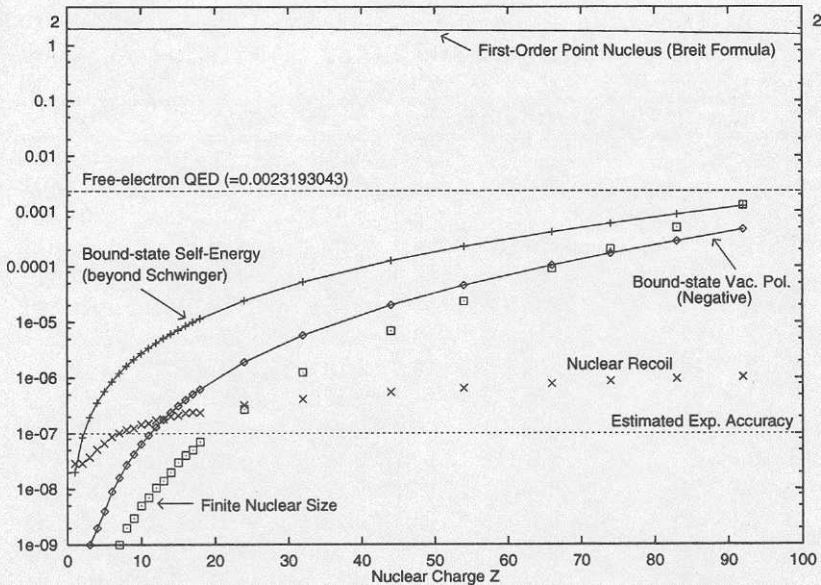


Figure 6.2: Contributions to the bound electron g factor.

for low Z . To reach this accuracy, it was essential to compute the one-potential vertex and binding-energy terms separately in the semi-analytical way described in Chapters 3 and 5, since this part has a very slow convergence in the partial wave expansion. For example, at $Z = 1$ the partial wave expansion changes sign at $l = 84$ and to obtain the contribution from the tail accurately we included terms up to $l = 150$. The sign change occurs for lower l values when increasing Z and therefore it was necessary with the special treatment of this part only for $Z \leq 18$. In Table 6.9 where the self-energy corrections are presented in terms of the function $C^{(2)}(Z\alpha)$, the values for $Z \geq 24$ in column six are thus the sum of the one- and many-potential terms $E_{\text{h.o.}}^{\text{ve+be}} = E_{\text{mp}}^{\text{ve+be}} + E_{\text{op}}^{\text{ve+be}}$. The results presented in Table 6.9 agrees well in the high- Z region with a similar calculation performed by Blundell *et al.* [79], but for low Z our results are slightly larger.

From a $(Z\alpha)$ expansion consideration, beyond the Schwinger and Grotch term, one would expect terms of order $\alpha(Z\alpha)^4$ [80]. For $Z \leq 30$ we have performed different fittings of our numerical self-energy values, beyond the Schwinger correction, to formulas of the type

$$A\alpha(Z\alpha)^2 + \alpha(Z\alpha)^4[B + C \ln(Z\alpha) + D(Z\alpha)], \quad (6.11)$$

and obtained the Grotch coefficient, A , with an accuracy better than 1%. A plot of the numerical values and a fit to these can be found in Fig. 2 of Paper II. Since the displayed ratio in that figure becomes very sensitive for $Z = 1$ we get a safer prediction by using different fittings of the results from higher Z . Our fitted result of this ratio for $Z = 1$ is 1.007(2), where the uncertainty comes from excluding the log term in the fitting function. This value is also consistent with

our numerical value for $Z = 1$ given in Table 6.9. Even though the Grotch term and our all-order numerical result are almost identical for $Z = 1$, the deviation between the two grows rapidly with Z . This would lead to the wrong sign for the total bound-state QED correction for $Z \geq 60$ if using the Grotch prediction for the self-energy part.

To make a comparison with experiment one has to include the effects of nuclear recoil, finite nuclear size and QED corrections from diagrams involving two and more virtual photons. Additionally, for very high Z also effects from nuclear polarization might come in at the 10^{-7} level. The nuclear recoil correction can be obtained from the formulas derived by Grotch and Hegstrom [78], and is to the demanded accuracy given by the leading term $g_j^{\text{recoil}} = (Z\alpha)^2 m/M$. For high Z this can only be considered as a reliable order of magnitude estimation [81]. However, in this region this is sufficient since the recoil effect is small compared to the bound-state QED corrections. Furthermore, a careful investigation of the nuclear size effect on the dominating first-order contribution has been performed as described in Paper II. The uncertainty assigned to the nuclear-size effect in Table 6.10 corresponds to the experimental uncertainty in the R_{rms} values [70].

Concerning the QED effects involving two and more virtual photons, the free-electron part is significant. The corresponding bound-state corrections, which are still uncalculated, should be a factor (α/π) smaller than the calculated one-photon bound-state corrections.

In Table 6.10 we have added all different contributions to the bound $(g_j - 2)$ value, i.e., the one-photon bound-state radiative correction (column three), the nuclear-size effect (column four), the nuclear recoil (column five), the $(g_j - 2)$ from the Breit term (column six) and finally the free electron $(g_e - 2)$ value 0.0023193043 [74]. The contributions are further displayed in Fig. 6.2. The vacuum polarization results are taken from Table I of Paper II and the Schwinger term is here subtracted from the self-energy values. For low Z the free-electron part dominates while the Breit term gives the dominating contribution to $(g_j - 2)$ for medium and high Z . However, the uncertainty in the theoretical values are small compared to the bound-state QED effects for all Z . With an anticipated experimental uncertainty of 10^{-7} , this implies that the bound-state g factor measurements will constitute a good test of bound-state QED for all $Z \geq 10$.

6.3 Hyperfine structure

In the recent publication Paper I, we presented our calculations of the radiative corrections to the hyperfine-structure splitting in H-like ions. The paper contains the first complete evaluation of the one-photon radiative corrections to all orders in $(Z\alpha)$. To unambiguously incorporate the Wichmann-Kroll part the vacuum polarization correction to the measured nuclear magnetic moment was taken into account. An analysis of how the QED effects are affected by using an extended nuclear magnetization, in comparison with the point-dipole model, is also included. Here we have extended the calculations to cover the range of nuclear charges more fully. Tables 6.11–6.14 correspond to the Tables I–IV in the paper, but now completed such that all $Z \leq 10$ have been considered. For

Table 6.11: The low Z self-energy corrections given in terms of the function $F_{\text{se}}^{(2)}$. As a comparison the values of the $(Z\alpha)$ -expansion and the results of Ref. [42] are also given.

Z	$E_{\text{se}}^{\text{wf}}$	$E_{\text{zp}}^{\text{be}}$	$E_{\text{zp}}^{\text{ve}}$	$E_{\text{h.o.}}^{\text{ve+be}}$	Total SE	$F_{\text{se}}^{(2)}(Z\alpha)$	Ref. [42]
1	-0.0110	7.7895	-5.0795	-2.2610	0.4380(1)	0.43811	0.43808
2	-0.0294	6.4079	-3.8112	-2.1940	0.3734(1)	0.37351	0.37347
3	-0.0519	5.6036	-3.1124	-2.1318	0.3075(1)	0.30773	0.30759
4	-0.0774	5.0364	-2.6442	-2.0739	0.2410(1)	0.24137	0.24103
5	-0.1049	4.5996	-2.3008	-2.0197	0.1741(1)	0.17475	0.17405
6	-0.1343	4.2455	-2.0353	-1.9691	0.1068(1)	0.10809	0.10684
7	-0.1651	3.9487	-1.8226	-1.9215	0.0395(1)	0.04154	0.03950
8	-0.1972	3.6940	-1.6479	-1.8769	-0.0280(1)	-0.02481	-0.02791
9	-0.2301	3.4714	-1.5018	-1.8349	-0.0954(1)	-0.09086	-0.09535
10	-0.2639	3.2744	-1.3779	-1.7954	-0.1628(1)	-0.15657	-0.16283

the self-energy part we have further included some new results in the medium high range $Z = 18 - 54$ (Table 6.12). In this section a brief summary of the results will be given. For the full analysis we refer to the article.

The one-photon radiative corrections are conveniently expressed in terms of the function $F^{(2)}$, which is defined through

$$\Delta E_{\text{QED}}^{(2)} = \Delta E_{\text{F}} \frac{\alpha}{\pi} F^{(2)}, \quad (6.12)$$

where ΔE_{F} is the non-relativistic, point-nucleus first-order hyperfine splitting in ground state H-like ions [82]

$$\Delta E_{\text{F}} = \frac{4}{3} \alpha (Z\alpha)^3 mc^2 \frac{\mu}{\mu_N} \frac{m}{m_p} \frac{2I+1}{2I}. \quad (6.13)$$

Here μ is the nuclear magnetic moment, μ_N is the nuclear magneton, m_p is the proton mass and I is the nuclear spin. The vacuum polarization correction is separated in the wavefunction and the potential correction parts. They are here denoted by the electric (EL) and magnetic (ML) loop corrections, respectively. These names are due to the polarization loop connecting with the electric nuclear potential in the wavefunction part, and with the magnetic nuclear vector potential for the potential correction diagram. The known part of the $(Z\alpha)$ -expansion for the one-photon QED effects [3, 83–91] is for the self-energy corrections given by

$$\begin{aligned} F_{\text{se}}^{(2)}(Z\alpha) &= \frac{1}{2} + \left(\ln 2 - \frac{13}{4} \right) \pi (Z\alpha) \\ &+ \left[-\frac{8}{3} \ln^2(Z\alpha) + \left(-\frac{37}{36} + \frac{16}{3} \ln 2 \right) \ln(Z\alpha) + H_{\text{se}}^{(2)}(Z\alpha) \right] (Z\alpha)^2, \end{aligned} \quad (6.14)$$

where

$$H_{\text{se}}^{(2)}(Z\alpha) = 17.122 + \left[\left(-5 \ln 2 + \frac{191}{16} \right) \pi \ln(Z\alpha) \right] (Z\alpha) + \dots, \quad (6.15)$$

Table 6.12: The self-energy corrections for the medium and high Z region given in terms of $F_{\text{se}}^{(2)}$. In the last two columns the results of Refs. [41, 92] are given as a comparison. These values are scaled to our units by using the first-order values (uniform nuclear charge distribution) given in Table V of Paper I.

Z	$E_{\text{se}}^{\text{wf}}$	$E_{\text{zp}}^{\text{be}}$	$E_{\text{zp}}^{\text{ve}}$	$E_{\text{h.o.}}^{\text{ve+be}}$	Total SE	Ref. [92]	Ref. [41]
18	-0.5548	2.2170	-0.8126	-1.5499	-0.7003		
24	-0.7970	1.7422	-0.6298	-1.4255	-1.1100		
32	-1.1549	1.3028	-0.5173	-1.3201	-1.6895		
44	-1.8059	0.8621	-0.4942	-1.2552	-2.6932		
54	-2.5184	0.6007	-0.5600	-1.2715	-3.7491		
67	-3.8506	0.3309	-0.7515	-1.3894	-5.6605	-5.662	-5.6625
75	-5.0639	0.1818	-0.9484	-1.5295	-7.3599	-7.362	
82	-6.5211	0.0508	-1.1896	-1.7085	-9.3683		
83	-6.7694	0.0316	-1.2307	-1.7393	-9.7078	-9.707	-9.7111
92	-9.5874	-0.1535	-1.6906	-2.0876	-13.5192		

and the vacuum polarization parts are

$$F_{\text{vp-el}}^{(2)}(Z\alpha) = \frac{3}{8}\pi(Z\alpha) + \left[-\frac{8}{15}\ln(Z\alpha) + \left(\frac{214}{225} - \frac{8}{15}\ln 2 \right) \right] (Z\alpha)^2 - \frac{\pi}{6}\ln(Z\alpha)(Z\alpha)^3, \quad (6.16)$$

and

$$F_{\text{vp-ml}}^{(2)}(Z\alpha) = \frac{3}{8}\pi(Z\alpha) - \frac{4}{5}(Z\alpha)^2 - \frac{3}{8}\pi\ln(Z\alpha)(Z\alpha)^3. \quad (6.17)$$

The self-energy corrections are presented in Tables 6.11 and 6.12 for the low- and high- Z regions, respectively. As can be seen from the tables our values are consistent with the $(Z\alpha)$ -expansion and agrees well with the results of Refs. [41, 42, 92]. The low- Z values presented in [42] are still an order of magnitude more accurate than ours, so we can not add more information about the $(Z\alpha)$ -expansion comparison than was done in their paper. The limitations in our computation come mainly from the $E_{\text{h.o.}}^{\text{ve+be}}$ term where a large number of partial-wave terms have to be calculated in order to decrease the extrapolation error. We should be able to increase our accuracy substantially if we could evaluate the slowly converging one-potential vertex and binding-energy term semianalytically as was successfully accomplished in the g_j -factor calculation (see previous section). It would then also be necessary to improve the accuracy in the computation of the $E_{\text{se}}^{\text{wf}}$ term, which can be done by implementing the analytical form of the perturbed wavefunction (see Chapter 5).

Table 6.13: The low- Z Uehling vacuum-polarization corrections given in terms of the function $F_{\text{vp}}^{(2)}$. The results of the $(Z\alpha)$ -expansions are given in column three and five and in the last column the total numerical value is collected.

Z	$E_{\text{vp}}^{\text{el-ue}}$	$F_{\text{el}}^{(2)}(Z\alpha)$	$E_{\text{vp}}^{\text{ml-ue}}$	$F_{\text{ml}}^{(2)}(Z\alpha)$	Total num.
1	0.0087691	0.0087687	0.0085578	0.0085566	0.017327
2	0.017817	0.017805	0.017049	0.017039	0.034865
3	0.027112	0.027067	0.025487	0.025455	0.052599
4	0.036645	0.036535	0.033886	0.033810	0.070530
5	0.046414	0.046194	0.042257	0.042109	0.088670
6	0.056421	0.056033	0.050611	0.050358	0.107032
7	0.066671	0.066043	0.058960	0.058559	0.125631
8	0.077171	0.076217	0.067313	0.066715	0.144484
9	0.087929	0.086549	0.075681	0.074831	0.163610
10	0.098955	0.097033	0.084072	0.082908	0.183028

The results for the vacuum polarization corrections are presented in Tables 6.13 and 6.14. The low- Z values displayed in Table 6.13 are the results in the Uehling approximation since the $(Z\alpha)$ -expansion is evaluated in this approximation. The agreement between the numerical results and the $(Z\alpha)$ -expansion is seen to be very good for low Z . Using the analytical perturbed wavefunction it is, however, possible to evaluate the Uehling corrections exactly (to all orders in $(Z\alpha)$) [93], making the $(Z\alpha)$ -expansion superfluous. This should also be possible to elaborate for the wavefunction correction in the g factor case. For extended nuclear charge distributions the corrections have still to be calculated numerically in order to obtain the all order result.

In Table 6.14 the VP corrections for $Z \geq 10$ are presented. In the second last column the “renormalized” Wichmann-Kroll correction to the magnetic loop diagram is given. It represents the combined effect of the WK corrections to the magnetic loop diagram and to the nuclear magnetic moment, which can not be calculated directly for the point-dipole model (see Chapter 4 and the paper). In order to check the consistency of the calculation of the renormalized contribution, we analyzed the behavior at the point-dipole limit. Using that the parts and the combined WK effect are all well-defined and finite when cutting of the small distances, we performed the calculation for several values of the cutoff radius. The limit of zero cutoff radius corresponds to the point-dipole model. The results of this analysis is for $Z = 92$ displayed in Fig. 6.3 (boxes) together with a fit to these values (filled line). As is seen from the figure there is a smooth transition to the point-dipole model. The fit yields the value -0.7396 for zero cutoff radius and the direct calculation, using Eq. (4.41), gives -0.7397 . The direct calculation is increasingly harder to control numerically when going down in Z , and we obtained more accurate predictions by using such fitting procedures.

Our total (VP+SE) numerical values for the one-photon radiative corrections are displayed in Fig. 6.4 (dots) together with the prediction of the $(Z\alpha)$ -expansion (Eqs. 6.14-6.17). For low Z there is excellent agreement but for high Z the two results differ substantially due to higher-order terms in $(Z\alpha)$ not

Table 6.14: The vacuum polarization corrections given in terms of the function $F_{\text{vp}}^{(2)}$. The R_{rms} -values used for the nuclear electric charge distribution are given in the second column (fm). In column three and four the EL and ML Uehling parts are displayed. The Wichmann-Kroll part of the EL diagram is given in column five followed by the “renormalized” ML Wichmann-Kroll contribution.

Z	R_{rms}	$E_{\text{vp}}^{\text{el-ue}}$	$E_{\text{vp}}^{\text{ml-ue}}$	$E_{\text{vp}}^{\text{el-wk}}$	$E_{\text{vp}}^{\text{ml-wk-ren}}$	Total VP
10	2.99	0.094922	0.080275	-0.000054	-0.000271	0.174871
18	3.42	0.18865	0.14480	-0.00035	-0.00160	0.33150
24	3.64	0.27326	0.19626	-0.00084	-0.00389	0.46479
32	4.07	0.41176	0.27153	-0.00218	-0.00970	0.67141
44	4.48	0.7065	0.4102	-0.0067	-0.0286	1.0815
54	4.78	1.0831	0.5630	-0.0146	-0.0609	1.5707
67	5.21	1.900	0.847	-0.037	-0.147	2.562
75	5.351	2.742	1.102	-0.063	-0.249	3.533
82	5.497	3.843	1.404	-0.102	-0.391	4.754
83	5.519	4.038	1.455	-0.109	-0.418	4.967
92	5.860	6.377	2.016	-0.200	-0.740	7.453

included in the analytical expansion. The figure clearly shows the necessity of a nonperturbative treatment of the nuclear potential in calculating the QED effects for high- Z systems.

For the comparison with experiment we studied in Paper I the sensibility of the QED effects on the nuclear structure. Considering both the nuclear charge and magnetic moment distributions we found a very weak dependence of the radiative effects. This is in contrast to the dominating first-order energy, for which the lack of detailed knowledge of the magnetization distribution implies large uncertainties. The uncertainty of the Bohr-Weisskopf effect is typically of the same size as the total QED contribution (see Table VII in Paper I). Another source of error is the not fully reliable measurements of the nuclear magnetic moments [94]. These two uncertainties restrict today the possibility for a stringent test of the QED corrections to the hyperfine-structure splitting in H-like ions. Recently [92] a method was proposed for reducing the uncertainty due to the Bohr-Weisskopf effect in ground-state lithiumlike ions. This leads to a consistency check for the QED part since the method is based on the correctness of the QED corrections in the corresponding hydrogenlike ion.

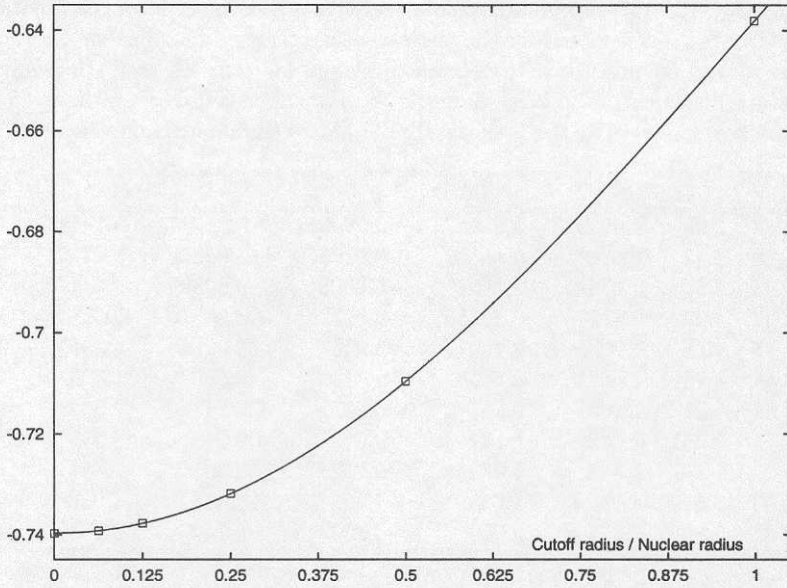


Figure 6.3: The renormalized Wichmann-Kroll contribution for uranium using different cutoff radii (in terms of $F_{\text{vp}}^{(2)}$). The boxes are our numerical values and the line is a fit to these values.

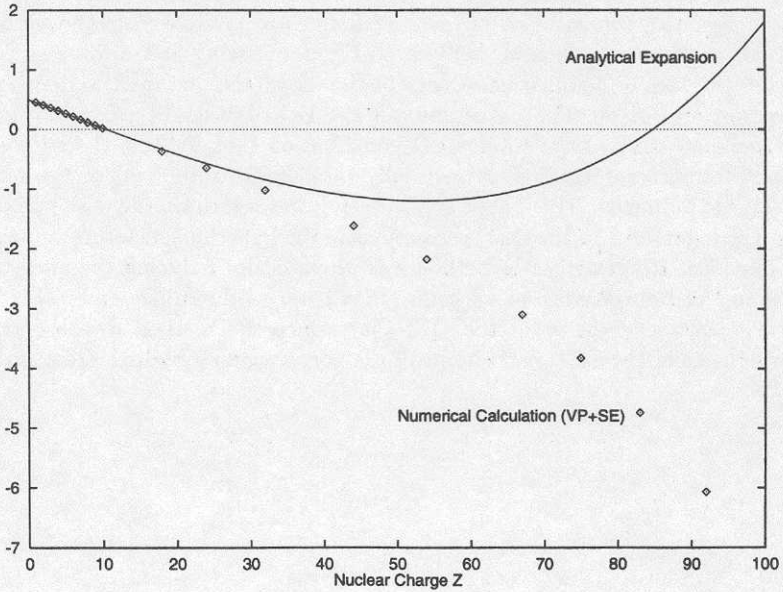


Figure 6.4: The total numerical hyperfine structure QED corrections, in units of $(\alpha/\pi)\Delta E_F$, plotted together with the results from the $(Z\alpha)$ -expansion.

7 Conclusions and Outlook

In recent years a considerable improvement has been gained in precision measurements on heavy highly-charged ions. These systems are fully relativistic and the electrons propagate in a very strong nuclear field. This provides a testing ground for both relativity and QED in a region not carefully investigated before. This has stimulated theory to perform accurate calculations for such systems, in the hope to uncover new effects or to verify the validity of existing theories in these extreme fields.

Several experiments on highly-charged ions have been carried out or are being planned in order to test bound-state QED [59, 60, 64, 95, 96]. Specifically, the ground-state hyperfine splitting of hydrogenlike bismuth and the two-electron contributions to the ground-state energy of heliumlike ions have both been measured with high precision. These accurate measurements, together with the bound electron g -factor experiment in progress at Mainz, have motivated a detailed theoretical study of the one-loop QED corrections, which have not been evaluated in a complete way before.

In this thesis we have presented the first complete evaluation of the one-loop QED corrections to the three different types of interactions mentioned above. These calculations have all been done non-perturbatively in the nuclear Coulomb field. For low Z we have compared our results with the known parts of the corresponding $(Z\alpha)$ -expansions, and we find in all cases excellent agreement. We have further made comparisons for all Z with other recent non-perturbative theoretical works and the results from these independent calculations coincide almost completely with ours. These facts suggest that we have a good understanding of how to evaluate these QED corrections, and that the numerical results can be considered to be reliable.

Considering the comparison with experiment in the two-electron case, we conclude that the experimental accuracy is not at present high enough to seriously test the QED parts. However, an improvement of one order of magnitude would be sufficient to achieve this. Such an improvement is expected in the near future [97].

Concerning the g -factor measurement it will constitute an excellent pure test of the bound-state QED effects at the percentage level, provided that the anticipated relative uncertainty of 10^{-7} is reached. The two-electron and g -factor cases both depend weakly on the nuclear structure. This is an important issue when comparing theory and experiment, since the nuclear uncertainties will not impair the QED test.

For the hyperfine splitting the picture is different. Here the lack of detailed knowledge of the nuclear magnetization distribution leads to such large uncertainties, in the dominating first-order contribution, that the QED part is completely obscured. On the other hand, trusting the QED parts one can extract information about the nuclear magnetization distribution [62].

Work is in progress in our group to generalize the presented calculation scheme to excited heliumlike systems, which are also interesting experimental test cases. This generalization will also be of importance for the theoretical investigation of the $2p_{1/2} - 2s_{1/2}$ transition in lithiumlike uranium, which recently have been measured with high accuracy [96]. The QED correction to the interaction between the core and the valence electron has earlier been treated only in an approximate way, which is not fully satisfactory. The almost perfect agreement between theory and experiment [98] is probably partly fortuitous since the missing contributions are estimated to be significant. To obtain an accurate theoretical prediction it is also essential to include the non-radiative QED effects as well as two-photon self-energy effects. The latter effects, which are essential also for the $1s$ Lamb shift in heavy hydrogenlike ions [95], are intensively investigated at present [99–102]. Due to the lack of detailed knowledge about the nuclear structure, it is at present not meaningful to go beyond the two virtual photon level in the evaluation of the QED effects.

Acknowledgements

First of all I want to acknowledge my close collaborators Docent Hans Persson and Docent Sten Salomonson. I owe you many thanks for your skillful guidance and your never ending support. These years together have really been stimulating.

I also want to express my gratitude to Professor Ingvar Lindgren, for valuable discussions and for the help with this thesis. Professor Eleanor Campbell is also greatly acknowledged.

I shared office with Dr Håkan Warston for a number of years, and I am very grateful for all his help during this time. Martin Gustavsson and Björn Åsén have both contributed to this work, not only in the practical meaning, but also as being good friends. I further would like to acknowledge associate Professor Ann-Marie Mårtensson-Pendrill for interesting discussions and comments.

The cooperation with the German group under the leadership of Professor Gerhard Soff has been fruitful and Dr Thomas Beier, Dr Stefan Schneider and Dr Günter Plunien are all greatly acknowledged.

I want to give very special thanks to all members of my family. Your support and encouragement during these years have been invaluable!

Finally I thank all previous and present members of the atomic physics group and the molecular physics group, for creating a friendly and stimulating atmosphere to work in.

APPENDICES

A Basic Theory of Bound State QED

The basic theory of bound-state QED will be discussed in some detail in this appendix. Second-quantized electron and electromagnetic fields will be introduced and the perturbative expansion of their interaction, the S-matrix expansion, and its connection to Feynman diagrams shall be discussed.

Despite the fact that our approach is explicitly frame dependent, since we attach the reference frame to a fixed atomic nucleus, we will be careful to develop a manifestly covariant formulation of bound-state QED. The covariance of the theory is important; it allows us to utilize well-established renormalization techniques to deal with the divergences which appear in QED.

A.1 Units and notations

In relativistic quantum field theory it is very convenient to work with *natural units*. In these units mass, action and velocity are taken to be the fundamental dimensions. Planck's constant, \hbar , is chosen to be the unit of action and the velocity of light, c , the unit of velocity. All quantities will then have the dimension of a power of mass. It is further expedient to put $\epsilon_0 = 1$ (the permittivity of vacuum) and consequently also $\mu_0 = 1$ (the permeability of vacuum). We can thus transform SI units to these new units by putting $\hbar = c = \epsilon_0 = \mu_0 = 1$. The dimensionless fine-structure constant, α , is for example given in SI units by the expression

$$\alpha = \frac{e^2}{4\pi\epsilon_0 c\hbar} \quad (\text{A.1})$$

and in natural units this reads

$$\alpha = \frac{e^2}{4\pi}. \quad (\text{A.2})$$

The electric charge, e , is thus dimensionless in natural units.

For the relativistic notation we use the metric tensor

$$g_{\mu\nu} = g^{\mu\nu} = \begin{pmatrix} 1 & 0 & 0 & 0 \\ 0 & -1 & 0 & 0 \\ 0 & 0 & -1 & 0 \\ 0 & 0 & 0 & -1 \end{pmatrix} \quad (\text{A.3})$$

which relates the covariant four-vector $x_\mu = (x_0, -\mathbf{x}) = (t, -\mathbf{x})$ to the contravariant $x^\mu = (x_0, \mathbf{x}) = (t, \mathbf{x})$ by

$$x_\mu = \sum_{\nu=0}^3 g_{\mu\nu} x^\nu = g_{\mu\nu} x^\nu. \quad (\text{A.4})$$

Here we have also introduced the convention that repeated indices, one contravariant and one covariant, are summed over. Greek indices ($\mu = 0, 1, 2, 3$) will label the components of four-vectors and Latin indices ($i = 1, 2, 3$) will be used to label three-vectors. The scalar product between four-vectors can be written in several ways

$$a \cdot b = a_\mu b^\mu = g_{\mu\nu} a^\nu b^\mu = \dots = a^0 b^0 - \mathbf{a} \cdot \mathbf{b}. \quad (\text{A.5})$$

The covariant and contravariant gradient operators are further defined by

$$\partial_\mu = \frac{\partial}{\partial x^\mu} = \left(\frac{\partial}{\partial t}, \nabla \right) \quad (\text{A.6})$$

$$\partial^\mu = \frac{\partial}{\partial x_\mu} = \left(\frac{\partial}{\partial t}, -\nabla \right) \quad (\text{A.7})$$

and from these definitions we introduce the four-divergence

$$\partial_\mu A^\mu = \frac{\partial A^0}{\partial t} + \nabla \cdot \mathbf{A} \quad (\text{A.8})$$

and finally the d'Alembertian operator

$$\square = \partial^\mu \partial_\mu = \frac{\partial^2}{\partial t^2} - \nabla^2. \quad (\text{A.9})$$

We will use the Dirac-Pauli representation of the gamma 4×4 matrices

$$\gamma^\mu = \gamma^0 \alpha^\mu \quad (\text{A.10})$$

where α^μ and $\gamma^0 (= \beta)$ are the standard Dirac matrices

$$\alpha^0 = \mathbf{1}, \quad \alpha = \begin{pmatrix} 0 & \boldsymbol{\sigma} \\ \boldsymbol{\sigma} & 0 \end{pmatrix}, \quad \gamma^0 = \begin{pmatrix} \mathbf{1} & 0 \\ 0 & -\mathbf{1} \end{pmatrix}, \quad (\text{A.11})$$

and where σ_k are the Pauli spin matrices

$$\sigma_1 = \begin{pmatrix} 0 & 1 \\ 1 & 0 \end{pmatrix}, \quad \sigma_2 = \begin{pmatrix} 0 & -i \\ i & 0 \end{pmatrix}, \quad \sigma_3 = \begin{pmatrix} 1 & 0 \\ 0 & -1 \end{pmatrix}. \quad (\text{A.12})$$

To simplify notations we also define the "slash" vector \not{p} by

$$\not{p} = \gamma^\mu p_\mu = \gamma^0 p^0 - \boldsymbol{\gamma} \cdot \mathbf{p}. \quad (\text{A.13})$$

We base further our definition of the bra state vector, $\langle a|$, on $\psi_a^\dagger(x)$ instead of $\bar{\psi}_a(x) = \psi_a^\dagger(x)\gamma^0$, which is the more commonly used convention. The γ^0 -matrix will here be associated with the operator and as an example, the first-order energy contribution from a perturbing potential, A^μ , will be written as

$$\Delta E^1 = \langle a | \gamma^0 A | a \rangle = \langle a | \alpha^\mu A_\mu | a \rangle = \langle a | A^0 - \boldsymbol{\alpha} \cdot \mathbf{A} | a \rangle. \quad (\text{A.14})$$

Correspondingly we associate an α^μ -matrix, rather than a γ^μ -matrix, to each vertex when formulating our Feynman diagram rules.

A.2 The non-interacting electron field

The non-interacting electron field is in our approach described by the solutions to the bound Dirac Hamiltonian. The electrostatic interaction with the nucleus is thus included from the very beginning and it is taken into account to all orders (all orders in $(Z\alpha)$). The matter field, expressed in terms of the eigenstates in the nuclear potential, is then canonically quantized (second quantization). This procedure for doing bound state QED is called the Furry interaction picture. It should be noted that we can also include other potentials when solving the Dirac equation, e.g. the vacuum polarization potential, in order to compute higher-order effects.

Starting from the Lagrangian density

$$\mathcal{L}(x) = \Psi^\dagger(x) \gamma^0 [i\partial - m + e\mathcal{A}] \Psi(x) \quad (\text{A.15})$$

we can derive the Dirac equation for an electron moving in a classical static electromagnetic potential $A^\mu(\mathbf{x})$

$$[i\partial - m + e\mathcal{A}(\mathbf{x})] \Psi(x) = 0. \quad (\text{A.16})$$

The solution set in the nuclear potential, $A^\mu(\mathbf{x}) = (\phi_{\text{nuc}}(\mathbf{x}), \mathbf{0})$, is then used to expand the electron field

$$\begin{aligned} \Psi(x) &= \sum_s^+ a_s \Phi_s(\mathbf{x}) e^{-iE_s t} + \sum_s^- b_s \Phi_s(\mathbf{x}) e^{-iE_s t} \\ \Psi^\dagger(x) &= \sum_s^+ a_s^\dagger \Phi_s^\dagger(\mathbf{x}) e^{iE_s t} + \sum_s^- b_s^\dagger \Phi_s^\dagger(\mathbf{x}) e^{iE_s t} \end{aligned} \quad (\text{A.17})$$

where $+$ and $-$ refers to positive and negative energy electron eigenstates. By imposing the anticommutation relations

$$[a_r, a_s^\dagger]_+ = [b_r, b_s^\dagger]_+ = \delta_{r,s} \quad (\text{A.18})$$

(all other anticommutators vanish) the field is quantized. These relations also guarantees that the electrons obey Fermi-Dirac statistics. Upon quantization the expansion coefficients turn into operators, and they have the interpretation that $\hat{a}^\dagger(\hat{b}^\dagger)$ and $\hat{a}(\hat{b})$ are the positive (negative) energy electron creation and annihilation operators. These operators act on number states, which are built up from the vacuum state $|0\rangle$, defined by

$$\hat{a}_r |0\rangle = \hat{b}_r^\dagger |0\rangle = 0 \quad \text{all } r. \quad (\text{A.19})$$

The vacuum state is thus the state with no positive energy electrons present, but with all the negative energy states occupied – *the Dirac sea*. The filled Dirac sea can alternatively be interpreted as an absence of positron states (with positive energy), since the creation of a positron is equivalent to the annihilation of a negative energy electron. We can thus turn to this positron-picture by replacing the creation (annihilation) operators of the negative energy electrons with annihilation (creation) operators of positive energy positrons.

One can further show that the Hamiltonian of this electron field has an infinite vacuum expectation value. This infinite constant is, however, harmless since only energy differences are observable. The same problem also occurs for other observables, e.g. the charge. To avoid these vacuum infinities, which originates from the Dirac sea, one can redefine the scale of energy, charge etc., such that all quantities are measured relative to the vacuum.

The electron propagator

We shall here introduce the Feynman electron propagator which is the Green's function for the Dirac equation. It describes the propagation of virtual particles of the electron field between two points in space-time. The Feynman propagator has the special property of simultaneously treating the two different time-orderings of a two point interaction. It has played an important role in the development of a systematic covariant perturbation theory.

The definition of the Feynman propagator reads

$$iS_F(x_2, x_1) = \langle 0 | T\{\hat{\Psi}(x_2)\hat{\Psi}^\dagger(x_1)\} | 0 \rangle \quad (\text{A.20})$$

where we have introduced the *time-ordered* product, defined by

$$T\{\hat{\Psi}(x_2)\hat{\Psi}^\dagger(x_1)\} = \begin{cases} \hat{\Psi}(x_2)\hat{\Psi}^\dagger(x_1), & t_2 > t_1 \\ -\hat{\Psi}^\dagger(x_1)\hat{\Psi}(x_2), & t_1 > t_2 \end{cases} \quad (\text{A.21})$$

The propagator thus contains two terms

$$\langle 0 | \Theta(t_2 - t_1)\hat{\Psi}(x_2)\hat{\Psi}^\dagger(x_1) - \Theta(t_1 - t_2)\hat{\Psi}^\dagger(x_1)\hat{\Psi}(x_2) | 0 \rangle \quad (\text{A.22})$$

where $\Theta(t)$ is the Heavyside step function which is equal to unity for positive arguments and zero otherwise.

For $t_2 > t_1$, the contribution to the propagator comes from the first term in Eq. (A.22). As $\hat{\Psi}^\dagger(x_1)$ acts on the vacuum state an electron is created at x_1 . This electron is then annihilated at x_2 by $\hat{\Psi}(x_2)$.

The second term contributes when $t_1 > t_2$, and results in an annihilation of a negative energy electron at x_2 , which is subsequently created at x_1 by the action of $\hat{\Psi}^\dagger(x_1)$. The negative energy electron can therefore be considered as propagating *backwards in time*. This absence of a negative energy electron, can alternatively be interpreted as the presence of a positive energy *positron*, propagating from x_2 to x_1 (forward in time). The Feynman electron propagator contains both these processes and we will represent it by a single *Feynman diagram*, in which there is no time-ordering of the interaction points (vertices) x_1 and x_2 . It is also worth noting that only when considering the two cases together, as in the full Feynman propagator, one obtains a manifestly covariant treatment.

We proceed now with deriving an expression for the propagator which is suitable for actual calculations. By using the expansion of the electron field and the anticommutation relations for the creation and absorption operators one

obtains

$$iS_F(x_2, x_1) = \Theta(t_2 - t_1) \sum_s^+ e^{-iE_s(t_2 - t_1)} \Phi_s(\mathbf{x}_2) \Phi_s^\dagger(\mathbf{x}_1) - \Theta(t_1 - t_2) \sum_s^- e^{-iE_s(t_2 - t_1)} \Phi_s(\mathbf{x}_2) \Phi_s^\dagger(\mathbf{x}_1). \quad (\text{A.23})$$

The propagator can further be expressed as an integral in the complex z -plane, separating out the time-dependence

$$S_F(x_2, x_1) = \int_{-\infty}^{\infty} \frac{dz}{2\pi} e^{-iz(t_2 - t_1)} S_F(\mathbf{x}_2, \mathbf{x}_1, z) \quad (\text{A.24})$$

where

$$S_F(\mathbf{x}_2, \mathbf{x}_1, z) = \sum_s \frac{\Phi_s(\mathbf{x}_2) \Phi_s^\dagger(\mathbf{x}_1)}{z - E_s(1 - i\eta)} \quad (\text{A.25})$$

and where s runs over the complete set of solutions. In the denominator a small positive number, η , is introduced to move the poles off the real axis; poles originating from states in the positive energy spectrum (also those which may have negative energy) is placed in the lower half-plane, whereas the negative energy poles are situated in the upper half-plane.

For bound state problems, in contrast to free electron QED, it is also necessary to define a propagator for equal coordinates. The time-ordering can for equal times be defined as

$$T\{\hat{\Psi}(x)\hat{\Psi}^\dagger(x)\} = \frac{1}{2} [\hat{\Psi}(x)\hat{\Psi}^\dagger(x) - \hat{\Psi}^\dagger(x)\hat{\Psi}(x)], \quad (\text{A.26})$$

which gives the equal-time propagator

$$iS_F(x) = \frac{1}{2} \sum_s \text{sign}(E_s) \Phi_s(\mathbf{x}) \Phi_s^\dagger(\mathbf{x}) \quad (\text{A.27})$$

where $\text{sign}(E_s)$ associate a minus sign to the terms from the negative energy spectrum. By straightforward integration it is seen that the integral form of S_F in Eq. (A.24) also holds for the equal-time case.

A.3 The electromagnetic field

It is well known that only the transverse radiation field corresponds to dynamical degrees of freedom for the electromagnetic field. Here we want to develop a covariant theory, i.e. we wish to treat all four components of the potential, $A^\mu = (\phi, \mathbf{A})$, on an equal footing. This implies that we introduce more dynamical degrees of freedom than the field possesses. In order to get this formulation consistent, suitable constraints have to be imposed. The theory of covariant quantization of the electromagnetic field is by no means trivial and leads to various difficulties, such as states with negative norm. These problems can be treated in a rigorous way within the Gupta-Bleuler formalism and a more

complete discussion of this subject can be found in the book of Mandl and Shaw [9] and the references therein. Here we just take over the results necessary for our description.

We start by expressing Maxwells equations in a covariant form. For this purpose we introduce the antisymmetric field tensor

$$F^{\mu\nu}(x) = \begin{pmatrix} 0 & E_x & E_y & E_z \\ -E_x & 0 & B_z & -B_y \\ -E_y & -B_z & 0 & B_x \\ -E_z & B_y & -B_x & 0 \end{pmatrix}, \quad (\text{A.28})$$

where \mathbf{E} and \mathbf{B} are the electric and magnetic fields, respectively. In terms of the field tensor and the charge-current density, $s^\mu = (\rho, \mathbf{j})$, Maxwells equations reads

$$\partial_\nu F^{\mu\nu}(x) = s^\mu(x) \quad (\text{A.29})$$

$$\partial^\lambda F^{\mu\nu}(x) + \partial^\mu F^{\nu\lambda}(x) + \partial^\nu F^{\lambda\mu}(x) = 0. \quad (\text{A.30})$$

The conservation of the charge-current density, $\partial_\mu s^\mu(x) = 0$, follows directly from the antisymmetric property of $F^{\mu\nu}$. From Eq. (A.30) we deduce that the fields can be expressed in terms of the four-potential $A^\mu(x)$,

$$F^{\mu\nu}(x) = \partial^\nu A^\mu(x) - \partial^\mu A^\nu(x) \quad (\text{A.31})$$

and in terms of the potential, Maxwells inhomogeneous equations becomes

$$\square A^\mu(x) - \partial^\mu(\partial_\nu A^\nu) = s^\mu(x). \quad (\text{A.32})$$

Furthermore, Eq. (A.31) ensures gauge invariance since a general gauge transformation

$$A^\mu(x) \longrightarrow \tilde{A}^\mu(x) = A^\mu(x) + \partial^\mu f(x) \quad (\text{A.33})$$

leaves the field tensor identically unchanged.

The proper Lagrangian density which generates Maxwells equations

$$\mathcal{L}_M(x) = -\frac{1}{4}F_{\mu\nu}(x)F^{\mu\nu}(x) - s^\mu(x)A_\mu(x) \quad (\text{A.34})$$

can not be used for covariant canonical quantization. This is a manifestation of the fact that the electromagnetic field has indeed only two degrees of freedom. This density leads to the conjugate fields

$$\pi^\mu(x) = \frac{\partial \mathcal{L}_M}{\partial \dot{A}_\mu} = -F^{\mu 0}(x) \quad (\text{A.35})$$

and in particular $\pi^0(x) \equiv 0$, which is incompatible with canonical quantization. This problem can be circumvented by choosing a particular gauge. We work here in the Feynman gauge in which the potential fulfills the constraint

$$\partial_\mu A^\mu(x) = 0 \quad (\text{A.36})$$

which is referred to as the Lorentz condition. The Lagrangian density is in the Feynman gauge modified to read

$$\mathcal{L}_F(x) = \mathcal{L}_M(x) - \frac{1}{2}(\partial_\mu A^\mu(x))^2 \quad (\text{A.37})$$

and it generates the field equations

$$\square A^\mu(x) = s^\mu(x) \quad (\text{A.38})$$

which is consistent with Eq. (A.32) due to the Lorentz condition. The potentials are, however, not uniquely defined by the Lorentz constraint since the constraint is invariant under gauge transformations, provided the gauge function satisfies $\square f(x) = 0$. Any gauge in which the Lorentz condition holds is called a Lorentz gauge. Besides the Feynman gauge the Fried-Yennie gauge is a widely used Lorentz gauge which we will return to later.

An important property of the Lorentz gauge is that the imposed constraint is a Lorentz-invariant. This is in contrast to the Coulomb gauge in which the condition $\nabla \cdot \mathbf{A} = 0$ is imposed. This gauge implies for the free field case (no charges present) the field equations $\square \mathbf{A} = 0$. The solutions are free transverse electromagnetic waves with the expected two polarization states. In the presence of charges we have to add the instantaneous Coulomb interaction, which in the Coulomb gauge is treated as a classical potential. The Coulomb gauge has the advantage of containing only the two dynamical degrees of freedom and no redundant information. However, the condition $\nabla \cdot \mathbf{A} = 0$ separates transverse and longitudinal components and is therefore manifestly frame-dependent. The Coulomb gauge is therefore not suitable for developing the general theory since we wish to establish an explicitly covariant formulation of bound-state QED. We will therefore hold on to the Lorentz gauge in order to achieve this.

The Feynman Lagrangian density, Eq. (A.37), is now used to quantize the field, ignoring the Lorentz condition. To end up with Maxwells equations, we impose the Lorentz constraint as a subsidiary condition after the quantization has been performed.

The field equations in Feynman gauge are in the free field case

$$\square A^\mu(x) = 0. \quad (\text{A.39})$$

All four components of the potential $A^\mu(x)$ can thus be expanded in terms of plane waves and the quantized photon field can be written as

$$\hat{A}^\mu(x) = \sum_{r,\mathbf{k}} \sqrt{\frac{1}{2V\omega_{\mathbf{k}}}} \epsilon_r^\mu(\mathbf{k}) \left[\hat{c}_r(\mathbf{k}) e^{-ik \cdot x} + \hat{c}_r^\dagger(\mathbf{k}) e^{ik \cdot x} \right] \quad (\text{A.40})$$

where $k^\mu = (\omega_{\mathbf{k}} = |\mathbf{k}|, \mathbf{k})$ is the wave vector of the photon. V is the quantization volume and the sum over \mathbf{k} runs over the wave vectors allowed by the imposed periodic boundary conditions. The summation over r runs from $r = 0$ to $r = 3$ and corresponds to the fact that for the four-vector potential $A^\mu(x)$ there exists, for each \mathbf{k} , four linearly independent polarization states. These states are described by the polarization vectors $\epsilon_r^\mu(\mathbf{k})$; $r = 1, 2$ corresponds to

the transverse field, $r = 0$ describes scalar photons and $r = 3$ corresponds to longitudinal photons. The expansion coefficients are operators satisfying the commutation relations

$$[\hat{c}_r(\mathbf{k}'), \hat{c}_s^\dagger(\mathbf{k})]_- = \zeta_r \delta_{r,s} \delta_{\mathbf{k},\mathbf{k}'} \quad (\text{A.41})$$

$$[\hat{c}_r(\mathbf{k}'), \hat{c}_s(\mathbf{k})]_- = [\hat{c}_r^\dagger(\mathbf{k}'), \hat{c}_s^\dagger(\mathbf{k})]_- = 0 \quad (\text{A.42})$$

where $\zeta_r = 1$ for $r = 1, 2, 3$ and $\zeta_r = -1$ for $r = 0$. Note that these commutation relations imply Bose-Einstein statistics. $\hat{c}_r(\mathbf{k})$ and $\hat{c}_r^\dagger(\mathbf{k})$ are interpreted as absorption and creation operators for transverse, longitudinal and scalar photons.

For the free-field case one can show that as a consequence of imposing the subsidiary Lorentz condition, it is only the transverse photons that contribute to observable quantities. Thus, the scalar and longitudinal photons do not show up as free particles. However, if there are charges present these two additional polarization states are important as they provide a covariant description of the instantaneous Coulomb interaction between charges.

The photon propagator

The covariant photon propagator describes the interaction between charges via the exchange of four kinds of virtual photons. The instantaneous Coulomb interaction emerges as an exchange of scalar and longitudinal photons and the transverse photons describe the transverse radiation field.

The Feynman photon propagator is defined, in analogy with the electron propagator, as the vacuum expectation value

$$iD_F^{\mu\nu}(x_1 - x_2) = \langle 0 | T \{ \hat{A}^\mu(x_1) \hat{A}^\nu(x_2) \} | 0 \rangle. \quad (\text{A.43})$$

In Feynman gauge this leads to

$$D_F^{\mu\nu}(x_1 - x_2) = -g^{\mu\nu} \int \frac{d^4k}{(2\pi)^4} \frac{e^{-ik \cdot (x_1 - x_2)}}{k^2 + i\delta}, \quad (\text{A.44})$$

where the k^0 -integration runs over $-\infty < k^0 < \infty$ and δ is a small positive number which defines the contour of integration.

In analogy with the electron case, we state a form of the photon propagator which separate out the time-dependence ($z = k^0$)

$$D_F^{\mu\nu}(x_1 - x_2) = \int_{-\infty}^{\infty} \frac{dz}{2\pi} e^{-iz(t_1 - t_2)} D_F^{\mu\nu}(\mathbf{x}_1 - \mathbf{x}_2, z) \quad (\text{A.45})$$

where

$$D_F^{\mu\nu}(\mathbf{x}_1 - \mathbf{x}_2, z) = -g^{\mu\nu} \int \frac{d^3\mathbf{k}}{(2\pi)^3} \frac{e^{i\mathbf{k} \cdot (\mathbf{x}_1 - \mathbf{x}_2)}}{z^2 - \mathbf{k}^2 + i\delta}. \quad (\text{A.46})$$

Using different gauges affects the photon propagator and the general form can be expressed as

$$D_F^{\mu\nu}(x_1 - x_2) = \int \frac{d^4k}{(2\pi)^4} e^{-ik \cdot (x_1 - x_2)} \frac{\tilde{D}^{\mu\nu}(k)}{k^2 + i\delta}, \quad (\text{A.47})$$

where $\tilde{D}^{\mu\nu}(k) = -g^{\mu\nu}$ retains the Feynman gauge. The Fried-Yennie gauge, which is particularly useful when treating infrared divergences, corresponds to $\tilde{D}_{\text{FY}}^{\mu\nu}(k) = -g^{\mu\nu} - 2k^\mu k^\nu / k^2$. In the Coulomb gauge we find the components $\tilde{D}_{\text{C}}^{00}(k) = k^2 / k^2$, $\tilde{D}_{\text{C}}^{i0}(k) = \tilde{D}_{\text{C}}^{0i}(k) = 0$ and $\tilde{D}_{\text{C}}^{ij}(k) = \delta_{ij} - k^i k^j / k^2$. Here we have the direct physical interpretation that $\tilde{D}_{\text{C}}^{00}$ gives the instantaneous Coulomb interaction and $\tilde{D}_{\text{C}}^{ij}$ corresponds to the transverse (magnetic) interaction.

A.4 The interacting fields

Here we shall consider the interaction between electrons and the electromagnetic field within the quantized field theory. The interaction is introduced by the minimal coupling

$$\partial_\mu \longrightarrow \partial_\mu - ieA_\mu. \quad (\text{A.48})$$

In addition to the interaction between electrons and the quantized photon field, we want here to study interactions with an external classical potential A_μ^{ext} . The electron Lagrangian density, Eq. (A.15), is therefore modified according to

$$\partial_\mu \longrightarrow \partial_\mu - ie \left[\hat{A}_\mu + A_\mu^{\text{ext}} \right], \quad (\text{A.49})$$

where \hat{A}_μ represents the quantized electromagnetic field. The total Lagrangian density for bound state QED can thus be written as

$$\mathcal{L}_{\text{QED}}(x) = \mathcal{L}_{\text{Electron}}(x) + \mathcal{L}_{\text{Photon}}(x) + \mathcal{L}_{\text{int}}(x) \quad (\text{A.50})$$

where $\mathcal{L}_{\text{Electron}}$ and $\mathcal{L}_{\text{Photon}}$ are given by Eqs. (A.15, A.37) and where the interaction density is given by

$$\mathcal{L}_{\text{int}}(x) = \hat{\Psi}^\dagger(x) \gamma^0 \left[e \hat{A}(x) + e A^{\text{ext}}(x) \right] \hat{\Psi}(x). \quad (\text{A.51})$$

The total Hamiltonian is divided into two parts

$$H_{\text{QED}}(t) = H_0(t) + H_I(t) \quad (\text{A.52})$$

where $H_0 = H_{\text{Electron}} + H_{\text{Photon}}$ is the Hamiltonian of the non-interacting fields and H_I is the interaction term

$$H_I(t) = \int d^3\mathbf{x} \mathcal{H}_I(x) = - \int d^3\mathbf{x} \hat{\Psi}^\dagger(x) \gamma^0 \left[e \hat{A}(x) + e A^{\text{ext}}(x) \right] \hat{\Psi}(x). \quad (\text{A.53})$$

To solve the time-development of a system with the Hamiltonian (A.52) is an extremely difficult problem, and this has only been done within perturbation theory. A perturbative expansion is of course only meaningful if the interaction is sufficiently weak. This is the case in QED where the interaction strength is given by the fine-structure constant $\alpha \approx 1/137$.

Up to now we have worked in the Heisenberg time-development picture (H.P.), where the operators (e.g. fields) carry the full time-dependence, whereas the state vectors are constants of motion. If we now go over to work in the Interaction picture (I.P.), which is well suited for the Hamiltonian (A.52), the

development of a perturbative expansion will be much simplified. Many of the results derived in the H.P. can directly be taken over to the I.P. The reason for this is that the time-development of the operators is in the I.P. determined by the free Hamiltonian, H_0 , and not by the full Hamiltonian H_{QED} .

In the I.P., the system is described by a time-dependent state vector, $|\Phi(t)\rangle$, which satisfies the equation of motion

$$i \frac{d}{dt} |\Phi(t)\rangle = H_I(t) |\Phi(t)\rangle, \quad (\text{A.54})$$

which is solved by the integral equation

$$|\Phi(t)\rangle = |\Phi(t_0)\rangle - i \int_{t_0}^t dt_1 H_I(t_1) |\Phi(t_1)\rangle. \quad (\text{A.55})$$

Defining the S-matrix operator, \hat{S} , by

$$|\Phi(\infty)\rangle = \hat{S} |\Phi(-\infty)\rangle \quad (\text{A.56})$$

we can, from Eq. (A.55), obtain the iterative solution for the S-matrix

$$\begin{aligned} \hat{S} &= \sum_{n=0}^{\infty} (-i)^n \frac{1}{n!} \int_{-\infty}^{\infty} dt_1 \int_{-\infty}^{\infty} dt_2 \dots \int_{-\infty}^{\infty} dt_n T \{ H_I(t_1) \dots H_I(t_n) \} \\ &= \sum_{n=0}^{\infty} (-i)^n \frac{1}{n!} \int d^4 x_1 \int d^4 x_2 \dots \int d^4 x_n T \{ \mathcal{H}_I(x_1) \dots \mathcal{H}_I(x_n) \}. \end{aligned} \quad (\text{A.57})$$

The S-matrix defined here was originally designed for scattering processes where the interacting particles approach each other from $t = -\infty$, collide (i.e. interact) at $t = 0$, and then finally fly apart again at $t = \infty$. In bound-state QED the interaction is present all the time, and we must therefore change the formalism slightly in order to take over the S-matrix approach to the bound state problem. We do this by adopting the adiabatic hypothesis, introduced by Gell-Mann and Low [103], which modifies the interaction Hamiltonian according to

$$H_I(t) \rightarrow H_I(t, \gamma) = e^{-\gamma|t|} H_I(t) \quad (\text{A.58})$$

where $\gamma > 0$ is the adiabatic parameter. The modified interaction is then switched off as $t \rightarrow \pm\infty$ and at $t = 0$ we have the full interaction $H_I(t)$. With the interaction (A.58) we generalize the S-matrix concept to be valid also for bound states. At the end of calculations we then put $\gamma = 0$ to restore the usual interaction.

In order to obtain the energy level shifts caused by the interaction H_I , we introduce the level shift formula

$$\Delta E_a = \lim_{\gamma \rightarrow 0} \frac{1}{2} i \gamma e \frac{\frac{\partial}{\partial e} \langle \Phi_a^0 | \hat{S}_\gamma | \Phi_a^0 \rangle}{\langle \Phi_a^0 | \hat{S}_\gamma | \Phi_a^0 \rangle} \quad (\text{A.59})$$

which was derived by Sucher [104], and where $|\Phi_a^0\rangle$ is the state vector of the atomic system considered. This formula can be expanded in a power series in

e and by introducing the abbreviation $\langle \hat{S}_\gamma^{(n)} \rangle = \langle \Phi_a^0 | \hat{S}_\gamma^{(n)} | \Phi_a^0 \rangle$, where the superscript indicates the order in e , we obtain up to order e^4 (α^2)

$$\begin{aligned} \Delta E_a = & \lim_{\gamma \rightarrow 0} \frac{1}{2} i\gamma \left\{ \langle \hat{S}_\gamma^{(1)} \rangle + [2\langle \hat{S}_\gamma^{(2)} \rangle - \langle \hat{S}_\gamma^{(1)} \rangle^2] + [3\langle \hat{S}_\gamma^{(3)} \rangle - 3\langle \hat{S}_\gamma^{(2)} \rangle \langle \hat{S}_\gamma^{(1)} \rangle + \langle \hat{S}_\gamma^{(1)} \rangle^3] \right. \\ & \left. + [4\langle \hat{S}_\gamma^{(4)} \rangle - 4\langle \hat{S}_\gamma^{(3)} \rangle \langle \hat{S}_\gamma^{(1)} \rangle + 4\langle \hat{S}_\gamma^{(2)} \rangle \langle \hat{S}_\gamma^{(1)} \rangle^2 - 2\langle \hat{S}_\gamma^{(2)} \rangle^2 - \langle \hat{S}_\gamma^{(1)} \rangle^4] + O(e^5) \right\} \end{aligned} \quad (\text{A.60})$$

There are two types of matrix elements that has to be distinguished; *reducible* and *irreducible*. An irreducible matrix element is, by definition, a matrix element which does not contain parts that can be written as a product of lower order matrix elements. The product terms in Eq. (A.60) are naturally reducible and it is only the “pure” terms ($\langle \hat{S}_\gamma^{(1)} \rangle, 2\langle \hat{S}_\gamma^{(2)} \rangle, 3\langle \hat{S}_\gamma^{(3)} \rangle, 4\langle \hat{S}_\gamma^{(4)} \rangle$) that can be irreducible. Even these terms can, however, contain reducible parts if an intermediate state in the spectral decomposition of the electron propagator coincides with some initial or final state (*reference state*).

For an irreducible matrix element, or an irreducible part of a reducible matrix element, the limit $\gamma \rightarrow 0$ can be taken in the beginning of the calculations and the energy level shift can then be written as

$$\Delta E_{a,\text{irr}}^{(n)} = iM^{(n)}, \quad (\text{A.61})$$

where $M^{(n)}$ is the Feynman amplitude defined by the relation

$$\langle \Phi_a^0 | \hat{S}^{(n)} | \Phi_a^0 \rangle = 2\pi \delta \left(\sum (E_{\text{in}} - E_{\text{out}}) \right) M^{(n)}. \quad (\text{A.62})$$

To calculate $M^{(n)}$ one can use simple time-independent Feynman rules which will be stated at the end of this chapter.

The calculation of reducible parts are done using the expansion (A.60) and will give rise to singularities in terms of γ^{-1} . Subtracting the appropriate lower-order matrix elements in Eq. (A.60) will, however, cancel the singularities and the γ -limit can be taken. For some cases there will also be a finite remainder. We will see an example of this procedure in Appendix E.

A.4.1 Wick's theorem

We will now introduce Wick's theorem [105], which is an operator identity that relates a time-ordered product of operators to a sum of *normal-ordered* products. The normal-ordering is defined such that all absorption operators stands to right of all creation operators in each product of operators. Applying Wick's theorem on the time-ordered Hamiltonians in the S-matrix will significantly simplify its evaluation. Before stating the theorem we first define the *contraction* between two field operators by

$$\underline{AB} = T\{AB\} - N\{AB\} = \langle 0 | T\{AB\} | 0 \rangle. \quad (\text{A.63})$$

The electron- and photon-propagators are thus defined as contractions of the corresponding fields. Note that the contraction is just a C -number, and it will therefore not be affected by normal-ordering.

Wick's theorem arise when one generalize the contraction to the case of several field operators, and it reads

$$\begin{aligned}
 & T\{ABCD\dots WXYZ\} = N\{ABCD\dots WXYZ\} \\
 & + N\{\underline{A}BCD\dots WXYZ\} + \dots + N\{ABCD\dots \underline{WXY}Z\} \\
 & + N\{\underline{AB} \underline{C}D\dots WXYZ\} + \dots + N\{ABCD\dots \underline{WX} \underline{Y}Z\} \\
 & + \dots
 \end{aligned} \tag{A.64}$$

The second line contains all possible contractions that can be formed by two of the operators, on the third line appears all possible combinations including two contractions and so on. Altogether, the right-hand side of Eq. (A.64) represents all possible contractions that can be formed by the interacting field operators $ABCD\dots WXYZ$.

Using Wick's theorem we can write down the S-matrix in a form where all uncontracted operators are normal-ordered. This implies that only those terms which contain the absorption and creation operators necessary to destroy the initial electrons and to create the final electrons will contribute. Note further that this form of Wick's theorem does not impose any restrictions on the possible contractions and therefore allows for equal-time propagators. This is not the case when the operators $ABC\dots$ consists of normal-ordered groups. It was for this reason that the interaction Hamiltonian, Eq. (A.53), was defined without the normal-ordering, which is the usual procedure for free-electron QED.

A.5 Rules for Feynman diagrams

We will here summarize the rules which can be used to write down the mathematical expression for a general Feynman diagram. When setting up these rules we have followed the notations given by Lindgren [106].

The energy shift for irreducible matrix elements can be expressed in terms of a Feynman amplitude, M , as

$$\Delta E_{\text{irr}}^{(n),j} = \frac{i}{2\pi} \langle \Phi_a^0 | \hat{S}^{(n),j} | \Phi_a^0 \rangle = iM^{(n),j}$$

where n denotes the order of the S-matrix contribution and j the special process considered. For reducible matrix elements one should use the energy level shift formula (A.60) to obtain the energy shifts. In this case the rules gives the particular matrix element considered

$$\langle \Phi_a^0 | \hat{S}_\gamma^{(n),j} | \Phi_a^0 \rangle = M_\gamma^{(n),j}.$$

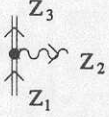
To obtain the Feynman amplitude, write down the following factors:



1. For each incoming electron line: $\Phi(\mathbf{x})$



2. For each outgoing electron line: $\Phi^\dagger(\mathbf{x})$



3. For each vertex: $ie\alpha^\mu$, associate $2\pi\Delta_\gamma(z_1 - z_3 - z_2)$ for reducible elements, in the irreducible case use energy conservation ($z_1 = z_3 + z_2$). For external lines z is replaced with the orbital energy E_a .



4. External potential interaction: $A_\mu^{\text{ext}}(\mathbf{x})$, energy parameter $z = 0$.



5. For each internal photon line:

$$iD_{\mu\nu}^F(\mathbf{x}_2 - \mathbf{x}_1, z) = -ig_{\mu\nu} \int \frac{d^3\mathbf{k}}{(2\pi)^3} \frac{e^{i\mathbf{k}\cdot(\mathbf{x}_2 - \mathbf{x}_1)}}{z^2 - \mathbf{k}^2 + i\delta}$$



6. For each internal electron line: $iS_F(\mathbf{x}_2, \mathbf{x}_1, z) = i \sum_s \frac{\Phi_s(\mathbf{x}_2)\Phi_s^\dagger(\mathbf{x}_1)}{z - E_s(1 - i\eta)}$

7. For each closed electron loop: Factor of (-1) and the trace symbol.

8. Integration over all \mathbf{x} and z variables. Include a factor of $(2\pi)^{-1}$ for each nontrivial z -integration.

B Interaction Potentials in Momentum Space

We shall here derive the momentum space expressions for the interaction potentials. For that purpose we start with transforming the expression for the first-order energy from coordinate to momentum space.

The first-order interaction energy is given in coordinate space by the integral

$$\Delta E^1 = -e \int d^3\mathbf{x} \Phi_a^\dagger(\mathbf{x}) \alpha^\mu A_\mu(\mathbf{x}) \Phi_a(\mathbf{x}), \quad (\text{B.1})$$

where A_μ is the potential of the given interaction. We now insert a delta function for each wavefunction and write

$$\Delta E^1 = -e \int d^3\mathbf{x} \int d^3\mathbf{y}_1 \int d^3\mathbf{y}_2 \Phi_a^\dagger(\mathbf{y}_1) \delta^3(\mathbf{x} - \mathbf{y}_1) \alpha^\mu A_\mu(\mathbf{x}) \delta^3(\mathbf{x} - \mathbf{y}_2) \Phi_a(\mathbf{y}_2).$$

Using the Fourier integral representation of the delta function

$$\delta^3(\mathbf{x} - \mathbf{y}) = \int \frac{d^3\mathbf{p}}{(2\pi)^3} e^{\pm i\mathbf{p}\cdot(\mathbf{x}-\mathbf{y})} \quad (\text{B.2})$$

yields

$$\begin{aligned} \Delta E^1 = & -e \int d^3\mathbf{x} \int d^3\mathbf{y}_1 \int d^3\mathbf{y}_2 \int \frac{d^3\mathbf{p}}{(2\pi)^3} \int \frac{d^3\mathbf{p}'}{(2\pi)^3} \\ & \times \Phi_a^\dagger(\mathbf{y}_1) e^{i\mathbf{p}\cdot(\mathbf{y}_1-\mathbf{x})} \alpha^\mu A_\mu(\mathbf{x}) e^{-i\mathbf{p}'\cdot(\mathbf{y}_2-\mathbf{x})} \Phi_a(\mathbf{y}_2). \end{aligned} \quad (\text{B.3})$$

We now define the momentum space wavefunction and potential by

$$\begin{aligned} \Phi_a(\mathbf{p}) &= \frac{1}{(2\pi)^{3/2}} \int d^3\mathbf{r} e^{-i\mathbf{p}\cdot\mathbf{r}} \Phi_a(\mathbf{r}) \\ A_\mu(\mathbf{q}) &= \frac{1}{(2\pi)^3} \int d^3\mathbf{r} e^{-i\mathbf{q}\cdot\mathbf{r}} A_\mu(\mathbf{r}) \end{aligned} \quad (\text{B.4})$$

and identification of these in Eq. (B.3) gives then the first-order energy in momentum space

$$\Delta E^1 = -e \int d^3\mathbf{p} \int d^3\mathbf{p}' \Phi_a^\dagger(\mathbf{p}) \alpha^\mu A_\mu(\mathbf{p} - \mathbf{p}') \Phi_a(\mathbf{p}'). \quad (\text{B.5})$$

We see here that the interaction potential depends on the difference $\mathbf{q} = \mathbf{p} - \mathbf{p}'$ where \mathbf{p} and \mathbf{p}' are the outgoing and incoming momenta, respectively. We shall now derive explicit forms of the momentum space potentials for the three different interactions considered in this thesis.

B.1 The electron potential

The electron potential is in coordinate space given by

$$A_\mu^{db}(\mathbf{x}) = -e \int d^3\mathbf{y} D_{\mu\nu}^F(\mathbf{x} - \mathbf{y}, 0) \Phi_d^\dagger(\mathbf{y}) \alpha^\nu \Phi_b(\mathbf{y}), \quad (\text{B.6})$$

and by using

$$D_{\mu\nu}^F(\mathbf{x} - \mathbf{y}, 0) = g_{\mu\nu} \int \frac{d^3\mathbf{k}}{(2\pi)^3} \frac{1}{k^2} e^{i\mathbf{k}\cdot(\mathbf{x}-\mathbf{y})}, \quad (\text{B.7})$$

we can write

$$A_\mu^{db}(\mathbf{x}) = \frac{-e}{(2\pi)^3} \int d^3\mathbf{k} e^{i\mathbf{k}\cdot\mathbf{x}} \frac{1}{k^2} \int d^3\mathbf{y} e^{-i\mathbf{k}\cdot\mathbf{y}} \Phi_d^\dagger(\mathbf{y}) \alpha_\mu \Phi_b(\mathbf{y}). \quad (\text{B.8})$$

From this expression we can directly identify the potential in momentum space

$$A_\mu^{db}(\mathbf{k}) = \frac{-e}{(2\pi)^3} \frac{1}{k^2} \int d^3\mathbf{y} e^{-i\mathbf{k}\cdot\mathbf{y}} \Phi_d^\dagger(\mathbf{y}) \alpha_\mu \Phi_b(\mathbf{y}). \quad (\text{B.9})$$

The Coulomb (scalar) and Breit (vector) parts of this potential will now be treated separately and the explicit momentum space expressions will be written down.

B.1.1 Coulomb potential

The atomic wavefunction can for a spherically symmetric potential be separated into an angular part and a radial part as

$$\Phi(\mathbf{r}) = \begin{pmatrix} f(r) \chi_\kappa^m(\hat{r}) \\ ig(r) \chi_{-\kappa}^m(\hat{r}) \end{pmatrix}, \quad (\text{B.10})$$

where $f(r)$ and $g(r)$ are the large and small radial components of the wave function, respectively, and $\chi_\kappa^m(\hat{r})$ is the ls -coupled spin-angular function. For the scalar interaction it is straightforward to obtain (only $m_b = m_d = \pm 1/2$ contributes)

$$\Phi_d^\dagger(\mathbf{r}) \Phi_b(\mathbf{r}) = \frac{1}{4\pi} [f^2(r) + g^2(r)]. \quad (\text{B.11})$$

The momentum transform is thus given by

$$A_0^{db}(\mathbf{q}) = \frac{-e}{(2\pi)^3} \frac{1}{q^2} \int d^3\mathbf{r} e^{-i\mathbf{q}\cdot\mathbf{r}} \frac{1}{4\pi} [f^2(r) + g^2(r)], \quad (\text{B.12})$$

and by performing the angular integration we obtain

$$A_0^{db}(\mathbf{q}) = \frac{-e}{(2\pi)^3} \frac{1}{q^2} \int dr r^2 j_0(qr) [f^2(r) + g^2(r)]. \quad (\text{B.13})$$

The potential depends on the difference $\mathbf{q} = \mathbf{p} - \mathbf{p}'$, and to separate the angular dependencies we use the general expansion of a function of $\cos \vartheta$ where ϑ is the angle between \mathbf{p} and \mathbf{p}'

$$V(p, p', \cos \vartheta) = \sum_{k=0}^{\infty} (2k+1) V_k(p, p') \mathbf{C}^k(\hat{p}) \cdot \mathbf{C}^k(\hat{p}'). \quad (\text{B.14})$$

Here we have introduced the \mathbf{C}^k tensor, which is related to the spherical harmonics Y_m^k by $C_m^k = \sqrt{4\pi/(2k+1)} Y_m^k$. The expansion coefficients $V_k(p, p')$ are given by

$$V_k(p, p') = \frac{1}{2} \int_{-1}^1 d \cos \vartheta V(p, p', \cos \vartheta) P_k(\cos \vartheta), \quad (\text{B.15})$$

where $P_k(\cos \vartheta)$ is the Legendre polynomial of order k . This way of separating angular dependencies will be used extensively throughout the thesis. The final form of the Coulomb potential in momentum space can now be written as

$$A_0^{db}(\mathbf{p} - \mathbf{p}') = \frac{-e}{(2\pi)^3} \sum_{k=0}^{\infty} (2k+1) V_k(p, p') \mathbf{C}^k(\hat{p}) \cdot \mathbf{C}^k(\hat{p}'), \quad (\text{B.16})$$

with

$$V(p, p', \cos \vartheta) = \frac{1}{q^2} \int dr r^2 j_0(qr) [f^2(r) + g^2(r)]. \quad (\text{B.17})$$

B.1.2 Breit potential

The momentum transform is given by the expression

$$\mathbf{A}^{db}(\mathbf{q}) = \frac{-e}{(2\pi)^3} \frac{1}{q^2} \int d^3 \mathbf{r} e^{-i\mathbf{q}\cdot\mathbf{r}} \Phi_d^\dagger(\mathbf{r}) \boldsymbol{\alpha} \Phi_b(\mathbf{r}), \quad (\text{B.18})$$

and to perform the angular integrations we use the spherical expansion of a plane wave

$$e^{-i\mathbf{q}\cdot\mathbf{r}} = \sum_{l=0}^{\infty} (2l+1) (-i)^l j_l(qr) \mathbf{C}^l(\hat{r}) \cdot \mathbf{C}^l(\hat{q}), \quad (\text{B.19})$$

which gives the expression

$$\begin{aligned} \mathbf{A}^{db}(\mathbf{q}) = & \frac{-ie}{(2\pi)^3} \frac{1}{q^2} \sum_{l=0}^{\infty} (2l+1) (-i)^l \mathbf{C}^l(\hat{q}) \int dr r^2 j_l(qr) f(r) g(r) \\ & \times \int d\Omega [\chi_{\kappa}^{m_a \dagger}(\hat{r}) \boldsymbol{\sigma} \mathbf{C}^l(\hat{r}) \chi_{-\kappa}^{m_b}(\hat{r}) - \chi_{-\kappa}^{m_a \dagger}(\hat{r}) \boldsymbol{\sigma} \mathbf{C}^l(\hat{r}) \chi_{\kappa}^{m_b}(\hat{r})]. \end{aligned} \quad (\text{B.20})$$

From the angular integration it is seen that only the $l = 1$ term in the expansion will contribute. The angular dependence of \mathbf{q} is separated by using

$$q \mathbf{C}^1(\hat{q}) = p \mathbf{C}^1(\hat{p}) - p' \mathbf{C}^1(\hat{p}'), \quad (\text{B.21})$$

followed by expanding

$$\begin{aligned} h(p, p', \cos \vartheta) &= \frac{1}{q^3} \int dr r^2 j_1(qr) f(r) g(r) \\ &= \sum_{k=0}^{\infty} (2k+1) h_k(p, p') \mathbf{C}^k(\hat{p}) \cdot \mathbf{C}^k(\hat{p}'), \end{aligned} \quad (\text{B.22})$$

using Eqs. (B.14) and (B.15). Inserting these expressions we can write the momentum space potential as

$$\begin{aligned} \mathbf{A}^{db}(\mathbf{p} - \mathbf{p}') &= \frac{-3e}{(2\pi)^3} \sum_{k=0}^{\infty} (2k+1) h_k(p, p') \mathbf{C}^k(\hat{p}) \cdot \mathbf{C}^k(\hat{p}') [p \mathbf{C}^1(\hat{p}) - p' \mathbf{C}^1(\hat{p}')] \\ &\quad \times \int d\Omega [\chi_{\kappa}^{m_d \dagger}(\hat{r}) \boldsymbol{\sigma} \mathbf{C}^1(\hat{r}) \chi_{-\kappa}^{m_b}(\hat{r}) - \chi_{-\kappa}^{m_d \dagger}(\hat{r}) \boldsymbol{\sigma} \mathbf{C}^1(\hat{r}) \chi_{\kappa}^{m_b}(\hat{r})]. \end{aligned} \quad (\text{B.23})$$

B.2 External magnetic potential

The external homogeneous magnetic field, \mathbf{B} , is described by the vector potential

$$\mathbf{A}^{\text{mag}}(\mathbf{r}) = -\frac{1}{2} \mathbf{r} \times \mathbf{B}, \quad (\text{B.24})$$

and it is straightforward to see that the \mathbf{r} operator transforms into the gradient of a delta function

$$\mathbf{r} \rightarrow -i \nabla_{\mathbf{q}} \delta^3(\mathbf{q}). \quad (\text{B.25})$$

This highly singular function is represented numerically by introducing a Gaussian cut-off function in coordinate space

$$\mathbf{r} \rightarrow \lim_{\rho \rightarrow 0} \mathbf{r} e^{-\left(\frac{\rho \mathbf{r}}{2}\right)^2}, \quad (\text{B.26})$$

with the momentum transform

$$\mathbf{A}^{\text{mag}}(\mathbf{q}) = \frac{1}{2(2\pi)^3} \mathbf{B} \times \int d^3 \mathbf{r} e^{-i\mathbf{q} \cdot \mathbf{r}} \mathbf{r} e^{-\left(\frac{\rho \mathbf{r}}{2}\right)^2}. \quad (\text{B.27})$$

The \mathbf{r} vector can be decomposed into spherical components as follows

$$\mathbf{r} = r \sqrt{\frac{4\pi}{3}} \sum_{k=-1}^1 (-1)^k Y_{1k}(\hat{r}) \hat{e}_{-k}^{[1]}, \quad (\text{B.28})$$

where the spherical base vectors are given by

$$\begin{aligned} \hat{e}_{-1}^{[1]} &= \frac{1}{\sqrt{2}} (\hat{x} - i\hat{y}) \\ \hat{e}_0^{[1]} &= \hat{z} \\ \hat{e}_1^{[1]} &= -\frac{1}{\sqrt{2}} (\hat{x} + i\hat{y}). \end{aligned} \quad (\text{B.29})$$

Using this together with the plane wave expansion Eq. (B.19) we obtain

$$\begin{aligned}
\mathbf{A}^{\text{mag}}(\mathbf{q}) &= \frac{4\pi}{2(2\pi)^3} \sqrt{\frac{4\pi}{3}} \mathbf{B} \times \sum_{l=0}^{\infty} \sum_{m=-l}^l (-i)^l \sum_{k=-1}^1 (-1)^k \hat{e}_{-k}^{[1]} Y_{lm}(\hat{q}) \\
&\quad \times \int dr r^3 j_l(qr) e^{-\left(\frac{\rho r}{2}\right)^2} \int d\Omega Y_{1k}(\hat{r}) Y_{lm}^*(\hat{r}) \\
&= \frac{4\pi}{2(2\pi)^3} \sqrt{\frac{4\pi}{3}} \mathbf{B} \times \sum_{l=0}^{\infty} \sum_{m=-l}^l (-i)^l \sum_{k=-1}^1 (-1)^k \hat{e}_{-k}^{[1]} Y_{lm}(\hat{q}) \\
&\quad \times \int dr r^3 j_l(qr) e^{-\left(\frac{\rho r}{2}\right)^2} \delta_{l,1} \delta_{k,m} \\
&= -\frac{2\pi i}{(2\pi)^3} \mathbf{B} \times \hat{q} \int dr r^3 j_1(qr) e^{-\left(\frac{\rho r}{2}\right)^2} \\
&= \frac{i}{\pi^{3/2} \rho^5} e^{-(q/\rho)^2} \mathbf{q} \times \mathbf{B}. \tag{B.30}
\end{aligned}$$

Eventually, the limit $\rho \rightarrow 0$ should be taken, but in practice it is enough to have a small finite value of ρ so that the introduced inhomogeneity in the magnetic field is negligible over the extension of the ion. By using the expansion Eq. (B.14) for $e^{-(q/\rho)^2}$ the angular dependence of q is separated.

B.3 Hyperfine potential

The point-dipole nuclear magnetic vector potential is given by

$$\mathbf{A}^{\text{hfs}}(\mathbf{r}) = \frac{1}{4\pi} \frac{\boldsymbol{\mu} \times \mathbf{r}}{r^3}, \tag{B.31}$$

and by using the expansions of Eqs. (B.19) and (B.28) we obtain the momentum space potential

$$\begin{aligned}
\mathbf{A}^{\text{hfs}}(\mathbf{q}) &= \frac{1}{4\pi(2\pi)^3} \boldsymbol{\mu} \times \int d^3\mathbf{r} e^{-i\mathbf{q}\cdot\mathbf{r}} \frac{\mathbf{r}}{r^3} \\
&= \frac{-i}{(2\pi)^3} \frac{\boldsymbol{\mu} \times \mathbf{q}}{q} \int dr j_1(qr) \\
&= \frac{-i}{(2\pi)^3} \frac{\boldsymbol{\mu} \times \mathbf{q}}{q^2}. \tag{B.32}
\end{aligned}$$

Using the extended magnetization model of Eq. (2.41) leads instead to the integral

$$\mathbf{A}^{\text{hfs,n}}(\mathbf{q}) = \frac{-i}{(2\pi)^3} \frac{\boldsymbol{\mu} \times \mathbf{q}}{q} \int dr j_1(qr) V_n(r), \tag{B.33}$$

which can be evaluated as the sum

$$\mathbf{A}^{\text{hfs,n}}(\mathbf{q}) = \frac{-i}{(2\pi)^3} \frac{\boldsymbol{\mu} \times \mathbf{q}}{q} \left\{ \frac{1}{q} + \int_0^{R_0} dr j_1(qr) [V_n(r) - 1] \right\}, \tag{B.34}$$

such that the last term gives directly the extended magnetization correction (Bohr-Weisskopf effect). For this model and for the point-dipole model we

separate the angular dependencies by using Eq. (B.14) for the parts beyond the vector product $\boldsymbol{\mu} \times \mathbf{q}$.

The potential for the DPM is very similar to the inter-electron case and it can be written as

$$\begin{aligned} \mathbf{A}^{\text{hfs,dpm}}(\mathbf{p} - \mathbf{p}') &= \frac{3e}{(2\pi)^3} \sum_{k=0}^{\infty} (2k+1) H_k(p, p') \mathbf{C}^k(\hat{p}) \cdot \mathbf{C}^k(\hat{p}') [p \mathbf{C}^1(\hat{p}) - p' \mathbf{C}^1(\hat{p}')] \\ &\quad \times \int d\Omega [\chi_{\kappa}^{m\dagger}(\hat{R}) \boldsymbol{\sigma} \mathbf{C}^1(\hat{R}) \chi_{-\kappa}^m(\hat{R}) - \chi_{-\kappa}^{m\dagger}(\hat{R}) \boldsymbol{\sigma} \mathbf{C}^1(\hat{R}) \chi_{\kappa}^m(\hat{R})] , \end{aligned} \quad (\text{B.35})$$

where $H_k(p, p')$ is the coefficient in the expansion Eq. (B.14) of

$$H_k(p, p', \cos \vartheta) = \int dr r^2 j_1(kr) f_N(r) g_N(r) , \quad (\text{B.36})$$

where $f_N(r)$ and $g_N(r)$ are the radial nuclear wavefunctions.

C Mass and Charge Renormalization

We will here discuss the concept of mass and charge renormalization following the lines of Mandl and Shaw [9]. The free electron case considered here is important, since the renormalization problem in bound-state QED can be brought back to the free field case, by means of an expansion in the binding potential.

The problem with the divergences which appear in higher-order QED can be associated with the way we describe the electrons and their interactions. The perturbation expansion starts from non-interacting “bare” electrons and describe their interaction in terms of the bare electron mass (m_0) and charge (e_0). The m 's and e 's present in the Hamiltonian Eq. (A.52), should thus be interpreted as the bare values until renormalization is performed. The QED interaction modifies the properties of the electron, the electron self-energy correction changes its mass and the photon self interaction changes its charge. The problem is that the shifts induced by those processes are infinite. For free electrons this is the only effect of those radiative corrections. When the electron is not free, however, they will also yield finite contributions to the concerned process. If we include these effects to all orders, the bare electron will be dressed by the interaction and it will end up as the real physical electron having the experimental mass (m) and charge (e).

There is, however, no such thing as a bare electron. The mass and charge that we observe in experiments include these radiative (dressing) effects from the very beginning. The theory thus have to be reformulated such that it is expressed in terms of the properties of the physical particles, and not in terms of the bare non-interacting ones. Using the real physical electron mass and charge in the calculations, we must, however, correct for the effects already taken into account when assigning these physical properties to the bare non-interacting electron. This is exactly the basic idea of renormalization. We insert the real physical mass and charge into the bare Hamiltonian and to adjust for this replacement certain counter terms has to be subtracted.

By renormalization, all divergent quantities will be absorbed in untestable equations relating bare and physical properties of the electron. The observable predictions of the theory will, however, only involve well-defined finite quantities. From a computational point of view, the task is now to isolate and find useful forms of these finite parts. To accomplish the renormalization explicitly, some kind of regularization scheme has to be applied for the divergent integrals. Regularization will be discussed in the subsequent appendix and we will assume in the following, when needed, that all quantities are properly regularized.

In addition to the electron self-energy and the photon self interaction also the vertex correction contains a divergent piece. This divergence is present also in the electron self-energy and it cancels between the two corrections. The three different radiative corrections appear in each order of the perturbation expansion and we can thus define, for example, the electron self-energy of order



Figure C.1: *The photon propagator modified by photon self interaction insertions.*

α , α^2 , ... and so on. We will here study the lowest-order corrections (order α) involving one virtual photon, the one-photon radiative corrections. The Feynman diagrams for these one-loop corrections are given by the second term in Figs. C.1, C.2 and C.4.

C.1 Photon self interaction

The photon self interaction effect convert bare non-interacting particles, with the bare charge e_0 , to real physical particles with the observable charge e . In addition it also gives finite contributions to the process in which it participates, so-called vacuum polarization corrections. This name comes from the fact that the photon self interaction involves the creation and subsequent annihilation of virtual electron-positron pairs, which are polarized in the presence of an electromagnetic field.

Fig. C.1 shows the modification of the photon propagator due to photon self-energy insertions. Considering the propagator to order α , we include the first two terms and write

$$iD_{\alpha\beta}^{F,(2)}(k) = iD_{\alpha\beta}^{F,(1)}(k) + iD_{\alpha\mu}^{F,(1)}(k) ie_0^2 \Pi^{\mu\nu,(1)}(k) iD_{\nu\beta}^{F,(1)}(k), \quad (\text{C.1})$$

where the first-order polarization tensor, $\Pi^{\mu\nu,(1)}(k)$, is given by

$$ie_0^2 \Pi^{\mu\nu,(1)}(k) = e_0^2 \int \frac{d^4p}{(2\pi)^4} \text{Tr}[\gamma^\mu iS_F(p)\gamma^\nu iS_F(p-k)]. \quad (\text{C.2})$$

Note that we use here the charge e_0 , the charge of bare non-interacting particles. From Lorentz invariance the polarization tensor (to any order) must have the form

$$\Pi^{\mu\nu}(k) = -g^{\mu\nu} A(k^2) + k^\mu k^\nu B(k^2), \quad (\text{C.3})$$

since this is the most general rank two tensor which can be formed using only the four-vector k^μ . Due to current conservation the $k^\mu k^\nu$ -term can be omitted. Since we deal only with the first-order polarization tensor here, we will from now on omit the superscript (1) on the tensor and its constituents.

Inserting Eq. (C.3) and the explicit form, $D_{\alpha\beta}^{F,(1)}(k) = -g_{\alpha\beta}/(k^2 + i\delta)$, in the second-order propagator yields

$$iD_{\alpha\beta}^{F,(2)}(k) = iD_{\alpha\beta}^{F,(1)}(k) \left[1 - e_0^2 A(k^2) \frac{1}{k^2 + i\delta} \right] = \frac{-ig_{\alpha\beta}}{k^2 + i\delta + e_0^2 A(k^2)} + O(e_0^4). \quad (\text{C.4})$$

This equation represents the propagator of a real physical photon accurate to terms in e_0^2 . In order to retain zero rest mass also for the physical photon, the propagator must have its pole at $k^2 = 0$. This implies

$$A(0) = 0, \quad (\text{C.5})$$

and we can therefore write $A(k^2)$ as

$$A(k^2) = k^2 A'(0) + k^2 \Pi^{\text{ren}}(k^2), \quad (\text{C.6})$$

where

$$A'(k^2) = \frac{dA(k^2)}{d(k^2)}. \quad (\text{C.7})$$

Substituting this form of $A(k^2)$ into the modified propagator (C.4), and multiplying with e_0^2 to incorporate the charges at the ends of the propagator, results in

$$e_0^2 i D_{\alpha\beta}^{F_i(2)}(k) = e_0^2 i D_{\alpha\beta}^{F_i(1)}(k) [1 - e_0^2 A'(0)] - e_0^2 i D_{\alpha\beta}^{F_i(1)}(k) e_0^2 \Pi^{\text{ren}}(k^2). \quad (\text{C.8})$$

We now introduce the concept of charge renormalization, relating the renormalized electronic charge ($-e$) to the charge ($-e_0$) of bare non-interacting electrons via the relation

$$e^2 = e_0^2 [1 - e_0^2 A'(0)]. \quad (\text{C.9})$$

A detailed analysis of the polarization tensor shows that the renormalization constant, $A'(0)$, is divergent while the remaining term, $\Pi^{\text{ren}}(k^2)$, is finite. Hence, the divergent part can be included in the untestable relation Eq. (C.9), and all observable predictions of the theory will contain the finite term Π^{ren} only. This result is generalizable to each order of the perturbation expansion pictured in Fig. C.1, with the appropriate reformulation of the polarization tensor.

The second order renormalized photon propagator can thus be written as

$$D_{\alpha\beta}^{F_i(2)}(k) = D_{\alpha\beta}^{F_i(1)}(k) [1 - e^2 \Pi^{\text{ren}}(k^2)]. \quad (\text{C.10})$$

The first term is just the first-order propagator and the second term gives finite vacuum polarization corrections (of order α) to any process involving the photon propagator in lowest-order perturbation theory. The interaction with an external potential is also modified by the photon self-energy process, and we obtain in a similar way as for the photon propagator

$$A_\mu^{(2)}(k) = A_\mu^{(1)}(k) [1 - e^2 \Pi^{\text{ren}}(k^2)]. \quad (\text{C.11})$$

The second term is referred to as the Uehling potential, after E. A. Uehling who derived this correction already in 1935 [44].

The finite part, Π^{ren} , can be extracted from Eq. (C.2), for example by the method of dimensional regularization, and the resulting expression reads

$$e^2 \Pi^{\text{ren}}(k^2) = -\frac{\alpha}{\pi} \int_1^\infty dt \sqrt{t^2 - 1} \left(\frac{2}{3t^2} + \frac{1}{3t^4} \right) \frac{k^2}{k^2 - 4m^2 t^2 + i\delta}. \quad (\text{C.12})$$

The imaginary term, $i\delta$, defines the way the pole, which appears only for $k^2 > 4m^2$, is circumvented.

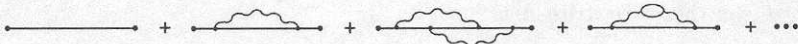


Figure C.2: *The electron propagator modified by electron self-energy insertions.*

C.2 Electron self-energy

We shall here discuss the electron self-energy, which is the self-interaction of an electron involving the emission and subsequent re-absorption of virtual photons. For a free electron, the process just modifies the electron mass. However, for bound electrons the self-energy also give rise to a detectable energy shift.

In analogy with the discussion of vacuum polarization, we start with an unrenormalized theory in which the non-interacting electron is described by its bare charge and mass, e_0 and m_0 . Fig. C.2 pictures the electron propagator dressed by self-energy insertions. To second order we take the first two terms into account and obtain

$$iS_F^{(2)}(p) = iS_F^{(1)}(p) - iS_F^{(1)}(p) i\Sigma^{(1)}(p) iS_F^{(1)}(p), \quad (\text{C.13})$$

where the first-order free electron self-energy operator is given by

$$\Sigma^{(1)}(p) = -ie_0^2 \int \frac{d^4k}{(2\pi)^4} \frac{1}{k^2 + i\delta} \gamma^\mu \frac{1}{\not{p} - \not{k} - m_0 + i\eta} \gamma_\mu. \quad (\text{C.14})$$

Using the explicit form of $S_F^{(1)}(p) = 1/(\not{p} - m_0 + i\eta)$, we can write

$$\begin{aligned} iS_F^{(2)}(p) &= \frac{i}{\not{p} - m_0 + i\eta} - \frac{i}{\not{p} - m_0 + i\eta} i\Sigma^{(1)}(p) \frac{i}{\not{p} - m_0 + i\eta} \\ &= \frac{i}{\not{p} - m_0 - \Sigma^{(1)}(p) + i\eta} + O(e_0^4). \end{aligned} \quad (\text{C.15})$$

This is the propagator, of order e_0^2 , of the real physical electron with the observable mass m . It should therefore have its pole at $\not{p} = m$, which implies

$$\Sigma^{(1)}(p) \Big|_{\not{p}=m} = m - m_0 = \delta m, \quad (\text{C.16})$$

where δm is the mass shift due to the electron self-energy. This equation represents the mass renormalization; the physical electron mass m is related to the bare mass m_0 via the on mass-shell ($\not{p} = m$) value of the free electron self-energy operator. The mass shift, δm , is divergent and is the analogue of the constant $A'(0)$ in the corresponding relation (Eq. (C.9)) for the charge renormalization. Considering here only the first-order self-energy, we now omit the (1) label on the self-energy operator.

The self-energy operator can, after proper regularization, be expanded around $\not{p} = m$

$$\Sigma(p) = \delta m + (\not{p} - m)B + (\not{p} - m)C(p), \quad (\text{C.17})$$

where B is a constant and $C(p)$ vanish linearly with $(\not{p} - m)$ as $\not{p} \rightarrow m$. $C(p)$ is the finite part which gives radiative corrections of order α due to the first-order



Figure C.3: *The two-line vertex, representing the mass counterterm. Each Feynman diagram containing the electron self-energy loop must be considered together, to account for mass renormalization, with the identical diagram in which the self-energy loop is replaced with this two-line vertex part.*

self-energy insertion. The constant B

$$B = \left. \frac{\partial \Sigma(p)}{\partial \not{p}} \right|_{\not{p}=m}, \quad (\text{C.18})$$

is divergent and is associated with charge renormalization

$$e^2 = Z_2 e_0^2 = e_0^2 [1 + B] + O(e_0^6), \quad (\text{C.19})$$

where Z_2 is a charge renormalization constant. The self-energy operator contains thus, in addition to the mass divergence, also a charge divergence. The associated charge renormalization is, however, fictitious since the divergence cancels between the electron self-energy and the vertex correction (see below).

The mass renormalization relation Eq. (C.16) is now inserted in the Hamiltonian, i.e. the bare mass m_0 is replaced with $m - \delta m$. The mass shift δm is combined with the interaction Hamiltonian, giving

$$\hat{H}'_I(t) = \hat{H}_I(t) - \delta m \int d^3 \mathbf{x} \hat{\Psi}^\dagger(x) \gamma^0 \hat{\Psi}(x). \quad (\text{C.20})$$

We thus use the physical mass for the non-interacting electrons, and to compensate for this we subtract the mass counterterm δm . The modified interaction gives additional contributions (of order e^2) to the S-matrix expansion, represented by Feynman graphs containing the two-line vertex part, shown in Fig. C.3. Hence, each Feynman graph that contains an electron self-energy loop, must be considered together with an identical graph in which the self-energy loop has been replaced by the mass counterterm. The resulting contribution to the Feynman amplitude, caused by the self-energy process, is therefore

$$\begin{aligned} \Sigma_{\text{ren}}^{\text{mass}}(p) &= \Sigma(p) - \delta m \\ &= (\not{p} - m)(Z_2 - 1) + \Sigma^{\text{ren}}(p), \end{aligned} \quad (\text{C.21})$$

where $\Sigma^{\text{ren}}(p) = (\not{p} - m)C(p)$.

C.3 Vertex correction

The modification of the vertex due to vertex corrections is shown in Fig. C.4 and the vertex function to second-order is given by the first two terms

$$ie_0 \Gamma_\mu^{(2)}(p, p') = ie_0 \gamma_\mu + ie_0 \Lambda_\mu^{(1)}(p, p'), \quad (\text{C.22})$$



Figure C.4: *The vertex modified due to vertex corrections.*

where the first-order vertex correction is given by

$$\Lambda_{\mu}^{(1)}(p, p') = -ie_0^2 \int \frac{d^4k}{(2\pi)^4} \frac{1}{k^2 + i\delta} \gamma^{\nu} \frac{1}{\not{p} - \not{k} - m} \gamma_{\mu} \frac{1}{\not{p}' - \not{k} - m} \gamma^{\nu}. \quad (\text{C.23})$$

This operator can be separated into one divergent piece and a finite remainder $\Lambda_{\mu}^{\text{ren}}(p, p')$, which is defined through (omitting the (1) superscript)

$$\Lambda_{\mu}(p, p') = \gamma_{\mu} L + \Lambda_{\mu}^{\text{ren}}(p, p'). \quad (\text{C.24})$$

The divergent constant L is associated with the charge renormalization

$$e = \frac{e_0}{Z_1} = e_0(1 + L) + O(e_0^5), \quad (\text{C.25})$$

where Z_1 is a charge renormalization constant. By virtue of Ward's identity [107]

$$\frac{\partial \Sigma(p)}{\partial p_{\mu}} = \Lambda^{\mu}(p, p), \quad (\text{C.26})$$

one can show that $L = -B$, where B is the divergent constant of the self-energy operator. This implies that $Z_1 = Z_2$, and we can therefore write the first-order free electron vertex operator as

$$\Lambda_{\mu}(p, p') = \gamma_{\mu}(1 - Z_2) + \Lambda_{\mu}^{\text{ren}}(p, p'). \quad (\text{C.27})$$

The divergent part will cancel against the self-energy operator and $\Lambda_{\mu}^{\text{ren}}$ is the finite part which gives radiative corrections of order α . As a consequence of Ward's identity one can further conclude that the photon self interaction is alone responsible for the renormalization of charge.

D Dimensional Regularization

The integrals over a loop-momentum which appear in the calculation of vacuum polarization, self-energy and vertex corrections contain divergent parts. The divergences are associated with the identification of real physical observables from the bare unphysical ones. When calculating an observable physical quantity, e.g. a cross section, divergences are absorbed in the mass and charge renormalization and only finite parts will enter the final result. To be able to evaluate the integral and to identify the divergent pieces some kind of regularization must be employed. It is important that the regularization scheme preserves the fundamental symmetries of QED, e.g. gauge and Lorentz invariance. Using a regulator that does not fulfill these demands can lead to erroneous results as for the case of using partial wave renormalization for the magnetic screened self-energy (see Paper V).

We use here the concept of dimensional regularization due to 't Hooft and Veltman [108]. The idea behind this scheme is to compute the quantity in question as an analytic function of the dimensionality of space-time, D . For sufficiently small D , any loop-momentum integral will be convergent and the divergent pieces will appear as terms proportional to inverse powers of $\epsilon = 4 - D$. Eventually all such terms will cancel out and the final result for any observable quantity will have a well-defined limit as $D \rightarrow 4$.

For a description of how to perform integrals in D -dimensional space we refer to Peskin and Schroeder [109], from which we take the results

$$\frac{1}{m^{D-2n}} \int \frac{d^D l}{(2\pi)^D} \frac{1}{(l^2 - w)^n} = i \frac{(-1)^n}{(4\pi)^{D/2}} \frac{\Gamma(n - \frac{D}{2})}{\Gamma(n)} \left(\frac{m^2}{w}\right)^{n - \frac{D}{2}} \quad (\text{D.1})$$

$$\frac{1}{m^{D-2n+2}} \int \frac{d^D l}{(2\pi)^D} \frac{l_\mu l_\nu}{(l^2 - w)^n} = i \frac{g_{\mu\nu}}{2} \frac{(-1)^{n-1}}{(4\pi)^{D/2}} \frac{\Gamma(n - \frac{D}{2} - 1)}{\Gamma(n)} \left(\frac{m^2}{w}\right)^{n - \frac{D}{2} - 1} \quad (\text{D.2})$$

where l_μ is a momentum variable and w is independent of l_μ . Note that we have made these expressions dimensionless by including the factors of m in front of the integrals. For convergent integrals the limit $D \rightarrow 4$ can be taken from the beginning. If the integral diverges we need the following expansions to obtain the behavior near $D = 4$

$$\left(\frac{m^2}{w}\right)^{\epsilon/2} = 1 - \frac{\epsilon}{2} \ln\left(\frac{w}{m^2}\right) + \dots \quad (\text{D.3})$$

$$\Gamma\left(\frac{\epsilon}{2}\right) = \frac{2}{\epsilon} - \gamma_E + \dots \quad (\text{D.4})$$

where γ_E is Euler's constant $\gamma_E \approx 0.57722$. It is convenient to work out the following combination which appear for the divergent integrals considered here

$$\frac{\Gamma(2 - \frac{D}{2})}{(4\pi)^{D/2}} \left(\frac{m^2}{w}\right)^{2 - \frac{D}{2}} = \frac{1}{(4\pi)^2} \left[\Delta - \ln\left(\frac{w}{m^2}\right) + O(\epsilon) \right], \quad (\text{D.5})$$

where $\Delta = 2/\epsilon - \gamma_E + \ln 4\pi$ is the divergent constant which will cancel out between different Feynman diagrams.

We must also generalize the γ -matrices to D -dimensional space and this implies the following corrections to the contraction relations for the γ -matrices

$$\begin{aligned} \gamma^\mu \gamma_\mu &= 4 - \epsilon \\ \gamma^\mu \gamma^\alpha \gamma_\mu &= -2\gamma^\alpha + \epsilon \gamma^\alpha \\ \gamma^\mu \gamma^\alpha \gamma^\beta \gamma_\mu &= 4g^{\alpha\beta} - \epsilon \gamma^\alpha \gamma^\beta \\ \gamma^\mu \gamma^\alpha \gamma^\beta \gamma^\gamma \gamma_\mu &= -2\gamma^\gamma \gamma^\beta \gamma^\alpha + \epsilon \gamma^\alpha \gamma^\beta \gamma^\gamma. \end{aligned} \quad (\text{D.6})$$

It should be noted that these ϵ -dependent corrections will give contributions when combined with divergent integrals.

To cast integrals into the form of Eqs. (D.1) and (D.2), we utilize Feynman parameterization for the propagator denominators

$$\frac{1}{AB} = \int_0^1 ds \frac{1}{[sA + (1-s)B]^2} \quad (\text{D.7})$$

$$\frac{1}{ABC} = 2 \int_0^1 ds \int_0^{1-s} dt \frac{1}{[sA + tB + (1-s-t)C]^3} \quad (\text{D.8})$$

where the two and three denominator cases will be used for the free-electron self-energy and vertex operator, respectively. The denominator will be a quadratic function of the momentum integration variable. By completing the square and shifting the integration variable to absorb the linear terms, the denominator will take the form $(l^2 - w)^n$. We will now turn to a detailed derivation of these two operators using dimensional regularization.

D.1 Free electron self-energy operator

The free electron self-energy operator is given by the integral

$$\Sigma(p) = -4\pi i \alpha \int \frac{d^4 k}{(2\pi)^4} \gamma^\mu \frac{\not{p} - \not{k} + m}{(p-k)^2 - m^2} \gamma_\mu \frac{1}{k^2}, \quad (\text{D.9})$$

which can be shown to diverge logarithmically in the ultraviolet limit. By using the contraction identities of Eq. (D.6) and Feynman parameterization, we obtain

$$\Sigma(p) = -4\pi i \alpha \int_0^1 ds \int \frac{d^D k}{(2\pi)^D} \frac{(-2 + \epsilon)(\not{p} - \not{k}) + (4 - \epsilon)m}{[sk^2 + (1-s)[(p-k)^2 - m^2]]^2}. \quad (\text{D.10})$$

The substitution $l_\mu = k_\mu - p_\mu(1-s)$ leads to the form

$$\Sigma(p) = -4\pi i\alpha \int_0^1 ds \int \frac{d^D l}{(2\pi)^D} \frac{(-2 + \epsilon)(s\not{p} - \not{l}) + (4 - \epsilon)m}{[l^2 - w(s)]^2}, \quad (\text{D.11})$$

where

$$w(s) = m^2 [\rho(1-s) + (1-\rho)(1-s)^2], \quad (\text{D.12})$$

and $\rho = (m^2 - p^2)/m^2$. The \not{l} -term will vanish due to symmetry and the integral to evaluate is of the type of Eq. (D.1). Using the expansion in Eq. (D.5) we are left with the parameterization integral

$$\Sigma(p) = (m^{-\epsilon}) \frac{\alpha}{4\pi} \int_0^1 ds [(-2 + \epsilon)s\not{p} + (4 - \epsilon)m] \left[\Delta - \ln \left(\frac{w(s)}{m^2} \right) \right], \quad (\text{D.13})$$

which is straightforward to evaluate. The appearance of the factor $(m^{-\epsilon})$ is due to the fact that the dimension of $\Sigma(p)$ is altered by dimensional regularization. Expanding this factor (with Eq. (D.3)) will lead to a term $-\ln m^2$ on the same level as the divergence Δ . Such a term will also appear for the vertex operator and these terms will thus cancel out. Subtracting the on-mass-shell value ($\delta m = \Sigma(p)|_{\not{p}=m}$) we obtain for the mass renormalized self-energy operator

$$\begin{aligned} \Sigma_{\text{ren}}^{\text{mass}}(p) &= \Sigma(p) - \delta m \\ &= -\frac{\alpha}{4\pi} \left\{ (\not{p} - m) \left[\Delta + 2 + \frac{\rho}{1-\rho} \left(1 + \frac{2-\rho}{1-\rho} \ln \rho \right) \right] \right. \\ &\quad \left. + \frac{m\rho}{1-\rho} \left(1 - \frac{2-3\rho}{1-\rho} \ln \rho \right) \right\}. \end{aligned} \quad (\text{D.14})$$

D.2 Free electron vertex operator

The free electron vertex operator is given by

$$\Lambda_\mu(p, p') = -4\pi i\alpha \int \frac{d^4 k}{(2\pi)^4} \gamma_\nu \frac{\not{p} - \not{k} + m}{(p-k)^2 - m^2} \gamma_\mu \frac{\not{p}' - \not{k} + m}{(p'-k)^2 - m^2} \gamma_\nu \frac{1}{k^2}, \quad (\text{D.15})$$

and it is logarithmically ultraviolet divergent. The numerator exhibits three different forms of k -dependence $[1, k_\mu, k_\mu k_\nu]$ for which we define the following coefficient functions [36]

$$\begin{aligned} &\int \frac{d^4 k}{(2\pi)^4} \frac{[1, k_\mu, k_\mu k_\nu]}{k^2 [(p-k)^2 - m^2] [(p'-k)^2 - m^2]} \left(\frac{i}{16\pi^2} \right)^{-1} \\ &= [-C_0, p_\mu C_{11} + p'_\mu C_{12}, \\ &\quad -p_\mu p_\nu C_{21} - p'_\mu p'_\nu C_{22} - (p_\mu p'_\nu + p'_\mu p_\nu) C_{23} + g_{\mu\nu} C_{24}]. \end{aligned} \quad (\text{D.16})$$

All the coefficient functions C_{ij} are convergent except C_{24} which contains the ultraviolet divergence Δ .

The integral for C_0 can be parameterized to read

$$C_0 = -2 \left(\frac{i}{16\pi^2} \right)^{-1} \int_0^1 ds \int_0^{1-s} dt \int \frac{d^D k}{(2\pi)^D} \frac{1}{[s[(p-k)^2 - m^2] + t[(p'-k)^2 - m^2] + (1-s-t)k^2]^3}, \quad (\text{D.17})$$

performing the momentum integral in the variable $l_\mu = k_\mu - (sp_\mu + tp'_\mu)$ we end up with the integration

$$m^2 C_0 = \int_0^1 ds \int_0^{1-s} dt \frac{m^2}{w(s, t)} \quad (\text{D.18})$$

where

$$w(s, t) = s(s-1)p^2 + t(t-1)p'^2 + 2stp \cdot p' + (s+t)m^2. \quad (\text{D.19})$$

This can be put into a particularly simple form through the substitution

$$\begin{cases} x = s+t, & s = xy, & 0 \leq x \leq 1 \\ y = s/(s+t), & t = x(1-y), & 0 \leq y \leq 1 \end{cases} \quad (\text{D.20})$$

and $dsdt \rightarrow x dx dy$. We obtain then

$$m^2 C_0 = \int_0^1 \int_0^1 dx dy \frac{1}{ax+b} = \int_0^1 dy \frac{1}{a} \ln \left(\frac{a+b}{b} \right) \quad (\text{D.21})$$

where

$$\begin{aligned} b &= y\rho - (1-y)\rho' \\ a+b &= 1 - y(1-y)q^2/m^2 \end{aligned} \quad (\text{D.22})$$

and where $q^2 = (p-p')^2$. We choose here to evaluate this integral, as well as the corresponding integrals for the other coefficient functions, numerically since they are very easy to control. The expression for numerical evaluation of the scalar coefficient function is thus given by

$$m^2 C_0 = \int_0^1 dy \frac{\ln[1 - y(1-y)q^2/m^2] - \ln[y\rho + (1-y)\rho']}{[1 - y(1-y)q^2/m^2] - [y\rho + (1-y)\rho']}. \quad (\text{D.23})$$

Since only the numerator differs between the scalar, vector and tensor coefficient functions, we have here the same l_μ (and $w(s, t)$) as was introduced in the C_0 case. Using $k_\mu = l_\mu + (sp_\mu + tp'_\mu)$ for the numerators k_μ and $k_\mu k_\nu$ will lead to linear terms in l_μ which again will vanish upon integration. Proceeding like this it is straightforward to obtain

$$m^2 [p_\mu C_{11} + p'_\mu C_{12}] = - \int_0^1 ds \int_0^{1-s} dt \left[sp_\mu \frac{m^2}{w(s, t)} + tp'_\mu \frac{m^2}{w(s, t)} \right] \quad (\text{D.24})$$

and by using the substitution Eq. (D.20) the resulting expressions are

$$m^2 C_{11} = - \int_0^1 \int_0^1 dx dy \frac{xy}{ax+b} = - \int_0^1 dy \frac{y}{a} \left[1 - \frac{b}{a} \ln \left(\frac{a+b}{b} \right) \right] \quad (\text{D.25})$$

and

$$m^2 C_{12} = - \int_0^1 \int_0^1 dx dy \frac{x(1-y)}{ax+b} = - \int_0^1 dy \frac{1-y}{a} \left[1 - \frac{b}{a} \ln \left(\frac{a+b}{b} \right) \right]. \quad (\text{D.26})$$

For the tensor part we have the integral

$$\begin{aligned} & -p_\mu p_\nu C_{21} - p'_\mu p'_\nu C_{22} - (p_\mu p'_\nu + p'_\mu p_\nu) C_{23} + g_{\mu\nu} C_{24} \\ & = 2 \left(\frac{i}{16\pi^2} \right)^{-1} \int_0^1 ds \int_0^{1-s} dt \int \frac{d^D l}{(2\pi)^D} \frac{s^2 p_\mu p_\nu + t^2 p'_\mu p'_\nu + st (p_\mu p'_\nu + p'_\mu p_\nu) + l_\mu l_\nu}{[l^2 - w(s, t)]^3}, \end{aligned} \quad (\text{D.27})$$

from which it is easy to identify the coefficient functions

$$\begin{aligned} m^2 C_{21} &= \int_0^1 \int_0^1 dx dy \frac{x^2 y^2}{ax+b} = \int_0^1 dy \frac{y^2}{a} \left[\frac{1}{2} - \frac{b}{a} + \left(\frac{b}{a} \right)^2 \ln \left(\frac{a+b}{b} \right) \right] \\ m^2 C_{22} &= \int_0^1 \int_0^1 dx dy \frac{x^2 (1-y)^2}{ax+b} = \int_0^1 dy \frac{(1-y)^2}{a} \left[\frac{1}{2} - \frac{b}{a} + \left(\frac{b}{a} \right)^2 \ln \left(\frac{a+b}{b} \right) \right] \\ m^2 C_{23} &= \int_0^1 \int_0^1 dx dy \frac{x^2 y (1-y)}{ax+b} = \int_0^1 dy \frac{y(1-y)}{a} \left[\frac{1}{2} - \frac{b}{a} + \left(\frac{b}{a} \right)^2 \ln \left(\frac{a+b}{b} \right) \right]. \end{aligned} \quad (\text{D.28})$$

The divergent coefficient C_{24} comes from the $l_\mu l_\nu$ -term. Using the integral in Eq. (D.2) and the expansion Eq. (D.5) we can write

$$\begin{aligned} C_{24} &= (m^{-\epsilon}) \frac{1}{2} \int_0^1 ds \int_0^{1-s} dt \left[\Delta - \ln \left(\frac{w(s, t)}{m^2} \right) \right] \\ &= \frac{(m^{-\epsilon})}{4} \Delta - \frac{(m^{-\epsilon})}{2} \int_0^1 ds \int_0^{1-s} dt \ln \left(\frac{w(s, t)}{m^2} \right), \end{aligned} \quad (\text{D.29})$$

where we again meet the canceling quantity $(m^{-\epsilon})$, see the discussion for the self-energy operator. Letting $s, t \rightarrow x, y$ and performing the x -integration we obtain

$$C_{24} = \frac{1}{4} \left\{ \Delta + 1 - \int_0^1 dy \frac{b}{a} \left[1 - \frac{b}{a} \ln \left(\frac{a+b}{b} \right) \right] - \int_0^1 dy \ln(a+b) \right\}. \quad (\text{D.30})$$

Comparing with the expressions for C_{11} and C_{12} in Eqs. (D.25, D.26) and using the definition of b , it can be seen that the first y -integral of C_{24} can be written as

$$- \int_0^1 dy \frac{b}{a} \left[1 - \frac{b}{a} \ln \left(\frac{a+b}{b} \right) \right] = \rho m^2 C_{11} + \rho' m^2 C_{12}. \quad (\text{D.31})$$

The last integral yields further

$$-\int_0^1 dy \ln(a+b) = 2 - v \ln\left(\frac{v+1}{v-1}\right) \quad (\text{D.32})$$

where $v = \sqrt{1 - 4m^2/q^2}$. We can thus finally write

$$C_{24} = \frac{1}{4} \left[\Delta + 3 + \rho m^2 C_{11} + \rho' m^2 C_{12} - v \ln\left(\frac{v+1}{v-1}\right) \right]. \quad (\text{D.33})$$

Since C_{24} contains the $2/\epsilon$ -term we must keep the ϵ -dependent terms when contracting the numerator in the vertex operator. From Eq. (D.15) we see that C_{24} is to be combined with

$$g_{\alpha\beta} C_{24} \gamma_\nu \gamma^\alpha \gamma_\mu \gamma^\beta \gamma^\nu = C_{24} \gamma_\nu \gamma^\alpha \gamma_\mu \gamma_\alpha \gamma^\nu, \quad (\text{D.34})$$

and by using the contraction identities of Eq. (D.6) we obtain the following contribution from the ϵ -dependent terms

$$\frac{1}{4} \left(\frac{2}{\epsilon} \right) \gamma_\nu \gamma^\alpha \gamma_\mu \gamma_\alpha \gamma^\nu = \frac{1}{4} \left(\frac{2}{\epsilon} \right) (-4\epsilon \gamma_\mu) = -2\gamma_\mu. \quad (\text{D.35})$$

Putting all the terms together we obtain finally the complete covariant vertex operator

$$\begin{aligned} \Lambda_\mu(p, p') = & \frac{\alpha}{4\pi} \left\{ \gamma_\mu \left[4C_{24} - 2 + 2m^2 C_0 - 4p \cdot p' (C_0 + C_{11} + C_{12} + C_{23}) \right. \right. \\ & \left. \left. - 2p^2 (C_{11} + C_{21}) - 2p'^2 (C_{12} + C_{22}) \right] \right. \\ & + \not{p} p_\mu [4(C_{11} + C_{21})] \\ & + \not{p}' p'_\mu [4(C_0 + C_{11} + C_{12} + C_{23})] \\ & + \not{p}' p_\mu [4(C_0 + C_{11} + C_{12} + C_{23})] \\ & + \not{p}' p'_\mu [4(C_{12} + C_{22})] \\ & - \not{p}' \gamma_\mu \not{p}' [2(C_0 + C_{11} + C_{12})] \\ & - p_\mu [4m(C_0 + 2C_{11})] \\ & \left. - p'_\mu [4m(C_0 + 2C_{12})] \right\}. \quad (\text{D.36}) \end{aligned}$$

E Derivation of the Binding-Energy Correction

We shall here consider the reducible part of the external line self-energy diagram for the two-electron case. As discussed in Appendix A, we have to subtract the lower-order diagrams shown in Fig. E.1 (b) and (c), to obtain a non-singular expression. The finite remainder is called the binding-energy correction. In this appendix we will use the notation E_0 for the one-electron energies of the $1s^2$ reference states $E_0 = E_a = E_b = E_c = E_d$. Moreover, the degeneracy condition $E_t = E_c = E_0$ implies that the intermediate state $|t\rangle$ must in this case be identical with the reference state $|c\rangle$.

From Feynman rules we obtain the amplitude

$$\begin{aligned}
 M_\gamma^{4,(a)} &= e^4 \int d^3\mathbf{x}_1 \dots \int d^3\mathbf{x}_4 \int_{-\infty}^{\infty} dz_1 \dots \int_{-\infty}^{\infty} dz_4 \\
 &\times \Delta_\gamma(z_3 + z_4 - E_0) \Delta_\gamma(-z_1) \frac{\Delta_\gamma(E_0 + z_1 - z_2) \Delta_\gamma(z_2 - z_3 - z_4)}{z_2 - E_0(1 - i\eta)} \\
 &\times \Phi_c^\dagger(\mathbf{x}_1) \alpha^\mu D_{\mu\nu}^F(\mathbf{x}_1 - \mathbf{x}_2, z_4) S_F(\mathbf{x}_1, \mathbf{x}_2, z_3) \alpha^\nu \Phi_c(\mathbf{x}_2) \\
 &\times \Phi_c^\dagger(\mathbf{x}_3) \alpha^\sigma D_{\sigma\lambda}^F(\mathbf{x}_3 - \mathbf{x}_4, z_1) \Phi_a(\mathbf{x}_3) \Phi_d^\dagger(\mathbf{x}_4) \alpha^\lambda \Phi_b(\mathbf{x}_4).
 \end{aligned} \tag{E.1}$$

By performing the z_2 -integration we obtain

$$\int_{-\infty}^{\infty} dz_2 \frac{\Delta_\gamma(z_2 - z_3 - z_4) \Delta_\gamma(E_0 + z_1 - z_2)}{z_2 - E_0(1 - i\eta)} = \frac{1}{\pi^2} f_\gamma(-z_1, z_3 + z_4 - E_0) \tag{E.2}$$

where we have introduced the function $f_\gamma(z_1, z_2)$, defined by

$$f_\gamma(z_1, z_2) = \frac{\pi\gamma}{(z_1 + z_2)^2 + 4\gamma^2} \frac{(z_1 - z_2 - 4i\gamma)}{(z_1 - i\gamma)(z_2 + i\gamma)}. \tag{E.3}$$

Furthermore, by introducing the functions

$$g_{cadb}(z_1) = \int d^3\mathbf{x}_3 \int d^3\mathbf{x}_4 \Phi_c^\dagger(\mathbf{x}_3) \alpha^\sigma \Phi_a(\mathbf{x}_3) D_{\sigma\lambda}^F(\mathbf{x}_3 - \mathbf{x}_4, z_1) \Phi_d^\dagger(\mathbf{x}_4) \alpha^\lambda \Phi_b(\mathbf{x}_4) \tag{E.4}$$

and

$$h_c(z_3, z_4) = \int d^3\mathbf{x}_1 \int d^3\mathbf{x}_2 \Phi_c^\dagger(\mathbf{x}_1) \alpha^\mu S_F(\mathbf{x}_1, \mathbf{x}_2, z_3) D_{\mu\nu}^F(\mathbf{x}_1 - \mathbf{x}_2, z_4) \alpha^\nu \Phi_c(\mathbf{x}_2) \tag{E.5}$$

we can write $M_\gamma^{4,(a)}$ in the compact form

$$\begin{aligned}
 M_\gamma^{4,(a)} &= \frac{e^4}{\pi^2} \int_{-\infty}^{\infty} dz_1 \int_{-\infty}^{\infty} dz_3 \int_{-\infty}^{\infty} dz_4 \Delta_\gamma(z_3 + z_4 - E_0) \Delta_\gamma(-z_1) \\
 &\times g_{cadb}(z_1) h_c(z_3, z_4) f_\gamma(-z_1, z_3 + z_4 - E_0).
 \end{aligned} \tag{E.6}$$

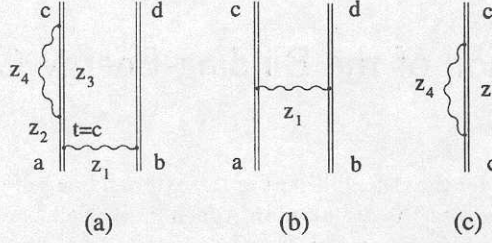


Figure E.1: The reducible graph (a) together with the corresponding counterparts (b) and (c).

Following Feynman rules, we can write the counterparts in Fig. E.1(b,c) as

$$M_\gamma^{2,(b)} = -2\pi i \epsilon^2 \int_{-\infty}^{\infty} dz_1 g_{cadb}(z_1) [\Delta_\gamma(-z_1)]^2 \quad (\text{E.7})$$

and

$$M_\gamma^{2,(c)} = e^2 \int_{-\infty}^{\infty} dz_3 \int_{-\infty}^{\infty} dz_4 h_c(z_3, z_4) [\Delta_\gamma(z_3 + z_4 - E_0)]^2. \quad (\text{E.8})$$

The identity

$$-2i\pi^3 \Delta_\gamma(z_3 + z_4 - E_0) \Delta_\gamma(-z_1) = f_\gamma(-z_1, z_3 + z_4 - E_0) + f_\gamma(z_3 + z_4 - E_0, -z_1) \quad (\text{E.9})$$

allow us to write the product of counterparts as

$$\begin{aligned} M_\gamma^{2,\text{tot}} &= M_\gamma^{2,(b)} \times M_\gamma^{2,(c)} \\ &= \frac{e^4}{\pi^2} \int_{-\infty}^{\infty} dz_1 \int_{-\infty}^{\infty} dz_3 \int_{-\infty}^{\infty} dz_4 \Delta_\gamma(z_3 + z_4 - E_0) \Delta_\gamma(-z_1) \\ &\quad \times g_{cadb}(z_1) h_c(z_3, z_4) [f_\gamma(-z_1, z_3 + z_4 - E_0) + f_\gamma(z_3 + z_4 - E_0, -z_1)]. \end{aligned} \quad (\text{E.10})$$

It is now straightforward to perform the subtraction as prescribed by Sucher's formula (A.60)

$$\begin{aligned} 4M_\gamma^{4,(a)} - 2M_\gamma^{2,\text{tot}} &= 2 \frac{e^4}{\pi^2} \int_{-\infty}^{\infty} dz_1 \int_{-\infty}^{\infty} dz_3 \int_{-\infty}^{\infty} dz_4 \\ &\quad \times \Delta_\gamma(z_3 + z_4 - E_0) \Delta_\gamma(-z_1) g_{cadb}(z_1) h_c(z_3, z_4) \\ &\quad \times [f_\gamma(-z_1, z_3 + z_4 - E_0) - f_\gamma(z_3 + z_4 - E_0, -z_1)]. \end{aligned} \quad (\text{E.11})$$

The limit $\gamma \rightarrow 0$ can, however, not be taken at this stage. Both the z_3 - and z_1 -integrations have to be performed first. To evaluate the z_3 -integration we reduce the factor in square brackets to read

$$\begin{aligned} F_\gamma(z_1, z_3, z_4) &= [f_\gamma(-z_1, z_3 + z_4 - E_0) - f_\gamma(z_3 + z_4 - E_0, -z_1)] \\ &= \frac{2\pi\gamma}{4\gamma^2 + (z_3 + z_4 - z_1 - E_0)^2} \frac{(z_3 + z_4 + z_1 - E_0)(3\gamma^2 - z_1(z_3 + z_4 - E_0))}{(z_1^2 + \gamma^2)(z_3 + z_4 - E_0 - i\gamma)(z_3 + z_4 - E_0 + i\gamma)}. \end{aligned} \quad (\text{E.12})$$

By extracting the z_3 -dependence out of $h_c(z_3, z_4)$, and assuming E_u to be positive, we have poles at $z_3 = E_0 - z_4 + i\gamma$ and $z_3 = E_0 + z_1 - z_4 + 2i\gamma$ in the upper half plane. Using calculus of residues enclosing these poles yields

$$\begin{aligned} \int_{-\infty}^{\infty} dz_3 \frac{\gamma}{\pi} \frac{F_\gamma(z_1, z_3, z_4)}{(z_3 - E_u(1 - i\eta))(\gamma^2 + (E_0 - z_3 - z_4)^2)} \\ = \frac{G_\gamma(z_1, z_4)}{(z_1^2 + \gamma^2)(z_1^2 + 9\gamma^2)[z_4 - z_1 - E_0 + E_t(1 - i\eta) - 2i\gamma]} \end{aligned} \quad (\text{E.13})$$

where $G_\gamma(z_1, z_4)$ is a very lengthy function not written out for the sake of brevity. In a similar way we perform the z_1 -integration, with poles at $z_1 = +i\gamma$, $z_1 = +3i\gamma$ and $z_1 = -k_1 + i\delta$ as follows from Eq. (E.13) and $g_{cadb}(z_1)$. $k_1 = |\mathbf{k}_1|$ is the momentum of the ladder photon, the photon which connects the two electrons. Finally we can take the limit $\gamma \rightarrow 0$ which yields

$$\begin{aligned} \lim_{\gamma \rightarrow 0} \frac{i\gamma}{2} \int_{-\infty}^{\infty} dz_1 \frac{\gamma}{\pi} \frac{G_\gamma(z_1, z_4)}{(z_1^2 - k_1^2 + i\delta)(z_1^2 + \gamma^2)^2(z_1^2 + 9\gamma^2)[z_4 - z_1 - E_0 + E_u(1 - i\eta) - 2i\gamma]} \\ = \frac{\pi i}{8} \frac{1}{k_1^2 [E_0 - z_4 - E_u(1 - i\eta)]^2}. \end{aligned} \quad (\text{E.14})$$

Although the result (E.14) has been derived for $E_u > 0$, it holds also for negative intermediate energies. Proceeding with the z_4 -integration

$$\int_{-\infty}^{\infty} dz_4 \frac{1}{[E_0 - z_4 - E_u(1 - i\eta)]^2(z_4^2 - k_2^2 + i\delta)} = \frac{-\pi i}{k_2 [E_0 - E_u - \text{sign}(E_u)k_2]^2} \quad (\text{E.15})$$

where $k_2 = |\mathbf{k}_2|$ is the momentum of the self-energy photon. Collecting everything we can finally write the reference state contribution as

$$\Delta E_{\text{se}}^{\text{be}} = \Delta E^1 \times 2\pi\alpha \int \frac{d^3\mathbf{k}_2}{(2\pi)^3} \sum_u \frac{\langle c | \alpha^\nu e^{i\mathbf{k}_2 \cdot \mathbf{x}_1} | u \rangle \langle u | \alpha_\nu e^{-i\mathbf{k}_2 \cdot \mathbf{x}_2} | c \rangle}{k_2 [E_0 - E_u - k_2 \text{sign}(E_u)]^2}, \quad (\text{E.16})$$

which can be converted to the form in Eq. (3.86) by performing the angular part of the \mathbf{k}_2 -integration and using the spherical wave expansion Eq. (3.42).

F Free Electron Solutions

F.1 Plane waves

We will follow the notations and conventions given in [9]. For convenience, we explicitly write out c (the velocity of light) in this appendix. The time-dependent Dirac equation possesses plane-wave solutions

$$\Phi_p(x) = \text{Const} \begin{Bmatrix} u_r(\mathbf{p}) \\ v_r(\mathbf{p}) \end{Bmatrix} e^{\mp i p x / \hbar} \quad (\text{F.1})$$

where $p = (p_0, \mathbf{p}) = (E_p/c, \mathbf{p})$ and $E_p = +\sqrt{m^2 c^4 + \mathbf{p}^2 c^2}$. The index $r = 1, 2$ labels two independent solutions for each four momentum p .

$u_r(\mathbf{p})$ corresponds to a particle of momentum \mathbf{p} and positive energy E_p . $v_r(\mathbf{p})$ corresponds to, in the language of negative energy states, a negative energy electron with momentum $-\mathbf{p}$.

The four-spinors $u_r(\mathbf{p})$ and $v_r(\mathbf{p})$, and their adjoints

$$\begin{aligned} \bar{u}_r(\mathbf{p}) &= u_r^\dagger(\mathbf{p}) \gamma^0 \\ \bar{v}_r(\mathbf{p}) &= v_r^\dagger(\mathbf{p}) \gamma^0 \end{aligned} \quad (\text{F.2})$$

satisfy the time-dependent Dirac equation (the on mass-shell conditions)

$$(\not{p} - mc)u_r(\mathbf{p}) = 0 \quad (\not{p} + mc)v_r(\mathbf{p}) = 0 \quad (\text{F.3})$$

$$\bar{u}_r(\mathbf{p})(\not{p} - mc) = 0 \quad \bar{v}_r(\mathbf{p})(\not{p} + mc) = 0 \quad (\text{F.4})$$

Using the orthonormality condition

$$u_r^\dagger(\mathbf{p})u_s(\mathbf{p}) = v_r^\dagger(\mathbf{p})v_s(\mathbf{p}) = \delta_{r,s} \quad (\text{F.5})$$

leads to the completeness relation

$$\sum_{r=1}^2 u_r(\mathbf{p})u_r^\dagger(\mathbf{p}) - v_r(\mathbf{p})v_r^\dagger(\mathbf{p}) = \begin{pmatrix} I & 0 \\ 0 & I \end{pmatrix} \quad (\text{F.6})$$

where I is the 2×2 identity matrix.

The normalization requirement in Eq. (F.5) gives the explicit form of the spinors

$$u_r(\mathbf{p}) = \frac{1}{\sqrt{2p_0(p_0 + mc)}} \begin{pmatrix} (p_0 + mc)\chi_r \\ \boldsymbol{\sigma} \cdot \mathbf{p} \chi_r \end{pmatrix} \quad (\text{F.7})$$

$$v_r(\mathbf{p}) = \frac{1}{\sqrt{2p_0(p_0 + mc)}} \begin{pmatrix} \boldsymbol{\sigma} \cdot \mathbf{p} \chi'_r \\ (p_0 + mc)\chi'_r \end{pmatrix} \quad (\text{F.8})$$

where we have introduced the two-component spinors

$$\chi_1 = \chi'_2 = \begin{pmatrix} 1 \\ 0 \end{pmatrix} \quad (\text{F.9})$$

$$\chi_2 = \chi'_1 = \begin{pmatrix} 0 \\ 1 \end{pmatrix} \quad (\text{F.10})$$

We also define the projection operators $\Lambda^\pm(\mathbf{p})$ which project out the positive (negative) energy solution when acting on a linear combination of the spinors

$$\Lambda^\pm(\mathbf{p}) = \frac{\pm \not{\mathbf{p}} + mc}{2mc} \quad (\text{F.11})$$

or one can show the alternative relations

$$\Lambda^+(\mathbf{p}) = \sum_{r=1,2} u_r(\mathbf{p})u_r^\dagger(\mathbf{p}) \quad (\text{F.12})$$

$$\Lambda^-(\mathbf{p}) = - \sum_{r=1,2} v_r(\mathbf{p})v_r^\dagger(\mathbf{p}) \quad (\text{F.13})$$

Alternatively, we can use the normalization condition $\bar{u}_r(\mathbf{p})u_r(\mathbf{p}) = \delta_{r,s}$ which gives similar relations where $u_r^\dagger(\mathbf{p})$ is replaced by $\bar{u}_r(\mathbf{p})$.

F.2 Spherical waves

Separating out the time-dependency in the Dirac equation, we can obtain free-electron solutions for a spherical symmetry of the form

$$\Phi_E(\mathbf{x}) = \frac{1}{r} \begin{pmatrix} F_{E,\kappa}(pr) & \chi_{\kappa,m}(\theta, \phi) \\ iG_{E,\kappa}(pr) & \chi_{-\kappa,m}(\theta, \phi) \end{pmatrix}$$

where $F_{E,\kappa}(pr)$ and $G_{E,\kappa}(pr)$ are the upper and lower component radial functions and $\chi_{-\kappa,m}(\theta, \phi)$ is the spin-angular function. p is the one-dimensional positive momenta related to the energy E_p as $E_p = +\sqrt{m^2c^4 + \mathbf{p}^2c^2}$. Furthermore, for each solution of the time-independent Dirac equation we have two roots of the energy E , given by $E = \pm E_p$, with corresponding radial eigenfunctions of the form

$$F_{E,\kappa}(pr) = A_E pr j_l(pr) \quad (\text{F.14})$$

and

$$G_{E,\kappa}(pr) = B_E pr j_{\bar{l}}(pr) \quad (\text{F.15})$$

where

$$l = \begin{cases} \kappa & \kappa > 0 \\ -\kappa - 1 & \kappa < 0 \end{cases}$$

$$\bar{l} = \begin{cases} \kappa - 1 & \kappa > 0 \\ -\kappa & \kappa < 0 \end{cases}$$

Using the energy normalization

$$\int_0^\infty (F_{E,\kappa}(pr)F_{E',\kappa}(p'r) + G_{E,\kappa}(pr)G_{E',\kappa}(p'r) dr = \delta(E - E') \quad (\text{F.16})$$

yields the normalization constants

$$A_E = \sqrt{\frac{E + mc^2}{\pi E}} \quad (\text{F.17})$$

$$B_E = \text{sgn}(E) \frac{\kappa}{|\kappa|} \sqrt{\frac{E - mc^2}{\pi E}} \quad (\text{F.18})$$

To summarize, we can write the upper and lower radial component as

$$F_{E,\kappa}(pr) = \sqrt{\frac{E + mc^2}{\pi E}} pr j_i(pr) \quad (\text{F.19})$$

and

$$G_{E,\kappa}(pr) = \text{sgn}(E) \frac{\kappa}{|\kappa|} \sqrt{\frac{E - mc^2}{\pi E}} pr j_{\bar{i}}(pr) \quad (\text{F.20})$$

References

- ¹ W. E. Lamb, Jr. and R. C. Retherford, *Physical Review* **72**, 241 (1947).
W. E. Lamb, Jr. and R. C. Retherford, *Physical Review* **86**, 1014 (1952).
- ² H. A. Bethe, *Physical Review* **72**, 339 (1947).
- ³ J. Schwinger, *Phys. Rev.* **73**, 416 (1948).
- ⁴ P. Kusch and H. M. Foley, *Physical Review* **74**, 250 (1948).
- ⁵ F. J. Dyson, *Physical Review* **75**, 1736 (1949).
- ⁶ A. Salam, *Physical Review* **82**, 217 (1951).
- ⁷ J. C. Ward, *Proc. Phys. Soc.*, **A64**, 54 (1951).
- ⁸ J. J. Sakurai, *Advanced Quantum Mechanics*, Addison-Wesley (1967).
- ⁹ F. Mandl and G. Shaw, *Quantum Field Theory*, Wiley (1984).
- ¹⁰ J. M. Jauch and F. Rohrlich, *The Theory of Photons and electrons*, Springer-Verlag (1955).
- ¹¹ W. Greiner, B. Müller, J. Rafelski, *Quantum Electrodynamics of Strong Fields*, Springer-Verlag (1985).
- ¹² M. Finkbeiner, B. Fricke, and T. Kühl, *Phys. Lett A* **176**, 113 (1993).
- ¹³ L. N. Labzowsky, W. R. Johnson, S. M. Schneider, and G. Soff, *Phys. Rev.* **A51**, 4597 (1995).
- ¹⁴ N. M. Kroll and W. E. Lamb, *Physical Review* **73**, 388 (1949).
- ¹⁵ J. B. French and V. Weisskopf, *Physical Review* **75**, 1240 (1949).
- ¹⁶ R. P. Feynman, *Physical Review* **74**, 1430 (1949), and correction in *Physical Review* **76**, 769 (1949), footnote 13.
- ¹⁷ J. Schwinger, *Physical Review* **76**, 790 (1949).
- ¹⁸ H. Fukuda, Y. Miyamoto, and S. Tomonaga, *Progress in Theoretical Physics (Japan)* **4**, 47 and 121 (1948).
- ¹⁹ G. E. Brown, J. S. Langer, and G. W. Schaefer, *Proceedings of the Royal Society (London)* **251**, 92 (1959).
- ²⁰ G. E. Brown and D. F. Mayers, *Proceedings of the Royal Society (London)* **251**, 105 (1959).

- ²¹ A. M. Desiderio and W. R. Johnson, *Physical Review A* **3**, 1267 (1971).
- ²² P. J. Mohr, *Annals of Physics* **88**, 26 (1974).
- ²³ P. J. Mohr, *Annals of Physics* **88**, 52 (1974).
- ²⁴ P. J. Mohr, *Physical Review A* **26**, 2338 (1982).
- ²⁵ P. J. Mohr, *Physical Review A* **46**, 4421 (1992).
- ²⁶ M. Baranger, H. A. Bethe and R. P. Feynman, *Physical Review* **92**, 482 (1953).
- ²⁷ S. Blundell, *Physical Review A* **46**, 3762 (1992).
- ²⁸ S. Blundell, *Physical Review A* **47**, 1790 (1993).
- ²⁹ K. T. Cheng, W. R. Johnson and J. Sapirstein, *Physical Review Letters* **66**, 2960 (1991).
- ³⁰ K. T. Cheng, W. R. Johnson and J. Sapirstein, *Physical Review A* **47**, 1817 (1993).
- ³¹ P. Indelicato and P. J. Mohr, *Theoretical Chemical Acta* **80**, 207 (1991).
- ³² H. M. Quiney and I. P. Grant, *Physica Scripta T* **46**, 132 (1993)
- ³³ H. Persson, I. Lindgren and S. Salomonson, *Physica Scripta T* **46**, 125 (1993)
- ³⁴ I. Lindgren, H. Persson, S. Salomonson, and A. Ynnerman, *Physical Review A* **47**, R4555 (1993)
- ³⁵ S. A. Blundell and N. J. Snyderman, *Physical Review A* **44**, R1427 (1991).
- ³⁶ N. J. Snyderman, *Annals of Physics (N.Y.)* **211**, 43 (1991).
- ³⁷ H. M. Quiney and I. P. Grant, *J. Phys.* **B27**, L199 (1994).
- ³⁸ H. Persson, doctoral thesis, Göteborg 1993, unpublished.
- ³⁹ V. M. Shabaev, *Izv. Vuz. Fiz.* **33** (1990) 43, [*Sov. Phys. J.* **33** (1990) 660].
V. M. Shabaev and I. G. Fokeeva, *Physical Review A* **49**, 4489 (1994).
V. A. Erokhin and V. M. Shabaev, *Sov. Phys. JETP* **83**, 39 (1996).
- ⁴⁰ P. Indelicato, and P. J. Mohr, *Theor. Chem. Acta* **80**, 207 (1991).
- ⁴¹ S. A. Blundell, K. T. Cheng, and J. Sapirstein, *Phys. Rev.* **A55**, 1857 (1997).
- ⁴² S. A. Blundell, K. T. Cheng, and J. Sapirstein, *Phys. Rev. Lett.* **78**, 4914 (1997).
- ⁴³ I. Lindgren, J. Morrison, *Atomic Many-Body Theory*, (Springer, Berlin, 1982).

- 44 E. A. Uehling, *Physical Review* **48**, 55 (1935).
- 45 G. Soff and P. J. Mohr, *Phys. Rev. A* **38**, 5066 (1988).
- 46 M. Gyulassy, *Nuclear Physics A* **244**, 497 (1975).
- 47 A. N. Artemyev, V. M. Shabaev, and V. A. Yerokhin *Phys. Rev. A* **56**, 3529 (1997).
- 48 J. Aldins *et al.* *Phys. Rev. D* **1**, 2378 (1970).
- 49 J. Calmet, S. Narison, M. Perrottet, and E. de Rafael *Rev. Mod. Phys* **40**, 21 (1977).
- 50 B. E. Lautrup and M. A. Samuel *Phys. Lett.* **B72**, 114 (1977).
- 51 A. I. Milstein and A. S. Yelkhovsky *Phys. Lett.* **B233**, 11 (1989).
- 52 A. S. Yelkhovsky and A. I. Milstein, *Sov. Phys. JETP* **72**, 592 (1991).
- 53 S. Salomonson, P. Öster, *Physical Review A* **40**, 5548 (1989).
- 54 V.M. Shabaev, *J. Phys. B* **24**, 4479 (1991).
- 55 M.B. Shabaeva and V.M. Shabaev, *Physical Review A* **52**, 2811 (1995).
- 56 I Lindgren, H Persson, S Salomonson and L Labzowsky, *Phys. Rev. A* **51**, 1167, (1995).
- 57 A.P. Prudnikov, Yu.A. Brychkov and O.I. Marichev, *Integrals and Series*, Vol 2: Special Functions, Gordon and Breach (1986).
- 58 I. S. Gradshteyn and I. M. Ryzhik, *Table of Integrals, Series and Products*, Academic Press (1980).
- 59 R. E. Marrs, S. R. Elliot and Th. Stöhlker, *Physical Review A* **52**, 3577 (1995).
- 60 I. Klafit, S. Borneis, T. Engel, B. Fricke, R. Grieser, G. Huber, T. Kühl, D. Marx, R. Neumann, S. Schröder, P. Seelig, and L. Völker, *Phys. Rev. Lett.* **73**, 2425 (1994).
- 61 J. R. Crespo Lopez-Urrutia, P. Beiersdorfer, D. Savin, and K. Widman, *Phys. Rev. Lett.* **77**, 826 (1996).
- 62 J. R. Crespo Lopez-Urrutia, P. Beiersdorfer, K. Widmann, B. B. Birkett, A.-M. Mårtensson-Pendrill and M. G. H. Gustavsson, *Phys. Rev.* **A57**, (1998).
- 63 P. Seelig *et al.* to be published.
- 64 K. Hermanspahn, W. Quint, S. Stahl, M. Tönges, G. Bollen, H.-J. Kluge, R. Ley, R. Mann and G. Werth, *Acta Physica Polonica B* **27**, 357 (1996).

- ⁶⁵ K T Cheng, W R Johnson and J Sapirstein, Phys. Rev. Lett **66**, 2960 (1991).
- ⁶⁶ I Lindgren, H Persson, S Salomonson, and A Ynnerman, Phys. Rev. A **47**, R4555 (1993).
- ⁶⁷ S Blundell, P J Mohr, W R Johnson and J Sapirstein, Phys. Rev. A **48**, 2615 (1993).
- ⁶⁸ H Araki, Prog. Theor. Phys. **17**, 619 (1957).
J Sucher, Phys. Rev. **109**, 1010 (1958) and his Ph. D. Thesis Columbia University (1957), unpublished.
- ⁶⁹ V. A. Yerokhin, A. N. Artemyev, and V. M. Shabaev, Phys. Lett. A **234**, 361 (1997).
- ⁷⁰ H. De Vries, C. W. Jager, and C. De Vries, At. Data Nucl. Data Tables **36**, 495 (1987); E. G. Nadjakov, K. P. Marinova, and Yu. P. Gangrsky, *ibid.* **56**, 133 (1994); G. Fricke *et al.*, *ibid.* **60**, 177 (1995).
- ⁷¹ G Drake, Can. J. Phys. **66**, 586 (1988) and ref. [59].
- ⁷² D R Plante, W R Johnson, and J Sapirstein, Phys. Rev. A **49**, 3519, (1994).
- ⁷³ P Indelicato, taken from ref. [59].
P Indelicato, O. Gorceix, and J. P. Desclaux, J. Phys. B **20**, 651 (1987).
- ⁷⁴ T. Kinoshita, Phys. Rev. Lett. **75**, 4728 (1995).
- ⁷⁵ G. Breit, Nature **122**, 649 (1928).
- ⁷⁶ R. A. Hegstrom, Phys. Rev. **184**, 17 (1969).
- ⁷⁷ H. Grotch, Phys. Rev. Lett. **24**, 39 (1970).
- ⁷⁸ H. Grotch and R. A. Hegstrom, Phys. Rev. A **4**, 59 (1971).
- ⁷⁹ S.A. Blundell, K.T. Cheng, and J. Sapirstein, Phys. Rev. A **55**, 1857 (1997).
- ⁸⁰ K. Pachucki, Private Communication (1996).
- ⁸¹ A. N. Artemyev, V. M. Shabaev and V. A. Yerokhin, Phys. Rev. A **52**, 1884 (1995).
- ⁸² E. Fermi, Z. Phys. **60**, 320 (1930).
- ⁸³ N. M. Kroll, and F. Pollock, Phys. Rev. **85**, 876 (1952).
- ⁸⁴ R. Karplus, and A. Klein, Phys. Rev. **85**, 927 (1952).
- ⁸⁵ D. E. Zwanziger, Phys. Rev. **121**, 1128 (1961).
- ⁸⁶ S. J. Brodsky, and G. W. Erickson, Phys. Rev. **148**, 26 (1966).

- ⁸⁷ J. R. Sapirstein, Phys. Rev. Lett. **51**, 985 (1983).
- ⁸⁸ S. M. Schneider, G. Soff, and W. Greiner, Phys. Rev. A**50**, 118 (1994).
- ⁸⁹ S. G. Karshenboim, Z. Phys. D **36**, 11 (1996).
- ⁹⁰ K. Pachucki, Phys. Rev. A**54**, 1994 (1996).
- ⁹¹ M. Nio, T. Kinoshita, Phys. Rev. D**55**, 7267 (1997).
- ⁹² V. M. Shabaev, M. B. Shabaeva, I. I. Tupitsyn, V. A. Yerokhin, A. N. Artemyev, T. Kühl, M. Tomaselli, and O. M. Zherebtsov, Phys. Rev. A**57**, 149 (1998).
- ⁹³ S. G. Karshenboim, V. G. Ivanov, and V. M. Shabaev, Can. J. Phys. **76**, No. 5 July (1998).
- ⁹⁴ M. G. H. Gustavsson and A.-M. Mårtensson-Pendrill, Phys. Rev. A**58**, (1998).
- ⁹⁵ H. F. Beyer *et al.*, Z. Phys. D**35**, 169 (1995).
- ⁹⁶ J. Schweppe *et al.*, Phys. Rev. Lett. **66**, 1434 (1991).
- ⁹⁷ Th. Stöhlker, R. E. Marrs, and S. R. Elliot, Hyp. Int. **99**, 217 (1996).
- ⁹⁸ H. Persson, I. Lindgren, L. N. Labzowsky, G. Plunien, T. Beier, and G. Soff, Phys. Rev. A **54**, 2805, (1996).
- ⁹⁹ I. Lindgren, H. Persson, S. Salomonson, and P. Sunnergren, Phys. Rev. A **58**, 1001 (1998).
- ¹⁰⁰ L. N. Labzowsky and A. O. Mitrushenkov, Phys. Rev. A **53**, 3029 (1996).
- ¹⁰¹ S. Mallampali and J. Sapirstein, Phys. Rev. A **57**, 1548 (1998).
- ¹⁰² S. Mallampali and J. Sapirstein, Phys. Rev. Lett. **80**, 5297 (1998).
- ¹⁰³ M. Gell-Mann and F. Low, Physical Review **84**, 350 (1951).
- ¹⁰⁴ J. Sucher, Physical Review **107**, 1448 (1957).
- ¹⁰⁵ G. C. Wick, Physical Review **80**, 268 (1950).
- ¹⁰⁶ I. Lindgren, Physica Scripta **T34**, 36 (1991).
- ¹⁰⁷ J. C. Ward, Physical Review **78**, 182 (1950).
- ¹⁰⁸ G. 't Hooft, M. J. G. Veltman, Nucl. Phys. B**44**, 189 (1972).
- ¹⁰⁹ M. E. Peskin, D. V. Schroeder, *An Introduction to Quantum Field Theory*, Addison-Wesley (1995).

På grund av upphovsrättsliga skäl kan vissa ingående delarbeten ej publiceras här.
För en fullständig lista av ingående delarbeten, se avhandlingens början.

Due to copyright law limitations, certain papers may not be published here.
For a complete list of papers, see the beginning of the dissertation.



Tyckt & Bunden
Vaastadens Bekbinderi A.B
1998

